AD-A164 192 STORAGE RING TECHNOLOGY FOR FREE ELECTRON LASERS(U) 1/3
STANFORD UNIV CA J M MADEY ET AL. APR 84
AFOSR-TR-85-1223 F49620-83-K-0030

UNCLASSIFIED F/G 20/5 NL

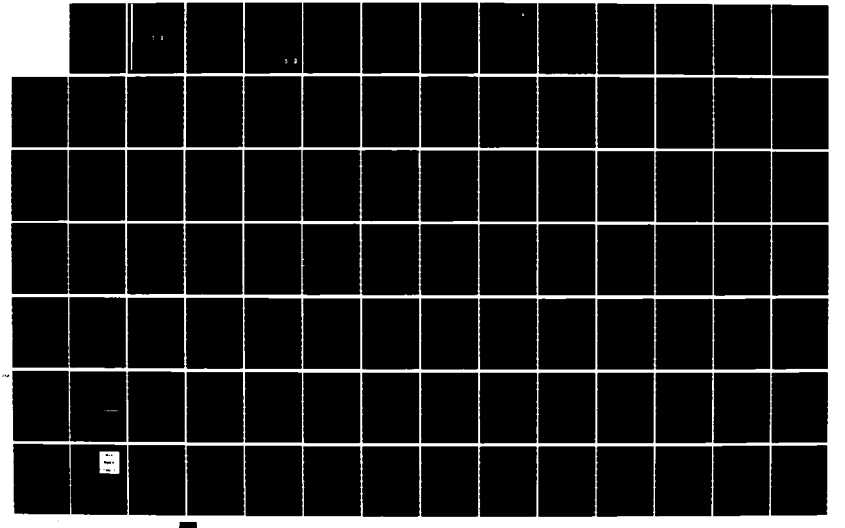

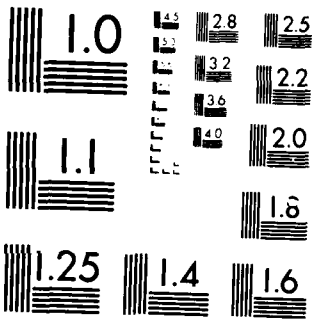

AFOSR-TR- 85-1223

AD-A164 192

DTIC
ELECTE
FEB 1 3 1986
S D
D

DTIC FILE COPY

Approved for public release;
distribution unlimited.

DISCLAIMER NOTICE

THIS DOCUMENT IS BEST QUALITY PRACTICABLE. THE COPY FURNISHED TO DTIC CONTAINED A SIGNIFICANT NUMBER OF PAGES WHICH DO NOT REPRODUCE LEGIBLY.

(1)

UNCLASSIFIED
SECURITY CLASSIFICATION OF THIS PAGE

REPORT DOCUMENTATION PAGE

1a. REPORT SECURITY CLASSIFICATION: UNCLASSIFIED	1b. RESTRICTIVE MARKINGS
2a. SECURITY CLASSIFICATION AUTHORITY	3. DISTRIBUTION/AVAILABILITY OF REPORT: Approved for public release, distribution unlimited
2b. DECLASSIFICATION/DOWNGRADING SCHEDULE	
4. PERFORMING ORGANIZATION REPORT NUMBER(S)	5. MONITORING ORGANIZATION REPORT NUMBER(S): AFOSR-TR-86-0023
6a. NAME OF PERFORMING ORGANIZATION: Stanford University; 6b. OFFICE SYMBOL (If applicable)	7a. NAME OF MONITORING ORGANIZATION: AFOSR
6c. ADDRESS (City, State and ZIP Code): Board of Trustees of the Leland Stanford Univ. SPO Office, Attn: Ms. Ruth Kaempf, Encina Hall, Stanford, CA 94305	7b. ADDRESS (City, State and ZIP Code): Bolling Air Force Base, DC 20332
8a. NAME OF FUNDING/SPONSORING ORGANIZATION: AFOSR; 8b. OFFICE SYMBOL (If applicable): NA	9. PROCUREMENT INSTRUMENT IDENTIFICATION NUMBER: AFOSR-83-K-0030
8c. ADDRESS (City, State and ZIP Code): Bolling AFB, DC 20332-6448	10. SOURCE OF FUNDING NOS. — PROGRAM ELEMENT NO.: 61102F; PROJECT NO.: 2301; TASK NO.: A1; WORK UNIT NO.: N/A
11. TITLE (Include Security Classification): Storage Ring Technology for Free Electron Lasers	
12. PERSONAL AUTHOR(S): J.M.J. Madey and D.A.G. Deacon	
13a. TYPE OF REPORT: Final Technical; 13b. TIME COVERED: FROM 04/25/83 TO 04/24/86; 14. DATE OF REPORT (Yr., Mo., Day): 1986; 15. PAGE COUNT: 224	
16. SUPPLEMENTARY NOTATION	
17. COSATI CODES — FIELD / GROUP / SUB. GR.; 18. SUBJECT TERMS (Continue on reverse if necessary and identify by block number)	

19. ABSTRACT (Continue on reverse if necessary and identify by block number)

Laser operation was achieved and a series of discoveries on the operational characteristics of storage ring lasers were made including self pulsing and transverse mode coupling. The self pulsing phenomenon was observed to permit the continuous variation of the peak output power of the device. Analysis of the data taken on the optical klystron and the laser induced bunch lengthening was completed.

20. DISTRIBUTION/AVAILABILITY OF ABSTRACT: UNCLASSIFIED/UNLIMITED X SAME AS RPT. DTIC USERS	21. ABSTRACT SECURITY CLASSIFICATION: UNCLASSIFIED
22a. NAME OF RESPONSIBLE INDIVIDUAL: Major Michael R. Schlosberg	22b. TELEPHONE NUMBER (Include Area Code): (202) 767-4963; 22c. OFFICE SYMBOL: NP

DD FORM 1473, 83 APR — EDITION OF 1 JAN 73 IS OBSOLETE.

UNCLASSIFIED
SECURITY CLASSIFICATION OF THIS PAGE

Final Technical Report
to the
AFOSR

Contract F49620-83-K-0030

April 25, 1983 to April 24, 1984

During this period, the central technical milestone of the program was achieved: the free electron laser was made to oscillate for the first time on a storage ring device.

Laser operation on ACO proved to be moderately reliable and easy to obtain. We were therefore able to extract an enormous volume of information on the operation of the system. In contrast to the other operating FELs, the steady availability and good reproducibility of operation has permitted the investigation of questions important to the future of the field but which are difficult to observe in present machines.

The laser operation was discovered to exhibit a self pulsing behavior under conditions of free running operation. We have measured the dependence of the pulsing phenomena on the current, and the cavity length detuning. We discovered that the pulses could be modulated by driving the electron beam in either transverse position or RF frequency. Theoretically, the dependence of the peak power on the driving frequency provided an unambiguous identification of the mechanism of the pulsing phenomenon. We report these results in the papers:

First operation of a storage ring free electron laser, SPIE Vol 453 (1984)

Results of the free electron laser oscillation experiments on the ACO storage ring, J. Physique 45, (1984)

First Operation of a storage-ring free-electron laser, Phys. Rev. Lett 51, (1983)

A further discovery during the contract was the existence of transverse mode coupling due to the finite cross section of the electron beam. We devised a technique to measure this effect which relies on the interference of the excited modes with the fundamental. We were able to show that the higher order modes excited in this way could be predicted by the theory in a particularly simple case, and that the mode evolution had the appropriate behavior as a function of longitudinal position. These results, both experimental and theoretical, are reported in:

Measurement of stimulated transverse mode mixing in a free electron laser, IEEE J. Quant. Elect. (1985)

Transverse Mode dynamics in a free electron laser, Appl. Phys B33, (1984)

A series of other issues were addressed, including the effects of divergence on the Madey theorem. We were able to show that indeed the divergence of the optical mode shifts the gain and spontaneous spectra in a systematic way. These results are described in:

Measurement of the violation of the Madey Theorem induced by a diverging wave, IEEE J. Quant. Elect (1985)

Observation of the diffraction induced violation of the Madey theorem, in the Proceedings of the 1984 Castelgandalfo Conference, Nucl. Instr. & Meth. A237, (1985)

The analysis of the optical klystron experiments, including the application to energy spread measurement in a storage ring, are in:

Optical klystron experiments for the ACO storage ring free electron laser, Appl. Phys. B34 (1984)

The bunch lengthening analysis presented in

Characterization of free electron laser bunch lengthening on the ACO storage ring, Appl. Phys. B (1984),

completes the comparison between the theory and the experiment, and describes a unique experimental approach for measuring the momentum compaction factor in a storage ring. The other publications for the period include:

Inhomogeneous Broadening calculation with a single integral, HEPL Technical Note TN-84-2

Realization of a variable aperture diaphragm working in ultra high vacuum, Applied Optics 23, (1984)

Copies of these papers are attached.

Realization of a variable aperture diaphragm working in ultra high vacuum

M. Velghe, D. A. G. Deacon, and J. M. Ortega

An adjustable iris has been developed to operate in the 10^{-10}-Torr vacuum environment of a storage ring. It was baked out at 300°C and has been used more than 100 times. Measurements have been carried out using the spontaneous emission of an undulator set on the storage ring. They show that the iris could be centered and adjusted accurately from outside the vacuum chamber and used as a mode selector for free electron lasers.

I. Introduction

Laser transverse mode selection by an iris placed inside the optical cavity has been extensively studied in the past (Ref. 1 and references therein). Since the optical gain of a free electron laser (FEL) may develop in several transverse modes,[2] the Orsay FEL group decided to install an iris inside the laser optical cavity. Although laser oscillation was finally obtained[3] on the TEM_{00} mode without the help of that iris due to the extremely low value of the gain,[4] future high gain systems are expected to operate multimode. It is useful to look at the technical solutions which have led to an ultra high vacuum variable aperture diaphragm and to its practical operation. This is the purpose of this paper.

Due to the weakness of the optical gain in the Orsay experiment on the ACO storage ring it was impossible to insert any optical element, such as a window, between the laser medium (high energy electrons passing through the undulator) and the cavity mirrors. For that reason the iris, as well as the cavity mirrors, has to be placed in a vacuum chamber. The pressure inside this chamber is then necessarily as low as the pressure inside the storage ring, that is, between 10^{-9} and 10^{-10} Torr, since the two chambers communicate (Fig. 1).

The technical problems posed by the requirements for three fine mechanical motions (two translations and one rotational for the iris aperture) are severe in this environment. In addition the whole chamber has to be baked to at least 200°C (for degassing) to reach the desired vacuum. No such device is commercially available (existing iris diaphragms are designed for pressures above 10^{-7} Torr).

When this work was done M. Velghe was with Universite de Paris-Sud, Laboratoire de Photophysique Moleculaire, 91405 Orsay, France; he is now with Stanford University, High Energy Physics Laboratory, Stanford, California 94305. D. A. G. Deacon is with Deacon Research, 754 Duncardine Way, Sunnyvale, California 94087, and J. M. Ortega is with Ecole Superieure de Physique et Chimie, 10 rue Vauquelin, 75231 Paris CEDEX 05, France.

Received 4 April 1984.
0003-6935/84/213851-03$02.00/0.

II. Description of the Device

We have designed and tested a device which satisfied the three following requirements (Fig. 2):

(1) Given the limited space available in the chamber the iris has to be movable in a direction perpendicular to the light beam axis so that it can be replaced by a mirror. This mirror, oriented at 45° with respect to the beam axis, is used to extract the light when the optical cavity is not in use. Therefore, the iris and the mirror are mounted on the same axis, and switching from one to another is made by a translation stage operated from outside the chamber.

(2) The iris centering has to be adjusted mechanically over a distance typically of ±5 mm in any direction in the plane perpendicular to the light beam axis. Vertical adjustment is ensured by the micrometer stage mentioned above. The horizontal displacement is realized by a second stage mounted perpendicularly to the first (Fig. 2). The two displacements are allowed by the same ultra high vacuum bellows (Fig. 2, bellows 1).

(3) The aperture of the iris is controlled from outside the vacuum chamber. The rotational motion needed to change the iris dimension is accomplished by means of a 15-mm vertical linear translation, given by a third translation stage, allowing any aperture ranging from 1.6 to 18 mm in diameter (Fig. 2, bellows 2).

The mechanical assembly of these various parts is shown in Fig. 3. The whole chamber may be baked at 300°C. The ultra high vacuum requirements mean that grease cannot be used to lubricate mechanical parts. We shall now discuss the solution we used to move the delicate pieces of a diaphragm under ultra high vacuum.

III. Lubrication of the Diaphragm

Commercial irises are usually made of aluminum or brass and are painted or coated with Teflon for lubrication. None of these materials is usuable in ultra high vacuum because of their outgassing and structural changes which occur during bake out. We have fabricated a greaseless stainless steel iris diaphragm.

Initial tests at 4×10^{-10} Torr terminated abruptly

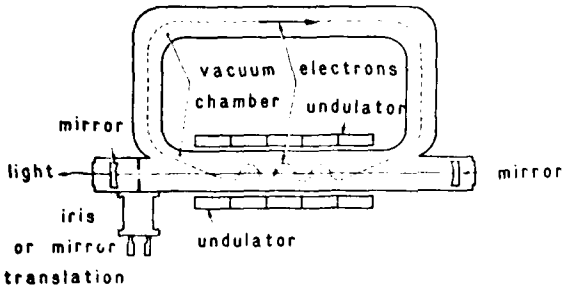

Fig. 1. General setup of the undulator experiment on the ACO storage ring FEL.

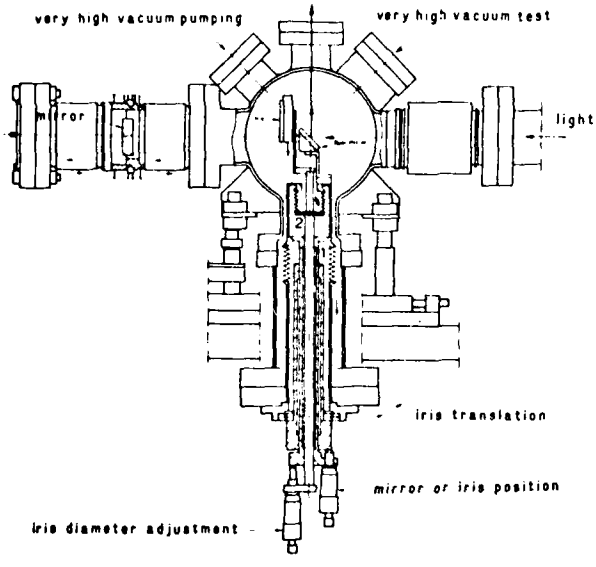

Fig. 2. Design of the iris rear mirror device within its vacuum chamber.

when a spring clip which held together the two movable posts fell off. The bake out temperature of 300°C probably annealed the piece which lost its elasticity. Upon extracting and inspecting the iris we also observed that the two moving parts that rotate coaxially showed some mutual scratching. Since lubrication was not possible we had to specify a certain clearance between the two pieces. One of the two parts undergoes a strain perpendicular to its rotation axis and, therefore, rubs strongly against the other piece.

Device modification was necessary to avoid these problems. We used a dry lubrication with very low outgassing. In this process a jet of a molybdenum disulfide plasma is projected onto both moving parts. The plasma is adsorbed by the surfaces to a depth of ~1 μm. In addition the spring clip mentioned previously was replaced by a threaded ring which holds the two moving parts more firmly and which can be baked out at 300°C. Finally the stainless lamellae of the iris, which had developed little burrs due to embossing, were carefully polished with a soft stone.

After these improvements the iris diaphragm has worked properly for more than 100 cycles (opening-closing) in a vacuum of $\sim 5 \times 10^{-10}$ Torr after a bake out at 300°C.

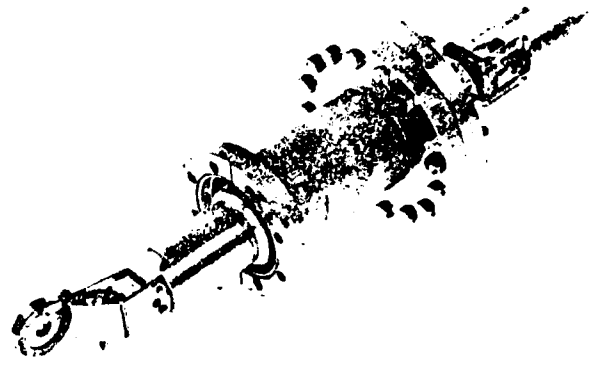

Fig. 3. Iris rear mirror device.

IV. Experiment

To test the iris operation we measured its effect on the light stored in the optical cavity. The light was emitted by the electrons of the ACO storage ring passing through an undulator[5,6] (see Fig. 1). We centered the iris in the colored rings emitted by the undulator (Fig. 4). The fine adjustment was made by maximizing the intensity transmitted by the output mirror of the cavity of the resonant wavelength (λ = 6300 Å in our case). We then measured the intensity of the light at this wavelength as a function of the iris aperture (Fig. 5). The measured intensity drops sharply when closing the diagram below a diameter of ~4 mm due to the very high quality of the optical cavity whose losses[7] are very low (1.2×10^{-3} in this experiment). Since the light is stored for $\sim 10^3$ round trips in the cavity a small loss at each pass on the diaphragm produces a large variation in the resulting intensity.

The spontaneous emission in the undulator of the electron beam at 235 MeV diverges with a half-angle

$$\theta \sim \left(\frac{2.8\lambda}{N\lambda_0\pi}\right)^{1/2} \simeq 0.66 \text{ mrad}, \quad (1)$$

where $N = 17$ is the number of periods and $\lambda_0 = 7.8$ cm is the magnet period. This angle is only a factor of 2.7 larger than the divergence angle $\lambda/\pi w_0$ of the TEM_{00} mode. In these conditions the spontaneous emission is expected to be stored on the first three of four cylindrical modes of the cavity.[8]

The intensity transmitted by the system can be easily calculated for various cylindrical transverse modes if one makes the assumption that the form of the modes is unchanged when closing the diaphragm. This assumption is probably not too bad in our case since the apertures of the iris for which the stored intensity vanishes is much larger than the beam waist at the iris location (a factor of 4–5 in our case). The loss at each passage through the iris is then found by integrating the mode intensity in the space surrounding the aperture. Since the iris is only separated from the cavity mirror by ~25 cm this power reduction occurs only once each round trip. If we include the power lost at the mirrors

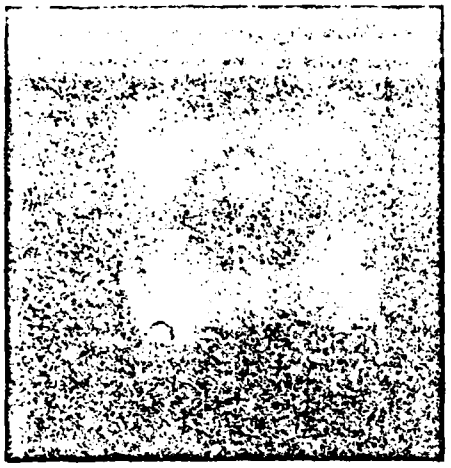

Fig. 4. Spontaneous emission produced by 235-MeV electrons traveling through the undulator.

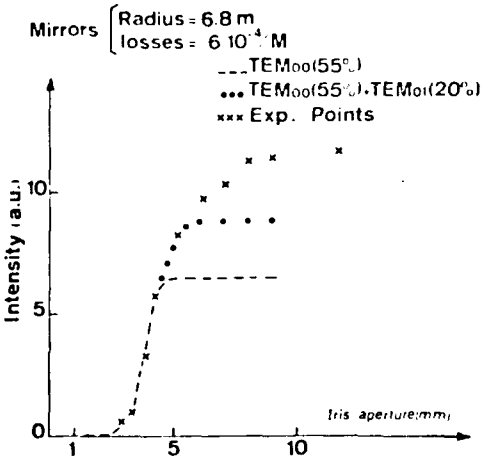

Fig. 5. Spontaneous emission intensity vs aperture of the iris.

and sum over all the round trips, we find that the intensity in the lowest-order mode is reduced from its value for the iris fully open by the factor

$$\frac{I_{00}(a)}{I_{00}(\infty)} = \frac{\Gamma}{\Gamma + \exp(-2a^2/w^2)}, \tag{2}$$

where a is the iris aperture, $w = 1.03$ mm is the size of the mode at the iris, and Γ is the total cavity losses per round trip. For the TEM_{10} cylindrical mode, the expression is

$$\frac{I_{10}(a)}{I_{10}(\infty)} = \frac{\Gamma}{\Gamma + \left(1 + \frac{a^2}{w^2}\right)\exp(-2a^2/w^2)}. \tag{3}$$

Fitting these curves to the data of Fig. 5, we can see that 55% of the output power is contained in the lowest-order mode, and 45% of the remainder is contained in the TEM_{01} within the accuracy of the fit.

This result is in good agreement with a previous analysis using a mathematical analysis of the spontaneous emission patterns.[9] Therefore, this approximate theory describes the data satisfactorily and shows that the iris has been centered and operated properly.

V. Conclusion

We have constructed a variable aperture iris capable of operating in the very difficult conditions of an ultra high vacuum environment. This device has been useful in the analysis of the mode structure of the light emitted by our undulator. Also it appears that it will be able to serve as a mode selector on the future storage ring free electron lasers particularly in the VUV spectral range where a high vacuum will be probably needed, for various reasons[3,7] in the whole optical resonator.

The authors acknowledge the vacuum staff of LURE for their assistance during these experiments. This work was supported by the CNRS (France), by the AFOSR contract F49620-83-K-0030, and by DRET contract 81:131 and was performed in part by Deacon Research under contract to Stanford University.

This work was done at Laboratoire LURE, Bâtiueent 209C, Université de Paris-Sud, 91405 Orsay, France.

References

1. M. Piche, P. Lavigne, F. Martin, and P. A. Belanger, "Modes of Resonators with Internal Apertures," Appl. Opt. **22**, 1999 (1983).
2. P. Elleaume and D. A. G. Deacon, "Transverse Mode Dynamics in Free Electron Laser," Appl. Phys. B **33**, 9 (1984).
3. M. Billardon *et al.*, "First Operation of a Storage Ring Free Electron Laser," Phys. Rev. Lett. **51**, 1652 (1983).
4. P. Elleaume *et al.*, "Results of the Free Electron Laser Oscillation Experiments on the ACO Storage Ring," J. Phys. Paris **45**, 989 (1984).
5. J. M. Ortega, C. Bazin, D. A. G. Deacon, C. Depeautex, and P. Elleaume, "Realization of the Permanent Magnet Undulator NOEL," Nucl. Instrum. Methods **206**, No. 1-2, 281 (1983).
6. M. Billardon *et al.*, "Recent Results of the ACO Storage Ring FEL Experiment," J. Phys. Paris C1, Suppl. 2 **44**, 29 (1983).
7. P. Elleaume, M. Velghe, M. Billardon, and J. M. Ortega, "Mesures vers 650 nm de la Dégradation de Réflectivité de Miroirs Multicouches Utilisés pour le Laser à Électrons Libres," J. Opt. **15**, (1984).
8. H. Kogelnik and T. Li, "Laser Beams and Resonators," J. Appl. Phys. **5**, 1550 (1966).
9. M. Billardon, Ecole Nationale Superieure de Physique et Chimie de Paris; private communication.

TN-84-2

JANUARY 1984

INHOMOGENOUS BROADENING CALCULATION WITH A SINGLE INTEGRAL*

David A. G. Deacon

High Energy Physics Laboratory
Stanford University
Stanford, California 94305

* This note was prepared under contract for HEPL by Deacon Research.

Abstract

The complex problem of calculating the inhomogenous broadening in an FEL with arbitrary energy spread, and horizontal and vertical angular spreads is reduced to a single well conditioned integral which can easily be performed on a microcomputer.

The calculation of the gain in an FEL driven by a "hot" beam in a recurring problem for FEL system designers. A knowledge of the gain reduction produced by a given energy spread and emittance is essential in designing short wavelength lasers or short interaction length systems in which the available gain approaches the net cavity losses.

The problem is conceptually simple, as it involves nothing more than a convolution of the single electron gain spectrum with the effective energy distribution of the electron beam. No closed form expression exists for the convolutions, and results must be obtained numerically. However, the general case involves separate convolution integrals for the energy spread, the horizontal angular spread, and the vertical angular spread. A numerical solution to this problem involving three integration steps can become impossibly time consuming on the computer, and complex to set up due to the divergences in the effective energy distribution of the angular spread, and due to the divergence of the denominator in the gain expression at $\nu=0$. In this paper, I present a solution to these problems using the properties of the Fourier transform, which reduces the triple integration with divergences to a single integration of an analytic functio The resulting expression takes only a few seconds to evaluate on a microcomputer, and can therefore be incorporated as a subroutine into a larger progream which evaluates the performance of a proposed design.

I assume the "hot" electron beam can be approximated by a Gaussian distribution in energy, angle, and position. The resonance parameter, ν, of an arbitrary electon is:

$$\nu \equiv 2\pi N \left(1 - \frac{\lambda_o}{2\gamma^2\lambda}\left(1 + \frac{K^2}{2} + \gamma^2\theta^2\right)\right) \tag{1}$$

for a planar undulator where N is the number of periods in the undulator, λ_o and λ are the undulator and light wavelengths, and γmc^2 and K are the electron energy and trajectory parameter $K = 2\pi e\hat{B}/mc^2\lambda_o$. If we take as our reference the resonance parameter x of an axial electron at the central energy γ_o,

$$x \equiv 2\pi N \left(1 - \frac{\lambda_o}{2\gamma^2\lambda}\left(1 + \frac{K^2}{2}\right)\right) \tag{2}$$

we find, for $\nu << N$,

$$y = x + 4\pi N \frac{\delta\gamma}{\gamma} - \frac{2\pi N}{1 + \frac{K^2}{2}}\gamma^2\theta^2 \tag{3}$$

where $\delta\gamma \equiv \gamma - \gamma_o$. The gain curve of the hot beam must be expressed in terms of x.

The numerical distribution $P(\delta\gamma, \theta_x^2, \theta_y^2)$ of electrons is assumed to be separable.

$$P(\delta\gamma, \theta_x^2, \theta_y^2) = P_1(\delta\gamma)\, P_2(\theta_x)\, P_3(\theta_y) \tag{4}$$

The average gain is then

$$\langle G(x)\rangle = \int_{-\infty}^{\infty} d\gamma\, P_1(\delta\gamma) \int_{-\infty}^{\infty} d\theta_x\, P_2(\theta_x) \int_{-\infty}^{\infty} d\theta_y\, P_3(\theta_y)\, G\left(\nu(x, \delta\gamma, \theta_x, \theta_y)\right) \tag{5}$$

which can be reduced to the convolution integrals

$$\langle G\rangle = E(x) * A_x(x) * A_y(x) * G(\nu(x)) \tag{6}$$

where

$$E(x) \equiv \frac{1}{\sqrt{2\pi\sigma^2}}\, e^{-x^2/2\sigma^2} \qquad \sigma \equiv 4\pi N \frac{\sigma_\gamma}{\gamma} \tag{7}$$

$$A(x) \equiv \theta(x)\, \frac{e^{-x/a}}{\sqrt{\pi a x}} \qquad a \equiv \frac{4\pi N \gamma^2 \sigma_\theta^2}{1 + \frac{K^2}{2}} \tag{8}$$

and $\theta(x)$ is the step function $\theta(x > 0) = 1$; $\theta(x < 0) = 0$.

Let us neglect the constant in $G(\nu)$, and use the analytic expression

for the small signal gain spectrum, including the phase shift of the slowly varying wave

$$G(\nu) = \frac{1 - \cos\nu - \frac{\nu}{2}\sin\nu}{\nu^3} - i\,\frac{\nu + \nu\cos\nu - 2\sin\nu}{\nu^3} \qquad (9)$$

It is clear from (8) and (9) that care must be taken in performing the three integrals in (6) to correctly handle the divergent denominators.

Equation (6) can most simply be handled by taking the Fourier transform, and using the convolution-product theorem:

$$\langle G(x)\rangle = \frac{1}{2\pi}\int_{-\infty}^{\infty} d\alpha\, e^{i\alpha\nu}\, E(\alpha)\, A_x(\alpha)\, A_y(\alpha)\, G(\alpha) \qquad (10)$$

where $E(\alpha)$, $A_x(\alpha)$, etc., are the Fourier transform of $E(x)$, $A(x)$, etc.

$$E(\alpha) \equiv \int_{-\infty}^{\infty} dx\; E(x)\, e^{-i\alpha x} = e^{-\alpha^2\sigma^2/2} \qquad (11)$$

$$A(\alpha) = (1 + ia\alpha)^{-1/2} = (1 + a^2\alpha^2)^{-1/4} \exp\left\{-\frac{i}{2}\tan^{-1}a\alpha\right\} \qquad (12)$$

The transform of $G(\nu)$ can most simply be obtained if we use the expression:

$$G(x) = \frac{i}{2} \int_0^1 d\tau \int_0^{\tau} d\tau' \int_0^{\tau'} d\tau'' \, e^{ix(\tau''-\tau)} \tag{13}$$

The transform is

$$G(\alpha) = -i\pi\alpha\,(1+\alpha)\,\Theta(-\alpha)\,\Theta(1+\alpha) \tag{14}$$

Inserting (11), (12), and (14) into (10), we obtain the final result:

$$\langle G(x) \rangle = \frac{1}{2} \int_0^1 d\alpha \, \frac{\alpha(1-\alpha)\, e^{-\alpha^2\sigma^2/2}}{\sqrt[4]{\left(1+a_x^2\alpha^2\right)\left(1+a_y^2\alpha^2\right)}} \left(\sin\Psi + i\cos\Psi\right)$$

$$\Psi \equiv \alpha x - \frac{i}{2}\tan^{-1} a_x\alpha - \frac{i}{2}\tan^{-1} a_y\alpha \tag{15}$$

This integral can be evaluated on a microcomputer with the simplest of codes. There are no divergent denominators, the functions are slowly varying, and the limits are independent of the electron beam parameters. Tables of $\mathrm{Re}\left\{\langle G(x_o)\rangle\right\}$ for optimum x_o and a range of τ, a_x, and a_y have been included in the appendix.

Equation (15) permits the calculation of both the real and imaginary parts of the inhomogeneous broadened gain spectrum as a function of x, which was defined in (2) as the resonance parameters of an ideal filamentary beam. It is valid in the small signal regime for an undulator with zero taper. In the large signal regime, the inhomogeneous broadening is of less interest since the gain is above threshold, but one can obtain the gain reduction by convolving the numerically obtained gain spectrum with the beam function B(x).

$$B(x) \equiv \frac{1}{\pi} \int_0^\infty d\alpha \, \frac{e^{-\alpha^2\sigma^2/2} \cos\left(\alpha x - \frac{i}{2}\tan^{-1} a_x\alpha - \frac{i}{2}\tan^{-1} a_y\alpha\right)}{\sqrt[4]{\left(1 + a_x^2\alpha^2\right)\left(1 + a_y^2\alpha^2\right)}} \qquad (16)$$

The other effects which reduce the gain are independent of the inhomogeneous broadening (15). The longitudinal effects, of course, do not couple with the inhomogeneous broadening term, and have been calculated in [1] and [2]. The same is true for the transverse effects, which can be included as a multiplicative filling factor [3] for low divergence optical and electron beam. The optical mode divergence will at some value reduce and distort [4] the gain curve; the effects of large electron beam divergence are also undesirable, although they have not been calculated.

The effects of the quadratic dependence of the undulator field on one of the transverse dimensions could have been included in (15) in an approximate way (the position distribution is identical to (8) with

$$a \longrightarrow \frac{(2\pi)^3 N \sigma_x^2}{\left(1+\frac{\kappa'}{2}\right)\lambda_0^2} \tag{17}$$

but this effect should really be handled in a transverse mode calculation such as [3]. The assumption of separability made in [4] is valid for most systems, and produces a worst-case estimate for coupled systems.

References

1. W. B. Colson, S. K. Ride, Physics of Quantum Electronics, 7, 377, (Addison-Wesley, Reading, MA, 1980).
2. P. Elleaume, "Macro-Temporal Structure of Storage Ring Free Electron Lasers," submitted to "Jouranl de Physique", Nov. 1983.
3. P. Elleaume, D. A. G. Deacon, Appl. Phys. B33 (1984), 9.
4. W. B. Colson and P. Elleaume, Appl. Phys. B29 (1982), 101.

Appendix

These tables list the values of $< G(x_o) >/G_{max}$ and x_o for values of σ, a_x and a_y between 0 and 5. $< G >/G_{max}$ for each entry is listed above x_o, which is the resonance parameter at the peak of the inhomogeneously broadened gain curve. The normalization $G_{max} = .0675$ is the maximum value of the gain curve attained with no broadening effects.

SIG = 0.00

Ax\Ay	0.00	0.50	1.00	1.50	2.00	2.50	3.00	3.50	4.00	4.50	5.00
0.00	1.000	0.980	0.928	0.865	0.803	0.746	0.695	0.651	0.612	0.578	0.547
	2.61	2.86	3.09	3.27	3.41	3.52	3.60	3.67	3.73	3.78	3.82
0.50	0.980	0.960	0.910	0.849	0.788	0.732	0.682	0.639	0.601	0.567	0.537
	2.86	3.11	3.34	3.52	3.66	3.77	3.86	3.93	3.99	4.04	4.08
1.00	0.928	0.910	0.864	0.806	0.748	0.696	0.648	0.607	0.571	0.539	0.511
	3.09	3.34	3.57	3.75	3.90	4.01	4.10	4.17	4.23	4.28	4.32
1.50	0.865	0.849	0.806	0.752	0.699	0.650	0.606	0.567	0.533	0.503	0.476
	3.27	3.52	3.75	3.94	4.09	4.21	4.30	4.37	4.43	4.49	4.53
2.00	0.803	0.788	0.748	0.699	0.649	0.604	0.563	0.526	0.495	0.467	0.442
	3.41	3.66	3.90	4.09	4.24	4.36	4.46	4.53	4.60	4.65	4.69
2.50	0.746	0.732	0.696	0.650	0.604	0.561	0.523	0.489	0.459	0.433	0.409
	3.52	3.77	4.01	4.21	4.36	4.48	4.58	4.66	4.73	4. 8	4.83
3.00	0.695	0.682	0.648	0.606	0.563	0.523	0.487	0.455	0.427	0.402	0.380
	3.60	3.86	4.10	4.30	4.46	4.58	4.68	4.76	4.83	4.89	4.94
3.50	0.651	0.639	0.607	0.567	0.526	0.489	0.455	0.425	0.399	0.375	0.355
	3.67	3.93	4.17	4.37	4.53	4.66	4.76	4.85	4.92	4.97	5.02
4.00	0.612	0.601	0.571	0.533	0.495	0.459	0.427	0.399	0.374	0.352	0.332
	3.73	3.99	4.23	4.43	4.60	4.73	4.83	4.92	4.99	5.05	5.10
4.50	0.578	0.567	0.539	0.503	0.467	0.433	0.402	0.375	0.352	0.331	0.312
	3.78	4.04	4.28	4.49	4.65	4.78	4.89	4.97	5.05	5.11	5.16
5.00	0.547	0.537	0.511	0.476	0.442	0.409	0.380	0.355	0.332	0.312	0.294
	3.82	4.08	4.32	4.53	4.69	4.83	4.94	5.02	5.10	5.16	5.21

SIG = 0.50

Ax\Ay	0.00	0.50	1.00	1.50	2.00	2.50	3.00	3.50	4.00	4.50	5.00
0.00	0.960 2.63	0.941 2.89	0.893 3.11	0.833 3.30	0.774 3.44	0.719 3.55	0.671 3.64	0.628 3.71	0.590 3.77	0.557 3.82	0.528 3.86
0.50	0.941 2.89	0.923 3.14	0.876 3.37	0.817 3.55	0.759 3.69	0.706 3.81	0.658 3.90	0.617 3.97	0.580 4.03	0.547 4.08	0.519 4.12
1.00	0.893 3.11	0.876 3.37	0.832 3.60	0.777 3.78	0.722 3.93	0.671 4.04	0.626 4.14	0.587 4.21	0.552 4.27	0.521 4.32	0.493 4.36
1.50	0.833 3.30	0.817 3.55	0.777 3.78	0.726 3.97	0.675 4.12	0.628 4.24	0.586 4.34	0.548 4.41	0.516 4.48	0.487 4.53	0.461 4.57
2.00	0.774 3.44	0.759 3.69	0.722 3.93	0.675 4.12	0.628 4.28	0.584 4.40	0.544 4.50	0.510 4.57	0.479 4.64	0.452 4.69	0.428 4.74
2.50	0.719 3.55	0.706 3.81	0.671 4.04	0.629 4.24	0.584 4.40	0.543 4.52	0.506 4.62	0.473 4.70	0.445 4.77	0.419 4.83	0.397 4.88
3.00	0.671 3.64	0.658 3.90	0.626 4.14	0.586 4.34	0.544 4.50	0.506 4.62	0.472 4.73	0.441 4.81	0.414 4.88	0.390 4.94	0.369 4.99
3.50	0.628 3.71	0.617 3.97	0.587 4.21	0.548 4.41	0.510 4.57	0.473 4.70	0.441 4.81	0.412 4.90	0.387 4.97	0.364 5.03	0.344 5.08
4.00	0.590 3.77	0.580 4.03	0.552 4.27	0.516 4.48	0.479 4.64	0.445 4.77	0.414 4.88	0.387 4.97	0.363 5.04	0.341 5.10	0.323 5.15
4.50	0.557 3.82	0.547 4.08	0.521 4.32	0.487 4.53	0.452 4.69	0.419 4.83	0.390 4.94	0.364 5.03	0.341 5.10	0.321 5.16	0.303 5.22
5.00	0.528 3.86	0.519 4.12	0.493 4.36	0.461 4.57	0.428 4.74	0.397 4.88	0.369 4.99	0.344 5.08	0.323 5.15	0.303 5.22	0.286 5.27

SIG = 1.00

Ax\Ay	0.00	0.50	1.00	1.50	2.00	2.50	3.00	3.50	4.00	4.50	5.00
0.00	0.855	0.839	0.798	0.747	0.695	0.647	0.605	0.567	0.533	0.504	0.478
	2.71	2.97	3.20	3.38	3.53	3.65	3.74	3.82	3.88	3.93	3.98
0.50	0.839	0.824	0.784	0.734	0.683	0.636	0.594	0.557	0.524	0.495	0.470
	2.97	3.22	3.45	3.64	3.79	3.91	4.00	4.08	4.14	4.19	4.24
1.00	0.798	0.784	0.746	0.699	0.651	0.607	0.567	0.532	0.500	0.473	0.448
	3.20	3.45	3.68	3.88	4.03	4.15	4.25	4.33	4.39	4.44	4.49
1.50	0.747	0.734	0.699	0.655	0.611	0.569	0.532	0.499	0.469	0.443	0.420
	3.38	3.64	3.88	4.07	4.23	4.35	4.45	4.53	4.60	4.66	4.70
2.00	0.695	0.683	0.651	0.611	0.570	0.531	0.496	0.465	0.437	0.413	0.391
	3.53	3.79	4.03	4.23	4.39	4.52	4.62	4.70	4.77	4.83	4.88
2.50	0.647	0.636	0.607	0.569	0.531	0.495	0.462	0.433	0.407	0.384	0.364
	3.65	3.91	4.15	4.35	4.52	4.65	4.75	4.84	4.91	4.97	5.03
3.00	0.605	0.594	0.567	0.532	0.496	0.462	0.431	0.404	0.380	0.358	0.339
	3.74	4.00	4.25	4.45	4.62	4.75	4.86	4.95	5.03	5.09	5.14
3.50	0.567	0.557	0.532	0.499	0.465	0.433	0.404	0.378	0.355	0.335	0.317
	3.82	4.08	4.33	4.53	4.70	4.84	4.95	5.04	5.12	5.19	5.24
4.00	0.533	0.524	0.500	0.469	0.437	0.407	0.380	0.355	0.333	0.314	0.297
	3.88	4.14	4.39	4.60	4.77	4.91	5.03	5.12	5.20	5.27	5.32
4.50	0.504	0.495	0.473	0.443	0.413	0.384	0.358	0.335	0.314	0.296	0.280
	3.93	4.19	4.44	4.66	4.83	4.97	5.09	5.19	5.27	5.33	5.39
5.00	0.478	0.470	0.448	0.420	0.391	0.364	0.339	0.317	0.297	0.280	0.264
	3.98	4.24	4.49	4.70	4.88	5.03	5.14	5.24	5.32	5.39	5.45

SIG = 1.50

Ax\Ay	0.00	0.50	1.00	1.50	2.00	2.50	3.00	3.50	4.00	4.50	5.00
0.00	0.717 2.85	0.705 3.11	0.673 3.34	0.633 3.54	0.592 3.70	0.553 3.82	0.517 3.93	0.486 4.01	0.458 4.08	0.433 4.14	0.411 4.19
0.50	0.705 3.11	0.693 3.36	0.662 3.60	0.623 3.80	0.582 3.96	0.544 4.08	0.510 4.19	0.479 4.27	0.451 4.34	0.427 4.40	0.405 4.45
1.00	0.673 3.34	0.662 3.60	0.633 3.84	0.596 4.04	0.558 4.20	0.522 4.33	0.488 4.44	0.459 4.52	0.433 4.60	0.409 4.66	0.388 4.71
1.50	0.633 3.54	0.623 3.80	0.596 4.04	0.562 4.24	0.526 4.41	0.492 4.54	0.461 4.65	0.433 4.74	0.408 4.82	0.386 4.88	0.366 4.93
2.00	0.592 3.70	0.582 3.96	0.558 4.20	0.526 4.41	0.492 4.58	0.460 4.72	0.431 4.83	0.405 4.92	0.382 5.00	0.361 5.07	0.343 5.12
2.50	0.553 3.82	0.544 4.08	0.522 4.33	0.492 4.54	0.460 4.72	0.431 4.86	0.403 4.99	0.379 5.07	0.357 5.15	0.338 5.22	0.320 5.28
3.00	0.517 3.93	0.510 4.19	0.488 4.44	0.461 4.65	0.431 4.83	0.403 4.98	0.378 5.10	0.355 5.20	0.334 5.28	0.316 5.35	0.299 5.41
3.50	0.486 4.01	0.479 4.27	0.459 4.52	0.433 4.74	0.405 4.92	0.379 5.07	0.355 5.20	0.333 5.30	0.314 5.39	0.296 5.46	0.281 5.52
4.00	0.458 4.08	0.451 4.34	0.433 4.60	0.408 4.82	0.382 5.00	0.357 5.15	0.334 5.28	0.314 5.39	0.295 5.47	0.278 5.55	0.264 5.62
4.50	0.433 4.14	0.427 4.40	0.409 4.66	0.386 4.88	0.361 5.07	0.338 5.22	0.316 5.35	0.296 5.46	0.278 5.55	0.263 5.63	0.249 5.70
5.00	0.411 4.19	0.405 4.45	0.388 4.71	0.366 4.93	0.343 5.12	0.320 5.28	0.299 5.41	0.281 5.52	0.264 5.62	0.249 5.70	0.235 5.76

SIG = 2.00

Ax\Ay	0.00	0.50	1.00	1.50	2.00	2.50	3.00	3.50	4.00	4.50	5.00
0.00	0.578	0.570	0.547	0.518	0.486	0.457	0.429	0.404	0.382	0.362	0.344
	3.06	3.32	3.56	3.77	3.94	4.08	4.19	4.29	4.37	4.44	4.49
0.50	0.570	0.561	0.539	0.511	0.480	0.451	0.424	0.399	0.377	0.357	0.339
	3.32	3.57	3.82	4.03	4.20	4.34	4.46	4.55	4.63	4.70	4.76
1.00	0.547	0.539	0.519	0.491	0.462	0.434	0.408	0.385	0.364	0.345	0.328
	3.56	3.82	4.06	4.28	4.45	4.59	4.71	4.81	4.89	4.97	5.03
1.50	0.518	0.511	0.491	0.466	0.438	0.412	0.388	0.365	0.345	0.327	0.311
	3.77	4.03	4.28	4.49	4.67	4.82	4.94	5.04	5.13	5.20	5.27
2.00	0.486	0.480	0.462	0.438	0.413	0.388	0.365	0.344	0.325	0.308	0.293
	3.94	4.20	4.45	4.67	4.85	5.01	5.13	5.24	5.33	5.41	5.47
2.50	0.457	0.451	0.434	0.412	0.388	0.365	0.344	0.324	0.306	0.290	0.275
	4.08	4.34	4.59	4.82	5.01	5.16	5.29	5.40	5.50	5.58	5.65
3.00	0.429	0.424	0.408	0.388	0.365	0.344	0.323	0.305	0.288	0.273	0.259
	4.19	4.46	4.71	4.94	5.13	5.29	5.43	5.54	5.64	5.72	5.80
3.50	0.404	0.399	0.385	0.365	0.344	0.324	0.305	0.287	0.271	0.257	0.244
	4.29	4.55	4.81	5.04	5.24	5.40	5.54	5.66	5.76	5.85	5.92
4.00	0.382	0.377	0.364	0.345	0.325	0.306	0.288	0.271	0.256	0.242	0.230
	4.37	4.63	4.89	5.13	5.33	5.50	5.64	5.76	5.86	5.95	6.03
4.50	0.362	0.357	0.345	0.327	0.308	0.290	0.273	0.257	0.242	0.229	0.218
	4.44	4.70	4.97	5.20	5.41	5.58	5.72	5.85	5.95	6.05	6.13
5.00	0.344	0.339	0.328	0.311	0.293	0.275	0.259	0.244	0.230	0.218	0.206
	4.49	4.76	5.03	5.27	5.47	5.65	5.80	5.92	6.03	6.13	6.21

S(G = 2.50

Ax\Ay	0.00	0.50	1.00	1.50	2.00	2.50	3.00	3.50	4.00	4.50	5.00
0.00	0.459 3.34	0.453 3.60	0.438 3.85	0.417 4.07	0.395 4.26	0.373 4.41	0.352 4.54	0.333 4.65	0.315 4.75	0.299 4.83	0.285 4.89
0.50	0.453 3.60	0.448 3.86	0.433 4.11	0.412 4.33	0.390 4.52	0.369 4.68	0.348 4.81	0.329 4.92	0.312 5.01	0.296 5.09	0.282 5.16
1.00	0.438 3.85	0.433 4.11	0.419 4.36	0.399 4.59	0.378 4.78	0.357 4.94	0.338 5.07	0.319 5.18	0.303 5.28	0.288 5.36	0.274 5.44
1.50	0.417 4.07	0.412 4.33	0.399 4.59	0.381 4.82	0.361 5.01	0.342 5.17	0.323 5.31	0.306 5.43	0.290 5.53	0.275 5.61	0.262 5.69
2.00	0.395 4.26	0.390 4.52	0.378 4.78	0.361 5.01	0.343 5.21	0.324 5.38	0.306 5.52	0.290 5.64	0.275 5.75	0.262 5.84	0.249 5.91
2.50	0.373 4.41	0.369 4.68	0.357 4.94	0.342 5.17	0.324 5.38	0.307 5.55	0.290 5.70	0.275 5.82	0.260 5.93	0.248 6.03	0.236 6.11
3.00	0.352 4.54	0.348 4.81	0.338 5.07	0.323 5.31	0.306 5.52	0.290 5.70	0.274 5.85	0.260 5.98	0.246 6.09	0.234 6.19	0.223 6.28
3.50	0.333 4.65	0.329 4.92	0.319 5.18	0.306 5.43	0.290 5.64	0.275 5.82	0.260 5.98	0.246 6.11	0.233 6.23	0.222 6.33	0.211 6.42
4.00	0.315 4.75	0.312 5.01	0.303 5.28	0.290 5.53	0.275 5.75	0.260 5.93	0.246 6.09	0.233 6.23	0.221 6.35	0.210 6.46	0.200 6.55
4.50	0.299 4.83	0.296 5.09	0.288 5.36	0.275 5.61	0.262 5.84	0.248 6.03	0.234 6.19	0.222 6.33	0.210 6.46	0.200 6.57	0.190 6.66
5.00	0.285 4.89	0.282 5.16	0.274 5.44	0.262 5.69	0.249 5.91	0.236 6.11	0.223 6.28	0.211 6.42	0.200 6.55	0.190 6.66	0.181 6.76

SIG = 3.00

Ax\Ay	0.00	0.50	1.00	1.50	2.00	2.50	3.00	3.50	4.00	4.50	5.00
0.00	0.364 3.69	0.361 3.95	0.351 4.21	0.337 4.44	0.321 4.64	0.305 4.81	0.289 4.96	0.275 5.09	0.261 5.20	0.249 5.29	0.238 5.37
0.50	0.361 3.95	0.357 4.21	0.348 4.47	0.334 4.70	0.318 4.90	0.302 5.08	0.287 5.22	0.273 5.35	0.259 5.46	0.247 5.56	0.236 5.64
1.00	0.351 4.21	0.348 4.47	0.338 4.73	0.325 4.96	0.310 5.17	0.294 5.34	0.280 5.49	0.266 5.62	0.253 5.73	0.241 5.83	0.230 5.92
1.50	0.337 4.44	0.334 4.70	0.325 4.96	0.312 5.20	0.298 5.41	0.283 5.59	0.269 5.75	0.256 5.88	0.244 5.99	0.233 6.09	0.222 6.18
2.00	0.321 4.64	0.318 4.90	0.310 5.17	0.298 5.41	0.285 5.62	0.271 5.81	0.257 5.97	0.245 6.10	0.233 6.22	0.223 6.33	0.213 6.42
2.50	0.305 4.81	0.302 5.08	0.294 5.34	0.283 5.59	0.271 5.81	0.258 6.00	0.245 6.16	0.233 6.30	0.222 6.43	0.212 6.54	0.203 6.63
3.00	0.289 4.96	0.287 5.22	0.280 5.49	0.269 5.75	0.257 5.97	0.245 6.16	0.233 6.33	0.222 6.48	0.212 6.60	0.202 6.72	0.193 6.82
3.50	0.275 5.09	0.273 5.35	0.266 5.62	0.256 5.88	0.245 6.10	0.233 6.30	0.222 6.48	0.211 6.63	0.201 6.76	0.192 6.88	0.184 6.98
4.00	0.261 5.20	0.259 5.46	0.253 5.73	0.244 5.99	0.233 6.22	0.222 6.43	0.212 6.60	0.201 6.76	0.192 6.90	0.183 7.02	0.175 7.12
4.50	0.249 5.29	0.247 5.56	0.241 5.83	0.233 6.09	0.223 6.33	0.212 6.54	0.202 6.72	0.192 6.88	0.183 7.02	0.175 7.14	0.167 7.25
5.00	0.238 5.37	0.236 5.64	0.230 5.92	0.222 6.18	0.213 6.42	0.203 6.63	0.193 6.82	0.184 6.98	0.175 7.12	0.167 7.25	0.159 7.37

SIG = 3.50

Ax\Ay	0.00	0.50	1.00	1.50	2.00	2.50	3.00	3.50	4.00	4.50	5.00
0.00	0.292 4.09	0.291 4.35	0.284 4.62	0.275 4.86	0.263 5.07	0.252 5.26	0.240 5.42	0.229 5.57	0.219 5.69	0.209 5.80	0.201 5.89
0.50	0.291 4.35	0.289 4.61	0.282 4.88	0.273 5.12	0.261 5.34	0.250 5.52	0.239 5.69	0.228 5.83	0.218 5.95	0.208 6.06	0.199 6.16
1.00	0.284 4.62	0.282 4.88	0.276 5.14	0.267 5.39	0.256 5.60	0.245 5.79	0.234 5.96	0.223 6.10	0.213 6.23	0.204 6.34	0.195 6.44
1.50	0.275 4.86	0.273 5.12	0.267 5.39	0.258 5.63	0.248 5.85	0.237 6.05	0.226 6.22	0.216 6.37	0.207 6.49	0.198 6.61	0.190 6.71
2.00	0.263 5.07	0.261 5.34	0.256 5.60	0.248 5.85	0.238 6.08	0.228 6.28	0.218 6.45	0.208 6.60	0.199 6.74	0.191 6.85	0.183 6.96
2.50	0.252 5.26	0.250 5.52	0.245 5.79	0.237 6.05	0.228 6.28	0.218 6.48	0.209 6.66	0.200 6.81	0.191 6.95	0.183 7.07	0.175 7.19
3.00	0.240 5.42	0.239 5.69	0.234 5.96	0.226 6.22	0.218 6.45	0.209 6.66	0.200 6.84	0.191 7.00	0.183 7.14	0.175 7.27	0.168 7.38
3.50	0.229 5.57	0.228 5.83	0.223 6.10	0.216 6.37	0.208 6.60	0.200 6.81	0.191 7.00	0.183 7.17	0.175 7.31	0.167 7.44	0.160 7.56
4.00	0.219 5.69	0.218 5.95	0.213 6.23	0.207 6.49	0.199 6.74	0.191 6.95	0.183 7.14	0.175 7.31	0.167 7.46	0.160 7.60	0.154 7.72
4.50	0.209 5.80	0.208 6.06	0.204 6.34	0.198 6.61	0.191 6.85	0.183 7.07	0.175 7.27	0.167 7.44	0.160 7.60	0.153 7.73	0.147 7.86
5.00	0.201 5.89	0.199 6.16	0.195 6.44	0.190 6.71	0.183 6.96	0.175 7.18	0.168 7.38	0.160 7.56	0.154 7.72	0.147 7.86	0.141 7.99

SIG = 4.00

Ax\Ay	0.00	0.50	1.00	1.50	2.00	2.50	3.00	3.50	4.00	4.50	5.00
0.00	0.240 4.53	0.238 4.79	0.234 5.06	0.227 5.31	0.219 5.53	0.210 5.73	0.202 5.91	0.193 6.07	0.185 6.20	0.178 6.33	0.171 6.44
0.50	0.238 4.79	0.236 5.05	0.232 5.32	0.225 5.57	0.218 5.79	0.209 6.00	0.201 6.17	0.192 6.33	0.184 6.47	0.177 6.59	0.170 6.70
1.00	0.234 5.06	0.232 5.32	0.228 5.58	0.221 5.84	0.214 6.06	0.205 6.27	0.197 6.45	0.189 6.60	0.181 6.74	0.174 6.87	0.167 6.98
1.50	0.227 5.31	0.225 5.57	0.221 5.84	0.215 6.09	0.208 6.32	0.200 6.53	0.192 6.71	0.184 6.87	0.177 7.01	0.170 7.14	0.163 7.25
2.00	0.219 5.53	0.218 5.79	0.214 6.06	0.208 6.32	0.201 6.55	0.193 6.76	0.186 6.95	0.178 7.12	0.171 7.26	0.164 7.39	0.158 7.51
2.50	0.210 5.73	0.209 6.00	0.205 6.27	0.200 6.53	0.193 6.76	0.186 6.98	0.179 7.17	0.172 7.34	0.165 7.49	0.159 7.62	0.152 7.74
3.00	0.202 5.91	0.201 6.17	0.197 6.45	0.192 6.71	0.186 6.95	0.179 7.17	0.172 7.36	0.165 7.54	0.159 7.69	0.153 7.83	0.147 7.95
3.50	0.193 6.07	0.192 6.33	0.189 6.60	0.184 6.87	0.178 7.12	0.172 7.34	0.165 7.54	0.159 7.71	0.153 7.87	0.147 8.01	0.141 8.14
4.00	0.185 6.20	0.184 6.47	0.181 6.74	0.177 7.01	0.171 7.26	0.165 7.49	0.159 7.69	0.153 7.87	0.147 8.03	0.141 8.18	0.135 8.31
4.50	0.178 6.33	0.177 6.59	0.174 6.87	0.170 7.14	0.164 7.39	0.159 7.62	0.153 7.83	0.147 8.01	0.141 8.18	0.135 8.33	0.130 8.46
5.00	0.171 6.44	0.170 6.70	0.167 6.98	0.163 7.25	0.158 7.51	0.152 7.74	0.147 7.95	0.141 8.14	0.135 8.31	0.130 8.46	0.125 8.60

SIG = 4.50

Ax\Ay	0.00	0.50	1.00	1.50	2.00	2.50	3.00	3.50	4.00	4.50	5.00
0.00	0.199 4.99	0.198 5.25	0.195 5.52	0.190 5.77	0.184 6.01	0.178 6.22	0.171 6.41	0.165 6.58	0.159 6.73	0.153 6.86	0.147 6.98
0.50	0.198 5.25	0.197 5.51	0.194 5.78	0.189 6.03	0.183 6.27	0.177 6.48	0.170 6.67	0.164 6.84	0.158 6.99	0.152 7.13	0.147 7.25
1.00	0.195 5.52	0.194 5.78	0.191 6.04	0.186 6.30	0.180 6.54	0.174 6.75	0.168 6.94	0.162 7.11	0.156 7.27	0.150 7.40	0.145 7.52
1.50	0.190 5.77	0.189 6.03	0.186 6.30	0.182 6.56	0.176 6.80	0.170 7.01	0.164 7.21	0.158 7.38	0.152 7.54	0.147 7.67	0.142 7.80
2.00	0.184 6.01	0.183 6.27	0.180 6.54	0.176 6.80	0.171 7.04	0.166 7.26	0.160 7.46	0.154 7.63	0.148 7.79	0.143 7.93	0.138 8.06
2.50	0.178 6.22	0.177 6.48	0.174 6.75	0.170 7.01	0.166 7.26	0.160 7.48	0.155 7.68	0.149 7.86	0.144 8.02	0.138 8.17	0.133 8.30
3.00	0.171 6.41	0.170 6.67	0.168 6.94	0.164 7.21	0.160 7.46	0.155 7.68	0.149 7.89	0.144 8.07	0.139 8.23	0.134 8.38	0.129 8.52
3.50	0.165 6.58	0.164 6.84	0.162 7.11	0.158 7.38	0.154 7.63	0.149 7.86	0.144 8.07	0.139 8.26	0.134 8.43	0.129 8.58	0.124 8.72
4.00	0.159 6.73	0.158 6.99	0.156 7.27	0.152 7.54	0.148 7.79	0.144 8.02	0.139 8.23	0.134 8.43	0.129 8.60	0.124 8.75	0.120 8.90
4.50	0.153 6.86	0.152 7.13	0.150 7.40	0.147 7.67	0.143 7.93	0.138 8.17	0.134 8.38	0.129 8.58	0.124 8.75	0.120 8.91	0.116 9.06
5.00	0.147 6.98	0.147 7.25	0.145 7.52	0.142 7.80	0.138 8.06	0.133 8.30	0.129 8.52	0.124 8.72	0.120 8.90	0.116 9.06	0.112 9.21

SIG = 5.00

Ax\Ay	0.00	0.50	1.00	1.50	2.00	2.50	3.00	3.50	4.00	4.50	5.00
0.00	0.167 5.46	0.166 5.72	0.164 5.99	0.161 6.25	0.157 6.49	0.152 6.71	0.147 6.91	0.142 7.09	0.137 7.25	0.132 7.40	0.128 7.53
0.50	0.166 5.72	0.166 5.98	0.164 6.25	0.160 6.51	0.156 6.75	0.151 6.97	0.146 7.17	0.141 7.35	0.137 7.51	0.132 7.66	0.127 7.79
1.00	0.164 5.99	0.164 6.25	0.161 6.51	0.158 6.77	0.154 7.02	0.149 7.24	0.145 7.44	0.140 7.62	0.135 7.79	0.130 7.94	0.126 8.07
1.50	0.161 6.25	0.160 6.51	0.158 6.77	0.155 7.04	0.151 7.28	0.147 7.51	0.142 7.71	0.137 7.89	0.133 8.06	0.128 8.21	0.124 8.34
2.00	0.157 6.49	0.156 6.75	0.154 7.02	0.151 7.28	0.147 7.53	0.143 7.76	0.138 7.96	0.134 8.15	0.129 8.32	0.125 8.47	0.121 8.61
2.50	0.152 6.71	0.151 6.97	0.149 7.24	0.147 7.51	0.143 7.76	0.139 7.99	0.134 8.20	0.130 8.38	0.126 8.56	0.122 8.71	0.118 8.85
3.00	0.147 6.91	0.146 7.17	0.145 7.44	0.142 7.71	0.138 7.96	0.134 8.20	0.130 8.41	0.126 8.60	0.122 8.78	0.118 8.94	0.114 9.08
3.50	0.142 7.09	0.141 7.35	0.140 7.62	0.137 7.89	0.134 8.15	0.130 8.38	0.126 8.60	0.122 8.80	0.118 8.98	0.114 9.14	0.110 9.29
4.00	0.137 7.25	0.137 7.51	0.135 7.79	0.133 8.06	0.129 8.32	0.126 8.56	0.122 8.78	0.118 8.98	0.114 9.16	0.110 9.32	0.107 9.48
4.50	0.132 7.40	0.132 7.66	0.130 7.94	0.128 8.21	0.125 8.47	0.122 8.71	0.118 8.94	0.114 9.14	0.110 9.32	0.107 9.49	0.103 9.65
5.00	0.128 7.53	0.127 7.79	0.126 8.07	0.124 8.34	0.121 8.61	0.118 8.85	0.114 9.08	0.110 9.29	0.107 9.48	0.103 9.65	0.100 9.81

Ax = 0.00

SIG\Ay	0.00	0.50	1.00	1.50	2.00	2.50	3.00	3.50	4.00	4.50	5.00
0.00	1.000	0.980	0.928	0.865	0.803	0.746	0.695	0.651	0.612	0.578	0.547
	2.61	2.86	3.09	3.27	3.41	3.52	3.60	3.67	3.73	3.78	3.82
0.50	0.960	0.941	0.892	0.833	0.774	0.719	0.671	0.628	0.590	0.557	0.528
	2.63	2.88	3.11	3.30	3.44	3.55	3.64	3.71	3.77	3.82	3.86
1.00	0.855	0.838	0.798	0.747	0.695	0.647	0.605	0.567	0.533	0.504	0.478
	2.71	2.97	3.21	3.38	3.53	3.65	3.74	3.82	3.88	3.93	3.98
1.50	0.717	0.705	0.673	0.633	0.592	0.553	0.517	0.486	0.458	0.433	0.411
	2.85	3.11	3.34	3.54	3.70	3.82	3.93	4.01	4.08	4.14	4.19
2.00	0.578	0.570	0.547	0.518	0.486	0.457	0.429	0.404	0.382	0.362	0.344
	3.06	3.32	3.56	3.77	3.94	4.08	4.19	4.29	4.37	4.44	4.49
2.50	0.459	0.453	0.438	0.417	0.395	0.373	0.352	0.333	0.315	0.299	0.285
	3.34	3.60	3.85	4.07	4.26	4.41	4.54	4.65	4.75	4.83	4.89
3.00	0.364	0.361	0.351	0.337	0.321	0.305	0.289	0.275	0.261	0.249	0.238
	3.69	3.95	4.21	4.44	4.64	4.81	4.96	5.09	5.20	5.29	5.37
3.50	0.293	0.291	0.284	0.275	0.263	0.252	0.240	0.229	0.219	0.209	0.201
	4.09	4.35	4.62	4.86	5.07	5.26	5.42	5.57	5.69	5.80	5.89
4.00	0.240	0.238	0.234	0.227	0.219	0.210	0.202	0.193	0.185	0.178	0.171
	4.53	4.79	5.06	5.31	5.53	5.73	5.91	6.07	6.20	6.33	6.44
4.50	0.199	0.198	0.195	0.190	0.184	0.178	0.171	0.165	0.159	0.153	0.147
	4.99	5.25	5.52	5.77	6.01	6.22	6.41	6.58	6.73	6.86	6.98
5.00	0.167	0.166	0.164	0.161	0.157	0.152	0.147	0.142	0.137	0.132	0.128
	5.46	5.72	5.99	6.25	6.49	6.71	6.91	7.09	7.25	7.40	7.53

Ax = 0.50

SIG\Ay	0.00	0.50	1.00	1.50	2.00	2.50	3.00	3.50	4.00	4.50	5.00
0.00	0.980	0.960	0.910	0.849	0.788	0.732	0.682	0.639	0.601	0.567	0.537
	2.86	3.11	3.34	3.52	3.66	3.77	3.86	3.93	3.99	4.04	4.08
0.50	0.941	0.923	0.876	0.817	0.759	0.706	0.658	0.617	0.580	0.547	0.519
	2.89	3.14	3.37	3.55	3.69	3.81	3.90	3.97	4.03	4.08	4.12
1.00	0.839	0.824	0.784	0.734	0.683	0.636	0.594	0.557	0.524	0.495	0.470
	2.97	3.22	3.45	3.64	3.79	3.91	4.00	4.08	4.14	4.19	4.24
1.50	0.705	0.693	0.662	0.623	0.582	0.544	0.510	0.479	0.451	0.427	0.405
	3.11	3.36	3.60	3.80	3.96	4.08	4.19	4.27	4.34	4.40	4.45
2.00	0.570	0.561	0.539	0.511	0.480	0.451	0.424	0.399	0.377	0.357	0.339
	3.32	3.57	3.82	4.03	4.20	4.34	4.46	4.55	4.63	4.70	4.76
2.50	0.453	0.448	0.433	0.412	0.390	0.369	0.348	0.329	0.312	0.296	0.282
	3.60	3.86	4.11	4.33	4.52	4.68	4.81	4.92	5.01	5.09	5.16
3.00	0.361	0.357	0.348	0.334	0.318	0.302	0.287	0.273	0.259	0.247	0.236
	3.95	4.21	4.47	4.70	4.90	5.08	5.22	5.35	5.46	5.56	5.64
3.50	0.291	0.289	0.282	0.273	0.261	0.250	0.239	0.228	0.218	0.208	0.199
	4.35	4.61	4.88	5.12	5.34	5.52	5.69	5.83	5.95	6.06	6.16
4.00	0.238	0.236	0.232	0.225	0.218	0.209	0.201	0.192	0.184	0.177	0.170
	4.79	5.05	5.32	5.57	5.79	6.00	6.17	6.33	6.47	6.59	6.70
4.50	0.198	0.197	0.194	0.189	0.183	0.177	0.170	0.164	0.158	0.152	0.147
	5.25	5.51	5.78	6.03	6.27	6.48	6.67	6.84	6.99	7.13	7.25
5.00	0.166	0.166	0.164	0.160	0.156	0.151	0.146	0.141	0.137	0.132	0.127
	5.72	5.98	6.25	6.51	6.75	6.97	7.17	7.35	7.51	7.66	7.79

A_x = 1.00

SIG\A_y	0.00	0.50	1.00	1.50	2.00	2.50	3.00	3.50	4.00	4.50	5.00
0.00	0.928	0.910	0.864	0.806	0.748	0.696	0.648	0.607	0.571	0.539	0.511
	3.09	3.34	3.57	3.75	3.90	4.01	4.10	4.17	4.23	4.28	4.32
0.50	0.893	0.876	0.832	0.777	0.722	0.671	0.626	0.587	0.552	0.521	0.493
	3.11	3.37	3.60	3.78	3.93	4.04	4.14	4.21	4.27	4.32	4.36
1.00	0.798	0.784	0.746	0.699	0.651	0.607	0.567	0.532	0.500	0.473	0.448
	3.20	3.45	3.68	3.88	4.03	4.15	4.25	4.33	4.39	4.44	4.49
1.50	0.673	0.662	0.633	0.596	0.558	0.522	0.488	0.459	0.433	0.409	0.388
	3.34	3.60	3.84	4.04	4.20	4.33	4.44	4.52	4.60	4.66	4.71
2.00	0.547	0.539	0.519	0.491	0.462	0.434	0.408	0.385	0.364	0.345	0.329
	3.56	3.82	4.06	4.28	4.45	4.59	4.71	4.81	4.89	4.97	5.03
2.50	0.438	0.433	0.419	0.399	0.378	0.357	0.338	0.319	0.303	0.288	0.274
	3.85	4.11	4.36	4.59	4.78	4.94	5.07	5.18	5.28	5.36	5.44
3.00	0.351	0.348	0.338	0.325	0.310	0.294	0.280	0.266	0.253	0.241	0.230
	4.21	4.47	4.73	4.96	5.17	5.34	5.49	5.62	5.73	5.83	5.92
3.50	0.284	0.282	0.276	0.267	0.256	0.245	0.234	0.223	0.213	0.204	0.195
	4.62	4.88	5.14	5.39	5.60	5.79	5.96	6.10	6.23	6.34	6.44
4.00	0.234	0.232	0.228	0.221	0.214	0.205	0.197	0.189	0.181	0.174	0.167
	5.06	5.32	5.58	5.84	6.06	6.27	6.45	6.60	6.74	6.87	6.98
4.50	0.195	0.194	0.191	0.186	0.180	0.174	0.168	0.162	0.156	0.150	0.145
	5.52	5.78	6.04	6.30	6.54	6.75	6.94	7.11	7.27	7.40	7.52
5.00	0.164	0.164	0.161	0.158	0.154	0.149	0.145	0.140	0.135	0.130	0.126
	5.99	6.25	6.51	6.77	7.02	7.24	7.44	7.62	7.79	7.94	8.07

Δx = 1.50

SIG\Δy	0.00	0.50	1.00	1.50	2.00	2.50	3.00	3.50	4.00	4.50	5.00
0.00	0.865	0.849	0.806	0.752	0.699	0.650	0.606	0.567	0.533	0.503	0.476
	3.27	3.52	3.75	3.94	4.09	4.21	4.30	4.37	4.43	4.49	4.53
0.50	0.833	0.817	0.777	0.726	0.675	0.628	0.586	0.548	0.516	0.487	0.461
	3.30	3.55	3.78	3.97	4.12	4.24	4.34	4.41	4.48	4.53	4.57
1.00	0.747	0.734	0.699	0.655	0.611	0.569	0.532	0.499	0.469	0.443	0.420
	3.38	3.64	3.88	4.07	4.23	4.35	4.45	4.53	4.60	4.66	4.70
1.50	0.633	0.623	0.596	0.562	0.526	0.492	0.461	0.433	0.408	0.386	0.366
	3.54	3.80	4.04	4.24	4.41	4.54	4.65	4.74	4.82	4.88	4.93
2.00	0.518	0.511	0.491	0.466	0.438	0.412	0.388	0.365	0.345	0.327	0.311
	3.77	4.03	4.28	4.49	4.67	4.82	4.94	5.04	5.13	5.20	5.27
2.50	0.417	0.412	0.399	0.381	0.361	0.342	0.323	0.306	0.290	0.275	0.262
	4.07	4.33	4.59	4.82	5.01	5.17	5.31	5.43	5.53	5.61	5.69
3.00	0.337	0.334	0.325	0.312	0.298	0.283	0.269	0.256	0.244	0.233	0.222
	4.44	4.70	4.96	5.20	5.41	5.59	5.75	5.88	5.99	6.09	6.18
3.50	0.275	0.273	0.267	0.258	0.248	0.237	0.226	0.216	0.207	0.198	0.190
	4.86	5.12	5.39	5.63	5.85	6.05	6.22	6.37	6.49	6.61	6.71
4.00	0.227	0.225	0.221	0.215	0.208	0.200	0.192	0.184	0.177	0.170	0.163
	5.31	5.57	5.84	6.09	6.32	6.53	6.71	6.87	7.01	7.14	7.25
4.50	0.190	0.189	0.186	0.182	0.176	0.170	0.164	0.158	0.152	0.147	0.142
	5.77	6.03	6.30	6.56	6.80	7.01	7.21	7.38	7.54	7.67	7.80
5.00	0.161	0.160	0.158	0.155	0.151	0.147	0.142	0.137	0.133	0.128	0.124
	6.25	6.51	6.77	7.04	7.28	7.51	7.71	7.89	8.06	8.21	8.34

Ax = 2.00

SIG\Ay	0.00	0.50	1.00	1.50	2.00	2.50	3.00	3.50	4.00	4.50	5.00
0.00	0.803	0.788	0.748	0.699	0.649	0.604	0.563	0.526	0.495	0.467	0.442
	3.41	3.66	3.90	4.09	4.24	4.36	4.46	4.53	4.60	4.65	4.69
0.50	0.774	0.759	0.722	0.675	0.628	0.584	0.544	0.510	0.479	0.452	0.428
	3.44	3.69	3.93	4.12	4.28	4.40	4.50	4.57	4.64	4.69	4.74
1.00	0.695	0.683	0.651	0.611	0.570	0.531	0.496	0.465	0.437	0.413	0.391
	3.53	3.79	4.03	4.23	4.39	4.52	4.62	4.70	4.77	4.83	4.88
1.50	0.592	0.582	0.558	0.526	0.492	0.460	0.431	0.405	0.382	0.361	0.343
	3.70	3.96	4.20	4.41	4.58	4.72	4.83	4.92	5.00	5.07	5.12
2.00	0.486	0.480	0.462	0.438	0.413	0.388	0.365	0.344	0.325	0.308	0.293
	3.94	4.20	4.45	4.67	4.85	5.01	5.13	5.24	5.33	5.41	5.47
2.50	0.395	0.390	0.378	0.361	0.343	0.324	0.306	0.290	0.275	0.262	0.249
	4.26	4.52	4.78	5.01	5.21	5.38	5.52	5.64	5.75	5.84	5.91
3.00	0.321	0.318	0.310	0.298	0.285	0.271	0.257	0.245	0.233	0.223	0.213
	4.64	4.90	5.17	5.41	5.62	5.81	5.97	6.10	6.22	6.33	6.42
3.50	0.263	0.261	0.256	0.248	0.238	0.229	0.218	0.208	0.199	0.191	0.183
	5.07	5.34	5.60	5.85	6.08	6.29	6.45	6.60	6.74	6.85	6.96
4.00	0.219	0.218	0.214	0.208	0.201	0.193	0.186	0.178	0.171	0.164	0.158
	5.53	5.79	6.06	6.32	6.55	6.76	6.95	7.12	7.26	7.39	7.51
4.50	0.184	0.183	0.180	0.176	0.171	0.166	0.160	0.154	0.148	0.143	0.138
	6.01	6.27	6.54	6.80	7.04	7.26	7.46	7.63	7.79	7.92	8.06
5.00	0.157	0.156	0.154	0.151	0.147	0.143	0.138	0.134	0.129	0.125	0.121
	6.49	6.75	7.02	7.29	7.53	7.76	7.96	8.15	8.32	8.47	8.61

Ax = 2.50

SIG\Ay	0.00	0.50	1.00	1.50	2.00	2.50	3.00	3.50	4.00	4.50	5.00
0.00	0.746	0.732	0.696	0.650	0.604	0.561	0.523	0.489	0.459	0.433	0.409
	3.52	3.77	4.01	4.21	4.36	4.48	4.58	4.66	4.73	4.78	4.83
0.50	0.719	0.706	0.671	0.628	0.584	0.543	0.506	0.473	0.445	0.419	0.397
	3.55	3.81	4.04	4.24	4.40	4.52	4.62	4.70	4.77	4.83	4.88
1.00	0.647	0.636	0.607	0.569	0.531	0.495	0.462	0.433	0.407	0.384	0.364
	3.65	3.91	4.15	4.35	4.52	4.65	4.75	4.84	4.91	4.97	5.03
.50	0.553	0.544	0.522	0.492	0.460	0.431	0.403	0.378	0.357	0.338	0.320
	3.82	4.08	4.33	4.54	4.72	4.86	4.98	5.07	5.15	5.22	5.28
2.00	0.457	0.451	0.434	0.412	0.388	0.365	0.344	0.324	0.306	0.290	0.275
	4.08	4.34	4.59	4.82	5.01	5.16	5.29	5.40	5.50	5.58	5.65
2.50	0.373	0.369	0.357	0.342	0.324	0.307	0.290	0.275	0.260	0.248	0.236
	4.41	4.68	4.94	5.17	5.38	5.55	5.70	5.82	5.93	6.03	6.11
3.00	0.305	0.302	0.294	0.283	0.271	0.258	0.245	0.233	0.222	0.212	0.203
	4.81	5.08	5.34	5.59	5.81	6.00	6.16	6.30	6.43	6.54	6.63
3.50	0.252	0.250	0.245	0.237	0.229	0.218	0.209	0.200	0.191	0.183	0.175
	5.26	5.52	5.79	6.05	6.28	6.48	6.66	6.81	6.95	7.07	7.18
4.00	0.210	0.209	0.205	0.200	0.193	0.186	0.179	0.172	0.165	0.159	0.152
	5.73	6.00	6.27	6.53	6.76	6.98	7.17	7.34	7.49	7.62	7.74
4.50	0.178	0.177	0.174	0.170	0.166	0.160	0.155	0.149	0.144	0.138	0.133
	6.22	6.48	6.75	7.01	7.26	7.48	7.68	7.86	8.02	8.17	8.30
5.00	0.152	0.151	0.149	0.147	0.143	0.139	0.134	0.130	0.126	0.122	0.118
	6.71	6.97	7.24	7.51	7.76	7.99	8.20	8.38	8.56	8.71	8.85

Ax = 3.00

SIG\Ay	0.00	0.50	1.00	1.50	2.00	2.50	3.00	3.50	4.00	4.50	5.00
0.00	0.695	0.682	0.648	0.606	0.563	0.523	0.487	0.455	0.427	0.402	0.380
	3.80	3.86	4.10	4.30	4.46	4.58	4.68	4.76	4.83	4.89	4.94
0.50	0.671	0.658	0.626	0.586	0.544	0.506	0.472	0.441	0.414	0.390	0.369
	3.64	3.90	4.14	4.34	4.50	4.62	4.73	4.81	4.88	4.94	4.99
1.00	0.605	0.594	0.567	0.532	0.496	0.462	0.431	0.404	0.380	0.358	0.339
	3.74	4.00	4.25	4.45	4.62	4.75	4.86	4.95	5.03	5.09	5.14
1.50	0.517	0.510	0.488	0.461	0.431	0.403	0.378	0.355	0.334	0.316	0.299
	3.93	4.19	4.44	4.65	4.83	4.98	5.10	5.20	5.28	5.35	5.41
2.00	0.429	0.424	0.408	0.388	0.365	0.344	0.323	0.305	0.288	0.273	0.259
	4.19	4.46	4.71	4.94	5.13	5.29	5.43	5.54	5.64	5.72	5.80
2.50	0.352	0.348	0.338	0.323	0.306	0.290	0.274	0.260	0.246	0.234	0.223
	4.54	4.81	5.07	5.31	5.52	5.70	5.85	5.98	6.09	6.19	6.28
3.00	0.289	0.287	0.280	0.269	0.257	0.245	0.233	0.222	0.212	0.202	0.193
	4.96	5.22	5.49	5.75	5.97	6.16	6.33	6.48	6.60	6.72	6.82
3.50	0.240	0.239	0.234	0.226	0.218	0.209	0.200	0.191	0.183	0.175	0.168
	5.42	5.69	5.96	6.22	6.45	6.66	6.84	7.00	7.14	7.27	7.38
4.00	0.202	0.201	0.197	0.192	0.186	0.179	0.172	0.165	0.159	0.153	0.147
	5.91	6.17	6.45	6.71	6.95	7.17	7.36	7.54	7.69	7.83	7.95
4.50	0.171	0.170	0.168	0.164	0.160	0.155	0.149	0.144	0.139	0.134	0.129
	6.41	6.67	6.94	7.21	7.46	7.68	7.89	8.07	8.23	8.38	8.52
5.00	0.147	0.146	0.145	0.142	0.138	0.134	0.130	0.126	0.122	0.118	0.114
	6.91	7.17	7.44	7.71	7.96	8.20	8.41	8.60	8.78	8.94	9.08

Ax = 3.50

SIG\Ay	0.00	0.50	1.00	1.50	2.00	2.50	3.00	3.50	4.00	4.50	5.00
0.00	0.651	0.639	0.607	0.567	0.526	0.489	0.455	0.425	0.399	0.375	0.355
	3.67	3.83	4.17	4.37	4.53	4.66	4.76	4.85	4.92	4.97	5.02
0.50	0.629	0.617	0.587	0.548	0.510	0.473	0.441	0.412	0.387	0.364	0.344
	3.71	3.97	4.21	4.41	4.57	4.70	4.81	4.90	4.97	5.03	5.08
1.00	0.567	0.557	0.532	0.499	0.465	0.433	0.404	0.378	0.355	0.335	0.317
	3.82	4.08	4.33	4.53	4.70	4.84	4.95	5.04	5.12	5.19	5.24
1.50	0.486	0.479	0.459	0.433	0.405	0.379	0.355	0.333	0.314	0.296	0.281
	4.01	4.27	4.52	4.74	4.92	5.07	5.20	5.30	5.39	5.46	5.52
2.00	0.404	0.399	0.385	0.365	0.344	0.324	0.305	0.287	0.271	0.257	0.244
	4.29	4.55	4.81	5.04	5.24	5.40	5.54	5.66	5.76	5.85	5.92
2.50	0.333	0.329	0.319	0.306	0.290	0.275	0.260	0.246	0.233	0.222	0.211
	4.65	4.92	5.18	5.43	5.64	5.82	5.98	6.11	6.23	6.33	6.42
3.00	0.275	0.273	0.266	0.256	0.245	0.233	0.222	0.211	0.201	0.192	0.184
	5.09	5.35	5.62	5.88	6.10	6.30	6.48	6.63	6.76	6.88	6.98
3.50	0.229	0.228	0.223	0.216	0.208	0.200	0.191	0.183	0.175	0.167	0.160
	5.57	5.83	6.10	6.37	6.60	6.81	7.00	7.17	7.31	7.44	7.56
4.00	0.193	0.192	0.189	0.184	0.178	0.172	0.165	0.159	0.153	0.147	0.141
	6.07	6.33	6.60	6.87	7.12	7.34	7.54	7.71	7.87	8.01	8.14
4.50	0.165	0.164	0.162	0.158	0.154	0.149	0.144	0.139	0.134	0.129	0.124
	6.59	6.84	7.11	7.38	7.63	7.86	8.07	8.26	8.43	8.58	8.72
5.00	0.142	0.141	0.140	0.137	0.134	0.130	0.126	0.122	0.118	0.114	0.110
	7.09	7.35	7.62	7.89	8.15	8.38	8.60	8.80	8.98	9.14	9.29

Ax = 4.00

SIG\Ay	0.00	0.50	1.00	1.50	2.00	2.50	3.00	3.50	4.00	4.50	5.00
0.00	0.612	0.601	0.571	0.533	0.495	0.459	0.427	0.399	0.374	0.352	0.332
	3.73	3.99	4.23	4.43	4.60	4.73	4.82	4.92	4.99	5.05	5.10
0.50	0.590	0.580	0.552	0.516	0.479	0.445	0.414	0.387	0.363	0.341	0.323
	3.77	4.03	4.27	4.48	4.64	4.77	4.88	4.97	5.04	5.10	5.15
1.00	0.533	0.524	0.500	0.469	0.437	0.407	0.380	0.355	0.333	0.314	0.297
	3.88	4.14	4.39	4.60	4.77	4.91	5.03	5.12	5.20	5.27	5.32
1.50	0.458	0.451	0.433	0.408	0.382	0.357	0.334	0.314	0.295	0.278	0.264
	4.08	4.34	4.60	4.82	5.00	5.15	5.28	5.38	5.47	5.55	5.62
2.00	0.382	0.377	0.364	0.345	0.325	0.306	0.288	0.271	0.256	0.242	0.230
	4.37	4.63	4.89	5.13	5.33	5.50	5.64	5.76	5.86	5.95	6.03
2.50	0.315	0.312	0.303	0.290	0.275	0.260	0.246	0.233	0.221	0.210	0.200
	4.75	5.01	5.28	5.53	5.75	5.93	6.09	6.23	6.35	6.46	6.55
3.00	0.261	0.259	0.253	0.244	0.233	0.222	0.212	0.201	0.192	0.183	0.175
	5.20	5.46	5.73	5.99	6.22	6.43	6.60	6.76	6.90	7.02	7.12
3.50	0.219	0.218	0.213	0.207	0.199	0.191	0.183	0.175	0.167	0.160	0.154
	5.69	5.95	6.23	6.49	6.74	6.95	7.14	7.31	7.46	7.60	7.72
4.00	0.185	0.184	0.181	0.177	0.171	0.165	0.159	0.153	0.147	0.141	0.135
	6.20	6.47	6.74	7.01	7.26	7.49	7.69	7.87	8.03	8.18	8.31
4.50	0.159	0.158	0.156	0.152	0.148	0.144	0.139	0.134	0.129	0.124	0.120
	6.72	6.99	7.27	7.54	7.79	8.02	8.23	8.43	8.60	8.75	8.90
5.00	0.137	0.137	0.135	0.133	0.129	0.126	0.122	0.118	0.114	0.110	0.107
	7.25	7.51	7.79	8.06	8.32	8.56	8.78	8.98	9.16	9.32	9.48

Ax = 4.50

SIG\Ay	0.00	0.50	1.00	1.50	2.00	2.50	3.00	3.50	4.00	4.50	5.00
0.00	0.578	0.567	0.539	0.503	0.467	0.433	0.402	0.375	0.352	0.331	0.312
	3.78	4.04	4.28	4.49	4.65	4.79	4.89	4.97	5.05	5.11	5.16
0.50	0.557	0.547	0.521	0.487	0.452	0.419	0.390	0.364	0.341	0.321	0.303
	3.82	4.08	4.32	4.53	4.69	4.83	4.94	5.03	5.10	5.16	5.22
1.00	0.504	0.495	0.473	0.443	0.413	0.384	0.358	0.335	0.314	0.296	0.280
	3.93	4.19	4.44	4.66	4.83	4.97	5.09	5.19	5.27	5.33	5.39
1.50	0.433	0.427	0.409	0.386	0.361	0.338	0.316	0.296	0.278	0.263	0.249
	4.14	4.40	4.66	4.88	5.07	5.22	5.35	5.46	5.55	5.63	5.70
2.00	0.382	0.357	0.345	0.327	0.308	0.290	0.273	0.257	0.242	0.229	0.218
	4.44	4.70	4.97	5.20	5.41	5.58	5.72	5.85	5.95	6.05	6.13
2.50	0.299	0.296	0.288	0.275	0.262	0.248	0.234	0.222	0.210	0.200	0.190
	4.82	5.09	5.36	5.61	5.84	6.03	6.19	6.33	6.46	6.57	6.66
3.00	0.249	0.247	0.241	0.233	0.223	0.212	0.202	0.192	0.183	0.175	0.167
	5.29	5.56	5.83	6.09	6.33	6.54	6.72	6.88	7.02	7.14	7.25
3.50	0.209	0.208	0.204	0.198	0.191	0.183	0.175	0.167	0.160	0.153	0.147
	5.80	6.06	6.34	6.61	6.85	7.07	7.27	7.44	7.60	7.73	7.86
4.00	0.178	0.177	0.174	0.170	0.164	0.159	0.153	0.147	0.141	0.135	0.130
	6.33	6.59	6.87	7.14	7.39	7.62	7.83	8.01	8.18	8.33	8.46
4.50	0.153	0.152	0.150	0.147	0.143	0.138	0.134	0.129	0.124	0.120	0.116
	6.86	7.13	7.40	7.67	7.93	8.17	8.38	8.58	8.75	8.91	9.06
5.00	0.132	0.132	0.130	0.128	0.125	0.122	0.118	0.114	0.110	0.107	0.103
	7.40	7.66	7.94	8.21	8.47	8.71	8.94	9.14	9.32	9.49	9.65

Ax = 5.00

SIG\Ay	0.00	0.50	1.00	1.50	2.00	2.50	3.00	3.50	4.00	4.50	5.00
0.00	0.547	0.537	0.511	0.476	0.442	0.409	0.380	0.355	0.332	0.312	0.294
	3.82	4.08	4.32	4.53	4.69	4.83	4.94	5.02	5.10	5.16	5.21
0.50	0.528	0.519	0.493	0.461	0.428	0.397	0.369	0.344	0.323	0.303	0.286
	3.86	4.12	4.36	4.57	4.74	4.88	4.99	5.08	5.15	5.22	5.27
1.00	0.478	0.470	0.448	0.420	0.391	0.364	0.339	0.317	0.297	0.280	0.264
	3.98	4.24	4.49	4.70	4.88	5.03	5.14	5.24	5.32	5.39	5.45
1.50	0.411	0.405	0.388	0.366	0.343	0.320	0.299	0.281	0.264	0.249	0.235
	4.19	4.45	4.71	4.93	5.12	5.29	5.41	5.52	5.62	5.70	5.76
2.00	0.344	0.339	0.328	0.311	0.293	0.275	0.259	0.244	0.230	0.218	0.206
	4.49	4.76	5.03	5.27	5.47	5.65	5.80	5.92	6.03	6.13	6.21
2.50	0.285	0.282	0.274	0.262	0.249	0.236	0.223	0.211	0.200	0.190	0.181
	4.89	5.16	5.44	5.69	5.91	6.11	6.28	6.42	6.55	6.66	6.76
3.00	0.238	0.236	0.230	0.222	0.213	0.203	0.193	0.184	0.175	0.167	0.159
	5.37	5.64	5.92	6.18	6.42	6.63	6.82	6.98	7.12	7.25	7.37
3.50	0.201	0.199	0.195	0.190	0.183	0.175	0.168	0.160	0.154	0.147	0.141
	5.89	6.16	6.44	6.71	6.96	7.18	7.38	7.56	7.72	7.86	7.99
4.00	0.171	0.170	0.167	0.163	0.158	0.152	0.147	0.141	0.135	0.130	0.125
	6.44	6.70	6.98	7.25	7.51	7.74	7.95	8.14	8.31	8.46	8.60
4.50	0.147	0.147	0.145	0.142	0.138	0.133	0.129	0.124	0.120	0.116	0.112
	6.98	7.25	7.52	7.80	8.06	8.30	8.52	8.72	8.90	9.06	9.21
5.00	0.128	0.127	0.126	0.124	0.121	0.118	0.114	0.110	0.107	0.103	0.100
	7.53	7.79	8.07	8.34	8.61	8.85	9.08	9.29	9.48	9.65	9.81

Submitted to
Applied Physics B

HEPL 952
April 1984

CHARACTERIZATION OF FREE-ELECTRON LASER BUNCH-LENGTHENING ON THE ACO STORAGE-RING*

Kem Edward Robinson, David A. G. Deacon[a], John M. J. Madey,
Michel F. Velghe[b]

High Energy Physics Laboratory
Stanford University, Stanford, California 94305

and

C. Bazin, M. Bergher, M. Billardon[c], P. Elleaume[d], J. M. Ortega[c],
and Y. Petroff

Laboratoire pour l'Utilisation du Rayonment Electromagnetique
Université de Paris-Sud, F-91405 Orsay Cedex, France

*Work supported in part by AFOSR under contract F 49620-80-C-0068, the DGRST under contract 79-7-0163, and the DRET under contract 9-073 and 81-131.

[a] *Permanent address:* Deacon Research, 754 Duncardine Way, Sunnyvale, CA 84087

[b] *Permanent address:* Laboratoire de Photophysique Moléculaire, Bâtiment 213, Université de Paris-Sud, 91405, Orsay, France.

[c] *Permanent address*: Ecole Supérieure de Physique et Chimie, 10 rue Vauquelin, 75231 Paris Cedex 05, France.

[d] *Permanent address*: Départment de Physico-Chimie, Service de Photophysique, Centre D'Etudes Nucléaire Saclay, Gif-sur-Yvette, France.

ABSTRACT

This paper summarizes the basic low-current laser-induced bunch-lengthening measurements that have been made on the ACO Storage-Ring Free-Electron Laser (SRFEL). The measurements provide verification of both the functional dependence and absolute magnitude of SRFEL theoretical models. The method of measurement, which is is explained, exploits frequency-domain techniques and is capable of accuracies comparable to those of a streak camara. The measurements are in good agreement with existing SRFEL theory and provide an important base for future work.

PACS: 42.55T, 29.20, 41.80D

INTRODUCTION

Operation of a free-electron laser as part of a storage ring [SRFEL] will cause an increase in the nominal energy spread of the electron bunch if the optical phase of the electrons is uncorrelated from pass to pass. This increase in energy spread results in an enlargement of the bunch length. The increased bunch length and energy spread cause a reduction in gain and can lead to the saturation of the SRFEL for low gain systems. As part of the LURE/Stanford ACO-SRFEL project this FEL-induced bunch lengthening was measured for the first time on the superconducting undulator mounted on ACO in 1981 [1,2]. In order to measure this FEL-induced bunch lengthening, we have developed a frequency-domain technique which measures induced bunch-length changes to 1 part in 10^3 and absolute bunch lengths to a precision of 1% as established by data taken on stored electron beams.

In this paper we present an outline of the measurement theory, experimental technique, and a complete description of the basic, low-current results of the laser-induced bunch lengthening obtained on ACO. We present results which provide a graphic demonstration of the scaling of FEL interaction, of the storage ring scaling, and absolute magnitude of the FEL-induced bunch lengthening as a function of laser intensity. An appendix is also included which summarizes the techniques used for measuring the storage ring parameters necessary to compare the data with theory.

At high currents on ACO electron beam interactions with the environment cause anomalous bunch lengthening [3]. This causes strong nonlinear, anomalous coupling with the FEL altering both the quantitative and qualitative heating effects. The nature and scaling of the FEL interaction at high currents on ACO, which is indicative of fine structure on the electron beam, have been reported elsewhere [4–7]. We will restrict this paper to those results which apply to the verification of existing SRFEL theory.

Measurement Theory and Procedure

All measurements presented in this paper were made while operating the SRFEL as an amplifier to an external laser. This is the same configuration used for the gain measurments [8,9]. Figure 1 is a schematic diagram of the ACO-SRFEL and external laser. An argon-ion laser, D, is aligned coaxial to the electron beam in the undulator through a mode matching telescope and optical transport system, E. Synchrotron light from a bending magnet, F, is then detected on a fast photodiode. The bending magnet chosen was to prevent any spurious light from the laser or undulator from reaching the photodiode.

Figure 2 is a schematic of the electronic-detection system used for the bunch-lengthening measurements. The synchrotron light, focused by cylindrical mirrors, is detected by a fast photodiode (B &H OC3002LN, or ITL3181) and sent via a low dispersion cable (RG 331) to an RF-spectrum analyzer (AILTECH Model 757) which is interfaced directly with a computer. The interface between the spectrum analyzer and the computer is used for the aquistion of global spectra. When monitoring the bunch length changes, the analyzer is operated as a phase-locked receiver tuned to a harmonic of the orbit frequency. The analyzer output can either be input to a lock-in amplifier for synchronous detection at the frequency of the laser chopper, or time averaged measurements can be made using an averaging digital oscilloscope. In all cases the detected signal is recorded on the data aquisition system together with the storage ring parameters including the RF voltage, the storage ring current, and the output power of the external laser.

After injection of ACO is completed the undulator is closed and the magnetic optics of the machine are compensated for the focusing induced by the undulator. ACO is operated at the coupling resonance of the betatron tunes. This assures nearly round beams for facilitating interpretation of the filling factors. Corrector coils are used to change the orbit from the nominal, injection orbit to one which is centered in the undulator as established by imaging the electrons in the undulator.

With the electron optics of the machine established through the undulator, the laser is aligned onto the electron beam. After optimization of the magnetic field and laser alignment, bunch lengthening data are taken.

Since the cumulative effect of the additional FEL-induced energy spread is the principal concern, the description of the electrons in the storage ring can be restricted to the synchrotron motion, including synchrotron oscillation and damping, in the longitudinal dimension. Several works exist which give a complete description of storage ring theory [10–12]. In linearized form the equation for synchrotron motion has the form of a damped harmonic-oscillator driven by a noise source [10]:

$$\frac{d^2\varsigma}{dt^2} + \frac{2}{\tau_e}\frac{d\varsigma}{dt} + \Omega^2\varsigma = \delta\epsilon_q + \delta\epsilon_{fel}. \tag{1}$$

In this equation ς is the longitudinal phase of the electron measured with respect to the *synchronous* or *design* electron in units of the orbit period T_o. The incoherent energy damping time is τ_e , and Ω is the angular synchrotron frequency of the electrons. The two terms on the right-hand side of Eqn. (1) are the driving terms arising from fluctuations as a result of the discrete nature of the synchrotron radiaton $\delta\epsilon_q$ [10], and the interaction of the electrons with the optical field in the FEL, $\delta\epsilon_{fel}$ [13]. Under idealized conditions, the quantum fluctuations give rise to steady-state Gaussian electron distributions in energy σ_ϵ and phase σ_ς [10]. The scaling factor between the two distributions is the ratio of the momentum-compaction factor and the angular synchrotron frequency

$$\sigma_\varsigma^2 = \frac{\alpha^2}{\Omega^2}\sigma_\epsilon^2. \tag{2}$$

The first-order interaction between the electrons and the optical field $\delta\epsilon_{fel}$ in Eqn. (1) causes an increase of the nominal energy spread. In storage rings, since the electrons are recirculated, the first-order damping of this increased energy spread will occur from the normal synchrotron damping of the storage ring. (There is a

possible FEL-induced damping but it is of higher order and becomes important only at optical intensities much greater than those accessible on ACO [14-16].)

Generally the optical phase of an electron in a SRFEL will be uncorrelated from pass to pass in the undulator. This will be true unless deliberate action is taken in the design of the storage ring as is the case with the isochronous-storage-ring [17]. Because of the uncorrelated contributions, the FEL interaction will behave as an additional stochastic noise term in Eqn. (1). Its contribution will be scaled by the energy damping time of the ring [1]. In the small-signal case the Central-Limit Theorem [18] provides the value of the expected increase in the steady-state energy spread in the presence of the FEL:

$$\sigma_\epsilon^2 = {\sigma_{\epsilon_o}}^2 + \frac{4\tau_\epsilon}{T_o}\langle(\delta\epsilon_{fel})^2\rangle_\psi. \tag{3}$$

Here, σ_{ϵ_o} is the nominal relative energy spread of the storage ring resulting from quantum fluctuations [10]. The optical phase of the electrons ψ is averaged over to obtain the second moment of the FEL interaction $\langle(\delta\epsilon_{fel})^2\rangle_\psi$. At higher power levels, where the FEL term in Eqn. (1) is comparable to σ_{ϵ_o}, the small-signal case is no longer valid. Under these circumstances the energy dependence of the FEL-induced spread must be taken into account as Renieri and others have done for the idealized SRFEL operating as an amplifier and oscillator [13,15,19-21].

A major consequence from the accumulated energy spread is the mechanism of gain saturation of the SRFEL for low-gain systems [6]. The gain may be depressed and saturate in one of two processes: (1) the increased energy spread of the electrons fills the energy acceptance of the undulator reducing the number of gain contributing particles, or (2) the increased energy spread will increase the bunch length, and thereby decreases the charge density and the gain which is proportional to the charge density. Both of these mechanisms are central to the operation of SRFEL's, and underscore the importance of the bunch-heating phenomena [22].

The synchrotron radiation from a normal bending magnent in storage ring is generally assumed to have no coherent or interference effects present [23]. The

bending magnet may be considered as an isolated element of the system, and the electron phases are uncorrelated [24]. Since the emitted radiation is incoherent, the number of photons emitted through a given solid angle of the bending magnent is proportional to the number of electrons. Equivalently, the instantaneous intensity of the synchrotron radiation $I_s(t)$ is proportional to the charge density $\rho(t)$:

$$I_s(t) \propto \rho(t). \tag{4}$$

The time dependence of the synchrotron radiation is characterized by a series of pulses separated by a time T_o/k, where T_o is the orbit period of the storage ring (73.4 nanoseconds on ACO) and k is the number of bunches stored in the ring. The pulses will have a temporal length σ_τ which corresponds to the longitudinal length of the electron pulse. One way of measuring the length of the electron bunch is to simply measure the length of the optical pulse $I_s(t)$ emitted by the electrons. However, in practice unless a streak camara is used, this technique is incapable of providing the precision required for adequate bunch length and induced bunch-lengthening measurements.

In order to obtain the precision needed for measurement we adopted a frequency-domain technique which measures the shape of the Fourier transform of $I_s(t)$. The Fourier transform of the charge density and the synchrotron radiation intensity are also proportional:

$$\tilde{I}_s(\omega) \propto \tilde{\rho}(\omega), \tag{5}$$

If a detector is placed in the synchrotron radiation from the bending magnet the signal recorded $f(t)$ will be proportional to the convolution of the detector time response to a delta function and the detected signal: $f(t) \propto p(t) \otimes I_s(t)$. In order to measure the pulse (bunch) length the response of the the detector must be deconvolved from the recorded signal. This is relatively simple if the signal and detector response are Gaussian, but in practice detector response is rarely Gaussian

[7]. In the frequency domain the temporal convolution becomes a product and $\tilde{I}_s(\omega)$ can be obtained quickly from $F(\omega)$ by dividing out the detector response $P(\omega)$.

If $I_s(t)$ is modeled the inverse bunch length can be estimated by fitting the compensated spectrum $F(\omega)/P(\omega)$ to the apropriate envelope. Under idealized conditions the longitudinal electron distribution will be Gaussian [10], so that the transform envelope is also Gaussian. Figure 3 is the uncompensated signal $\log F(\omega)$ from an actual electron beam stored in ACO. The spectrum was taken during a typical synchrotron radiation run with moderately high current. The electron energy was 536 MeV and the RF accelerating voltage was 17.5 kV. After compensation for the photodiode response, the fit to a Gaussian envelope gives an electron bunch-length of $\sigma_\tau = 665\,\text{psec} \pm 1.4\%$. The mean-squared correlation of the fit $R^2 > 0.992$ which gives a confidence factor in the Gaussian fit very near 100%. At lower currents, such as those used for zero-current bunch-lengthening measurements at 240 MeV, the typical bunch length measured is $\sim$200 psec with an uncertainty of $\sim 2\%$ and a mean-squared correlation $R^2 > 0.98$. This is in good agreement with the theoretical previsions for ACO [25].

For FEL-induced bunch lengthening the fractional bunch-length change is the principal quantity of interest. The method of measurement is simplier for induced changes than that used for measuring absolute bunch lengths. If the induced bunch-length changes are relatively small, or maintain their functional form, scaling relations from Fourier tranform analysis require that the product of the second moments remain constant because the total area under the pulse remains constant [26]. For the storage ring this is applicable since the total charge of the electron bunch is conserved. This invariance remains valid even under more general pulse modifications as a special case of Parseval's theorem, and is related to the bandwidth theorem and Schwartz's inequality [26]. If a single harmonic of the comb spectrum of $F(\omega)$ is examined the change in the amplitude will be inversely proportional to the bunch-length change. On ACO, where the direct measurements of the bunch length have shown that the electron distribution is essentially Gaussian, a change

from σ_{t_i} to σ_{t_f} results in a change of $F(\omega)$ of

$$\ln\left(\frac{F_f(\omega)}{F_i(\omega)}\right) = \frac{-\omega^2 \Delta\sigma_\tau^2}{2}, \tag{6}$$

where $\Delta\sigma_\tau^2 \equiv \sigma_{t_f}^2 - \sigma_{t_i}^2$. The change in the signal amplitude, induced by a change in the bunch length, scales as the square of the frequency at which the measurement is made. It is important to note that measurement of the fractional bunch-length change is independent of the response of the detector system.

Figure 4 is a plot of the detected bunch-lengthening signal from ACO as a function of the detection harmonic during a single bunch-lengthening measurement. The least-squares-fit parabola shows clearly that for harmonics as high as $100\omega_o$ the low current bunch on ACO remains Gaussian. This justifies the use of the Gaussian model for the electron bunch. The error bars are calculated directly from the fluctuations on the measurement and represent $\pm 1\sigma$. Since the fluctuations of the electron bunch length are the source of the uncertainty the signal-to-noise should remain essentially constant as long as the noise levels of the detection system are not significant. Measurements at higher harmonics are dominated by the decreasing, continuous-carrier harmonic level. The noise level of the detection system begins to dominate at extremely high harmonics for which the carrier amplitude is too small. This effectively imposes a limit assuring that measurements on ACO will be performed in the frequency regime where the electron RF spectrum is Gaussian. The data of Figure 4 were taken using synchronous detection.

Combining Eqns. (2), (3), and (6) the induced fractional bunch-length change $\Delta\sigma_\tau^2$ may be directly related to the theoretical predictions for free-electron-laser bunch lengthening:

$$\Delta\sigma_\tau^2 = \frac{\alpha^2 \tau_e}{4 T_o \Omega^2} \langle (\delta\epsilon_{fel})^2 \rangle_\psi. \tag{7}$$

This permits direct verification of FEL bunch-heating models without recourse to the absolute bunch length which must be compensated for the dectector response.

The sensitivity and precision achievable by the frequency-domain measurements is superior to that achievable with the available temporal methods. The detection system response is largely eliminated, or is easily compensated, for even non-Gaussian-response systems. Rapid oscillations of the electron bunch results only in sidebands at the carrier harmonics which can easily be eliminated. The frequency-domain technique is applicable to situations where disimilar multiple bunches are present in the storage ring [7]. Additionally, the bunch lengthening can be monitored continously for time-dependent response [6]. While streak cameras have comparable resolution, precise absolute measurements require multiple corrections for electron transit-time spread and film density. No such corrections are required in our frequency domain measurements in which transit-time spread in the photodiode has no effect on the detected signal.

Basic Experimental Results

The measurements presented in this paper were made with the NOEL permanent-magnet undulator and optical klystron mounted on ACO [27]. They were also made at total average currents of less than 1 mA. This current level is dictated by the thresholds of anomalous bunch lengthening on ACO [2,4]. The FEL oscillator could never acheive ignition if operation was ever attempted at this current level so all of the bunch-lengthening data were obtained while operating the SRFEL as an amplier to an external laser [8,9]. All of the measurements presented here were obtained with synchronous detection with the exception of the time-resolved response of the electron bunch (Figure 5).

Table I outlines the experimental parameters present at the time the time-resolved data, Figure 5, were aquired. These parameters are typical for all of the basic results presented. Any differences will be noted with the individual measurement.

Figure 5 is the time-averaged response of the induced quadratic bunch-length change as a function of time. In the small-signal stochastic-heating model of SRFEL the induced energy spread has the characteristic scaling given by the ratio of the energy damping to the orbit period of the ring as can be seen in Eqn. (7). Note that a decrease in signal $\log F(\omega)$ is an increase in bunch length. The measured characteristic damping time is $\tau_e/2 = 30 \pm 3\,\mathrm{msec}$. The error on the indivudual measurements of the damping time were actually much smaller than this and the majority of the uncertainty arises from shifts in the mean energy of ACO from run to run. The damping time was obtained by making a nonlinear fit of the time-averaged response from several runs to the equation:

$$f(t) = A_1 \exp(tA_2) + A_o. \tag{8}$$

The fits were made using a χ^2 reduction search. The confidence ratio of the fit is $> 98\%$. The theoretical damping time for ACO at 240 MeV is $\tau_e = 65\,\mathrm{msec}$. Thus the measured characteristic time is in excellent agreement with theory. The induced bunch lengthening on Figure 5 corresponds to an increase in bunch length of $\sim 5\%$. The data were obtained by using a digital oscilloscope and averaging over 64 scans. The magnitude of the bunch lengthening and the exponential response are consistent with existing bunch-lengthening models [1,13,15,20].

Figure 6 plots the detected quadratic-bunch-length change as a function of the RF-accelerating voltage for a constant external-laser intensity. The constant of proportionality between the scaling of the energy spread and the bunch length is given by the ratio of the momentum-compaction factor and the synchrotron frequency as seen in Eqn. (2). Additionally,

$$\Omega \propto \hat{V}^{-1}. \tag{9}$$

The nominal bunch length is proportional to $1/\hat{V}^{1/2}$, where $\hat{V}$ is the peak RF-accelerating voltage of the cavity [10]. The detected signal $\Delta\sigma_\tau^2$ should also obey the $1/\hat{V}$ scaling as long as the FEL-induced effects on the beam do not alter the

synchrotron frequency, or the coupling between the energy spread and the bunch length. The solid line in Figure 6 is the least-squares fit to $\Delta\sigma^2 = b\hat{V}$. The errors for each of the data points is smaller than the symbols representing them and so are not included. The proportionality of Eqn. (9) should hold as long as the RF over-voltage is large compared to the energy loss per turn, ($U_o = 280\,\mathrm{eV}$ on ACO at 240 MeV). At RF voltages comparable to the energy loss per turn the potential well, which determines the synchrotron frequency, contains higher order terms. These higher order terms become comparable to the quadratic terms resulting in a departure from the $1/\hat{V}$ scaling as $\hat{V} \rightarrow U_o$.

This scaling verification is important since numerical simulations indicate that at high laser intensity a reduction of the synchrotron frequency should occur [21]. This will change the coupling between the bunch length and the energy spread. Because of the possible coupling modifications it was necessary to verify that the measurements maintained the proper functional dependence of scaling for quantative comparision. Unfortunately, the argon-ion laser and optical-transport system on ACO are incapable of providing sufficient optical intensities to permit the examination of possible synchrotron-frequency depression. Because of this, and as Figure 6 indicates, all measurements remained in a region of intensity where the coupling between the bunch length and energy spread remains constant.

Figure 7 is a plot of bunch lengthening as a function of the transverse alignment of the external laser with respect to the electron beam. Both the laser beam and the electron beam have finite transverse dimensions so that the laser intensity seen by an electron will not be constant but will vary from pass to pass. The finite transverse beam size of the laser reduces the average intensity by a factor which originates from the integral over the transverse distribution of the electrons and transverse-laser mode. If the beams are coaxial the filling factor, $\mathcal{F}_x$, is

$$\mathcal{F}_x = \left[\left(\frac{4\sigma_y^2}{w^2} + 1\right)\left(\frac{4\sigma_x^2}{w^2} + 1\right)\right]^{-1/2}, \qquad (10)$$

for transverse electron beam dimensions σ_x and σ_y, and a laser beam waist w. If the

beams are colinear, that is parallel but having a transverse displacement between their maxima, the filling factor has the form

$$\mathcal{F} = \mathcal{F}_x \mathcal{F}_l. \tag{11}$$

where

$$\mathcal{F}_l = \exp\left[-\left(\frac{x_o^2}{2(w^2/4+\sigma_x^2)} + \frac{y_o^2}{2(w^2/4+\sigma_y^2)}\right)\right]. \tag{12}$$

The transverse displacement being x_o and y_o. The FEL-induced bunch lengthening should have a Gaussian dependence as a function of transverse alignment of the electron and optical beams if both have Gaussian profiles.

Figure 7 verifies the colinear filling factor $\mathcal{F}_l$. The solid curve is a weighted least-squares-fit Gaussian to the data. The errors bars are the calculated statistical uncertainty of the measurements and represent $\pm 1\sigma$. Its $\sigma = .75\,\mathrm{mm}$ which is in good agreement with the predicted value of $(.6\,\mathrm{mm})^2 + (.4\,\mathrm{mm})^2 = (.72\,\mathrm{mm})^2$, where $w/2$ was measured at .6 mm for the laser and σ_x of the electrons was measured at .4 mm for the electron beam.

Madey has demonstrated, as part of the Gain-Spread Theorem, that the FEL-induced energy-spread is proportional to the spontaneous emission power of the undulator [28]:

$$\langle(\delta\epsilon_{fel})^2\rangle_\omega = \frac{d^2 I}{d\Omega\, d\omega}. \tag{13}$$

For a constant-period undulator this results in

$$\langle(\delta\epsilon_{fel})^2\rangle_\omega = \mathcal{F}\frac{I_l r_e \lambda_o^2 \pi K^2 N^2}{mc^3\gamma_o^4}\left[J_{\frac{1}{2}(n-1)}(\xi) - J_{\frac{1}{2}(n+1)}(\xi)\right]^2\left[\frac{\sin\eta}{\eta}\right]^2, \tag{14}$$

and for the symmetric transverse optical klystron [16,29]:

$$\left[\langle(\delta\epsilon_{fel})^2\rangle_\omega\right]_{\mathrm{OpKly}} = 2(1+\cos\tilde{\eta})\left[\langle\delta\epsilon_{fel}(\tfrac{1}{2}N)\rangle_\omega\right]_{\mathrm{Und}}. \tag{15}$$

In these equations I_l is the peak intensity of the optical field, and r_e the classical electron radius. The total number of periods of the undulator, or optical klystron, is N. The harmonic of the on-axis radiation is n (n is odd); $\mathcal{F}$ is the *filling-factor*, or electron beam — optical mode overlap function. The undulator detuning parameter, $\eta \equiv 2\pi n N \delta\epsilon_r$, and $\tilde{\eta} \equiv 4\pi(\frac{1}{2}N + N_d)$, is the optical klystron detuning parameter with N_d a characteristic of the dispersive section [16,29]. The period of the undulator is λ_o. $K \equiv eB_o\lambda_o/2\pi mc^2$ is a dimensionless measure of the magnetic field and is referred to as the wiggler K parameter, and $\xi = nK^2/(4+2K^2)$. The resonant energy difference is $\delta\epsilon_r \equiv (\gamma - \gamma_r)/\gamma_r$, where

$$\gamma_r^2 = \frac{\lambda_o}{2\lambda}\left(1 + \tfrac{1}{2}K^2\right). \tag{16}$$

is the resonant energy of the linear undulator.

Figure 8 is the verification of the Madey Gain-Spread Theorem for the undulator as a function of magnetic-pole-face gap. Figure 9 is the equivalent verification for the optical klystron. Figures 8(a) and 9(a) are the quadratic laser-induced bunch-lengthening curves. Figures 8(b) and 9(b) are the spontaneous emission curves taken in identical conditions at the laser-beam wavelength of 5145Å. The excellent agreement with the Madey Theorem is immediately evident. The vertical scales are the quadratic-bunch-length change measured. They correspond to a $\delta\sigma/\sigma \approx 6\%$. The horizontal scales represent the magnetic-pole-face gap of the undulator, which can be equated to the magnetic field strength [27], and the wiggler K parameter. The resonant energy may be obtained from Eqn. (16). The central axis corresponds to magnetic-pole-face gap of 36.7 mm, $K = 1.93$, and a resonant energy of 238 MeV for the undulator. For the optical klystron the central axis represents a gap of 36.8 mm, $K = 1.92$, and a resonant energy of 237 MeV.

If the difference in the peak laser intensity and transverse filling factor is taken into account for the two curves the ratio of the bunch lengthening observed on the undulator and the optical klystron is equal to the square of the total number of periods in each device:

$$\frac{[\Delta\sigma^2]_{\text{Und}}}{[\Delta\sigma^2]_{\text{OpKly}}} = 1.5 \approx \left(\frac{N_{\text{Und}}}{N_{\text{OpKly}}}\right)^2 = \left(\frac{17}{14}\right)^2. \tag{17}$$

This is in agreement with the theoretical prediction based on Eqns. (14) and (15).

The small-signal stochastic-heating model of the SRFEL predicts that for low pump-laser intensities

$$\Delta\sigma_\tau^2 \propto \langle(\delta\epsilon_{fel})^2\rangle_\psi \propto I_l. \tag{18}$$

On ACO the verification of the linear response of the bunch lengthening to the pump laser was done as follows: Since the NOEL-undulator magnetic field is linear polarized in the vertical, y, direction the electrons oscillate in the horizontal plane. The laser is normally linearly polarized in the veritcal direction. It is rotated in the horizontal plane by using a half-wave plate. The initial angle of the half-wave plate is optimized by the bunch-lengthening signal, and bunch-lengthening measurements are then made as a function of the half-wave plate orientation. Angles are selected for measurement such that the points are evenly distributed in a linear space.

Figure 10 plots the bunch lengthening as a function of the laser intensity. The deviations from the straight line appear to be systematic errors since they were present in identical form over different experimental runs. They apparently were not induced by either a transvese displacement of the laser beam as the half-wave plate is rotated, or the result of an elliptical polariztion of the laser beam, causing an additional component with the proper polarization to be continually present. The elliptical-polarization error would cause all intermediate points to lie above a straight line whereas the majority of the deviations lie below. An additional possibility of a transverse-mode deformation was eliminated as measurements of the laser transverse dimensions as a function of polarization rotation indicate little or no deformation. One possibility remaining is stress-induced birefringence of the vacuum window, resulting in a polarization rotation of the laser beam as it enters the undulator vacuum chamber.

The horizontal uncertainty bars result from the inaccuracies in the knowledge of the power transmission of the optical transport system. The solid line is the least-squares fit of the data to a straight line with x and y intercepts at the origin. Its slope is $1.8 \pm .1 \times 10^{-23}$ sec^2-cm^2/W.

The theoretical values are also plotted on Figure 10. The small-signal stochastic-heating model predicts a slope of $2.07 \pm .05 \times 10^{-23}$ sec^2-cm^2/W under the operating conditions of the experiment and is represented on Figure 10 by the *dashed* line. The uncertainty in the theoretical value is the cumulative result of the inaccuracies of measurement in the filling factor in the undulator, and the other storage ring parameters. The solution of the Fokker-Planck Equation at the power levels of these data is indistinguishable from the small-signal stochastic-heating model [13]. The '$\times$' symbols represent heating values predicted by numerical simulation of the ACO-SRFEL amplifier [21]. The basic experimental results show good agreement with FEL theory in both functional scaling and absolute magnitude, demonstrating that the basic interaction between the electrons and the laser is well characterized.

Conclusion

The experimental results suggest several important conclusions concerning the beam-heating aspects of the SRFEL. The SRFEL is a stable system. The induced heating, resulting from the FEL on the storage ring, can be compensated for by the incoherent synchrotron-radiation damping. At low current, where interactions between the electrons and the envirnoment are small and no collective effects are present, the experimental results of the FEL heating are completely consistent with basic theory of the SRFEL. The argeement with theory is not only in the functional dependence of the scaling relations, but in the absolute magnitudes of the heating predicted by theory and numerical simulations. In addition, on ACO, the data show that the small-signal heating model gives results that are adequate for explaining behavior and predicting the magnitude of the laser-induced electron-beam heating.

The differences of the small-signal heating model and and solution of the Fokker-Planck equation and numerical simulations [13,15,21] will only become important at optical field densities much higher than those accessible on the ACO-SRFEL system.

With the energy aperature of the storage ring dictating the output power limit and efficiency of the SRFEL, improvements must be made in the energy acceptance of storage rings. For SRFEL systems with linear wigglers [13]

$$P_{laser} \approx \sigma_{\epsilon_{max}} P_{sync}. \tag{19}$$

The output power of the laser is P_{laser}, the total synchrotron-radiation power is P_{sync}, and the maximum allowable energy spread of the storage ring is $\sigma_{\epsilon_{max}}$. In order to avoid catastrophic reduction in the the electron beam lifetime, the half-width energy aperature of the storage ring $\Delta\epsilon$ should be at least six times the energy spread of the electron beam, $\Delta\epsilon \geq 6\sigma_{\epsilon_{max}}$ [10]. This limit includes the energy-spread contribution resulting from FEL-induced beam heating. If the wiggler energy envelope is non-Gaussian, as is the case for a linear wiggler, the total energy spread can approach $\frac{1}{4}\Delta\epsilon$ [13,30]. Storage-ring technology is such that $\Delta\epsilon_{max} \approx 8\%$ as in the case of ADONE for the LEDA project [31]. To give an idea the limit imposed by the aperature on the output power, consider the ACO-SRFEL [5,6] and the proposed Stanford-SRFEL [32]. The maximum allowable energy spread for the ACO-SRFEL is $\sim 1\%$, and for the Stanford-SRFEL design it will be as large as $\sim 4 \rightarrow 6\%$. The Stanford-SRFEL has a proposed total average current of 1000 mA, and for this example consider ACO to have a total average current of 100 mA. Assume that both SRFEL's will be storage-ring acceptance limited. The maximum average power of the laser on ACO at 166 MeV (240 MeV) over such conditions would be $\sim$100 mW ($\sim$300 mW); and for the Stanford-SRFEL, which will operate at 1GeV, the corresponding average power limit is $\sim 500 \rightarrow 700$ W.

For short-wavelength applications in the ultraviolet, and x-ray regions of the electro-magnetic spectrum the limit imposed by the energy aperature will not be a

major concern, and present storage-ring design technology should be sufficient for sucessful operation [32]. Even for visable wavelengths the energy aperature limit still allows the SRFEL to be a very attractive high-power source of tunable coherent radiation. However, for high-power operation, or increased high efficiencies for the laser the energy acceptance must be increased. The energy aperature limit will remain a central concern in the full development of high-efficiency SRFEL's. Either storage ring technology must succeed in improving energy acceptances or alternative systems, such as the isochronous storage ring FEL [17], must be developed.

Acknowledgements

We would like acknowledge the contribution of Yves Farge who initiated the ACO-SRFEL project, and to thank the the admistrative and technical staffs of LURE and the Laboratoire de l'Accélérateur Linéaire at Orsay, France for their assistance. This work supported in part by AFOSR under contract F 49620-80-C-0068, the DGRST under contract 79-7-0163, and the DRET under contracts 9-073 and 81-131.

Appendix – Storage Ring Parameter Measurement

In this appendix we list the measurement techniques used for various storage ring parameters necessary for comparing the laser-induced bunch-lengthening data with theory. In order to obtain a quantitative measurement of the laser-induced bunch lengthening several control measurements are neccessary. In addition to the characterization of the external laser, the mean energy of the storage ring, the relative energy spread, the transverse dimensions of the electron beam, the betatron tunes, the synchrotron frequency, the momentum-compaction factor, and average stored current must be measured. Since the magnetic optics and the RF cavity

remain constant on the storage ring, it is necessary only to measure these quantities once, then monitor the peak RF-cavity voltage and the stored current.

The mean energy is normally obtained by measuring the current being drawn by the bending magnets in the storage ring and calculating the corresponding magnet field, and deducing the energy of the ring with a knowledge of the RF-cavity frequency [10]. On ACO this method of measurement is subject to errors of several percent. This is because of the temperature-induced voltage variations in the shunts used to monitor the current supplied to the bending magnets, and from non-standard cycling of the magnets. The most accurate method of calibrating the mean energy, well suited for permanent-magnet SRFEL's, is that of measuring the center wavelength of the spontaneous emission. The central wavelength of the spontaneous emission, either of the undulator or the optical klystron, and the known magnetic field given [27] as a function of the magnetic-pole-face gap determine the mean energy of the storage ring to great accuracy. For NOEL on ACO as a function of pole-face gap the on-axis magnetic field is a simply an exponential [27]. The resonant energy of the undulator, which is also the mean energy, is given by Eqn. (16).

The two principal techniques normally employed for measuring the energy spread on storage rings are not readily employable on ACO. The method of measuring the energy spread of the *core* of the electron distribution by imaging [10,33] is not realizable since at no point on ACO, where the beam is imaged, is the ring sufficiently dispersive to make a good quantitative measurment. Scrapers, usually used for measuring the *tails* of the distribution [33], were removed from ACO. A third method attempted on ACO for measuring energy spread was that of recording the betatron tune envelopes when modulated by the synchrotron oscillations [34]. The principal problem on ACO is that the horizontal tune is the most sensitive to these fluctuations, but there are no electrodes on the storage ring capable of effective horizontal excitation or detection.

The method which proved to be more successful and precise monitored the

depth of modulation of the spontaneous emission of the optical klystron in order to measure the energy spread. This technique permits the energy spread to be measured simultaneously with oscillator operation by passing the spontaneous emission through a monochromater and situating a photomultiplier at one of the minima of the spontaneous-emission curve. Changes in the energy spread result in a decrease in the modulation depth and a subsequent increase in the detected signal [16,29,35].

Figure 11 is a plot of the energy spread detected by this method while scanning RF voltage in a current regime where turbulent bunch-lengthening thresholds are present. The thresholds at $\sim$17 kV, 14 kV, and at $\sim$12 kV are clearly visible.

The transverse, electron-beam dimensions were measured by two techniques. The most accurate and reproducible method was that of imaging the synchrotron radiation from a bending magnet with a convergent lens onto a Reticon CCD [Charge Coupled Device], linear diode array. The signal from the CCD was then read on an oscilloscope at a known rate. The use of a digital oscilloscope with a GPIB interface allowed the transfer of the data for fitting. Alignment was accomplished by using an external signal generator and exciting one of the betatron tunes. This would cause the beam to enlarge in one of its transverse dimensions. Then, the CCD would be rotated until the widest pulse width was located. The other tune would then be excited establishing the other dimension. This assured that the two orthogonal axes of the electron beam were being measured.

Betatron tunes were measured principally by external excitation and by observing the transverse beam profile on one of the video cameras which imaged the beam in the storage ring. The frequency of excitation then was input to a mixer with the orbit frequency which gave an output signal at the frequency of that particular tune. This method suffered from two shortcomings. The excitation required for the two separate tunes was disproportionate in amplitude. The disproportionate excitation again was a result of there being no electrode plates on the storage ring capable of exciting the horizontal tune. Because of this it was easy to lose all of

the stored beam by accidently exciting the strongly coupled tune while seeking the weaker tune. Additionally, this method could be time consuming if an accurate measurement of the tunes was needed, since the resonances varied in their width and definition from run to run.

To avoid the problem of the external-excitation detection of the betatron tunes, a technique using a broadband noise generator and the RF spectrum analyzer connected to an electrode on the storage ring was attempted. However, the tunes themselves were only about $\sim$5 dB above the noise level, and were $\sim$70 dB down in amplitude from the orbit frequency signal. The value of this method was also reduced because of the unsuitable electrodes on ACO. However, it is the most typical method of measurement of the betatron tunes employed on the principal storage rings in operation.

The spectrum analyzer was employed for the measurement of the synchrotron frequency. It is by far the most effective and direct method of measurement. The synchrotron frequency could be measured by either modulating the RF-accelerating cavity voltage with an external low-frequency signal generator, $1 \rightarrow 20$ kHz, and detecting the level of coupling between the excitation and the electron beam. Or, a second technique, which is non-invasive, consists of recording one of the orbit harmonic's natural sideband spectrum. The peaks are subsequently fit to determine the synchrotron frequency.

The momentum-compaction factor is the constant of proportionality between the orbit path-length differences and the energy of the electrons [10]. It is most easily measured by changing the frequency of the RF accelerating cavity and recording the shift in the mean energy of the stored electrons. The most sensitive and direct method manner of making this measurement is to use the spontaneous emission of the optical klystron.

Figure 12 is a composite set of spontaneous emission spectra of the optical klystron taken as a function of magnetic-pole-face gap at various RF-cavity frequencies. The resonant energies can be obtained from Eqn. (16). The shifts in the

maxima and minima were measured and used to determine the induced change in energy of the electrons resulting from the change in RF frequency. The changes in energy were in turn least-spuares fit to a straight line in order to obtain the momentum-compaction factor. The measured value for α on ACO was 0.028 at 240 MeV.

The technique used for measuring the stored current on ACO was to monitor the average signal current from a photomultiplier illuminated by synchrotron radiation. Additionally, the signal amplitude of an electrode on an oscilloscope was used. Both of these techniques were calibrated with a DC transformer developed by M. Bergher [36]. Both allowed very good relative current measurements, but limitations on both techniques reduced the absolute precision of stored-current measurements An impedence mismatch caused the signal on the oscilloscope to be inconsistent from one vertical scale to the next. The photomultiplier tube was sensitive to stray magnetic fields and changes in energy of the storage ring. The signal from the photomultiplier tube varied from run to run because of changes in cycling of the ring magnets and operating point.

References

[1] C. Bazin, M. Billardon, D. A. G. Deacon, P. Elleaume, Y. Farge, J. M. J. Madey, J. M. Ortega, Y. Petroff, K. E. Robinson, M. Velghe, *Physics of Quantum Electronics* (Addison-Wesley, Reading, Mass., 1982), Vol. **8**, Chap. 4, pp. 89-118.

[2] K. E. Robinson, D. A. G. Deacon, M. F. Velghe, and J. M. J. Madey, *IEEE J. Quantum Electron.*, Vol. **QE-19**, No. 3 (March 1983), pp. 365-368.

[3] P. J. Channell, and A. M. Sessler, *Nucl. Instrum. Methods*, Vol. **136** (1976) pp 473-484.

[4] K. E. Robinson, J. M. J. Madey, M. F. Velghe, and D. A. G. Deacon, *IEEE Trans. Nucl. Sci.*, Vol. **NS-30**, No. 4 (August 1983), pp. 3088–3090.

[5] M. Billardon, P. Elleaume, J. M. Ortega, C. Bazin, M. Bergher, M. Velghe, Y. Petroff, D. A. G. Deacon, K. E. Robinson, and J. M. J. Madey, *Phys. Rev. Lett.*, Vol. **51**, No. 18 (31 October 1983), pp. 1652-1655.

[6] P. Elleaume, J. M. Ortega, M. Billardon, C. Bazin, M. Bergher, M. Velghe, Y. Petroff, and D. A. G. Deacon, K. E. Robinson, J. M. J. Madey, Submitted to *J. Phys. (Paris)*, December 1983.

[7] K. E. Robinson, Ph.D. Dissertation, HEPL Report No. 945, February 1984, High Energy Physics Laboratory, Stanford University, Stanford, CA 94305.

[8] D. A. G. Deacon, J. M. J. Madey, K. E. Robinson, C. Bazin, M. Billardon, P. Elleaume, Y. Farge, J. M. Ortega, Y. Petroff, and M. F. Velghe, *IEEE Trans. Nucl. Sci.*, Vol. **NS-28**, No. 3 (June 1981), pp. 3142-3145.

[9] M. Billardon, D. A. G. Deacon, P. Elleaume, J. M. Ortega, K. E. Robinson, C. Bazin, M. Bergher, J. M. J. Madey, Y. Petroff, and M. Velghe, *J. Phys. (Paris) Colloq.*, Vol. **44**, Supp. No. 2 (February 1983), pp. C1-29–71.

[10] M. Sands, "The Physics of Electron Storage Rings: An Introduction," SLAC report No. 121 (November 1970), Stanford Linear Accelerator Center, Stanford, CA 94305.

[11] H. BRUCK, *Accélérateurs Circulaires de Particules*, (Presses Universitaires de France, Paris, France, 1966).

[12] W. H. Backer, "Some Aspects of the Orbits in an Electron Storage Ring used as a Synchrotron Radiation Source," Doctoral dissertation, Wetenschappen aan de Technische Hogeschool Eindhoven, (PAMPUS), December 1979, Printed by Wibro Helmond, Eindhoven, Netherlands.

[13] A. Renieri, *Il Nuovo Cimento B*, Vol. **53B**, No. 1 (11 September 1979), pp. 160-178.

[14] J. M. J. Madey, and D. A. G. Deacon, *Cooperative effects in Matter and Radiation* (Plenum, New York, 1977), pp. 313-334

[15] L. R. Elias, J. M. J. Madey, and T. I. Smith, *Appl. Phys.*, Vol. **23**, No. 9 (December 1980), pp. 273-282.

[16] P. Elleaume, *Physics of Quantum Electronics* (Addison-Wesley, Reading, Mass., 1982), Vol. **8**, Chap. 5, pp. pp. 119-151.

[17] D. A. G. Deacon, *Physics Reports*, Vol. **76**, No. 5 (October 1981), pp. 349-391.

[18] F. Reif, *Fundamentals of Statistical and Thermal Physics* (McGraw-Hill Book, New York, 1965), Chap. 1, p. 39.

[19] G. Dattoli, and A. Renieri, *Il Nuovo Cimento*, Vol. **59B**, No. 1 (11 September 1980), pp. 1-39.

[20] C. Pellegrini, *IEEE Trans. Nucl. Sci.*, Vol. **NS-26**, No. 3 (June 1979), pp. 3791-3797.

[21] K. E. Robinson, and J. M. J. Madey, HEPL Report No. 953, May 1984, High Energy Physics Laboratory, Stanford, CA 94305, Submitted to *Part. Accel.*

[22] For a detailed account of FEL theory and the experimental work in progress, the reader is referred to G. Dattoli, A. Renieri, To be published in *Laser Handbook* (North Holland, Amsterdam), Vol. **4**.

[23] H. Winick, and A. Bienenstock, *Annual Rev. Nucl. Part. Sci.*, Vol. **28**, pp. 33-113.

[24] P. L. Csonka, *Part. Accel.*, Vol. **8** (1978), pp. 225-234.

[25] Groupe 'Orbite', Internal Note 16-67 A.C.O., Laboratoire de l'Accélérateur Linéaire, Orsay, France.

[26] D. C. Champeney, *Fourier Transforms and Their Physical Applications* (Academic Press, London, 1973), pp. 16-18, and Appen. F.

[27] J. M. Ortega, C. Bazin, D. A. G. Deacon, C. Depautex, P. Elleaume, *Nucl. Instrum. Methods*, Vol. **206**, Nos. 1,2 (Feburary 1983) pp. 281-288.

[28] J. M. J. Madey, *Il Nuovo Cimento B*, Vol. **50B**, No. 61 (March 1979), pp. 64-88.

[29] P. Elleaume, *J. Phys. (Paris) Colloq.*, Vol. **44**, Supp. No. 2 (February 1983), pp. C1-333-352.

[30] For the transverse gradient wiggler a factor of 1.5 appears on the right hand side of Eqn. (19) resulting in an apparent increase in the possible laser output power, but the energy envelope for the transverse gradient wiggler is Gaussian and the energy spread again must not exceed $\frac{1}{6}\Delta\epsilon$ and the increase is countered by the decrease in available energy spread. See N. M. Kroll, and M. N. Rosenbluth, *J. Phys. (Paris) Colloq.*, Vol. **44**, Supp. No. 2 (February 1983), pp. C1-85–107; and J. M. J. Madey, *J. Phys. (Paris) Colloq.*, Vol. **44**, Supp. No. 2 (February 1983), pp. C1-169–178.

[31] R. Barbini, G. Dattoli, T. Letardi, A. Marino, A. Renieri, and G. Vignola, *IEEE Trans. Nucl. Sci.*, Vol. **NS-26**, No. 3 (June 1979), pp. 3836-3838.

[32] H. Wiedemann, *J. Phys. (Paris) Colloq.*, Vol. **44**, Supp. No. 2 (February 1983), pp. C1-201–209.

[33] P. B. Wilson, R. Servranckx, A. P. Sabersky, J. Gareyte, G. E. Fischer, and A. W. Chao, *IEEE Trans. Nucl. Sci.*, Vol. **NS-24**, No. 3 (June 1977), pp. 1211-1214.

[34] M. P. Level, H. Petit, Rapport Technique 3-75, 19 June 1975, Groupe 'Anneaux de Collisions,' Laboratoire de l'Accélérateur Linéaire, Institut National de Physique Nucléaire et de Physique des Particules, Orsay, France.

[35] D. A. G. Deacon, M. Billardon, P. Elleaume, J. M. Ortega, K. E. Robinson, C. Bazin, M. Bergher, M. Velghe, J. M. J. Madey, Y. Petroff, Submitted to *Appl. Phys. B*, December 1983.

[36] M. Bergher, *IEEE Trans. Nucl. Sci.*, Vol. **NS-28**, No. 3 (June 1981), pp. 2375-2377.

TABLE I

Basic Experimental Parameters

Electron Energy	E	238 MeV
Momentum Compaction	α	0.028
Synchrotron Frequency	$\Omega/2\pi$	6490 Hz
Electron Bunch Length	σ	200 psec
Energy Damping Time	τ	65 msec
Electron Beam Width (Horiz.)	σ_x	0.34 mm
Electron Beam Width (Vert.)	σ_y	0.33 mm
Undulator K Value	K	1.93
Undulator Period	λ_o	7.78 cm
Laser Wavelength	λ	5145Å
Laser Peak Intensity	I_l	175 W/cm^2
Laser Beam Waist	w	1.2 mm
Orbit Frequency	$\omega_o/2\pi$	13.618 MHz
Detection Frequency	$\omega/2\pi$	1062.2 MHz*
Number of Bunches		1

*78th Harmonic

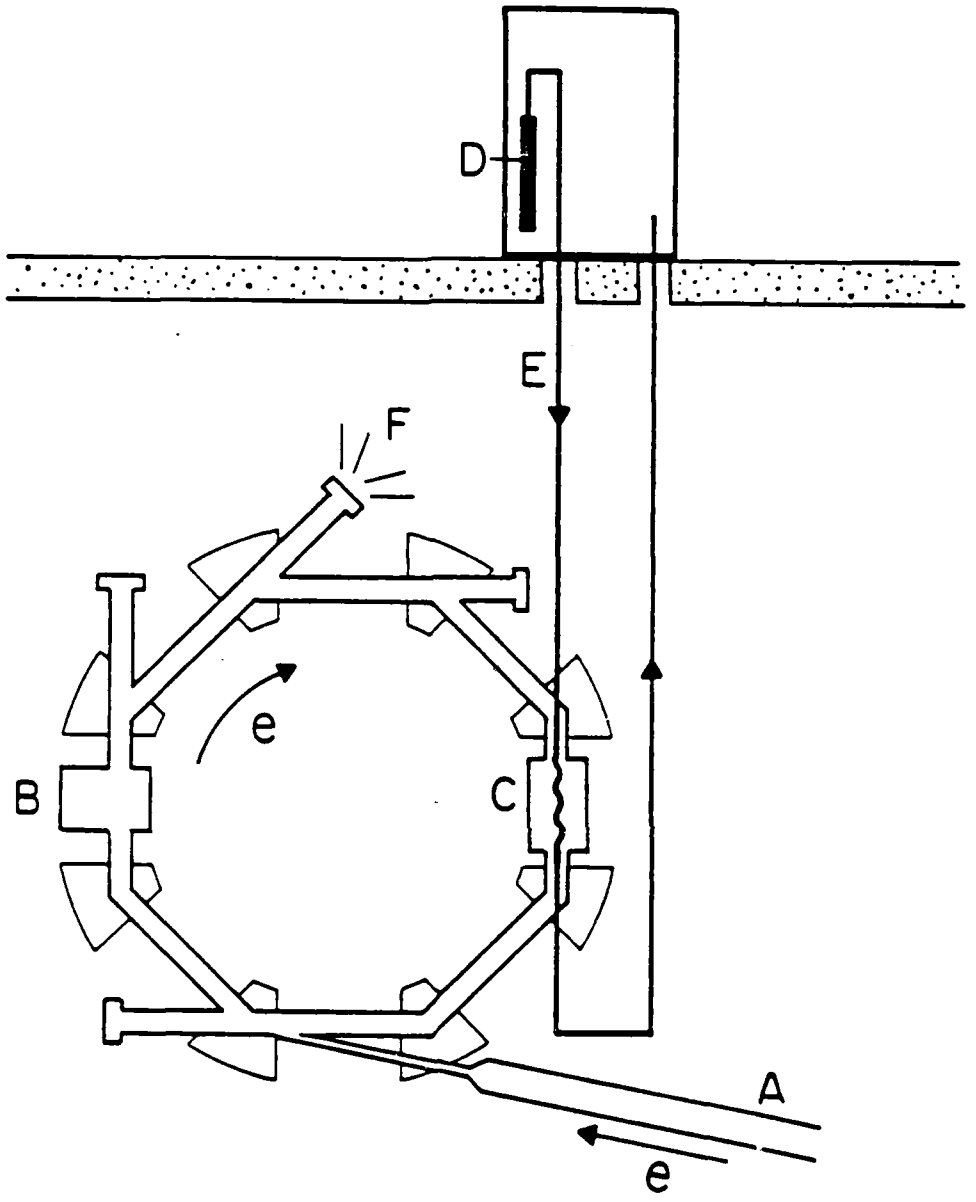

Figure 1 Schematic diagram of the ACO-SRFEL showing the injection line, A; the RF cavity, B; the undulator, C; the argon-ion laser, D, and the optical transport system, E, used for amplifier experiment. The synchrotron port, F, was used for bunch-lengthening measurements.

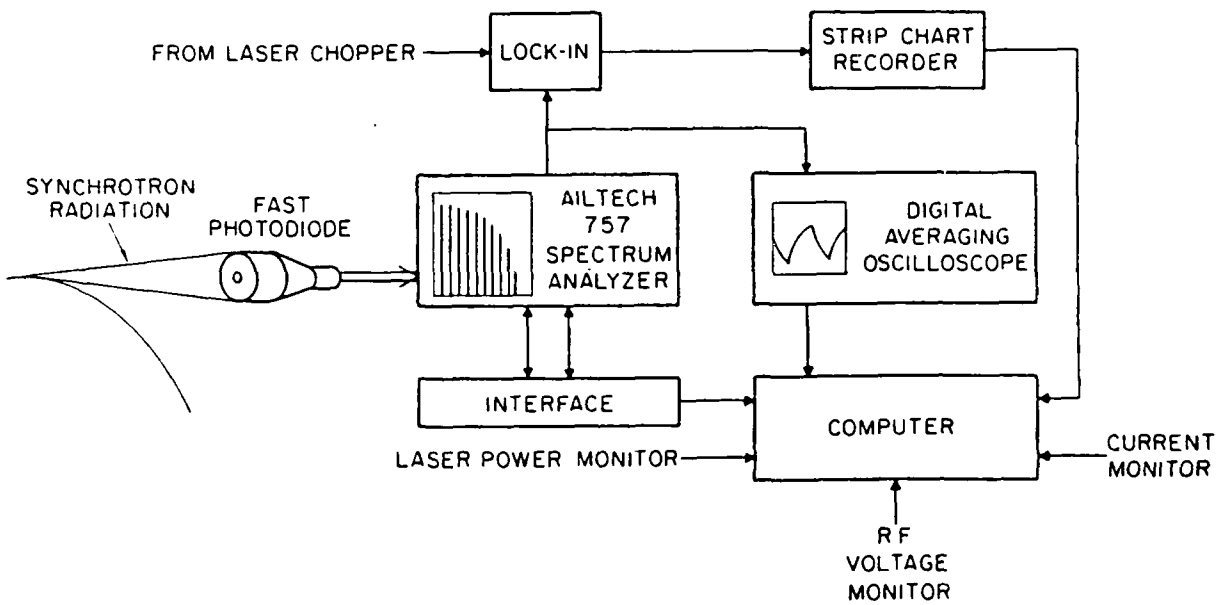

Figure 2 Schematic diagram of the laser-induced bunch-lengthening detection system.

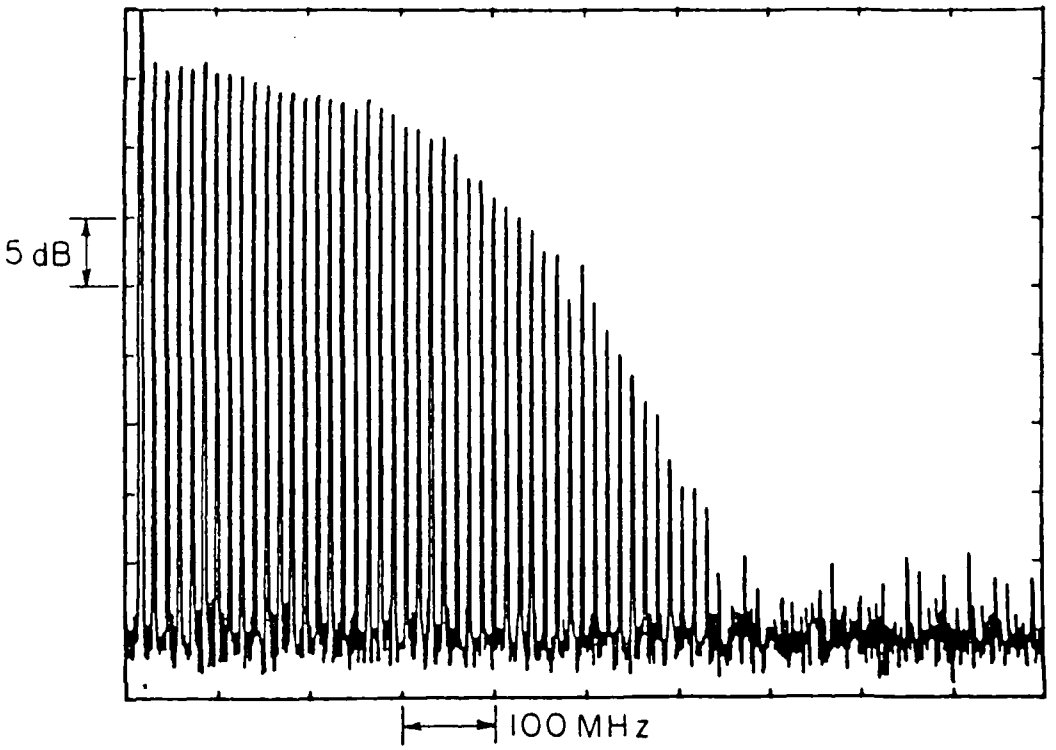

Figure 3 Spectrum Analyzer output showing the comb spectrum of the photodiode signal from synchrotron radiation from ACO. The horizontal scale is 100 MHz/div; the vertical is dB5/div. The first line is the zero frequency reference line and subsequent lines are spaced at 13.618 MHz – the orbit frequency of the storage ring. The spectral envelope corresponds to a compensated temporal bunch length of 665 picosecond with a mean-squared correlation of 99.2%. The spectrum was taken at an electron energy of 536 MeV, a current of 90 mA, and an RF accelerating voltage of 17.5 kV.

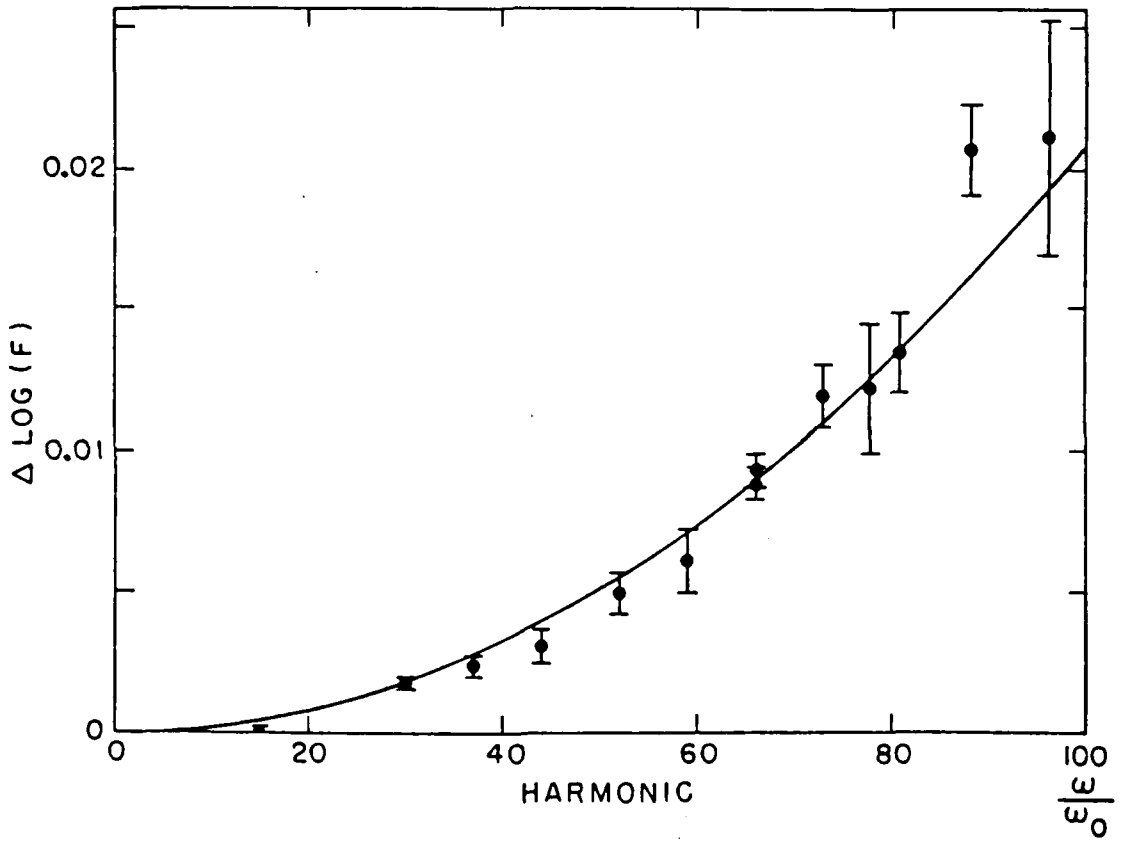

Figure 4 Plot of $\log F_i(\omega) - \log F_f(\omega)$ as a function of detection frequency measured as harmonics of the orbit frequency for a single bunch-lengthening measurement. The solid line is a least-squares fit of the data to a parabola, the response expected for a Gaussian beam. The error bars are measurement fluctuations of $\pm 1\sigma$.

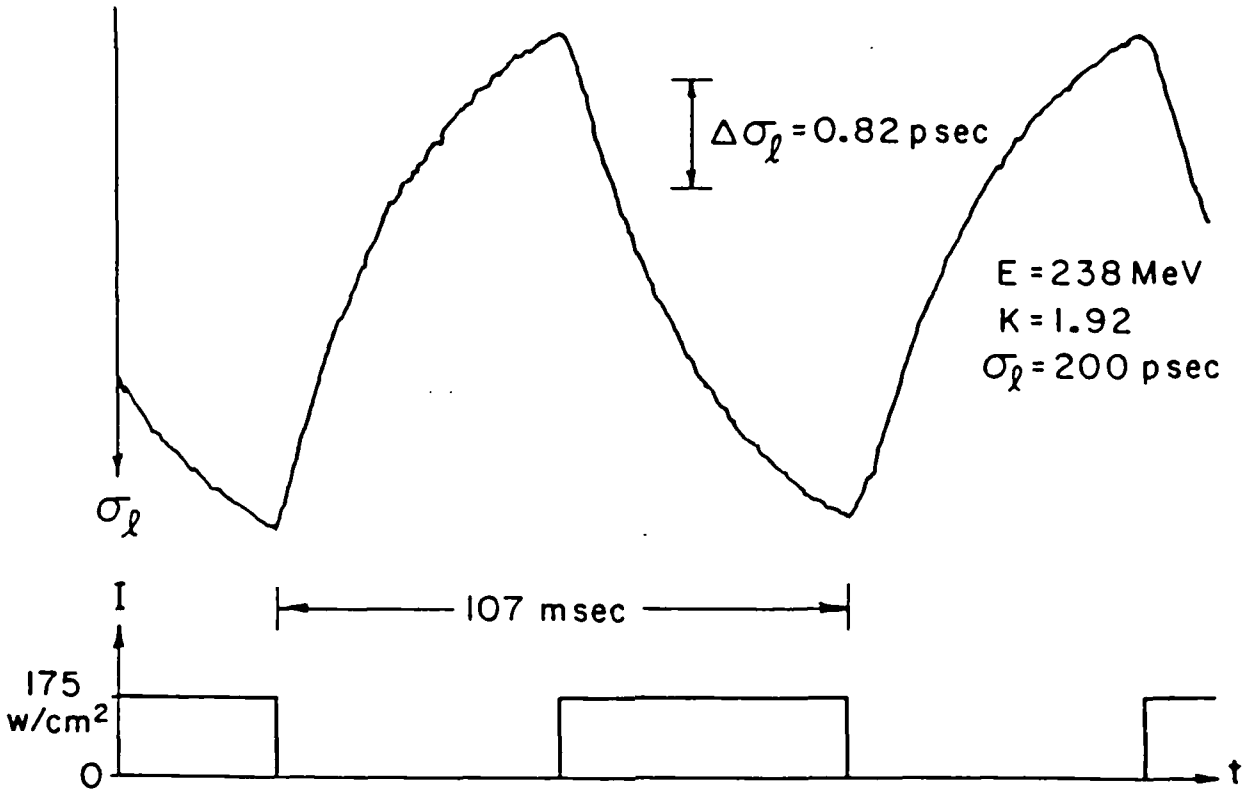

Figure 5 Time averaged response of the electron bunch length at low current to the external laser. The upper trace shows the time dependence of $\log F(\omega)$, the power output of the photodiode detector at the 78th harmonic of the orbit frequency (1062.2 MHz). As explained in the text, an increase in the bunch length corresponds to a decrease in signal amplitude of $\log F(\omega)$. The lower trace records the external laser intensity incident on the electron beam.

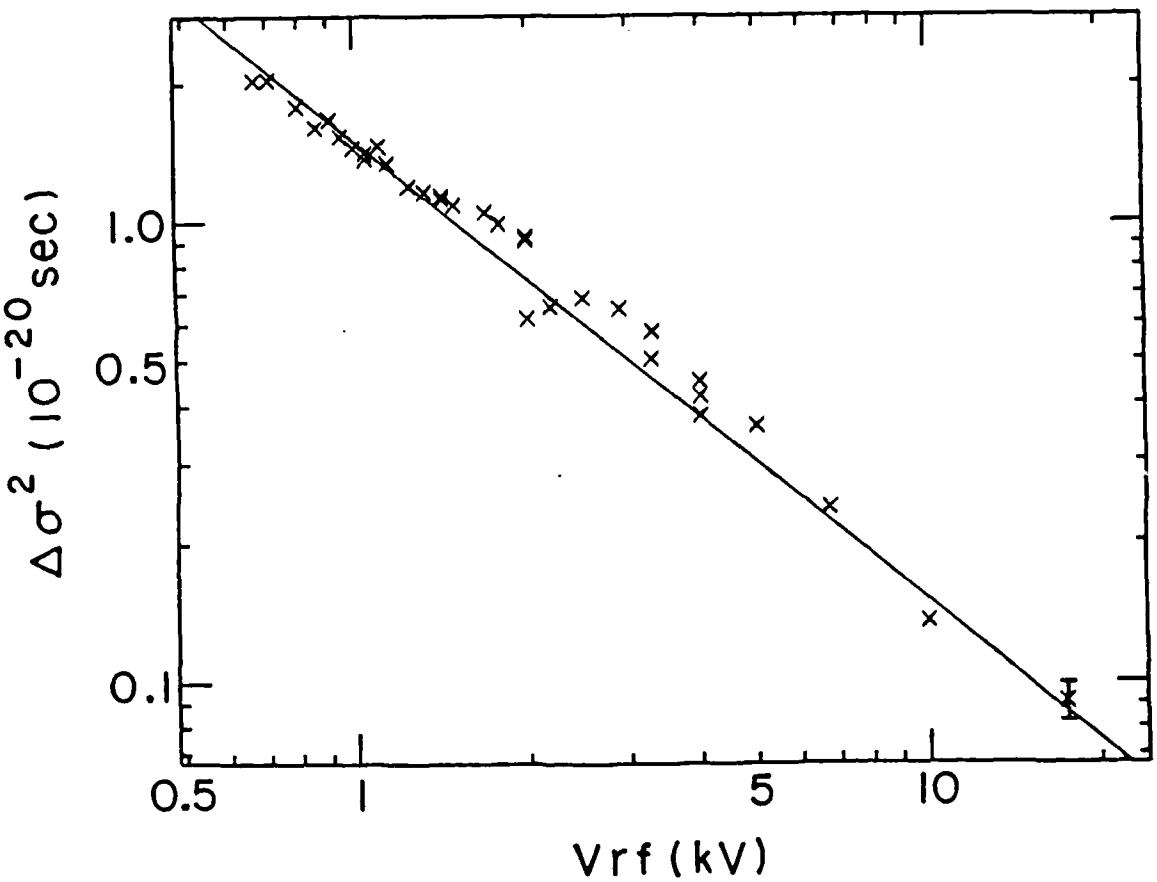

Figure 6 FEL-induced quadratic bunch-length change as a function of RF accelerating cavity voltage. The solid line is the least-squares fit of the data to $1/V_{rf}$. The statistical errors are smaller than the symbols representing the data points The data should scale as $1/V_{rf}$ as long as the FEL interaction does not effect the scaling between the energy spread and bunch length.

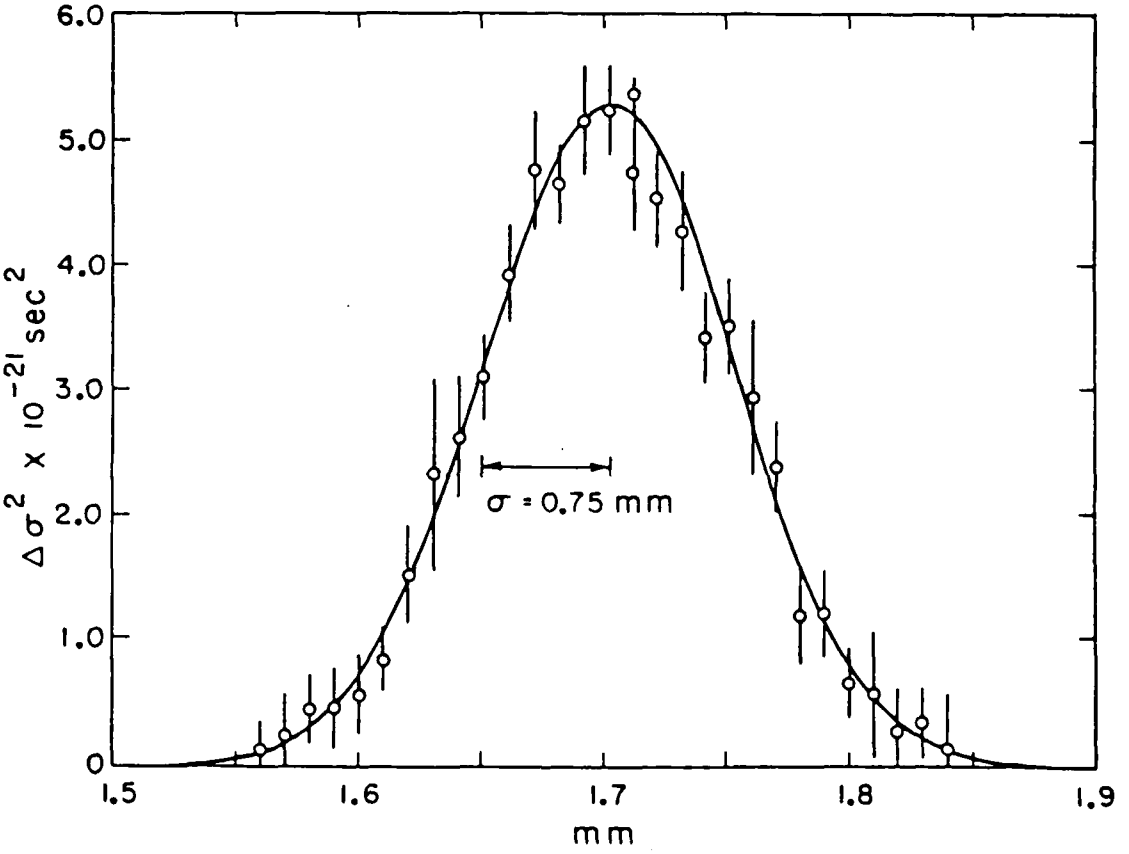

Figure 7 FEL-induced quadratic bunch-length change as a function of transverse laser alignment. The solid line is the weighted least-squares fit to a Gaussian with a $\sigma = 0.75$ mm, in good agreement with the theoretical value of 0.72 mm for the colinear filling factor. The error bars are measurement fluctuations of $\pm 1\sigma$.

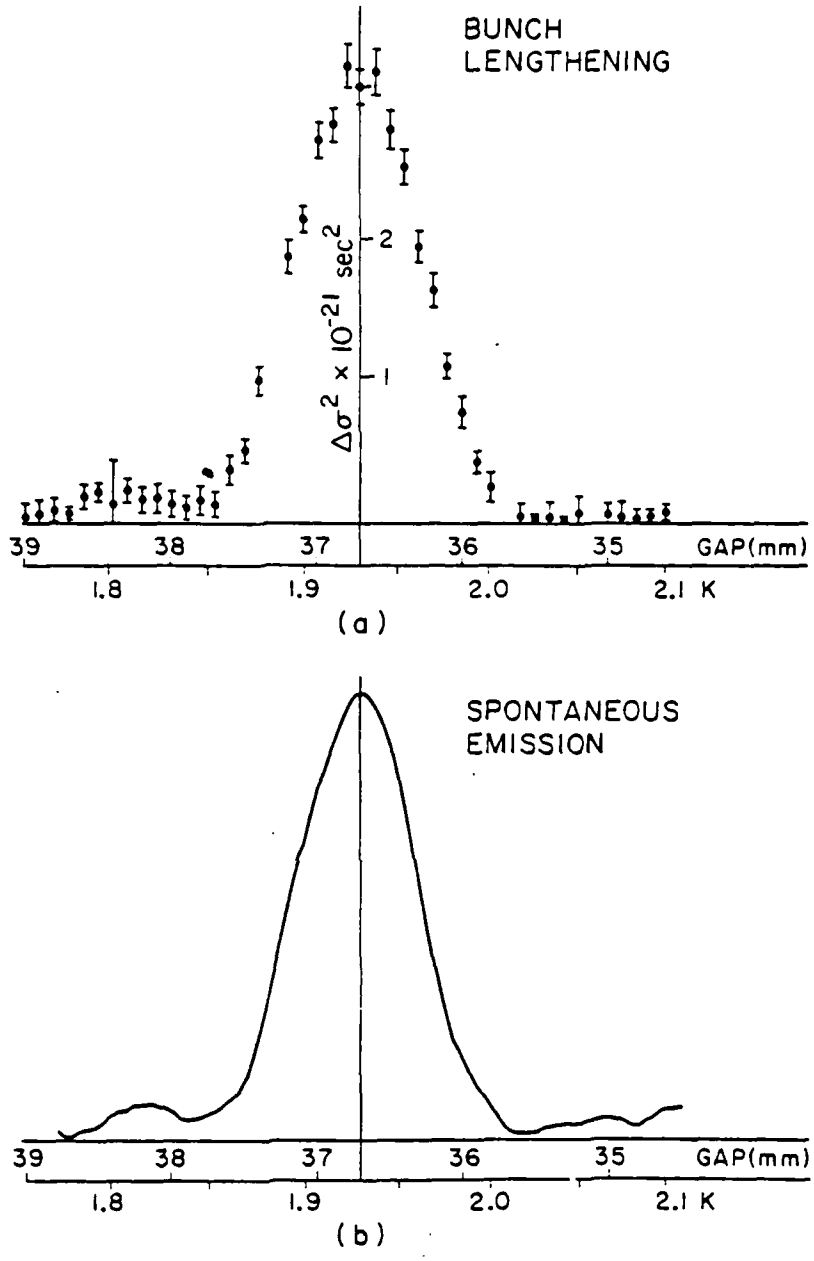

Figure 8 (a) FEL-induced bunch lengthening as a function of permanent-magnet undulator magnetic-pole-face gap. The maximum of the signal corresponds to a bunch lengthening of $\sim 6\%$ at a gap of 36.7 mm, equivalently a $K = 1.93$, or a resonant energy of 238 MeV. The error bars are measurement fluctuations of $\pm 1\sigma$. (b) Spontaneous emission of the permanent magnet undulator as a function of magnetic-pole-face gap at a fixed wavelength (5145Å).

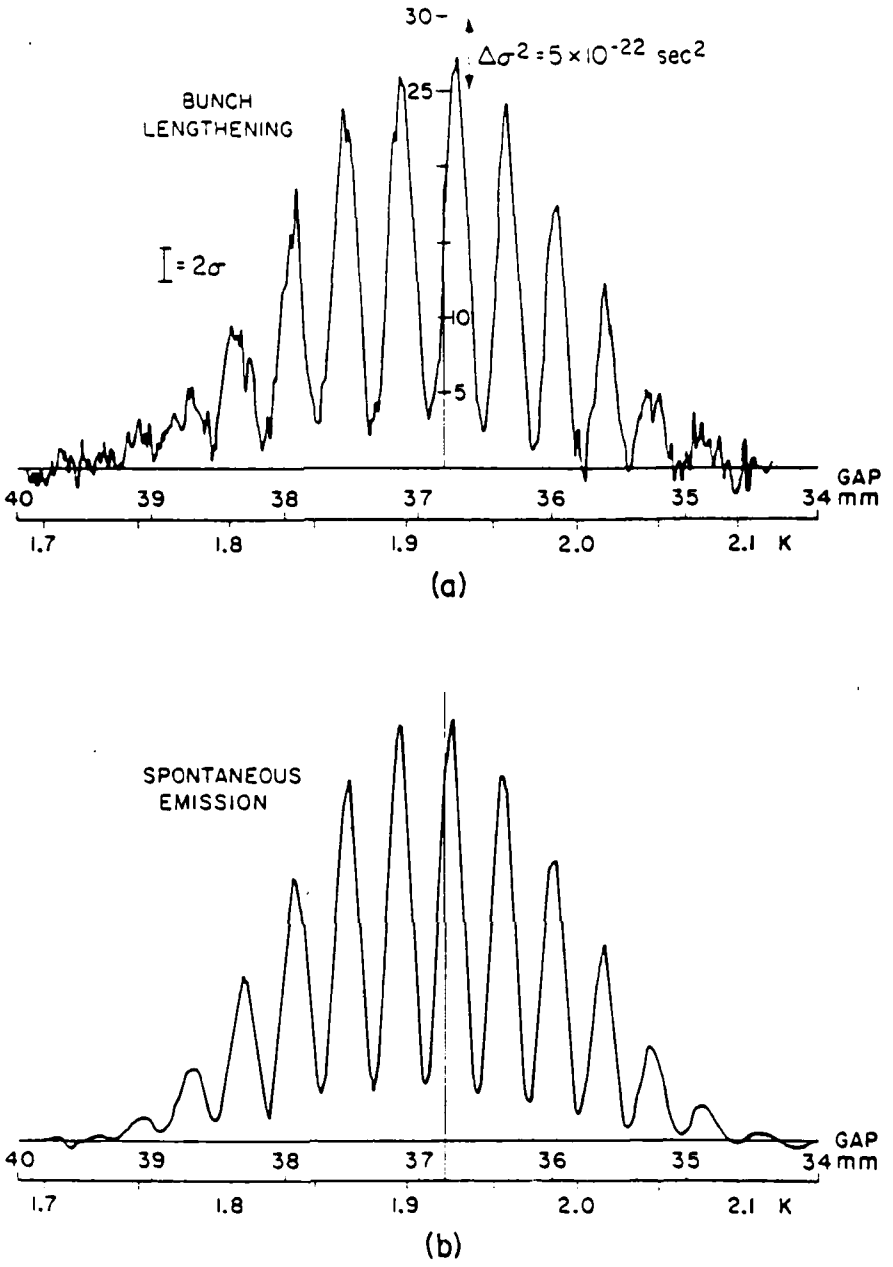

Figure 9 (a) FEL-induced bunch lengthening as a function of permanent-magnet optical klystron magnetic-pole-face gap. The central axis corresponds to a gap of 36.8 mm, a $K = 1.92$, and a resonant energy of 237 MeV. When difference in incident laser intensity is accounted for the maximum observed lengthening is a factor of 1.5 less than for the undulator in agreement with theory. The 2σ error bars shown are calculated from the statistical fluctuations of the signal before the scan was taken. (b) Spontaneous emission of the permanent-magnet optical klystron as a function of magnetic-pole-face gap at a fixed wavelength (5145Å).

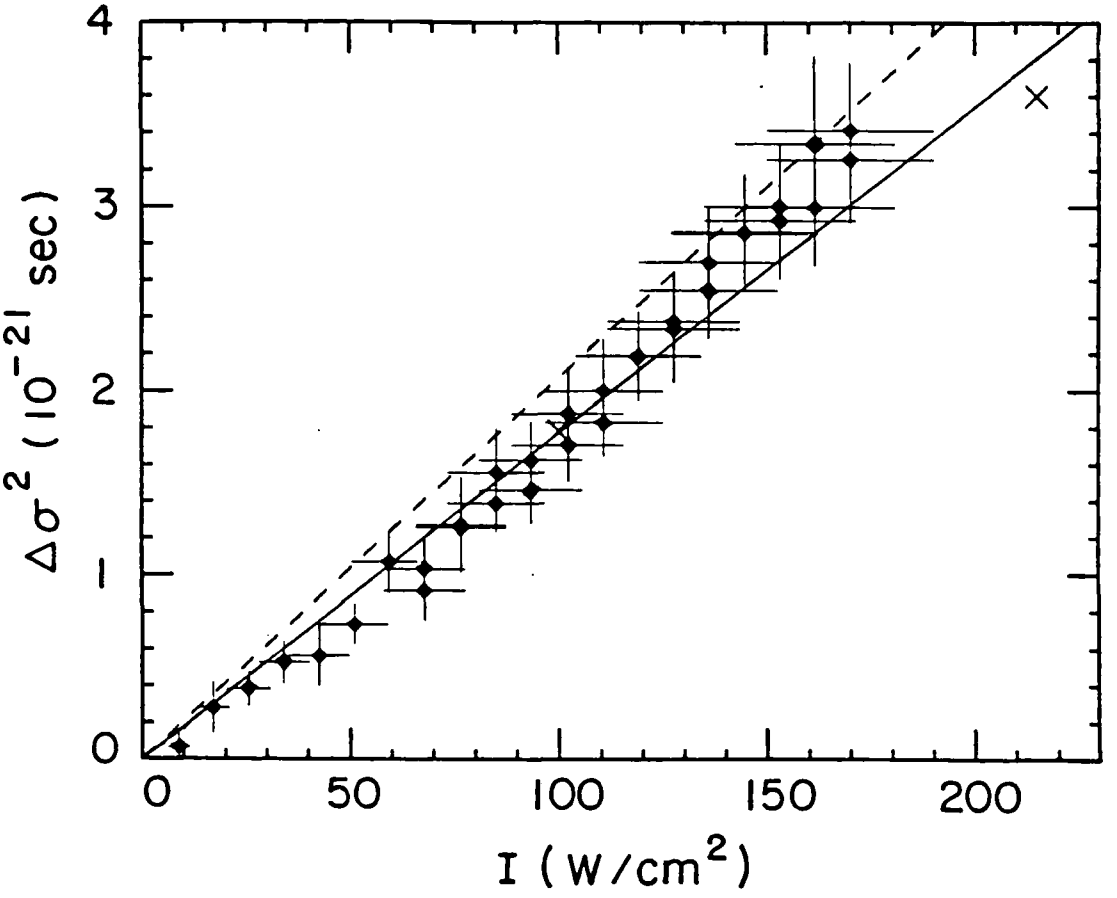

Figure 10 Quadratic laser-induced bunch lengthening as a function of peak laser intensity obtained by polarization rotation. The solid line is least-squares fit of to a straight line through the origin, and has a slope of $1.8 \pm .1 \times 10^{-23}$ sec^2-cm^2/W. The dashed line is the value predicted by the stochastic small-signal heating model based on the operating conditions present has a slope of $2.07 \pm .05 \times 10^{-23}$ sec^2-cm^2/W. The vertical error bars are are measurement fluctuations of $\pm 1\sigma$. The horizontal error bars are the result of laser-power transmission uncertainties.

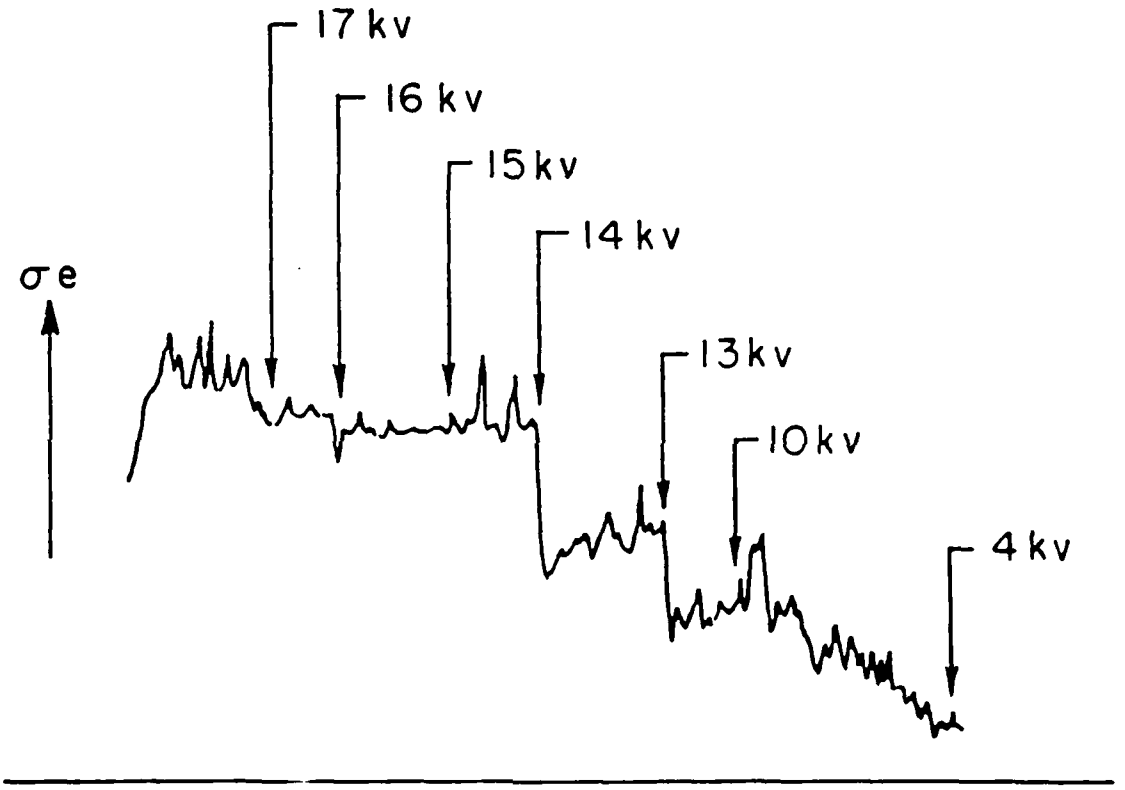

Figure 11 Electron beam energy spread measured with the optical-klystron spontaneous emission as a function of the RF-cavity. This scan was taken at moderate electron current in the ring at 238 MeV and shows anomalous bunch-lengthening thresholds.

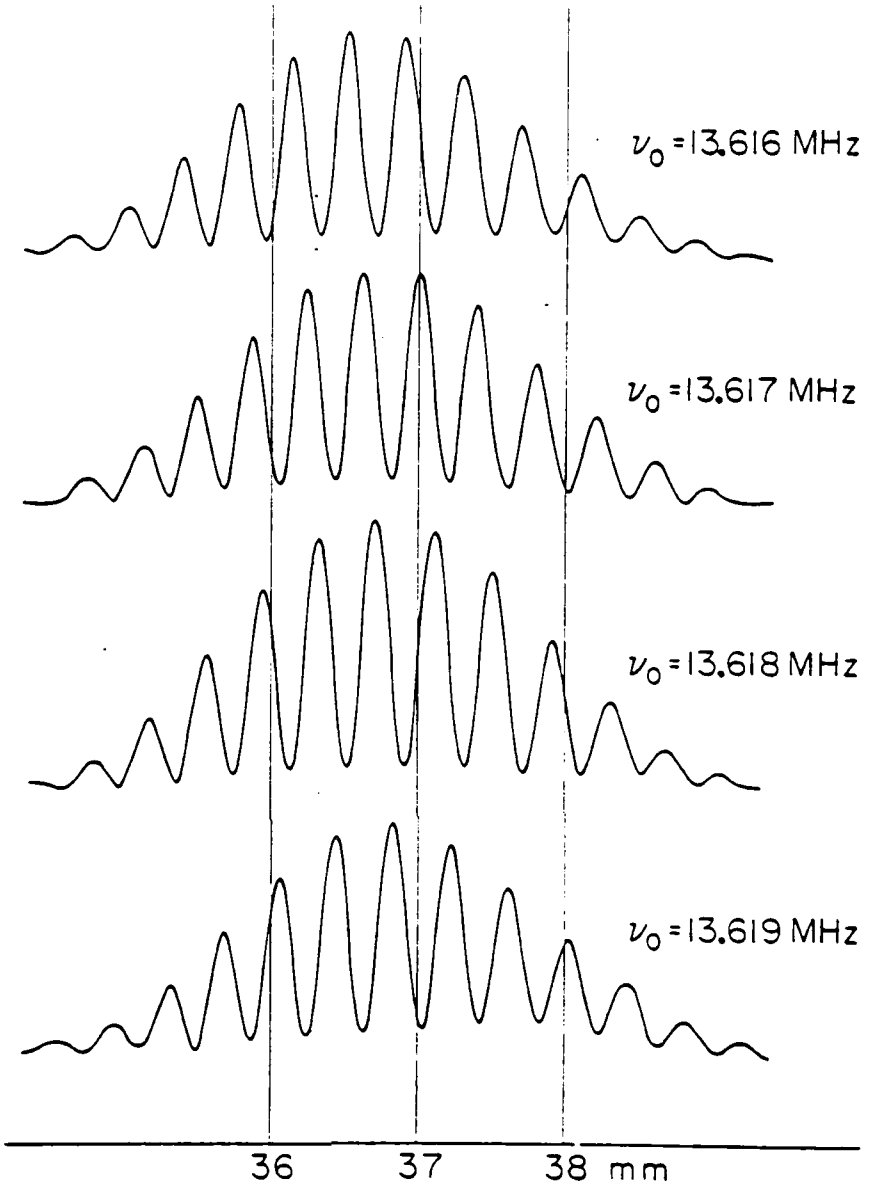

Figure 12 Optical-klystron spontaneous-emission curves as a function of magnetic-pole-face gap at a fixed wavelength (5145Å) for various RF-cavity frequencies. The energy shifts shown by the curves resulting from the changing of the frequency correspond to a momentum-compaction factor of 0.028.

Appl. Phys. B 34, 207–219 (1984)

Applied Physics B Photophysics and Laser Chemistry

Optical Klystron Experiments for the ACO Storage Ring Free Electron Laser

D. A. G. Deacon[1], M. Billardon[2], P. Elleaume[3], J. M. Ortega[2], K. E. Robinson[4], C. Bazin, M. Bergher, M. Velghe[5], J. M. J. Madey[4], and Y. Petroff

L.U.R.E., L.P. CNRS 008, Bâtiment 209-C,
Université de Paris-Sud, F-91405 Orsay, France

Received 2 January 1984/Accepted 20 March 1984

Abstract. To improve the gain in the Orsay storage ring Free Electron Laser (FEL) experiment, the 17 period permanent magnet undulator has been modified to form an optical klystron (OK). We report the measurement of spontaneous emission and the effects on it of energy spread and angular spread. Gain and laser induced bunch lengthening measurements with the OK are also reported and are in very good agreement with the FEL classical theory. The spontaneous emission spectrum which is easy to measure with good signal to noise ratio, turns out to be a very good diagnostic tool for *energy spread and angular spread measurements* on storage rings. The factor of four increase in the small gain obtained by converting the undulator NOEL into an OK was the critical factor in the recent operation of the ACO storage ring laser above threshold.

PACS: 42.60, 42.55

The main purpose of the Orsay experiment is to prove the feasability and test the theories of a storage ring free electron laser (FEL) in the visible range. A permanent magnet undulator has recently been built [1, 2] and has successfully operated on the electron storage ring ACO in the energy range 150–540 MeV [3]. However ACO is not optimized for FEL studies. The relatively low electron density (for storage rings) and the short length of the available straight section have conspired to limit the gain available with an undulator to 1 to $2\,10^{-4}$ per pass at a wavelength $\lambda = 6300$ Å and 240 MeV electron energy. Even with state-of-the-art mirrors, laser operation is impossible at this level of gain. Several directions have been followed to improve the gain. The most successful approach has been the modification of the undulator into an optical klystron (OK). In this paper we shall discuss our experience with the OK. The OK originally proposed by Vinokurov and Skrinsky [4] consists of two identical undulators separated by a dispersive section forcing the electron into a single large wiggle (Fig. 1). This configuration has a higher gain than an undulator of the same total length. Such a device can be used to advantage on electron beams with energy spread and it allows the maximization of the gain in an interaction region of fixed length.

Early results have already been reported [3]. In this paper we report on the dispersive section optimization (Sect. 1), spontaneous emission measurements (Sect. 2), gain measurements (Sect. 3) and laser induced bunch lengthening (Sect. 4). The spontaneous emission results are very detailed because they are easy to measure with a good signal to noise ratio and give much information on the OK FEL behaviour.

We use the notation of the theoretical description of optical klystrons of [5].

Permanent addresses:
[1] Deacon Research, 754 Duncardine Way, Sunnyvale, CA 94087, USA
[2] Ecole Supérieure de Physique et Chimie, 10, rue Vauquelin, F-75231 Paris Cedex 05, France
[3] Département de Physico-Chimie, Service de Photophysique, CEN Saclay, F-91191 Gif-sur-Yvette, France
[4] High Energy Physics Laboratory, Stanford University, Stanford, CA 94305, USA
[5] Laboratoire de Photophysique Moléculaire, Bâtiment 213, Université de Paris-Sud, F-91405 Orsay, France

away from the axis of the electron beam (Fig. 2). The calculated trajectory is shown in Fig. 1 which shows a large wiggle of about 2 mm amplitude for an electron energy of 240 MeV and a gap of 33 mm.

2. Spontaneous Emission

2.1. General Features of the Fundamental

As was done for the undulator, the electron beam is initially aligned by optical means into the axis of the vacuum chamber within ± 1 mm [3].

The spontaneous emission pattern of the optical klystron looks the same to the eye as that of an undulator [7, 6, 3], namely a series of concentric coloured rings with a similar pattern produced by each harmonic at progressively larger opening angles. The big difference appears in the spectrum.

The experimental set up used to measure the spontaneous emission spectrum has already been described [6]. It consists of a 1750 mm focal length spherical mirror placed at about 6.5 m from the center of the optical klystron.

The light transmitted by a 75 μm pinhole placed at the focal distance from the mirror is sent through a lens into an M20 uv Jobin Yvon monochromator (4 Å resolution with 0.1 mm slits). The output of the monochromator is then sent into a Hamamatsu R 928 photomultiplier. Fig. 3 shows a spontaneous emission spectrum of the fundamental at an energy of 240 MeV for a gap of 34.4 mm at low current in the ring.

We have compared the envelope of the oscillations with that of the emission spectrum of a perfect undulator having exactly N sinusoidal periods, the fields outside these periods being exactly zero. The emission spectrum $dI/d\lambda$ of such an undulator is:

$$\frac{dI}{d\lambda} \propto \frac{1}{\lambda^4}\left(\frac{\sin\delta}{\delta}\right)^2 \tag{3}$$

with $\delta = n\pi N(1-\lambda_R/\lambda)$,

where λ_R is the resonant wavelength and n is the harmonic number. Fitting the envelope to curves given by (3) gives $N = 8.1 \pm 0.1$ instead of 7. This discrepancy is probably due to the dispersive section field which could be partly resonant with the other 7 periods. It is certainly not due to the fringe field of the half periods which slightly decreases the effective number of periods. The envelope of oscillations also presents a long, short wavelength tail with the secondary maximum amplitude lower than expected. This effect was also seen in the 17 period undulator emission curves and is due to the parasitic tail of the ACO bending magnets fringe field [2]. Similar curves of emission were obtained as function of energy or field in the dispersive section (by changing the gap).

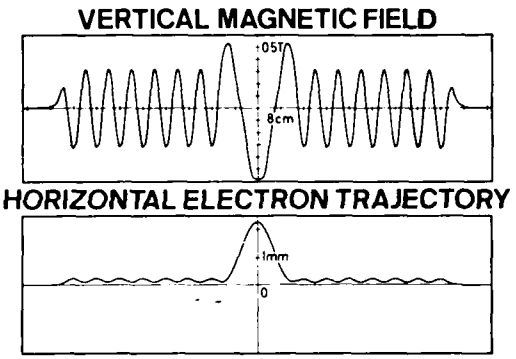

Fig. 1. Vertical magnetic field calculated for the Orsay optical klystron (gap: 33 mm) and the corresponding calculated horizontal electron trajectory at an energy of 240 MeV

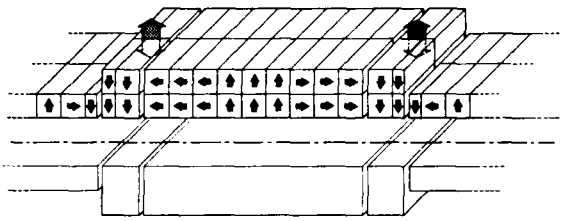

Fig. 2. Dispersive section permanent magnet configuration optimizing the low field gain

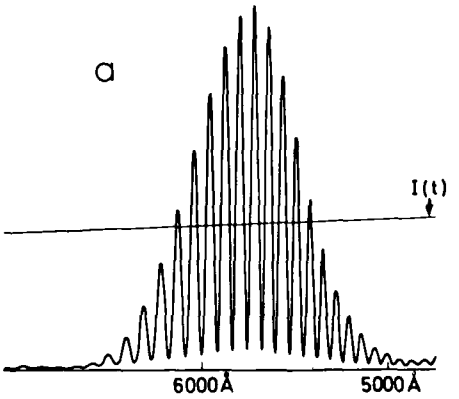

Fig. 3. Spontaneous emission spectrum $dI/d\lambda d\Omega$ measured for an electron energy of 238 MeV and a magnetic field parameter of $K = 2.09$ at low current where the modulation is almost total. The current decay $I(t)$ is superimposed

Plotting the N_d of each maximum as a function of $1/\lambda$, we verified a high linearity (0.9999 correlation coefficient in the range $0.3 < \lambda < 0.7$ [μm]). From the slope, we can calculate the experimental value of N_d which is $N_d = 65.3 \pm 0.2$ at $\gamma mc^2 = 240$ MeV and $\lambda = 6238$ Å for a dispersive section gap of 35 mm. This value is close to the value $N_d = 68$ predicted from the

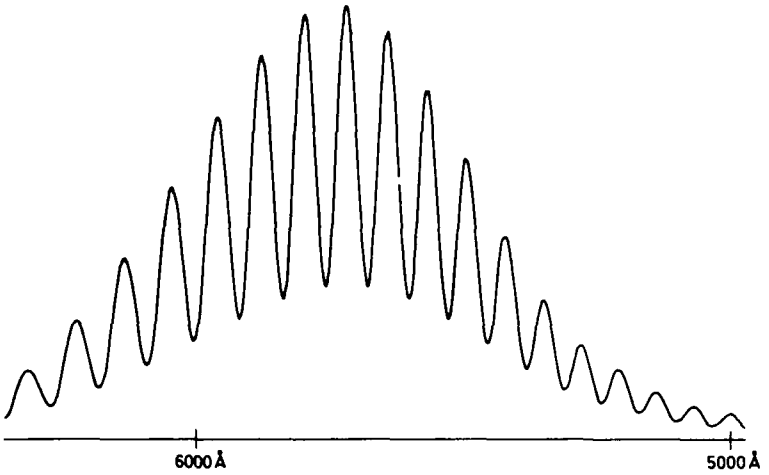

Fig. 4. Spontaneous emission spectrum $dI/d\lambda d\Omega$ measured for an electron energy of 240 MeV, a current of 40 mA and a magnetic gap of 35 mm. The non complete modulation is due to fractional energy spread of 1.2×10^{-3}

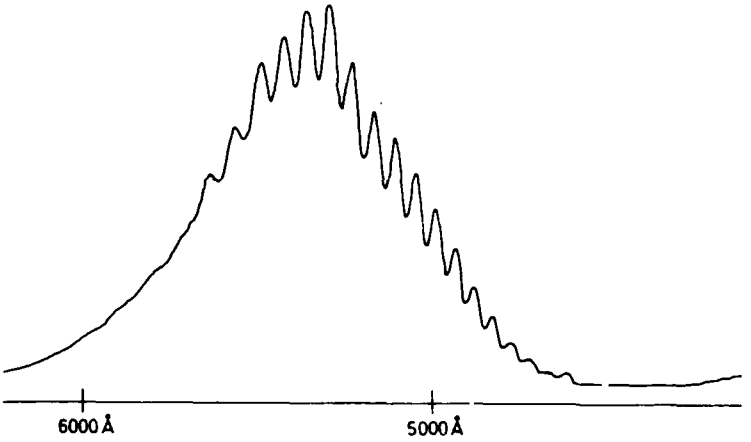

Fig. 5. Spontaneous emission spectrum $dI/d\lambda d\Omega$ measured at low curent and 240 MeV. The modulation is reduced below that of figure 3 by inducing large angular motion in the beam with a broad band noise source applied to an electrode in the vacuum chamber. Note the non-symmetric modulation characteristic of the angular spread as opposed to the symmetric modulation observed in the case of a dominant energy spread (Fig. 4)

attributed entirely to the energy spread in this case for two reasons. All the other contributions are predicted to be negligible as we will see in the next two sections, and the deduced energy spread [5], namely

$$\frac{\sigma_\gamma}{\gamma} = \frac{1}{4\pi(N+N_d)}\sqrt{-2\log f} = 1.2 \times 10^{-3}$$

is consistent with the value $1.4 \times 10^{-3} \pm 0.2$ predicted from the measured bunch length assuming constant synchrotron frequency.

The theory also predicts that for a Gaussian energy spread $f \sim \exp(-\sigma^2/2)$ with $\sigma \propto 1/\lambda$. Calculating for the eleven largest fine structure peaks one verifies the proportionality of σ versus $1/\lambda$ with a correlation coefficient of 0.95. Such a test is not powerful since $1/\lambda$ does not change much inside the bandwidth of the fundamental.

We have also measured f and deduced σ for the first three harmonics recorded at the same energy, current and gap. This data can be used for a more precise check of the λ dependence. Table 4 summarizes the measurements after deconvolution from the monochromator response.

In Table 4 the measured σ is compared to the predicted values from three different energy distribution shapes all normalized the fundamental. We observe a good agreement with the Gaussian energy spread predicted from storage ring theory [9]. The accuracy of this test on the energy distribution depends on the assumption that for a monoenergetic filament beam the modulation rate f is equal to 1. Residual modulation can be produced either by field errors in the OK, or an error in the pinhole positioning with respect to the mirror focal point. We have measured a 0.935 modulation depth at very low current, subtracted all

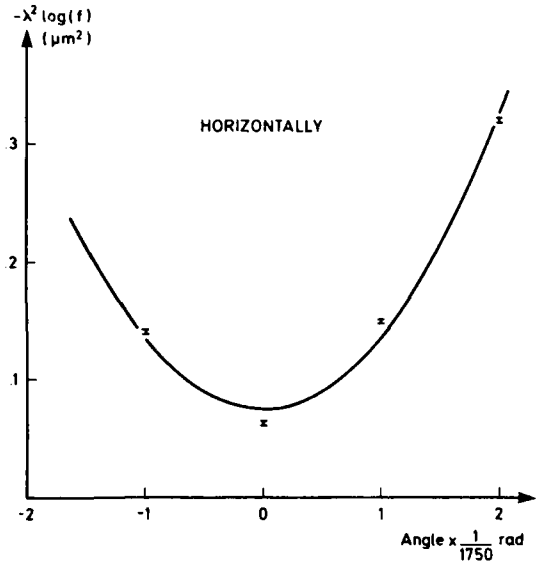

Fig. 6. Effect on the modulation rate of the horizontal angle of observation with respect to the electron trajectory axis. The curve plotted is the least squares fit of $-\lambda^2 \log$ (mdulation rate) to a second order polynomial of the angle. The fit gives the horizontal angular spread σ_θ 0.12 ± 0.01 mrad

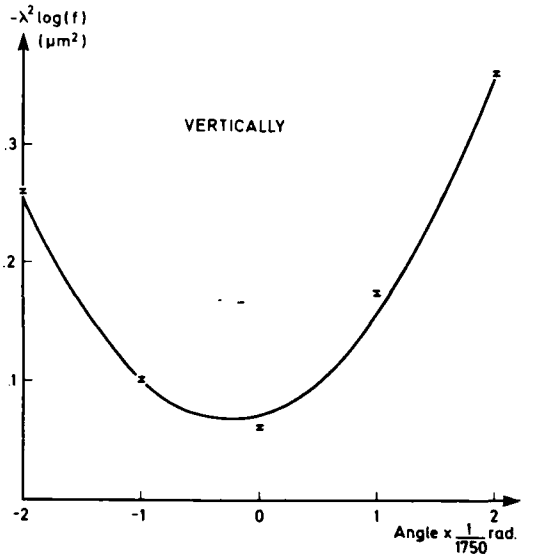

Fig. 7. Effect on the measured modulation rate of the vertical angle of observation with respect to the electron trajectory axis. The fit gives the vertical angular spread $\sigma_\theta = 0.12 \pm 0.005$ mrad

where σ_x and σ_y are the horizontal and vertical rms transverse spreads. Q_x and Q_y are coefficients connected to the field gradients in the dispersive section. They only depend on the field geometry and are equal to zero if the field is exactly uniform. $Q_y \cong 3.4 \times 10^{-4}\,\text{mm}^{-2}$ was deduced from field measurement; this value is just 10% lower than anticipated from the field calculation. These calculations also predicted $Q_x \cong 8.4 \times 10^{-5}\,\text{mm}^{-2}$, a value which has been roughly confirmed by the field measurements. Taking $\sigma_x = \sigma_y = 0.35$ mm (low current) and $\sigma_x = \sigma_y = 0.5$ mm (30 mA of current at 240 MeV) on has $f = 0.9985$ (low current) to $f = 0.997$ (high current). Such a tiny effect was covered experimentally by the energy spread and the angular spread. In some cases, verification may by possible by injecting the electron beam at a distance (x_0, y_0) from the dispersive section axis. Equation (12) still applies if one replaces $\sigma_x^4(\sigma_y^4)$ by $\sigma_x^4 + 2x_0^2\sigma_x^2$ $(\sigma_y^4 + 2y_0^2\sigma_y^2)$. Such an experiment was not possible on ACO because of the change in the beam focussing which would have occurred at the same time. The modulation rate only depends weakly on the injection point in the dispersive section. As in previous subsection one can define the apertures: horizontal aperture: ± 20 mm; vertical aperture: ± 4.7 mm.

2.3. Harmonics

Figures 8 and 9 show the second and third harmonics recorded at 240 MeV and a gap of 32.60 mm at 0.3 mA and 5 mA of current, respectively. As for a regular undulator, an ideal optical klystron does not emit any 2nd harmonic on axis and in fact, the measured peak intensity in Fig. 8 was only 8% of that of the fundamental. This residual intensity is due to the trajectory effect of the fringing fields of the two adjacent bending magnets of ACO. The third harmonic has a shape similar to the first harmonic. Fitting for N to the envelope curve of (3) gives $N = 3.8$ instead of 7. We know from the 3rd harmonic measurements on the 17 periods undulator that inhomogeneous effects are not responsible for this broadening [3]. The dispersive section must therefore be responsible for this effect either via an imperfect compensation or through a destructive interference introduced by the dispersive section at the undulator wavelength.

2.4. Dispersive Section Spontaneous Emission

The dispersive section is equivalent to a three pole wiggler and therefore, has a broad emission spectrum. If one is just interested in the FEL gain improvement, one can ignore the dispersive section intrinsi emission. However, apart from the OK fringes present across all the spectra we have observed (0.2 to 0.7 μm) and apart from the broadening or narrowing of the emission curves (which we have already discussed), there are some unique features which appear in the spontaneous

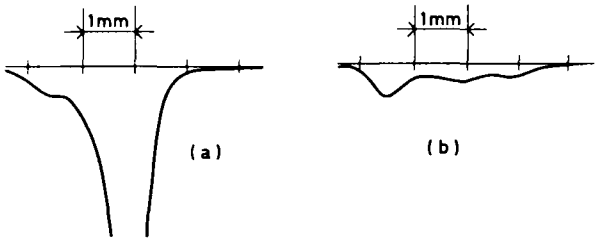

Fig. 11a and b. Transverse horizontal beam profiles of the light emitted by the electrons in the optical klystron. In (a) the interference filter center wavelength falls inside the undulator fundamental resonance; the peak is mainly due to the emission by electrons in the two undulators. The left hand shoulder is mainly due to the emission in the dispersive section. It is still present in (b) where the gap was decreased to suppress completely the undulator emission

and not in the vertical. The peak of Fig. 11b shows maximum definition when the CCD is positioned in the image plane of the dispersive section. This peak corresponds to light emitted from a source displaced about 1.5 mm from the undulator axis as compared to the theoretical 2 mm off axis excursion of the electrons in the dispersive section.

Optical Klystron Emission at Large Gap. At large gap the undulator field vanishes exponentially, much faster than the dispersive section field. The usual coloured ring [7, 6, 2] due to the interference of light from the undulator periods vanish. However one still sees a double interference structure centered about the undulator axis. A black and white reproduction is given in Fig. 13 for the gap series {142, 121, 182 mm} at 240 MeV. The dispersive section maximum field is {660, 1150, 1570 Gauss}, more than 20 times larger than the undulator peak field. This emission is not due to the undulator but is produced by the dispersive section with some contribution from the storage ring bending magnets fringe field.

The emission produced in the dispersive section is contained within the maximal tangent directions labeled A and B in Fig. 12a. At large distances the radiation pattern is symmetric about the axis 0. Schematically, due to the small $1/\gamma$ emission cone, an observer in the electron orbit plane between 0 and A will see the emission of the $t_1 - t_2$ part of trajectory shown in Fig. 12b. In the θ direction with respect to A, the emission is mainly due to small regions around tangent points t_1 and t_2 where the curvature is important (between t_1 and t_2 the curvature is very small and the emission of this part of trajectory can be neglected). Both points sources t_1 and t_2 interfere constructively when the difference in electron and photon transit times is an integral number of optical

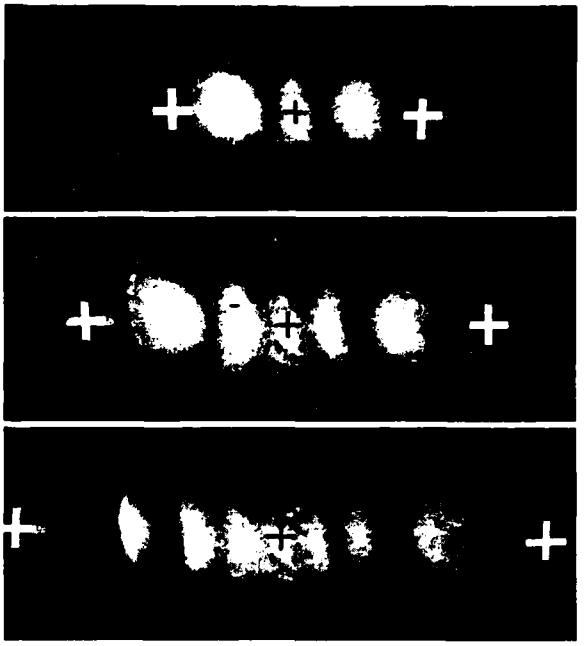

Fig. 13. Three photographs filtered at 5500 Å of the interference structure produced in the optical klystron at large gap. From top to bottom, the magnetic field is increased by closing the gap. The beam axis is marked by the black cross at the center of each pattern, and the points A and B calculated from the magnetic field strength in the OK are marked with white crosses

periods:

$$n\frac{\lambda}{c} = \int_{t_2}^{t_1} \frac{\delta s}{\beta c} - \frac{d}{c} \cong \frac{d}{2c\gamma^2}(1+\gamma^2\theta^2), \tag{13}$$

where d is practically half of dispersive section length and n is an integer.

For monochromatic light the interference maxima occur at a constant angle θ tracing out circles around A in the observation plane. Of course, the circles are incomplete because the angle of emission goes outside the electrons $1/\gamma$ forward cone, where the intensity drops to zero. The same interference pattern occurs around B direction, and one sees a double colored interference structure centered on A and B directions as illustrated in Fig. 13, for $\lambda = 5500$ Å and $E = 240$ MeV. Positions in fringe are in a rather good agreement with theoretical values calculated from (13), where $d \cong 8$ to 10 cm, the angle of A direction being 3.6 mrad, 6 mrad and 7.9 mrad, respectively, for each photographs.

Patterns like Fig. 13 have been recorded at 240, 540 MeV, and several different gaps. As the magnetic field in the dispersive section is increased by reducing the gap, the A–B angle increases, and more interference bands become visible. At small gap, the usual

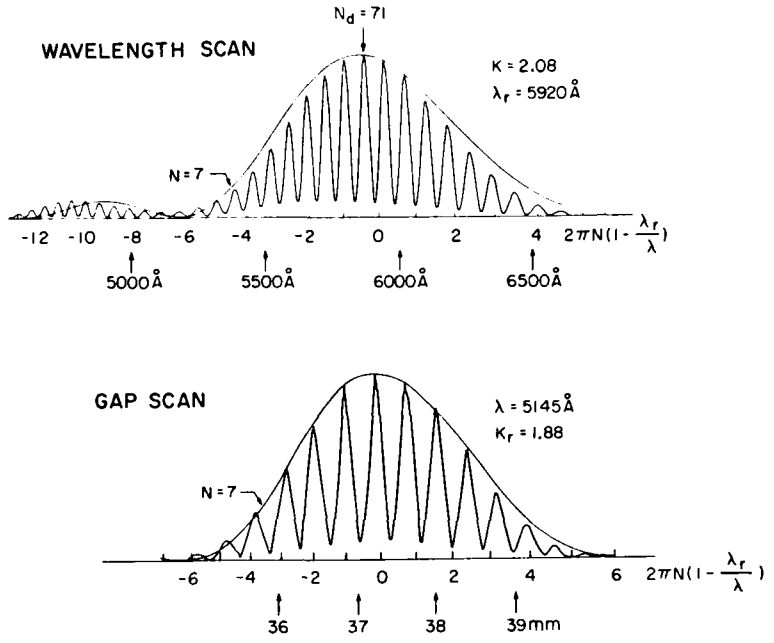

Fig. 15. The spontaneous emission spectrum as a function of wavelength and undulator gap or magnetic field are compared. The rapidly oscillating measured curves fit well into the theoretically calculated envelope curves with some small deviations in the case of the wavelength scan. The slower dependence of the dispersion parameter N_d on gap is visible in the lower curve. The gain as a function of gap is approximately the derivative of the gap scan, not the wavelength scan

where G_{ok}/G_{17} is the OK gain improvement with respect to the original 17 period undulator for a *monoenergetic filament beam*. It is given by (4); see also Table 3.

As before, f is the modulation rate and $\hat{G}_{17}$ is the 17 period undulator peak gain which is equal to [17]

$$\hat{G}_{17} = 1.5 \times 10^{-12} \frac{\lambda_0^2 N^3}{\gamma^3} K^2 [JJ]^2 \varrho_e F_f , \tag{15}$$

where λ_0 is the undulator period in cm, $[JJ]^2$ is the Bessel function factor [13]. $K = eB\lambda_0/2\pi mc$ is the peak field magnetic parameter, ϱ_e the peak electron density in cm ^{3}, and F_f is the filling factor which can be calculated from the overlap integral between the electron and laser beams. For coaxial weakly diverging beams [14].

$$F_f = \frac{1}{\sqrt{\left[1+\left(\frac{w_0}{2\sigma_h}\right)^2\right]\left[1+\left(\frac{w_0}{2\sigma_v}\right)^2\right]}}, \tag{16}$$

where w_0 is the laser beam waist and σ_h and σ_v the electron beam transverse rms sizes.

The theoretical peak gain predicted for the measurement shown on Fig. 14 is

$$(\hat{G}_{ok})_{th} = 4.0(\hat{G}_{17})_{th} = 6.6 \times 10^{-4} \pm 30\% \tag{17}$$

with $G_{OK}/G_{17} = 5.9$ (Table 3), $f = 0.67$ (measured on the spontaneous emission) and $(\hat{G}_{17})_{th}$ calculated from (15, 16). The 30% error bars originate primarily from the uncertainty in the β functions in the undulator. The measured peak gain is (Fig. 14):

$$(\hat{G}_{ok})_{meas} = 7\ 10^{-4}(\pm 0.3). \tag{18}$$

The agreement between the theoretically predicted (17) and measured (18) values is remarkably good, and certainly the best achieved to date. This was made possible by improvements in the alignment technique, and by thorough characterisation of the laser mode. Not only does the values of he gain reported here confirm the validity of the theory, but it also represents a large increase over the gain measured with the undulator NOEL.

4. Bunch Lengthening

Bunch lengthening experiments have been performed by superposing an argon laser colinear with the electron beam inside the optical klystron. The experimental set up has already been described [10, 3], good agreement was observed with stochastic heating models [15] at very low current while high current regimes are dominated by anomalous bunch lengthening effects. Figure 16 shows the bunch lengthening and spontaneous emission produced by the optical klystron. The vertical line indicates an undulator parameter K of 1.92. The results are in good agreement with the theorem demonstrated by Madey that the mean squared energy spread is proportional to the spontaneous power spectrum [8].

10. K.E. Robinson, D.A.G. Deacon, M.F. Velghe, J.M.J. Madey: IEEE J. QE-**19**, 365 (1983)
11. M.M. Nikitin, A.F. Medvedev, M.B. Moiseev: Sov. Tech. Phys. Lett. **5**, 347 (1979)
12. D.A.G. Deacon, J.M.J. Madey, K.E. Robinson, C. Bazin, M. Billardon, P. Elleaume, Y. Farge, J.M. Ortega, Y. Petroff, M. Velghe: IEEE Trans. NS-**28**, 3142 (1981)
13. D.A.G. Deacon, K. Robinson, J.M.J. Madey, C. Bazin, M. Billardon, P. Elleaume, Y. Farge, J.M. Ortega, Y. Petroff, M. Velghe: Opt. Commun. **40**, 373 (1982)
14. P. Elleaume, D.A.G. Deacon: Appl. Phys. B**33**, 9 (1984)
15. A. Renieri: IEEE Trans. NS-**26**, 3827 (1979).
    L.R. Elias, J.M.J. Madey, T.I. Smith: Appl. Phys. **23**, (1980)
    C. Pellegrini: IEEE Trans. NS-**26**, 3791 (1979)
    D.A.G. Deacon: Appl. Phys. **19**, 97 (1979)
16. J. Schwinger: Phys. Rev. **75**, 1912 (1949). The calculations are well detailed by J.D. Jackson, *Classical Electrodynamics*, 2nd ed. (Wiley, New York 1900) Chap. 14
17. W.B. Colson: Ph. D. Thesis, Standford University (1977)
18. M. Billardon, P. Elleaume, J.M. Ortega, C. Bazin, M. Bergher, M. Velghe, Y. Petroff, D.A.G. Deacon, K.E. Robinson, J.M.J. Madey: Phys. Rev. Lett. **51**, 1652 (1983)

Observation of the Diffraction Induced Violation of the Madey Theorem

David A. G. Deacon and Ming Xie[1]

Deacon Research, 754 Duncardine Way, Sunnyvale, CA 94087

1. High Energy Physics Lab, Stanford CA 94305

ABSTRACT

We have simultaneously measured [1] the spectra of the gain and the forward spontaneous radiation in the Orsay free electron laser so that we can extract the relative shift of these two curves. Our results are in agreement with the Madey theorem in the low divergence limit, and demonstrate the violation of the theorem produced as the Rayleigh range of the wave becomes comparable to or smaller than the length of the interaction region.

December 1984

Presented at
1984 Castelgandolfo FEL conference
September 1984

Introduction

The Madey theorem [2] has proved to be a valuable guide to research with free electron lasers. We will consider the form of the theorem with greatest experimental value: the gain spectrum is related to the derivative of the forward spontaneous emission spectrum.

$$G(\gamma) = - \frac{2\pi\rho\lambda^2 F_f}{mc} \frac{d}{d\gamma}\left\{\frac{dW(\gamma)}{d\Omega d\omega}\right\} \qquad (1)$$

The Madey theorem simplifies the calculation of the gain and the induced energy spread in an arbitrary magnetic structure [2,3,4], and shows that the easily measured spontaneous spectrum is a reliable diagnostic of the small signal gain [5], which is a difficult quantity to measure. In view of the value of this theorem, it is important to identify its limitations and where possible confirm them experimentally.

The derivations of the theorem [2,3,6,7,8] all assume low gain, an unsaturated electron-photon interaction, and a plane wave electromagnetic field. We have shown experimentally [9] that the theorem is obeyed when the above conditions are satisfied. A number of authors (see for example references [10], and [11]) have derived the theoretical result that the gain spectrum distorts as the saturated or the high gain regime is approached, although these results have not been experimentally confirmed.

Two papers, [12] and [13], have analyzed the effects on the small signal gain of a divergent optical wave, and found two deviations from the Madey theorem result: a shift of the gain curve combined with a distortion of the spectrum for large enough optical divergence. This paper summarizes the results of the first measurement [1] of the shift in resonance parameter between the gain spectrum observed on a diverging wave and the forward spontaneous spectrum.

To first approximation, the effect of the divergence of the wave is that a phase shift appears on axis as the wave passes through its focus. The part of this phase which is linear in z produces a local change in the wavelength of the probe beam which shifts the spectrum of the gain with respect to the Madey result. The nonlinear part of the phase shift distorts the shape of the curve. For large divergence, the gain curve has no simple relation to the spontaneous spectrum; the Madey theorem is maximally violated. We have been able to measure the resonance shift induced by a moderately divergent Gaussian TEM_{00} mode under conditions where the quadratic and higher order terms in the phase shift are negligible.

We have found the spontaneous and the gain spectra for the optical klystron including the effects of the divergence of the wave and the finite size of the electron beam in [1]. Using the notation of Elleaume [14],

$$\frac{d^2W}{d\Omega d\omega} \propto 1 + \cos\alpha$$
$$G \propto -\sin(\alpha+2\pi s) \qquad (2)$$

where the shift in the resonance parameter $2\pi s$ is defined in terms of the lengths of the first undulator L and the dispersive section d, the Rayleigh range z_0, and the standard filling factor F_f [16]

$$2\pi s \equiv \frac{L+d}{z_0} - \tan^{-1}\chi$$
$$\chi \equiv \frac{L+d}{2z_0} F_f \qquad (3)$$

The gain and spontaneous spectra are measured as a function of gap through filters of different wavelengths. If we define δg as the absolute shift of a gain peak from its corresponding spontaneous peak, and Δg as the local peak to peak change in the gap, the relative fringe shift $\delta g/\Delta g$ is

$$\frac{\delta g}{\Delta g} = \frac{1}{4} + s + (N+N_d)\frac{\delta\lambda}{\lambda} \qquad (4)$$

The first term of this expression is the Madey theorem result. The two terms included in the shift s are the on-axis phase shift and the correction term due to the reduced phase shift of the off-axis electrons. The last includes the effect of the different measurement wavelengths for the two spectra.

The Experiment

The principal difficulty in measuring the resonance shift of the spontaneous and the gain spectra is the small size of the effect compared to the 1/2N relative width of the spectra. The shift of an optimized TEM_{00} mode is difficult to identify in the presence of measurement noise. This difficulty is alleviated if the experiment is done with an optical klystron since the fine structure introduced onto the spectra increase the precision of the measurement. Our experiment was done with the optical klystron modification [17] of the undulator NOEL.

The measurement of the gain [18] requires the alignment of an external laser coaxial with the electron beam. It is preferable to measure the spontaneous spectrum simultaneously in order to eliminate the various sources of drift in the experiment. However, the laser beam which emerges perfectly aligned with the spontaneous radiation must be filtered out [1] to allow the variations in the weak spontaneous power to be observed. This is done by shifting the analyzing monochrometer away from the laser wavelength. Although the difference in wavelength will introduce another term in the resonance shift of the spectra, the effect of this extra term can be subtracted during the analysis of the data.

The resonance shift was measured for two values of the

probe laser beam divergence. The first experiment was performed after focussing the laser into the center of the optical klystron with a moderately large divergence characterized by the Rayleigh range $z_0 \equiv \pi w_0^2/\lambda = 1.1 \pm .1$ m. For the second experiment, the laser mode was configured essentially as a plane wave with a considerably smaller divergence and a Rayleigh range $z_0 = 2.3 \pm .1$ m.

For each scan the resonance shift is determined from the locations of the peaks and the valleys by multiple linear regression to two parallel lines in gap vs. peak number. The shift is normalized as in (4) to the mean peak separation. In the high divergence experiment, four scans were taken, two at 5130 Å which showed a shift of .09 and .11, and two at 5160 Å with a shift of .65, and .66. The mean of these values, and therefore the shift at the laser wavelength 5145 Å, is .38 ± .01. The theoretical value for this divergence is .32 ± .02, which is composed of the following parts: .32 = .25 (Madey Theorem) + .11 ± .01 (on axis divergence effect) - .04 ± .01 (finite beam size correction of divergence effect), where the divergence effects are calculated using the measured values of the electron beam size $\sigma \simeq 320\ \mu$ ± 20%. The agreement between the theoretical prediction and the experimental value is reasonably close (see the discussion of the systematic error below).

The wavelength detuning induced resonance shift which

MEASURED resonance parameter shift	THEORETICAL result	$(N+N_d)\frac{\delta\lambda}{\lambda}$	$\frac{L+d}{2\pi z_0}$	$\frac{-1}{2\pi}\tan^{-1}\frac{L+d}{2z_0}\bar{r}_f$	z_0	σ
.38 { .10	.32 { .05	=.25 -.27 (5130Å)	+.11	-.04	1.1 m	320 μ
.38 { .66	.32 { .59	=.25 +.27 (5160Å)	+.11	-.04	1.1 m	320 μ
.09	.13	=.25 -.15 (5137Å)	+.05	-.02	2.3 m	350 μ

Table I

appears in the above data is $\delta s = 1.8\times10^{-2}\delta\lambda$. This is identical to the value deduced theoretically from the measured value of $N_d = 90$: $\delta s = (N+N_d)\delta\lambda/\lambda = 1.9\times10^{-2}\delta\lambda \pm 5\%$.

In the low divergence experiment, four successive measurements were taken at one wavelength detuning. The mean value of the measured shift is .09 ± .01. This is to be compared to a theoretical value of .13 ± .02 = .25 - .15 ± .01 (wavelength detuning) + .05 ± .01 (divergence effect) -.02 (beam size correction) where the electron beam size is $\sigma \simeq 350\ \mu \pm 20\%$.

The small deviations from the theory in the above results are significant at two standard deviations, and arise from some systematic effect. We think the problem arises from the imperfect

characterization of the phase front curvature of the probe laser beam. The Strehl ratio was found to be $S \simeq .9$ by measuring the laser beam waist at several positions. Since a light beam is considered diffraction limited for $S \geq .8$, this beam is of very high quality. The RMS wavefront deviation σ_w is given from the Strehl ratio, for small σ_w/λ, by [19]

$$2\pi\frac{\sigma_w}{\lambda} = \sqrt{1-S} \tag{5}$$

which yields $\sigma_w/\lambda \simeq .05$ in our case. The actual evolution of the electromagnetic phase along the trajectory of an electron therefore contains an additional component due to the evolution of the wavefront distortion. If the laser beam is not too badly aberrated, the phase front distortion is slowly varying in the transverse dimensions, and all electrons see approximately the same effect. We expect under these circumstances that the optical wave will shift phase by an additional amount on the order of equation (5) as the probe beam goes through its focus, which means that the shift s in (3) contains an unknown additional component on the order of $\pm\sigma_w/\lambda$. This sets a fundamental linit on the precision of this type of experiment. The errors observed between the theoretical and experimental values of Table I are on the order of .05, in agreement with our hypothesis.

Although the high divergence maximal violation of the Madey theorem has been beyond our reach for this experiment, we have

been able to observe the linear resonance shift which occurs like a warning signal just before the strong distortion of the gain curve. We have shown experimentally that the Madey theorem is violated for divergent optical modes.

Acknowledgements

The authors are pleased to thank Pascal Elleaume, Olive Lee-Deacon, John Madey, and Michel Velghe for their experimental assistance and valuable suggestions during the execution of this work.

This work was performed by Deacon Research under contract to Stanford University and to the Air Force Office of Scientific Research, contract number F 49620-80-C-0068.

References

1.) D. A. G. Deacon, M. Xie, "Measurement of the Violation of the Madey Theorem Induced by a Diverging Wave", to be published in IEEE Journ. Quant. Elect., July (1985).

2.) J. M. J. Madey, "Relationship between mean radiated energy, mean squared radiated energy and spontaneous power spectrum in a power series expansion of the equations of motion in a free electron laser", Il Nuovo Cimento 50B, 64-88 (1979).

3.) N. M. Kroll, P. L. Morton, M. N. Rosenbluth, Appendix 1, "Free electron lasers with variable parameter wigglers", IEEE J. Quant. Elect. QE-17, 1436-1468 (1981).

4.) L. Grover, R. H. Pantell, "Simplified Analysis of free electron lasers using Madey's theorem", to be published; L. K. Grover, PhD thesis, Electrical Engineering Department, Stanford University, Dec. 1984.

5.) J. M. Ortega, C. Bazin, D. A. G. Deacon, "Optimization of a permanent magnet undulator for free electron laser studies on the ACO storage ring", J. Appl. Phys. 54, 4776-4783 (1983), shows that the gain produced in an undulator with a "perfect" spontaneous emission spectrum is also perfectly in agreement with the theory. The opposite situation in which

AD-A164 192 STORAGE RING TECHNOLOGY FOR FREE ELECTRON LASERS(U) 2/3
STANFORD UNIV CA J M MADEY ET AL. APR 84
AFOSR-TR-85-1223 F49620-83-K-0030

UNCLASSIFIED F/G 20/5 NL

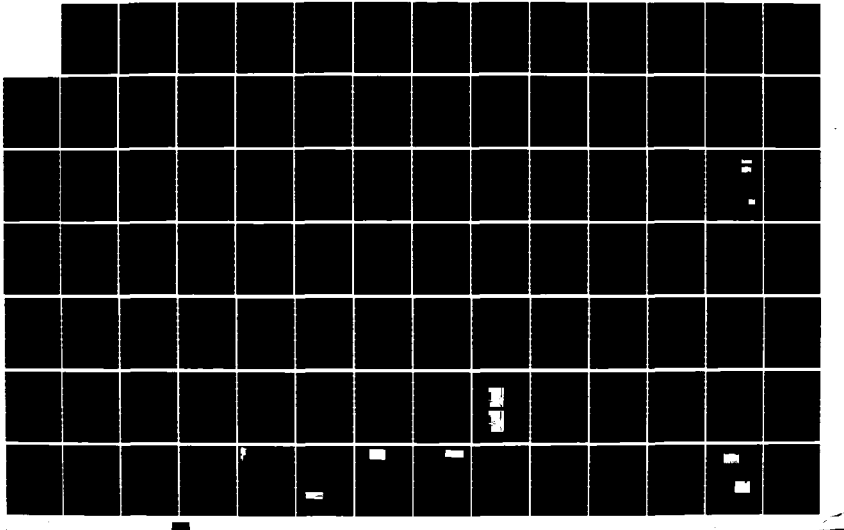

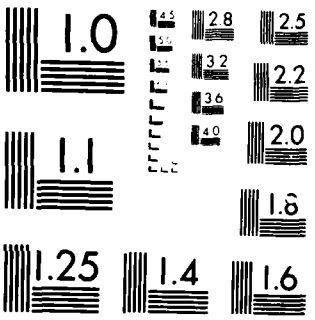

References

1.) D. A. G. Deacon, M. Xie, "Measurement of the Violation of the Madey Theorem Induced by a Diverging Wave", to be published in IEEE Journ. Quant. Elect., July (1985).

2.) J. M. J. Madey, "Relationship between mean radiated energy, mean squared radiated energy and spontaneous power spectrum in a power series expansion of the equations of motion in a free electron laser", Il Nuovo Cimento 50B, 64-88 (1979).

3.) N. M. Kroll, P. L. Morton, M. N. Rosenbluth, Appendix 1, "Free electron lasers with variable parameter wigglers", IEEE J. Quant. Elect. QE-17, 1436-1468 (1981).

4.) L. Grover, R. H. Pantell, "Simplified Analysis of free electron lasers using Madey's theorem", to be published; L. K. Grover, PhD thesis, Electrical Engineering Department, Stanford University, Dec. 1984.

5.) J. M. Ortega, C. Bazin, D. A. G. Deacon, "Optimization of a permanent magnet undulator for free electron laser studies on the ACO storage ring", J. Appl. Phys. 54, 4776-4783 (1983), shows that the gain produced in an undulator with a "perfect" spontaneous emission spectrum is also perfectly in agreement with the theory. The opposite situation in which

serious distortions exist in the spontaneous emission spectrum is analyzed in reference [9], where the distortions are shown to be mirrored in the gain measurements.

6.) N. M. Kroll, "A note on the Madey gain-spread theorem", in Physics of Quantum Electronics, 8, 315-323 (1982).

7.) S. Krinsky, J. M. Wang, P. Luchini, "Madey's gain-spread theorem for the FEL and the theory of stochastic processes", J. Appl. Phys., 53, 5453-5458 (1982).

8.) P. Elleaume, Appendix A, These du Doctorat d'Etat, (1984) unpublished, Universite de Paris Sud, 91405 Orsay, FRANCE.

9.) D. A. G. Deacon, K. E. Robinson, J. M. J. Madey, C. Bazin, M. Billardon, P. Elleaume, Y. Farge, J. M. Ortega, Y. Petroff, M. F. Velghe, "Gain measurements versus theory for the ACO storage ring laser", Opt. Commun., 40, 373-378 (1982).

10.) C. C. Shih, "Small signal gain spectrum of high gain free electron lasers", in Free electron generators of coherent radiation, SPIE Volume 453, 205-209 (1984).

11.) W. B. Colson, "Optical pulse evolution in the Stanford free electron laser and in a tapered wiggler", in Physics of Quantum Electronics, 8, 457-488 (1982).

12.) W. B. Colson, P. Elleaume, "Electron dynamics in free electron laser resonator modes", Appl. Phys. B29, 101-109 (1982).

13.) P. Luchini, G. Prisco, S. Solimeno, "Optimization of the gain of a free electron laser for a Gaussian beam", in Free Electron Generators of Coherent Radiation, SPIE Volume 453, 83-288 (1984).

14.) P. Elleaume, "Optical Klystrons", Journ. de Physique Colloque, 44, C1-333 - C1-352 (1983).

15.) C. Bazin, M.Billardon, D.A.G.Deacon, P. Elleaume, Y. Farge, J. M. J. Madey, J. M. Ortega, Y. Petroff, K. E. Robinson, M. Velghe, "Results of the first phase of the ACO storage ring laser experiment", in Physics of Quantum Electronics, 8, 89-118 (1982).

16.) P. Elleaume and D. A. G. Deacon, Appl. Phys. B33, 9-16 (1984).

17.) D. A. G. Deacon, M. Billardon, P. Elleaume, J. M. Ortega, K. E. Robinson, C. Bazin, M. Bergher, M. Velghe, J. M. J. Madey, Y. Petroff, "Optical Klystron Experiments for the ACO storage ring free electron laser", Appl. Phys. B34, 207-219 (1984).

18.) D. A. G. Deacon, J. M. J. Madey, K. E. Robinson, C. Bazin, M. Billardon, P. Elleaume, Y. Farge, J. M. Ortega, Y. Petroff, M. F. Velghe, "Gain measurement on the ACO storage ring laser", IEEE Trans. Nucl. Sci. NS-28, 3142-3144 (1981).

19.) M. Born and E. Wolf, Section 9.1, Principles of Optics, Pergamon Press (1975).

Measurement of the Violation of the Madey Theorem Induced by a Diverging Wave

David A. G. Deacon and Ming Xie[1]

Deacon Research, 900 Welch Road Suite 203, Palo Alto, CA 94304

1. High Energy Physics Lab, Stanford CA 94305

ABSTRACT

We have simultaneously measured the spectra of the gain and the forward spontaneous radiation in the Orsay free electron laser so that we can extract the relative shift of these two curves. Our results are in agreement with the Madey theorem in the low divergence limit, and demonstrate the violation of the theorem produced as the Rayleigh range of the wave becomes comparable to or smaller than the length of the interaction region. We extend the single particle theory to account for the divergence of the wave to first order. The predictions from this linearized model are in reasonable agreement with the experimental results in view of the fundamental limitations on this kind of experiment.

November 1984

To be published in:
IEEE Journal of Quantum Electronics
Special Issue on Free Electron Lasers, July 1985

Introduction

The Madey theorem [1] has proved to be a valuable guide to research with free electron lasers. Although the theorem can be divided into two parts and used in different contexts, we will consider the form of the theorem with greatest experimental value: the gain spectrum is related to the derivative of the forward spontaneous emission spectrum.

$$G(\gamma) = -\frac{2\pi e\lambda^2 F_f}{mc}\,\frac{d}{d\gamma}\left(\frac{d^2W(\gamma)}{d\Omega d\omega}\right) \qquad (1)$$

where $dW(\gamma)/d\Omega d\omega$ is the energy radiated per unit frequency interval per unit solid angle in the forward direction by one electron in a pass through a linearly polarized magnetic structure. The Madey theorem simplifies the calculation of the gain and the induced energy spread in an arbitrary magnetic structure [1,2,3], and shows that the easily measured spontaneous spectrum is a reliable diagnostic of the small signal gain [4], which is a difficult quantity to measure. In view of the value of this theorem, it is important to identify its limitations and where possible confirm them experimentally.

The derivations of the theorem [1,2,5,6,7] all assume low gain, an unsaturated electron-photon interaction, and a plane wave electromagnetic field. We have shown experimentally [8] that the theorem is obeyed when the above conditions are satisfied. A

number of authors (see for example references [9], and [10]) have derived the theoretical result that the gain spectrum distorts as the saturated or the high gain regime is approached, although these results have not been experimentally confirmed. Two papers, [11] and [12], have analyzed the effects on the small signal gain of a divergent optical wave, and found two deviations from the Madey theorem result: a shift of the gain curve, and a distortion of the spectrum for large enough optical divergence. Our paper reports the results of the first measurement of the shift in resonance parameter between the gain spectrum observed on a diverging wave and the forward spontaneous spectrum. Since the date of this work, the effects of divergence on the spectrum of the Orsay oscillator have also been observed and reported [13,7]. This latter work, however, suffers from the difficulty that the input mode content is not measurable so that a numerical comparison with the theory is not possible.

To first approximation, the effect of the divergence of the wave is that a phase shift appears on axis as the wave passes through its focus. The part of this phase which is linear in z produces a local change in the wavelength of the probe beam which shifts the spectrum of the gain with respect to the Madey result. The nonlinear part of the phase shift distorts the shape of the curve. For large divergence, the gain curve has no simple relation to the spontaneous spectrum; the Madey theorem is maximally violated. We have been able to measure the resonance

shift induced by a moderately divergent Gaussian TEM$_{00}$ mode under conditions where the quadratic and higher order terms in the phase shift are negligible.

The Linearized Theory

The forward spontaneous emission spectrum of an optical klystron with two identical undulators has been derived by Elleaume [14]

$$\frac{d^2W}{d\Omega d\omega}(O.K.) = 2\,\frac{d^2W}{d\Omega d\omega}(One\ Undulator)\times[1+\cos\alpha]$$

$$= \frac{N^2[JJ]^2r_e^2e^2K^2}{\theta\gamma^2c\gamma^2}\left[\frac{\sin(\nu/2)}{\nu/2}\right]^2[1+\cos\alpha] \qquad (2)$$

where

$$\nu \equiv L\left[k_0-\frac{k}{2\gamma^2}\left(1+\frac{K^2}{2}\right)\right]$$

$$\alpha \equiv 2\pi(N+N_d)-\nu \qquad (3)$$

$$N_d \equiv \frac{1}{2\gamma^2\lambda}\left(d-\frac{e^2}{m^2c^4}\int_0^d\left[\int_0^z\left[\int_0^z B_d(z)dz\right]dz\right]\right)$$

and where K and [JJ] are defined in [15], L and d are the lengths of one undulator and the dispersive section, ν is known as the resonance parameter, N_d is the number of optical wavelengths which pass over the electron in the dispersive section, N is the number of periods of length $\lambda_0 = 2\pi/k_0$ in one undulator, and B_d is the field in the dispersive section.

In order to find an analytic expression for the gain of a Gaussian mode, we consider the case with $(L+d)/z_0 < 1$, where z_0 is the Rayleigh range. This implies a low divergence optical beam, which is well satisfied in the Orsay experiment. The TEM_{00}

Gaussian mode [16]

$$E(r,z) = E_0 \frac{w_0}{w(z)} \exp\left\{i\left[kz - \tan^{-1}(z/z_0)\right] - r^2\left[\frac{1}{w^2(z)} - \frac{ik}{2R(z)}\right]\right\} \tag{4}$$

reduces to a simpler form in the low divergence limit

$$E(r,z) = E_0 \exp\left\{-\frac{r^2}{w_0^2} - i\left(k - \frac{1}{z_0} + \frac{kr^2}{2z_0^2}\right)z\right\} \tag{5}$$

since

$$w^2(z) = w_0^2\left(1 + \frac{z^2}{z_0^2}\right) \simeq w_0^2$$
$$R(z) = z + \frac{z_0^2}{z} \simeq \frac{z_0^2}{z} \tag{6}$$

We can obtain the gain by calculating the total radiated energy per electron to second order in the fields.

$$\langle \Delta\gamma^{(2)} \rangle = \exp\left(-\frac{2r^2}{w_0^2}\right)\left[\frac{-L^2 N e^2 \chi_0^2 J_0^2 z_0^2}{2m^2c^4\gamma^3}\right]\left\{(1+D)\left[\frac{\sin(\nu'/2)}{\nu'/2}\right]^2 \sin\alpha' + \frac{-4+4\cos\nu'+2\nu'\sin\nu'}{\nu'^2}[1+\cos\alpha']\right\} \tag{7}$$

where

$$D \equiv \frac{N_d}{N}\left(1 - \frac{\nu}{2\pi N}\right)^{-1} \simeq \frac{N_d}{N}$$
$$\nu' \equiv \nu - L\left(\frac{1}{z_0} - \frac{kr^2}{2z_0^2}\right) \tag{8}$$
$$\alpha' \equiv \alpha + (L+d)\left(\frac{1}{z_0} - \frac{kr^2}{2z_0^2}\right)$$

We assume a cold beam and straight line electron trajectories as is the case in the Orsay storage ring FEL, and integrate equation

(7) over the transverse electron distribution, which is assumed to be Gaussian. The gain is

$$G \equiv \frac{\int_0^{\infty}\int_0^{2\pi} -mc^2\langle \Delta\gamma^{(2)}\rangle_b \exp\left(-\frac{r^2}{2\sigma_r^2}\right) r\,dr\,d\theta}{\int_0^{\infty}\int_0^{2\pi} \frac{E_0}{B\rho}\exp\left(-\frac{2r^2}{w_f^2}\right) r\,dr\,d\theta} \tag{9}$$

$$= \frac{2A}{w_f^2}\left\{ \int_0^{\infty}\left[-(1+D)\left\{\frac{\sin(\nu'/2)}{\nu'/2}\right\}^2\right]\sin\alpha'\exp\left[\frac{-2r^2}{w_f^2F_f}\right]dr \right.$$

$$\left. + \int_0^{\infty}\left[\frac{4-4\cos\nu'-2\nu'\sin\nu'}{\nu'^2}\right](1-\cos\alpha')\exp\left[\frac{-2r^2}{w_f^2F_f}\right]dr \right\} \tag{10}$$

where

$$A \equiv \frac{4\pi^2 e^2 N_u^2 w_f^2 [JJ]^2 \eta_b}{mc^2\gamma_r^2} \tag{11}$$

The ν dependent envelope of the integrand varies slowly compared to the rapid oscillation of α'. If these terms are treated as constants and extracted from the integral, the result can be found analytically:

$$G = AF_f\left\{ -(1+D)\left\{\frac{\sin(\nu/2)}{\nu/2}\right\}^2\frac{\sin(\alpha+2\pi s)}{\sqrt{1+\chi^2}} \right.$$

$$\left. - \frac{4-4\cos\nu-2\nu\sin\nu}{\nu^2}\left\{1 - \frac{\cos(\alpha-2\pi s)}{\sqrt{1+\chi^2}}\right\}\right\} \tag{12}$$

where F_f is the standard gain filling factor [17], χ describes the effect of a finite beam size on the phase, and we have defined the shift in the resonance parameter to be $2\pi s$

$$\theta_s \equiv \frac{L+d}{z_0} - \tan^{-1}\chi$$
$$\chi \equiv \frac{L+d}{2z_0} F \qquad (13)$$

Applying the strong optical klystron condition $N_d N >> 1$, and neglecting the small effects of ν and χ on the amplitude, equations (2) and (12) become

$$\frac{d^2W}{d\hat{n}d\omega} \propto 1 - \cos\alpha$$
$$G \propto -\sin(\alpha+2\theta_s) \qquad (14)$$

The weak ν-dependence approximation we made in going from (10) to (12) and to (14) is adequate for our purposes, and we have checked numerically that it gives a value for the phase shift which is different from the exact value by less than 1%. The Madey theorem result is illustrated here if $s = 0$. The linear effect (5) of divergence produces little more than a relative shift of the two curves. If the nonlinear terms in (4) are large, the gain spectrum can become greatly distorted.

The values of the magnetic gap $g_m^{(S)}$ and $g_m^{(G)}$ which occur at the m^{th} maximum of the spontaneous emission and the gain spectra respectively (counting from zero photon energy), satisfy the relations

$$\alpha\left\{g_m^{(S)}\right\} = 2\pi m$$

$$\alpha\left\{(g_m^{(G)}\right\} - 2\pi s = 2\pi m - \frac{\pi}{2} \qquad (15)$$

The gain and spontaneous spectra are measured as a function of gap through filters of different wavelengths. If we define $\delta g \equiv g_m^{(G)} - g_m^{(S)}$ as the absolute shift of a gain peak from its corresponding spontaneous peak, $\Delta g \equiv g_m - g_{m+1}$ as the local peak to peak change in the gap, and $\delta\lambda \equiv \lambda^{(S)} - \lambda^{(G)}$ as the difference in the measurement wavelengths of the spontaneous from the gain spectra, the relative fringe shift $\delta g/\Delta g$ can be found by linearizing equations (15)

$$\frac{\delta g}{\Delta g} = \frac{1}{4} + s + (N+N_d)\,\frac{\delta\lambda}{\lambda} \qquad (16)$$

The first term of this expression is the Madey theorem result. The two terms included in the shift s are the on-axis phase shift produced in a Gaussian mode, and the correction term which accounts for the reduced phase shift experienced by the off-axis electrons. The last term accounts for the fact that the spontaneous and the gain spectra are measured at different wavelengths.

The Experiment

The principal difficulty in measuring the resonance shift of the spontaneous and the gain spectra is the small size of the effect compared to the 1/2N relative width of the spectra. The shift of an optimized TEM_{00} mode is difficult to identify in the presence of measurement noise. This difficulty is alleviated if the experiment is done with an optical klystron since the fine structure introduced onto the spectra increase the precision of the measurement. Our experiment was done with the optical klystron modification [18] of the undulator NOEL.

The comparison of two subsequent scans of the gain or the spontaneous emission spectra is complicated by the number of extraneous parameters which must be held constant, and in principle measured. Small resonance shifts of the spectrum can easily occur if the beam energy changes between scans (the magnet current control shunts are not temperature stabilized on ACO); if the electron orbit changes (due to energy or magnetic focussing or RF frequency drifts); or if there is play in the mechanical gap adjustment system. It is preferable to measure the two spectra simultaneously.

The measurement of the gain [19] requires the alignment of an external laser coaxial with the electron beam. If the spontaneous emission measurement is to be performed

simultaneously, the laser beam emerges perfectly aligned with the spontaneous radiation and may interfere with the measurement of its spectrum. We use spectral filtering (figure 1) to make possible the simultaneous measurements.

A semitransparent mirror splits off some of the radiation for analysis by the gain electronics, which performs its function without modification. The remainder of the light is directed to the spontaneous emission diagnostics [15]. If the monochromator is detuned from the Argon laser line by a sufficient margin, it is possible to filter out the laser light while allowing the variations in the relatively weak spontaneous power to be observed. Although the difference in wavelength will introduce another term in the resonance shift of the spectra, the effect of this extra term can be subtracted during the analysis of the data if the wavelengths are known.

The gain measurement is set up as usual on the 5145 A line of the Argon laser. The monochromator for analyzing the spontaneous radiation is detuned alternately to the short and the long wavelength side. Scans are taken as a function of the magnetic gap, overshooting enough on each side to eliminate mechanical backlash. The data is recorded, the locations of the peaks and the valleys are determined, and the relative shift of the gain spectrum is calculated by a linear regression analysis. Since the wavelength is displaced by the same amount in both

directions, the resonance parameter shift at the laser wavelength can be determined simply as the mean of the two shifts at the displaced wavelengths (see figure 2).

The laser mode matching was performed by measuring the laser mode size at several positions with the aid of a Reticon diode array. Alignment of the electron beam was obtained to a precision of about 80 μm by optimizing the measured gain with the aid of four horizontal and vertical steering coils. The experiment was performed at relatively low currents so that the product of the modulation depth of the spontaneous emission and the signal level of the gain would be a maximum. The electron beam size was also measured with the Reticon. The optical klystron parameter N_d was measured from a wavelength scan of the spontaneous emission at the central value of the magnetic gap. The fringe-to-fringe spacing $\Delta\lambda$ determines this quantity through $N + N_d = \lambda/\Delta\lambda$.

The resonance shift was measured for two values of the probe laser beam divergence. The first experiment was performed after focussing the laser into the center of the optical klystron with a moderately large divergence characterized by the Rayleigh range $z_0 \equiv \pi w_0^2/\lambda = 1.1 \pm .1$ m. For the second experiment, the laser mode was configured essentially as a plane wave with a considerably smaller divergence and a Rayleigh range $z_0 = 2.3 \pm .1$ m.

MEASURED resonance parameter shift	THEORETICAL result	$(N-N_1)\frac{\delta\lambda}{\lambda}$	$\frac{L+d}{2\pi z_0}$	$\frac{-1}{2\pi}\tan^{-1}\frac{L+d}{2z_0}\pi$	z_0	σ
.10	.05	=.25 -.27	+.11	-.04		
.38	.32	(5130Å)			1.1 m	320 μm
.66	.59	=.25 +.27	+.11	-.04		
		(5160Å)				
.09	.13	=.25 -.15	-.06	-.02	2.3 m	350 μm
		(5137Å)				

Table I

For each scan the resonance shift is determined from the locations of the peaks and the valleys by multiple linear regression to two parallel lines in gap vs. peak number. The shift is normalized to the mean peak separation. In the high divergence experiment, four scans were taken, two at 5130 Å which showed a shift of .09 and .11, and two at 5160 Å with a shift of .65, and .66. The mean of these values, and therefore the shift at the laser wavelength 5145 Å, is .38 ± .01. The theoretical value for this divergence is .32 ± .02, which is composed of the following parts: .32 = .25 (Madey Theorem) + .11 ± .01 (on axis divergence effect) - .04 ± .01 (finite beam size correction of divergence effect), where the divergence effects are calculated using the measured values of the electron beam size $\sigma \approx 320$ μm =

20%. The agreement between the theoretical prediction and the experimental value is reasonably close (see the discussion of the systematic error below).

The wavelength detuning induced resonance shift which appears in the above data is $\delta s = 1.8\times10^{-3}\delta\lambda$. This is identical to the value deduced theoretically from the measured value of $N_d = 90$: $\delta s = (N+N_c)\delta\lambda/\lambda = 1.9\times10^{-3}\delta\lambda \pm 5\%$.

In the low divergence experiment, which was performed almost one year following the first measurements, it was no longer possible to take simultaneous measurements. Because of the now large angular fluctuations of the probe laser, the noise level contributed by the laser in the spontaneous measurement completely dominated the spontaneous signal. The best which could be done was to take a series of measurements contiguous in time and alternating between gain and spontaneous emission. Seven such measurements were taken at low stored current so that the beam lifetime would be long. After normalizing for the varying scan rates of the optical klystron magnetic gap, we found that these seven measurements are consistent internally. This indicates that the uncontrolled external drifts were small during the time scale of the measurements, and we have been able to extract reliable information even in a set of non-simultaneous experiments. Although these measurements were taken at only one wavelength detuning, the behavior of the previous results verifies that we

know how to calculate the resonance parameter shift due to a wavelength detuning. Four successive measurements of the shift give a mean of .09 ± .01. This is to be compared to a theoretical value of .13 ± .02 = .25 - .15 ± .01 (wavelength detuning) + .05 ± .01 (divergence effect) -.02 (beam size correction) where the electron beam size is $\sigma \cong 350$ μm ± 20%.

Again, the agreement is reasonable. We note, however, that there is a small deviation of the measurements towards the extremes which may be significant. The high divergence measurements show a slightly larger shift and the low divergance results show a smaller shift than the theory predicts.

These deviations from the theory may be caused by the imperfect characterization of the phase front curvature of the probe laser beam. The Strehl ratio was found to be $S \cong .9$ by measuring the laser beam waist at several positions. Since a light beam is considered diffraction limited for $S \geq .8$, this beam is of very high quality. The RMS wavefront deviation σ_w is given from the Strehl ratio, for small σ_w/λ, by [20]

$$2\pi\frac{\sigma_w}{\lambda} = \sqrt{1-S} \qquad (17)$$

which yields $\sigma_w/\lambda \cong .05$ in our case. The actual evolution of the electromagnetic phase along the trajectory of an electron is then given by (5) with an additional component due to the evolution of

the wavefront distortion. If the laser beam is not too badly distorted, the distortion is slowly varying in the transverse dimensions, and all electrons see approximately the same effect. We expect under these circumstances that the linear part of the distorted component will shift phase by an amount on the order of equation (17) as the probe beam goes through its focus, which means that the shift s in (13) will have an unknown component on the order of $\pi\sigma_w/\lambda$. This sets a fundamental limit on the precision of this type of experiment. Indeed, the errors observed between the theoretical and experimental values of Table I are on the order of .05.

In summary, we have found in this experiment that: a) within the anticipated error bars, the divergence of the optical wave produces a resonance parameter shift of sign and magnitude predicted by the linearized small signal theory; and b) a sufficiently low divergence beam shows no shift, in agreement with the Madey theorem.

Although the high divergence maximal violation of the Madey theorem has been beyond our reach for this experiment, we have been able to observe the linear resonance shift which occurs like a warning signal just before the strong distortion of the gain curve. We have shown experimentally that the Madey theorem is violated for divergent optical modes. Any application of the theorem must test for low divergence $L/z_0 < 1$ (as well as low

gain and no saturation) as a condition of applicability.

Acknowledgement

The authors are pleased to thank Pascal Elleaume, Olive Lee-Deacon, John Madey, and Michel Velghe for their experimental assistance and valuable suggestions during the execution of this work.

This work was performed by Deacon Research under contract to Stanford University and to the Air Force Office of Scientific Research, contract number F 49620-80-C-0068.

Figure Captions

Figure 1 Schematic diagram of the experiment. The gain spectrum [8,19] is measured simultaneously with the forward spontaneous emission spectrum [18]. In the spontaneous measurements, the laser power is filtered out by setting the bandpass of the monochrometer at a wavelength displaced slightly from the Ar^+ line (see Table I).

Figure 2 The gain spectrum shown in the central trace is clearly displaced from the two spontaneous curves. The peak positions of a spontaneous spectrum taken at 5145 Å would fall midway between those of the top and bottom spontaneous curves. The shift of the gain peaks in a low divergence experiment is almost exactly .25 of the fringe spacing as predicted by the Madey theorem, once the wavelength shift is factored out. This figure shows an example of the increase of the shift (to .38) as a result of the violation of the Madey theorem induced by the divergence of the input laser (z_0 = 1.1 m in this case).

References

1.) J. M. J. Madey, "Relationship between mean radiated energy, mean squared radiated energy and spontaneous power spectrum in a power series expansion of the equations of motion in a free electron laser", Il Nuovo Cimento 50B, 64-88 (1979).

2.) N. M. Kroll, P. L. Morton, M. N. Rosenbluth, Appendix 1, "Free electron lasers with variable parameter wigglers", IEEE J. Quant. Elect. QE-17, 1436-1468 (1981).

3.) L. Grover, R. H. Pantell, "Simplified Analysis of free electron lasers using Madey's theorem", to be published; L. K. Grover, PhD thesis, Electrical Engineering Department, Stanford University, Dec. 1984.

4.) J. M. Ortega, C. Bazin, D. A. G. Deacon, "Optimization of a permanent magnet undulator for free electron laser studies on the ACO storage ring", J. Appl. Phys. 54, 4776-4783 (1983), shows that the gain produced in an undulator with a "perfect" spontaneous emission spectrum is also perfectly in agreement with the theory. The opposite situation in which serious distortions exist in the spontaneous emission spectrum is analyzed in reference [3], where the distortions are shown to be mirrored in the gain measurements.

5.) N. M. Kroll, "A note on the Madey gain-spread theorem", in Physics of Quantum Electronics, 8, 315-323 (1982).

6.) S. Krinsky, J. M. Wang, P. Luchini, "Madey's gain-spread theorem for the FEL and the theory of stochastic processes", J. Appl. Phys., 53, 5453-5458 (1982).

7.) P. Elleaume, Appendix A, These du Doctorat d'Etat, (1984) unpublished, Universite de Paris Sud, 91405 Orsay, FRANCE.

8.) D. A. G. Deacon, K. E. Robinson, J. M. J. Madey, C. Bazin, M. Billardon, P. Elleaume, Y. Farge, J. M. Ortega, Y. Petroff, M. F. Velghe, "Gain measurements versus theory for the ACO storage ring laser", Opt. Commun., 40, 373-378 (1982).

9.) C. C. Shih, "Small signal gain spectrum of high gain free electron lasers", in Free electron generators of coherent radiation, SPIE Volume 453, 205-209 (1984).

10.) W. B. Colson, "Optical pulse evolution in the Stanford free electron laser and in a tapered wiggler", in Physics of Quantum Electronics, 6, 457-468 (1982).

11.) W. B. Colson, P. Elleaume, "Electron dynamics in free electron laser resonator modes", Appl. Phys. B29, 101-109 (1982).

12.) P. Luchini, G. Prisco, S. Solimeno, "Optimination of the gain of a free electron laser for a Gaussian beam", in Free Electron Generators of Coherent Radiation, SPIE Volume 453, 83-288 (1984).

13.) P. Elleaume, J. M. Ortega, M. Billardon, C. Bazin, M. Bergher, M. Velghe, Y. Petroff, D. A. G. Deacon, K. E. Robinson, J. M. J. Madey, "Results of the free electron laser oscillation experiments on the ACO storage ring", J. Physique 45, 989-996 (1984).

14.) P. Elleaume, "Optical Klystrons", Journ. de Physique Colloque, 44, C1-333 - C1-352 (1983).

15.) C. Bazin, M.Billardon, D.A.G.Deacon, P. Elleaume, Y. Farge, J. M. J. Madey, J. M. Ortega, Y. Petroff, K. E. Robinson, M. Velghe, "Results of the first phase of the ACO storage ring laser experiment", in Physics of Quantum Electronics, 8, 89-118 (1982).

16.) A. Yariv, Chapter 6.6, Quantum Electronics, J. Wiley and Sons (1975).

17.) P. Elleaume and D. A. G. Deacon, Appl. Phys. B33, 9-16 (1984).

18.) D. A. G. Deacon, M. Billardon, P. Elleaume, J. M. Ortega, K. E. Robinson, C. Bazin, M. Bergher, M. Velghe, J. M. J. Madey, Y. Petroff, "Optical Klystron Experiments for the ACO storage ring free electron laser", Appl. Phys. B34, 207-219 (1984).

19.) D. A. G. Deacon, J. M. J. Madey, K. E. Robinson, C. Bazin, M. Billardon, P. Elleaume, Y. Farge, J. M. Ortega, Y. Petroff, M. J. Velghe, "Gain measurement on the ACO storage ring laser", IEEE Trans. Nucl. Sci. NS-28, 3142-3144 (1981).

20.) M. Born and E. Wolf, Section 9.1, Principles of Optics, Pergamon Press (1975).

5311-2

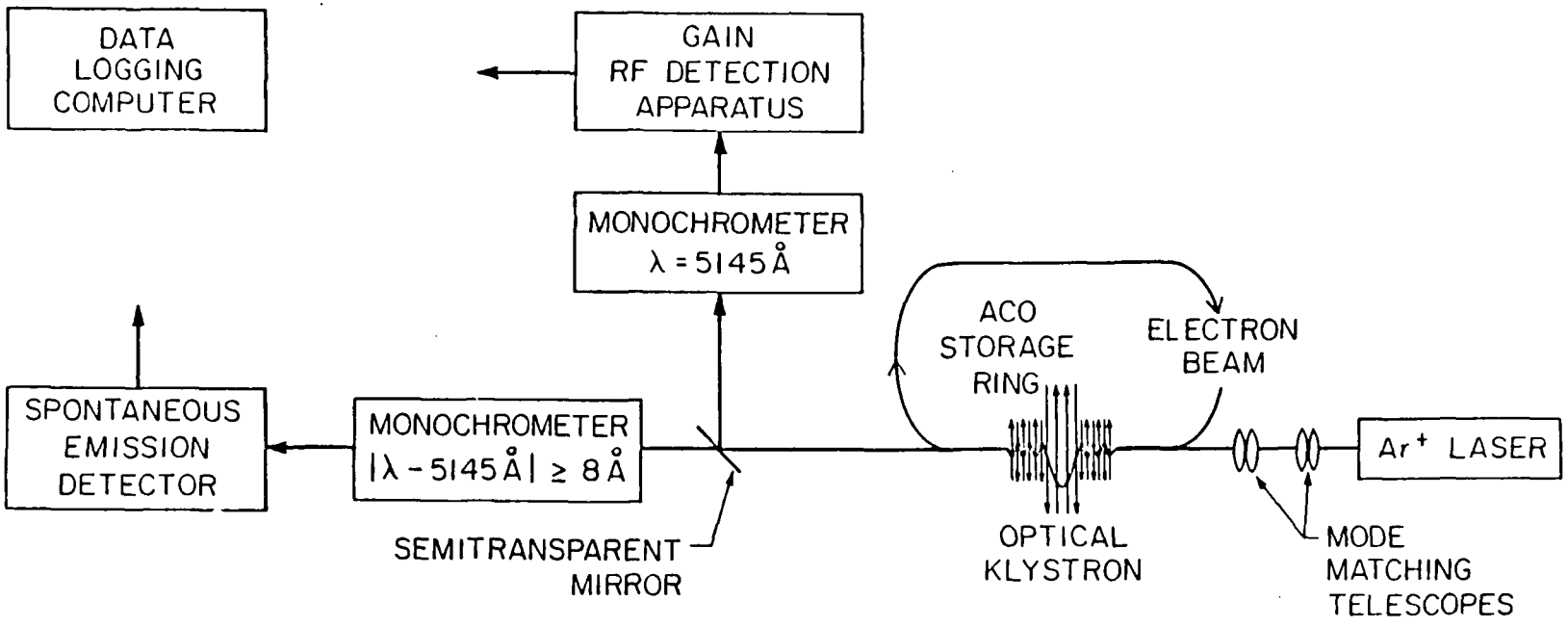

Figure 1

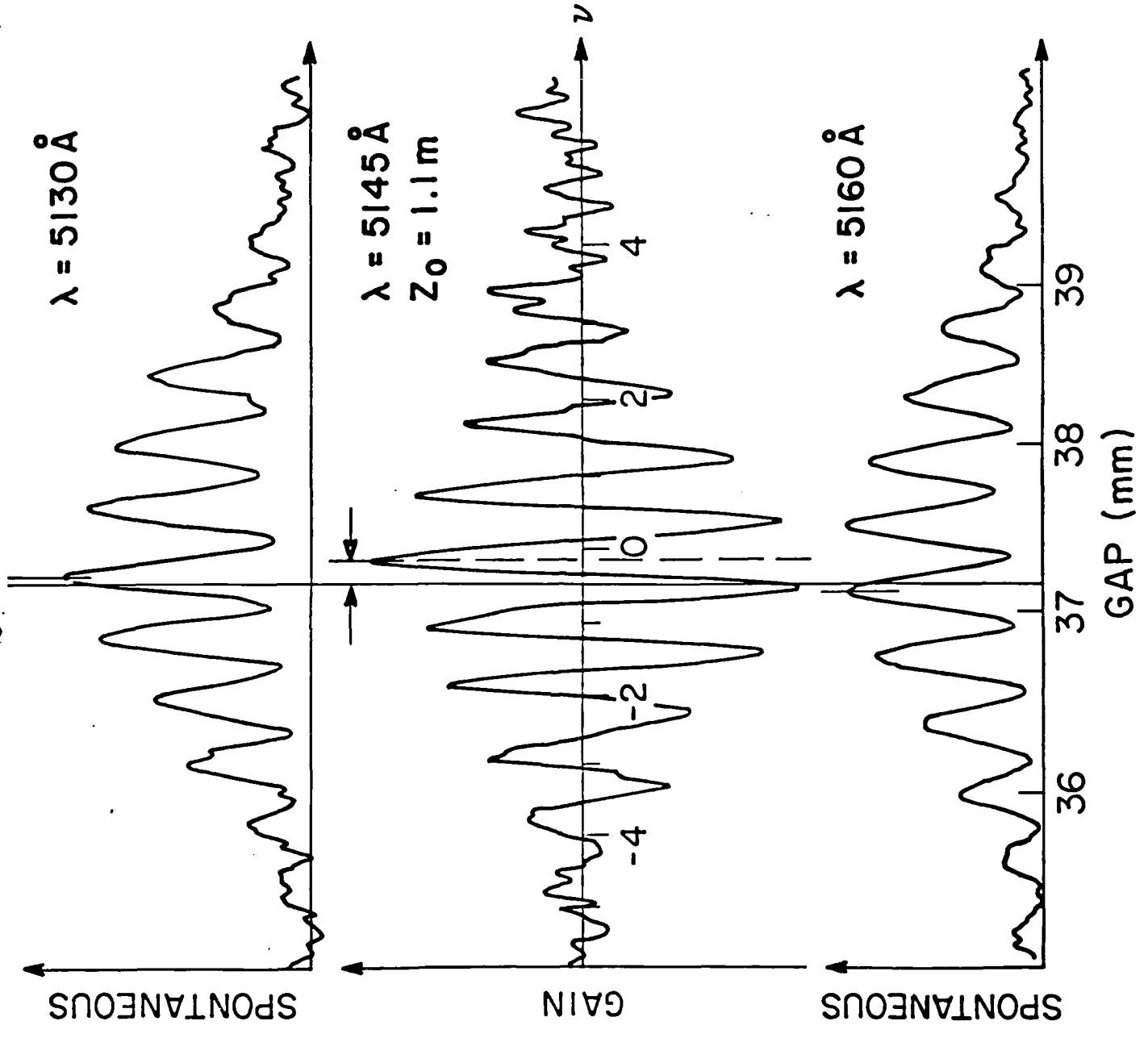
λ = 5130 Å
λ = 5145 Å
Z_o = 1.1 m
λ = 5160 Å
ν
4
2
0
-2
-4
39
38
37
36
GAP (mm)
SPONTANEOUS
GAIN
SPONTANEOUS

Figure 2

Appl. Phys. B 33, 9–16 (1984)

Applied Physics B Photophysics and Laser Chemistry

Transverse Mode Dynamics in a Free-Electron Laser

P. Elleaume[1] and D. A. G. Deacon[2]

LURE, Université de Paris-Sud, F-91405 Orsay, France

[1] CEN Saclay, DPC/SPP/SP, F-91190 Gif, France

[2] Deacon Research, 754 Duncardine Way, Sunnyvale, CA 94087, USA

Received 16 August 1983/Accepted 12 September 1983

Abstract. We derive the most general equations of motion for the electrons and the electromagnetic field in a free-electron laser including the effects of diffraction and pulse propagation. The field evolution is expressed in terms of the amplitudes and phases of a complete set of transverse modes. The analytic solution is given in the small-signal regime, where the theory is shown to be in excellent agreement with a recent experiment at Orsay.

PACS: 42.60, 42.20, 42.55

Stimulated by the original free-electron-laser experiments [1] in 1977, a number of authors have contributed to the development of a purely classical theory for the electron dynamics and the electromagnetic wave growth in these devices. The initial work assumed the light could be represented by a single-frequency plane wave [2, 3]. The first generalization was required to explain the extremely short pulse phenomena observed at Stanford [4, 5]. The inclusion of the longitudinal modes in the theory [6–8] permitted the explanation of the cavity detuning curve, and predicted a range of phenomena in the pulse structure which have yet to be observed. More recently, the theory has been broadened to include the transverse-mode structure of the optical beam [9–15]. Until our work at Orsay [16], no experimental information has been available to test the validity of these so-called 3D theories.

In this paper, we present a new approach to calculating the three-dimensional effects operative in free-electron lasers. The previously mentioned approaches consider the growth of the field $\delta(\mathbf{r}, t)$ along the propagation or z axis by evaluating its change at each point (x, y), and integrating numerically through the interaction region in the time domain [9–14] or in the frequency domain [15]. These techniques all demand long computer runs if they are to be applied to a real experimental situation. Our approach decomposes the problem into the minimum number of physically observable quantities: the transverse optical modes of the system. The field evolution is expressed in terms of a complete set of orthogonal transverse modes; equations are developed for the propagation of the amplitude and phase of each mode. In physical systems which operate on a few of the lowest-order modes, this approach greatly increases the accuracy, and may reduce the required computer time for the calculation by working in a vector space well matched to the solution of the problem. For the oscillator case, the appropriate choice of modes is the set of eigenmodes of the cavity. For the amplifier, the vector space of modes is determined by the characteristics of the input mode, which is presumably a TEM_{00} Gaussian mode. In either device, an optimum design would result in the excitation of as few of the higher-order modes as possible. The modal decomposition method is therefore well adapted to the prediction and optimization of the operation of the free-electron laser (FEL).

In the first section, we derive, in their most general form, the equations governing the dynamics of the complex mode amplitudes. The subsequent sections reduce these equations to the familiar case of the small signal, low-gain result (Sect. 2). Here, the problem becomes linear, the mode evolution can be described by a matrix transformation, and we retrieve the well known gain equation complete with filling factor. The

theory is then applied to the case of the Orsay experiment, where the results are in excellent agreement with an experiment [16] performed recently which exhibits the off-diagonal terms of the gain matrix.

1. Theoretical Development of the Fundamental Equations

The FEL system is properly described by the coupled Maxwell and Lorentz force equations. From these, we shall derive a self-consistent set of equations describing the electron and the transverse optical mode dynamics. We use the dimensionless notation originally developed by Colson (in fact this work is a generalization of Colson's work to include transverse modes and we shall stay as close as possible to his original notation). Let us recall his main equations describing the field and electron dynamics in the slowly varying phase and amplitude approximation [18]:

$$\frac{dv}{d\tau} = a' \cos(\zeta + \phi), \tag{1}$$

$$\frac{d\zeta}{d\tau} = v, \tag{2}$$

$$\frac{da'}{d\tau} = -r' \langle e^{-i\zeta} \rangle_{\zeta_0, v_0}, \tag{3}$$

where

$$\zeta(t) = (k + k_0) z(t) - \omega t \tag{4}$$

is the dimensionless electron phase,

$$v(t) = L[(k + k_0)\beta_z(t) - k] \tag{5}$$

the dimensionless resonance parameter,

$$\tau = \frac{ct}{L} \tag{6}$$

the dimensionless interaction time,

$$a'(z, t) = \frac{4\pi e N L K E(z, t) e^{i\phi(z,t)}}{\gamma^2 mc^2} \tag{7}$$

the dimensionless complex field amplitude, and

$$r'(z(t)) = \frac{8\pi^2 e^2 N L^2 K^2 \varrho(z(t))}{\gamma^3 mc^2} \tag{8}$$

the dimensionless gain parameter.

Here we consider an N-period helical undulator of length L, magnetic period $\lambda_0 = 2\pi/k_0$, peak magnetic field B, and deflection parameter $K = 93.4\,B$ [Gauss] λ_0 [cm]. An electron beam of energy γmc^2, and number density ϱ travels along the axis of the undulator; an individual electron has longitudinal coordinate $z(t)$ and longitudinal velocity $c\beta_z(t)$ at time t. A helically polarized *plane wave* of wavelength $\lambda = 2\pi/k$, frequency ω, and electric field $\delta(z, t) = E(z, t) \exp\{i[kz - \omega t + \phi(z, t)]\}$ interacts with the electrons. In (3), $\langle \rangle_{\zeta_0 v_0}$ is the average over the initial phase ζ_0 and resonance parameter v_0 of the electron population at the position z.

Equations (1, 2) are derived directly from the Lorentz force equation and describe the effect of the radiation field on the electrons. The work done by the longitudinal field on the electrons is neglected here, which is a good approximation provided that the modes are not too divergent [14] $\lambda/\omega_0 \ll 2\pi^2 K N \gamma$. Equation (3) is derived from the Maxwell equations and describes the effect of the electron on the radiation field. The set (1), (2), and (3) is *self-consistent*. Indeed, those equations are very close to being the most general classical equations describing the FEL dynamics. They apply to high and low gain devices ($r' \gg 1$ or $r' \ll 1$), high field and low field cases ($a' \gg 1$ or $a' \ll 1$), and include the effects of multiple longitudinal modes (laser lethargy effects) through the z dependence of r', E, and ϕ. Slight modifications allow their extension to the cases of:

- the planar undulator [19],
- the tapered undulator [18],
- the optical klystron [14], and
- space charge effects [19].

However, the plane-wave approximation cannot accurately describe the transverse effects produced by the finite transverse extent of the optical mode and the electron beam. A filling factor calculated with an ad-hoc overlap integral can be added to the results of this calculation, and gives satisfactory results in the small signal regime only so long as one is not interested in the exact transverse field profile.

To relieve this last restriction on the theory, we assume the field to be described in free space by the paraxial wave equation [20]:

$$\left(\frac{\partial^2}{\partial x^2} + \frac{\partial^2}{\partial y^2} - 2ik\frac{\partial}{\partial z}\right) E(\mathbf{r}, t) e^{i\phi(\mathbf{r},t)} = 0. \tag{9}$$

This equation is derived from the wave equation $(\nabla^2 - c^{-2}\partial^2/\partial t^2)\delta = 0$ in the slowly varying amplitude and phase approximation, and has been widely used in laser field calculations [17, 20]. The general solution of (9) can be expressed as a linear combination of a complete set of orthogonal modes. If we define these modes by the complex amplitude $E_m \exp(i\psi_m)$, where E_m is real and m is the generalized index of the mode (in the two-dimensional transverse space we consider, m represents two integer numbers), the most general expression for the field is

$$E(\mathbf{r}, t) e^{i\phi(\mathbf{r},t)} = \sum_m c_m(t)\, E_m(\mathbf{r}) e^{i\psi_m(\mathbf{r})}, \tag{10}$$

where c_m is complex and time-independent in free

space. The orthogonality relation reads

$$\int \frac{dx\,dy}{\pi w_0^2} E_m e^{i\psi_m} E_n e^{-i\psi_n} = \delta_{mn}, \tag{11}$$

where we have chosen a convenient normalization which makes the E_m dimensionless. The modes can be chosen in a variety of symmetries, but it is useful to exhibit their specific form in cylindrical symmetry:

$$E_{pl}(\mathbf{r}) = \sqrt{\frac{2^{l+2}p!}{(p+l)!(1+\delta_{0l})}} \frac{w_0}{w(z)} \left(\frac{r}{w(z)}\right)^l \begin{Bmatrix}\cos l\theta \\ \sin l\theta\end{Bmatrix} \cdot L_p^l\left(\frac{2r^2}{w^2(z)}\right) e^{-r^2/w^2(z)}, \tag{12}$$

$$\psi_{pl}(\mathbf{r}) = \frac{kr^2}{2R(z)} - (2p+l+1)\tan^{-1}\frac{z}{z_0}, \tag{13}$$

where r is the radial and θ is the azimuthal coordinate, w_0 is the beam waist, $L_p^l(2r^2/w^2)$ is the associated Laguerre polynomial, and

$$w^2(z) = w_0^2\left(1+\frac{z^2}{z_0^2}\right), \tag{14}$$

$$R(z) = z\left(1+\frac{z_0^2}{z^2}\right), \tag{15}$$

$$z_0 = \frac{\pi w_0^2}{\lambda}. \tag{16}$$

These modes are very useful for the case of a cylindrical electron beam aligned to the axis of the light beam. For an ellipsoidal electron beam profile, or off-axis electron injection, the rectangular eigenmodes are more appropriate. Although we will use the cylindrical modes in the examples, we proceed with the general theoretical development which makes no assumptions on the specific form of the modes.

In FEL, the coefficients in (10) become time dependent. We wish to calculate the evolution of the amplitude and phase of these mode coefficients. Proceeding through the derivation of (1–3), making only the slowly varying amplitude and phase approximation, but now using (10) and (11), we find

$$\frac{\partial v}{\partial \tau} = \sum_m |a_m| E_m \cos(\zeta + \psi_m + \phi_m), \tag{17}$$

$$\frac{\partial \zeta}{\partial \tau} = v, \tag{18}$$

$$\frac{\partial a_m}{\partial \tau} = -\int \frac{dx\,dy}{\pi w_0^2} r E_m e^{-i\psi_m} \langle e^{-i\zeta}\rangle_{z_0 v_0}, \tag{19}$$

where we have made the new definitions

$$a_m(z,t) \equiv \frac{4\pi e N L K}{\gamma^2 mc^2} c_m(z,t), \tag{20}$$

$$r(\mathbf{r},t) \equiv \frac{8\pi^2 e^2 N L^2 K^2}{\gamma^3 mc^2} \varrho(\mathbf{r},t), \tag{21}$$

$$c_m(z,t) = |c_m(z,t)| e^{i\phi_m(z,t)}. \tag{22}$$

As before, (17) and (18) describe the effect of the radiation field on the electrons, and (19) describes the growth or decay of the radiation field due to its interaction with the electrons. The change in (17) is quite straightforward. Equation (19) shows clearly the fact that the growth in the m^{th} mode amplitude and phase is given by the overlap integral of the inphase and out-of-phase components of the charge density with the complex conjugate of that mode, as one would expect. We note that the only assumptions made on the modes $E_m \exp(i\psi_m)$ used in (17–19) are orthogonality and completeness. This means these equations are also valid for the cases of waveguide modes and dielectrically loaded cavities. In this case, w_0 is no longer the mode waist in the usual Gaussian sense, but is defined by (11). As before, these equations are self-consistent. An example of this fact is the energy conservation equation

$$\frac{\partial}{\partial \tau}\sum_m |a_m|^2 = -2\int \frac{dx\,dy}{\pi w_0^2} r \left\langle \frac{\partial v}{\partial \tau}\right\rangle_{z_0 v_0} \tag{23}$$

which is derived from (17) and (19). The left-hand side of (23), the total energy gained by all the modes, is equal to the energy loss integrated over all of the electrons in the beam.

Equations (17–19) retain all of the generality of (1–3). They are valid for high and low fields, and high and low gain systems. They take into account the evolution of the transverse modes explicitly, and the evolution of the longitudinal modes implicitly, by keeping track of the z dependence of the charge density $r(\mathbf{r}, t)$ and of the mode amplitudes $a(z, t)$. For simplicity in the following development, we drop the explicit z dependence which has been thoroughly discussed by Colson [18], and concentrate on the transverse phenomena.

As discussed in [19], the generalization to the case of the planar undulator is no more than a change in the definition of the two parameters

$$a_m^{\text{lin}} = \frac{2\pi e N L K [JJ]}{\gamma^2 mc^2} c_m(t), \tag{24}$$

$$r^{\text{lin}} = \frac{4\pi^2 e^2 N L^2 K^2 [JJ]^2}{\gamma^3 mc^2} \varrho(\mathbf{r},t), \tag{25}$$

where

$$[JJ] \equiv J_0\left(\frac{K^2}{4+2K^2}\right) - J_1\left(\frac{K^2}{4+2K^2}\right). \tag{26}$$

Equations (17–19) can be integrated numerically to find the evolution of the optical wave in any Compton regime FEL. In a high-field experiment, (18) and (19) are nonlinear in a, and the wave evolution can only be obtained numerically. In this case, (17–19) provide a precise and efficient technique for solving the general

problem. In a low-field situation such as we find at Orsay, however, the problem becomes linear, and can be solved analytically. We proceed with the low field case in the next section.

2. The Low-Field Solution

The low-field case is defined by $|a_p| \ll 1$ for every mode. In other words, the electrons do not become overbunched. Experiments which operate in this domain include the low-field amplifier experiments, and storage ring FEL oscillators which saturate by mechanisms other than overbunching. The ignition of any FEL oscillator also occurs in this domain.

2.1. The Gain Matrix

Equations (17–19) can be solved by integrating (17) and (18) to lowest order in the fields a_m and inserting the result for ζ into (19). If the electrons are uniformly distributed initially in phase, we find

$$\frac{\partial a_m(\tau)}{\partial \tau} = \int_0^{\tau} d\tau' \int_0^{\tau'} d\tau'' M_{mn}(\tau, \tau'') a_n(\tau''), \tag{27}$$

where

$$M_{mn}(\tau, \tau'') = \frac{i}{2} \int \frac{dx\,dy}{\pi w_0^2} r(x, y)\, E_m(x, y, \tau)\, E_n(x, y, \tau'') \cdot e^{-i[\psi_m(x, y, \tau) - \psi_n(x, y, \tau'')]} \langle e^{i\nu_0(\tau - \tau'')} \rangle_{\nu_0}. \tag{28}$$

Equation (27) describes a linear evolution of the mode amplitudes, and upon integration, gives the relation

$$a_m(\tau = 1) = (I + G)_{mn} a_n(\tau = 0), \tag{29}$$

where I is the identity matrix, and G, which is generally not Hermitian, has elements

$$g_{mn} = \int_0^1 d\tau \int_0^{\tau} d\tau' \int_0^{\tau'} d\tau'' M_{mn}(\tau, \tau'') + \int_0^1 d\tau_1 \int_0^{\tau_1} d\tau_2 \int_0^{\tau_2} d\tau_3 M_{ml}(\tau_1, \tau_3) \cdot \int_0^{\tau_3} d\tau_4 \int_0^{\tau_4} d\tau_5 \int_0^{\tau_5} d\tau_6 M_{ln}(\tau_3, \tau_6) + \ldots . \tag{30}$$

The higher-order terms in g_{mn} are proportional to r^2 and higher powers of r, and are negligible in the low gain case.

Evidently this matrix is of great interest since multiple passes of the electron beam will result in multiple products of this matrix, greatly simplifying the calculation of the modes' growth. We shall discuss the consequences for an oscillation experiment in Sect. 2.2.

Let us note that this gain matrix is generally complex and defines the growth of the amplitude of the field. Sometimes people speak of the gain in a mode "m" as the energy gained by this mode in a pass through the undulator. This gain is simply $2\,\mathrm{Re}\{g_{mm}\} + |g_{mm}|^2$. Of course, one must keep in mind that energy is radiated into other modes, and that cross terms will mix a multiple mode input. If the input beam is truly monomode, the power radiated into the n^{th} mode is lower than that into the m^{th} mode by the ratio $|g_{mn}|^2 / 2\,\mathrm{Re}\{g_{mm}\}$ which is small for low gain ($r \ll 1$) systems. It is only in this case that it makes sense to speak of the gain of a mode. In high-gain systems, however, the off-diagonal terms can lead to substantial emission of energy into the higher-order transverse modes. If the input beam is multimode, of course, mode mixing occurs at all power levels.

Let us calculate g_{mn} in the simple case of experimental interest where the electron beam is cylindrical, and a good choice of modes is the cylindrical cavity eigenmodes (12) and (13). We restrict ourselves to the weakly diverging case $\pi w_0^2 \gg \lambda L$ where the gain takes on its most familiar form. The mode amplitudes and phases in (28) become independent of τ, and we can integrate the first term in (30) to find the gain. The average over the resonance parameter in (28) becomes, under the assumption of a Gaussian distribution of centroid ν_c and deviation σ_ν

$$\langle e^{i\nu_0(\tau - \tau'')} \rangle_{\nu_0} = e^{-\frac{1}{2}\sigma_\nu^2(\tau - \tau'')^2} e^{i\nu_c(\tau - \tau'')}. \tag{31}$$

Under the weak-divergence approximation, and assuming negligible pulse slippage effects (long electron bunch length $\sigma_l \gg N\lambda$), the only time-dependence in (28) is that of (31). For small spread $\sigma_\nu \ll 1$ the integral gives the well known gain spectrum

$$g_{mn} = \int \frac{dx\,dy}{\pi w_0^2} r(x, y)\, E_m(x, y)\, E_n(x, y)\, e^{-i\psi_m(x, y)}\, e^{i\psi_n(x, y)} \cdot \left\{ \frac{1 - \cos\nu_c - \frac{\nu_c}{2}\sin\nu_c}{\nu_c^3} + i \frac{-\frac{\nu_c}{2} - \frac{\nu_c}{2}\cos\nu_c + \sin\nu_c}{\nu_c^3} \right\}. \tag{32}$$

In the usual experimental case (unfortunately), $|g_{mn}| \ll 1$ and the energy gain G_m on the mode m becomes

$$G_m = 2\,\mathrm{Re}\{g_{mm}\} = \int \frac{dx\,dy}{\pi w_0^2} 2r E_m^2 \left(\frac{1 - \cos\nu_c - \frac{\nu_c}{2}\sin\nu_c}{\nu_c^3} \right). \tag{33}$$

This is exactly the gain one calculates by using the filling factor obtained by integrating the mode profile overlap with the gain profile. Specializing to the

TEM_{00} case with a Gaussian electron beam of width σ, we find

$$G_{00}=2r_0\left(\frac{1-\cos v_c-\frac{v_c}{2}\sin v_c}{v_c^3}\right)\frac{1}{1-\frac{w_0^2}{4\sigma^2}} \tag{34}$$

complete with the familiar filling factor.

The v_c dependence of G_m is the well known spectral dependence. The imaginary part of g_{mn} is not new. It describes the phase shift of the radiation field as described by Colson [18]. The inhomogeneous broadening term in (31) clearly distorts and reduces the magnitude of the gain spectrum if it is present in the integral of (30).

The effect of the divergence of the beam on the diagonal terms in G is, *to first order*, and for a filamentary electron beam, the addition of a time-varying phase which shifts the resonance curve in (32) by a constant depending on the mode

$$v_c \rightarrow v_c-\frac{\lambda L}{\pi w_0^2}(2p+l+1). \tag{35}$$

Equation (35) means that the gain curves of the modes are shifted with respect to each other. This effect has been calculated for the fundamental TEM_{00} mode in the energy loss approximation [14], and has recently been observed experimentally at Orsay [21]. It should be noted that for many practical situations where the cavity is optimized for gain on the TEM_{00} mode, this expression is valid for only the lowest-order mode. The higher modes become distorted in form as well as simply shifted in resonance parameter by (35).

2.2. *The Low-Field Oscillator*

We now discuss some consequence of the linearity of the low-field problem on the optimization of an optical cavity for an FEL oscillator experiment. In such an experiment the light pulses reflect n times on the cavity mirrors ($n \geqq 2$) between interactions with electrons in the undulator. The matrix governing the mode evolution from one amplification to the next is

$$(I+G)C, \tag{36}$$

where G in the gain matrix defined previously, and C is the cavity matrix describing the n reflections on the mirrors. In a set of cavity eigenmodes, C is diagonal

$$Cx^i=\mu_i x^i, \tag{37}$$

with $c_{jj}=\mu_j=\varrho_j\exp(i\alpha_j)$, where $1-\varrho_j^2$ are the total losses on the n reflections, including transmission, absorption, scattering, and diffraction. If diffraction is negligible, the eigenvectors x^i become the Gaussian TEM_{pl} modes, and the phase shift per round trip α_i becomes, for $n=2$ reflections per amplification and identical radius of curvature mirrors, $\alpha_{pl}=4(2p+l+1)\tan^{-1}(L_c/2z_0)$, where L_c is the optical cavity length.

The matrix (36) is the fundamental matrix of the problem. Its diagonalization allows the calculation of the mode evolution up to the onset of saturation:

$$(I+G)C=P\Lambda P^{-1}, \tag{38}$$

$$[(I+G)C]^m=P\Lambda^m P^{-1}, \tag{39}$$

where the columns of P are composed of the eigenvectors of $(I+G)C$, and Λ is diagonal. The fastest mode growth will be obtained with the eigenmode having the highest eigenvalue modulus. Optimization of the FEL oscillator will then consist of maximizing the desired eigenvalue of $(I+G)C$.

If the gain is low (as it is, unfortunately, for our system on ACO), one can diagonalize the evolution matrix (36)

$$(I+G)Cz^i=\lambda_i z^i \tag{40}$$

using the cavity eigenmodes x^i as the basis for a perturbation expansion of the new modes z^i. To first order in the non-degenerate case, the result is

$$\lambda_j=\varrho_j e^{i\alpha_j}(1+g_{jj}), \tag{41}$$

$$z^j=x^j+\sum_{m\neq j}\frac{\varrho_m e^{i\alpha_m}}{\varrho_j e^{i\alpha_j}-\varrho_m e^{i\alpha_m}}g_{mj}x^m. \tag{42}$$

Under these conditions, the FEL design is optimized by maximizing the diagonal term g_{jj} corresponding to the desired mode. From (33) and (12) it is clear that the beam size w_0 must be reduced down to the order of the electron-beam size in order to optimize the coupling, but if the mode becomes too divergent, the time dependent terms in E_m and E_n of (28) begin to reduce the gain. The optimal situation lies between these two extremes, and has been calculated in detail (using the energy loss approximation) by Colson and Elleaume [14].

The optimization procedure must also be limited by the stability condition [17] on the cavity. For the Orsay experiment, the radius of curvature chosen to optimize the small-signal gain was $R=3$ m, which is acceptably close to the stability limit of 2.75 m. There are cavity designs in which C is degenerate for which the optimization procedure is not necessary. For these designs, α_j is a constant independent of the index. In these cavities, any combination of modes reproduces itself after n reflections. If $n=2$ as in the Stanford and the Orsay experiments, the concentric and the plane-parallel cavities are degenerate, and the confocal cavity is degenerate on the p modes (quasi-degenerate). These

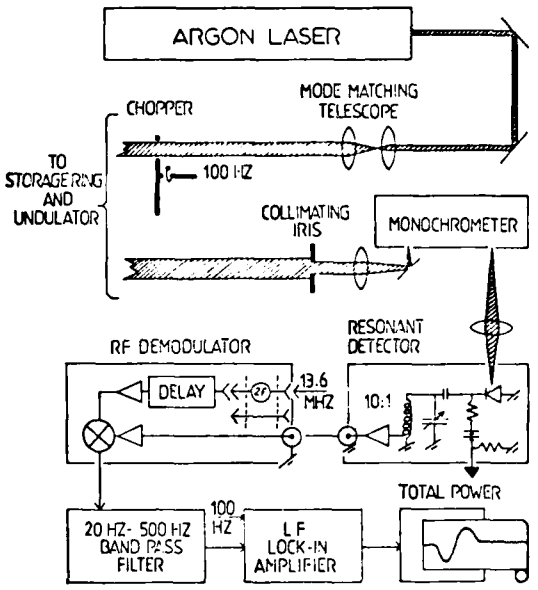

Fig. 1. Simplified schematic diagram of the gain-measurement apparatus [23] showing the argon-laser focussing system, the collimating iris, and the double demodulation detection system

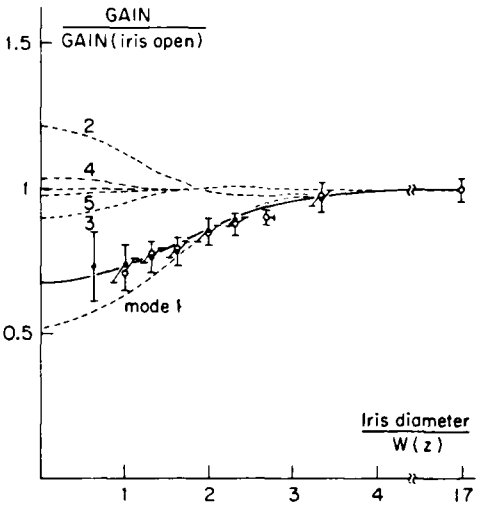

Fig. 2. The measured gain as a function of the iris diameter [16] normalized to the measured beam waist at the iris. The solid points were taken closing the iris and the open points while opening it. The error bars are the one sigma statistical errors. All points have the same horizontal error bar which is shown for the point at 2.7. The solid curve is calculated using the measured values for the electron and laser beam sizes. The effect of each higher-order mode is shown by the dashed curves

cavity designs, however, are useless since they stand critically on the stability boundary. The tolerance on the mirror radius of curvature is on the order of $|g_{00}|$ (obtained from the perturbation expansion) which is difficult to meet if the gain is low. For two-mirror devices where $n>2$, such as the Novosibirsk experiment where $n=8$, in general for mirrors of equal radius of curvature there exist $n/2+1$ cavity designs with a degenerate C matrix:

$$z_0 = \frac{L_c}{2\tan\dfrac{m\pi}{n}} \tag{43}$$

and $n/2$ with a quasi-degenerate C matrix in which the odd l modes change sign on every amplification. Only two of the degenerate and one of the quasi-degenerate cavities correspond to the unstable cavities; the others are potentially useable in an experiment. The value of a degenerate C matrix is that the eigenvectors of the amplifier plus cavity matrix (36) are equal to those of the gain matrix alone, multiplied by a constant. This degeneracy allows the cavity to oscillate on the most favorable combination of modes which best fits the electron beam shape. In this manner, the gain can be increased by factors of two or three over the gain of an optimized TEM_{00} mode, particularly if the electron beam size is smaller than the TEM_{00} mode. The tolerance on the mirror radius for the degeneracy of C will still be tight, and the experimental utility of these cavities remains to be investigated.

3. Application to Gain-vs-Aperture Experiment

3.1. Description of the Experiment

The gain of the Orsay FEL has recently been measured with the optical klystron in place [22] in an amplifier experiment using an external argon ion laser to provide the coherent mode. A detailed description of the apparatus can be found in [23], and a schematic description is given in Fig. 1. The laser beam is analyzed at a distance d from the optical klystron after passing through an adjustable collimating iris (Fig. 1), which is centered on the laser mode emerging from the interaction region. The gain is measured as the ratio of the power detected in phase with both the electron repetition frequency and the chopper frequency (the amplified power) divided by the power in phase with the chopper alone (the incident laser power). Calibration is performed as in [23].

The again is recorded as a function of the iris aperture, and large variations are observed [16]. One set of data points is reproduced in Fig. 2, where the gain is normalized to its value for the iris completely open, and the iris diameter is normalized to the measured beam waist at the iris. The data is taken at maximum gain, which means $v_c \approx 0$ for the optical klystron, and

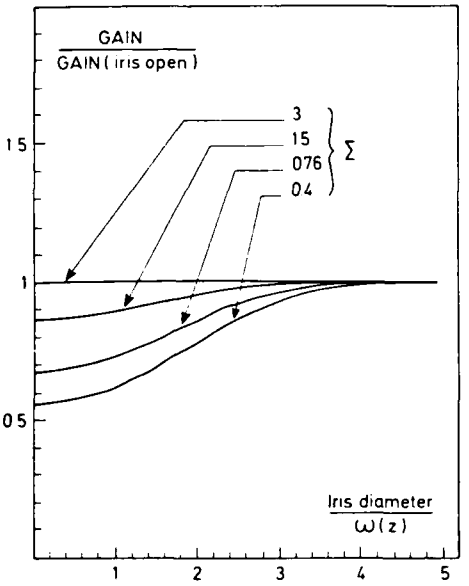

Fig. 3. Calculated curves for the gain as a function of iris diameter under the conditions of the Orsay experiment [16]. The electron beam dimension $\Sigma = \sigma \sqrt{\pi \lambda L}$ is varied to show the effects of the beam size on the excitation of the higher order modes. The value $\Sigma = 0.76$ corresponds to $\sigma = 0.35$ mm which is very close to the value at which the experimental points were recorded

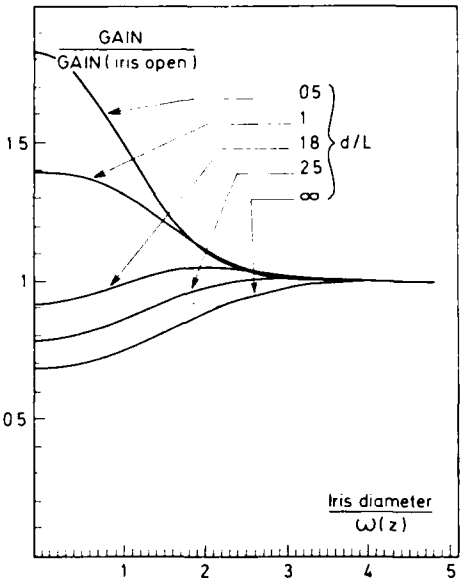

Fig. 4. Calculated gain as a function of iris diameter for several iris positions d, under the conditions of the Orsay experiment [16]. The ratio of the iris to optical klystron distance d divided by the optical klystron length L is varied through the range 0.5 to ∞. The experimental points of Fig. 2 were taken for $d/L = 9$

the laser beam was carefully aligned to within about 0.05 mm of the axis of the electron beam. The change in the measured gain as the iris is closed means that the laser is not uniformly amplified in its transverse profile. In fact, this experiment provides a very sensitive technique for measuring the power emitted into the higher-order modes even in the small gain limit and for a monomode input beam. Clearly a calculation of the g_{mn} is necessary in order to explain these results. In the next section, we apply the theory we have developed to the case at hand, and in Sect. 3.3, precise comparison is made between the experimental and the theoretical results.

3.2. *Multimode Emission in a Single-Mode Amplifier Experiment*

In this subsection, we assume the incident wave is a single mode TEM_{00} beam with a weak field ($|a_0| < 1$), and perfectly aligned onto the electron beam. As discussed previously, we take the cylindrical eigenmodes based on the form of the input beam. Using the notation of Sect. 1, the input laser field reads

$$E^I(\mathbf{r}) = c_0 E_0(\mathbf{r}) e^{i\psi_0(\mathbf{r})}, \tag{44}$$

where the subscript 0 refers to the TEM_{00} mode of (12) and (13). From (29), the output field $E^s(\mathbf{r})$ becomes

$$E^s = E^I + c_0 \sum_{j=0}^{x} g_{j0} E_j(\mathbf{r}) e^{i\psi_j(\mathbf{r})}. \tag{45}$$

Assuming low gain, the output power passing through the iris aperture is

$$\frac{8\pi P}{c} = \int dS |E^s|^2 \approx c_0^2 \int dS E_0^2 + 2c_0^2 \,\mathrm{Re} \cdot \left\{ \sum_{j=0}^{x} g_{j0} \int dS E_0 E_j e^{i(\psi_0 - \psi_j)} \right\}, \tag{46}$$

where $\int dS$ covers the iris aperture. The gain is therefore

$$G = \frac{2\,\mathrm{Re}\left\{ \sum_{j=0}^{x} g_{j0} \int dS E_0 E_j e^{i(\psi_0 - \psi_j)} \right\}}{\int dS E_0^2}. \tag{47}$$

For purely cylindrical $l = 0$ modes, G can be written

$$G = 2\,\mathrm{Re}\left\{ g_{00} + \sum_{p=1}^{x} g_{p0} e^{i2p\tan^{-1}\frac{z}{z_0}} \frac{\int_0^X L_p(x) e^{-x} dx}{\int_0^X e^{-x} dx} \right\}, \tag{48}$$

where z_0 is the Rayleigh range of the laser mode, z is the distance between the iris and the laser beam waist, and $X = r_0^2/2w^2(z)$ where r_0 is the iris diameter. There

are two interesting limiting cases:

$$G = 2\,\mathrm{Re}\{g_{00}\} \quad X \to \infty \text{ (iris open)}, \tag{49}$$

$$G = 2\,\mathrm{Re}\left\{(g_{00}) + \sum_{p=1}^{\infty} g_{p0} e^{i2p\tan^{-1}\frac{z}{z_0}}\right\}$$

$$X \to 0 \text{ (iris closed)}. \tag{50}$$

It is obvious from (48-50) that the gain changes with iris diameter in a way which depends on the magnitudes of the off-diagonal terms in the gain matrix. The generalization is straightforward to the case of the multimode input beam, and to imperfect alignment of the laser and electron beams, although the calculation becomes more difficult. This calculation also applies to high-power input laser beams ($a_0 \gg 1$) provided one keeps in mind that the g_{p0} are functions of a_0.

3.3. *Application to the Orsay Experiment*

The experimental points shown on Fig. 2 were taken under the following approximate conditions

laser beam:
- measured beam waist $w_0 = 0.67$ mm
- wavelength = 5145 Å
- measured beam waist at iris $w(z) = 2.7$ mm
- distance from optical klystron to iris $d = 11.6$ m,

electron beam:
- Gaussian and cylindrical with $\sigma \simeq 0.32$ mm,

optical klystron:
- Nd = 80 [19, 22, 24]
- resonance parameter corresponding to maximum gain with iris open.

The solid curve of Fig. 2 has been calculated using (27, 28, and 50) for the planar configuration (24 and 25), taking into account the 10 lowest order $l = 0$ modes. The dashed curves of Fig. 2 show the contribution of each individual mode. These curves are the same whether an undulator or optical klystron is used. Very similar curves (not shown) were calculated for other resonance parameters indicating that as expected, the diffraction effects do not change much as a function of detuning parameter for modes with low divergence.

Figure 3 shows the calculated effect for several dimensionless electron beam transverse dimensions $\Sigma = \sqrt{2}\,\sigma\pi/\lambda L = 0.4, 0.76, 1.5, 3$, where L is the length of the magnetic interaction region. $\Sigma = 0.76$ corresponds to the value $\sigma = 0.35$ mm, close to that used in Fig. 2. The flattening of the curves as Σ is increased to $\Sigma = 3$ is due to the vanishing of g_{0j}/g_{00} for $j \neq 0$ as σ increases.

Figure 4 shows the calculated effect for various iris distances d from the optical klystron center, normalized to the optical klystron length: $d/L = 0.5, 1, 1.8, 2.5$, and ∞. The experimental points of Fig. 2 were obtained for $d/L = 9$. The inversion of the effect is due primarily to the term $\exp[i2p\tan^{-1}(z/z_0)]$ with $p = 1$ in (50) which switches from $+1$ to -1 as z goes from zero to infinity (the mode $p = 1$ gives the predominant effect). At short distances the TEM_{10} mode interferes constructively on axis 1, and at long distances, it changes sign.

Acknowledgements. The authors would like to acknowledge stimulating discussions with W. B. Colson and J. M. J. Madey. The work was supported by the DRET, the Centre d'Etudes Nucleaires de Saclay DPC SPP SP, the Centre Nationale de la Recherche Scientifique, and was performed by Deacon Research under subcontract to HEPL, Stanford University, for the AFOSR.

References

1. D.A.G. Deacon, L.R. Elias, J.M.J. Madey, G.J. Ramian, H.A. Schwettman, T.I. Smith: Phys. Rev. Lett. **38**, 892 (1977)
2. IEEE J. QE-**17** (1981), Special Issue on Free-Electron Lasers (ed. by A. Szoke)
3. *Physics of Quantum Electronics*, Vols. 5 and 7-9 (Addison-Wesley, Reading, MA 1978-1982)
4. J.M.J. Madey et al.: Final Technical Report to ERDA: Contracts EY 76-S-03-0326 PA 48, and PA 49 (1977), available from the authors at HEPL, Stanford, CA 94305, USA
5. S. Benson, D.A.G. Deacon, J.N. Eckstein, J.M.J. Madey, K. Robinson, T.I. Smith, R. Taber: Phys. Rev. Lett. **48**, 235 (1982)
6. W.B. Colson, S.K. Ride: *Physics of Quantum Electronics* **7**, 377 (Addison-Wesley, Reading, MA 1980)
7. F.A. Hopf, T.G. Kuper, G.T. Moore, M.O. Scully: *Physics of Quantum Electronics* **7**, 31 (Addison-Wesley, Reading, MA 1980)
8. G. Dattoli, A. Marino, A. Renieri, F. Romanelli: IEEE J. QE-**17**, 1371 (1981)
9. C.-M. Tang, P. Sprangle: *Physics of Quantum Electronics* **9**, 627 (Addison-Wesley, Reading, MA 1982)
10. S.A. Mani, D.A. Korff, J. Blimmel: *Physics of Quantum Electronics* **9**, 557 (Addison-Wesley, Reading, MA 1982)
11. L.R. Elias, J.C. Gallardo: Phys. Rev. **24** A, 3276 (1981)
12. D. Prosnitz, R.A. Maas, S. Doss, R.J. Gelina: *Physics of Quantum Electronics* **9**, 1047 (Addison-Wesley, Reading, MA 1982)
13. B.J. Coffey, M. Lax, C.J. Eliott: IEEE J. QE-**19**, 297 (1983)
14. W.B. Colson, P. Elleaume: Appl. Phys. B **29**, 101 (1982)
15. W.B. Colson, J.L. Richardson: Phys. Rev. Lett. **50**, 1050 (1983)
16. D.A.G. Deacon, J.-M. Ortega et al.: In preparation
17. A. Yariv: *Quantum Electronics* (Wiley, New York 1975) Chaps. 6 and 7
18. W.B. Colson: *Physics of Quantum Electronics* **8**, 457 (Addison-Wesley, Reading, MA 1982)
19. W.B. Colson: IEEE J. QE-**17**, 1417 (1981)
20. M. Kogelnik, T. Li: Proc. IEEE **54**, 1312 (1966)
21. D.A.G. Deacon et al.: In preparation
22. M. Billardon, D.A.G. Deacon, P. Elleaume, J.-M. Ortega et al.: In preparation
23. D.A.G. Deacon, J.M.J. Madey, K.E. Robinson, C. Bazin, M. Billardon, P. Elleaume, Y. Farge, J.-M. Ortega, Y. Petroff, M.F. Velghe: IEEE Trans. NS-**28**, 3142 (1981)
24. P. Elleaume: J. Phys. (Paris) **44**, C1 333 (1983)

First Operation of a Storage-Ring Free-Electron Laser

M. Billardon,[a] P. Elleaume,[b] J. M. Ortega,[a] C. Bazin, M. Bergher, M. Velghe,[c] and Y. Petroff
Laboratoire pour l'Utilisation du Rayonnement Electromagnétique, Université de Paris-Sud, F-91105 Orsay, France

and

D. A. G. Deacon,[d] K. E. Robinson, and J. M. J. Madey
High Energy Physics Laboratory, Stanford University, Stanford, California 94305
(Received 1 August 1983)

A storage-ring free-electron laser oscillator has been operated above threshold at a visible wavelength $\lambda \simeq 6500$ Å.

PACS numbers: 42.60.-v

A free-electron laser (FEL) generates stimulated radiation by interaction of relativistic free electrons with a spatially oscillating magnetic field (undulator). The wavelength, λ, of the stimulated radiation emitted along the axis is given approximately by (in SI units)

$$\lambda = \frac{\lambda_0}{2\gamma^2}\left(1+\frac{K^2}{2}\right), \quad K = \frac{eB_0\lambda_0}{2\pi mc}, \tag{1}$$

where e and m are the electron charge and mass, c is the speed of light in vacuum, B_0 and λ_0 are the undulator peak magnetic field and period, and γ is the total electron energy divided by mc^2. The first operation[1] of a FEL has been demonstrated by the Stanford group at $\lambda = 3.4$ μm using 43-MeV electrons produced by a linear accelerator. In any practical design, $\lambda_0 \gtrsim 3$ cm; therefore it is obvious from Eq. (1) that operation of a visible or ultraviolet FEL needs a high-energy accelerator of $\gamma mc^2 \gtrsim 100$ MeV. In this energy range, storage rings are superior to linear accelerators in terms of electron density, energy spread, and emittance, thus resulting in a higher optical gain. In this Letter, we report the first operation of a storage-ring free-electron laser oscillator above threshold at $\lambda \simeq 6500$ Å.

We have used the Orsay storage ring ACO, an "older" machine, first operated in 1965. Its characteristics for this experiment are given in Table I. A permanent magnetic undulator of 17 periods optimized for electrons of 240-MeV energy has been built.[2] However, the limited straight-section length (1.3 m) available on ACO left us with a low gain of a few parts in 10^{-4} per pass in earlier work.[3] Laser oscillation was therefore impossible. Now, a gain enhancement by a factor 2 to 7 has been achieved by modifying the undulator into an optical klystron[4] (OK). This was done by replacing the three central periods by a three-pole wiggler (dispersive section). This section strongly enhances the bunching originating from electron and radiation interaction in the first undulator section and therefore gives a larger energy exchange between electrons and radiation field in the second undulator section.[4]

Mirror reflectivity degradation has been observed[3] at 240-MeV electron energy. This degradation is mainly due to the uv part of the spontaneous emission from the klystron. This problem was overcome by operating the OK at minimum K (by increasing the magnetic gap) to minimize the harmonic content of the spontaneous emission, and the storage ring at the minimum electron energy to also diminish the flux. It is

TABLE I. ACO characteristics in the FEL experiment.

Energy	160 – 166 MeV
Circumference	22 m
Bunch to bunch distance	11 m
Electron beam current for oscillation	16 to 100 mA
rms bunch length σ_l	0.5 to 1 ns
rms bunch transverse dimensions σ_x, σ_y	0.3 to 0.5 mm
rms angular spread σ_x', σ_y'	0.1 to 0.2 mrad
rms relative energy spread	$(0.9 \text{ to } 1.3) \times 10^{-3}$
Electron beam lifetime	60 to 90 min

TABLE II. Optical cavity characteristics.

Length	5.5 m
Mirror radius of curvature	3 m
Rayleigh range	1 m
Wavelength of maximum Q	620 to 680 nm
Average mirror reflectivity at 6328 Å	99.965%
Round trip cavity losses at 6328 Å	7×10^{-4}
Mirror transmission	3×10^{-5}

possible by decreasing both K and γ to keep λ constant around 6500 Å which gives the maximum reflectivity for the mirrors used in this experiment. The OK was finally operated at $K = 1.1$ to 1.2 with a dispersive section characterized by[5] $N_d \simeq 95$ where N_d is the number of laser optical wavelengths passing over an electron in the dispersive section. The optical cavity characteristics are given in Table II.

Laser oscillation was obtained after a careful alignment of the electron beam on the cavity axis (within 0.1 mm all along the 1.3-m OK length) and maximization of emission as a function of the storage-ring radio-frequency cavity voltage and the optical-cavity length. Laser operation requires very precise synchronism between light-pulse reflections and electron-bunch revolution frequency. To avoid backlash and mirror misalignment, fine tuning of the cavity length was performed by slightly changing the frequency instead of translating the mirrors. Laser oscillation lasted typically 1 h after each electron injection.

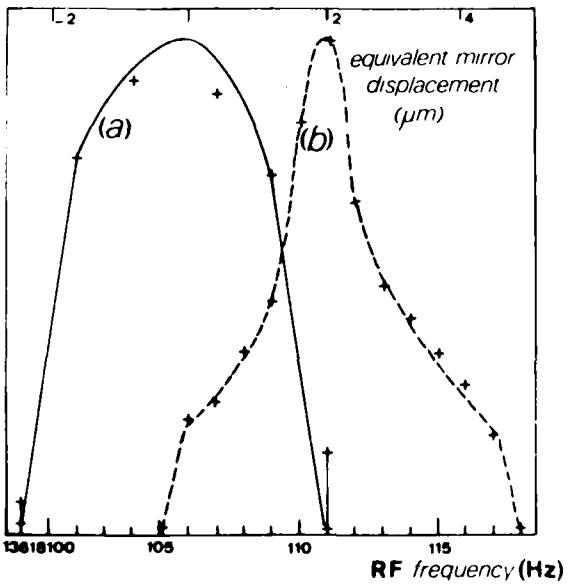

FIG. 1. Normalized laser power as a function of rf frequency and equivalent mirror displacement. Curve *a* is recorded close to the maximum gain/loss ratio and curve *b* close to the laser threshold. The shift between the two curves is probably due to some slight cavity-length drift.

Figure 1 shows two "detuning curves" of laser power (normalized to the maximum) versus frequency variation and equivalent mirror displacement. Curve (*a*) has a 3.4 μm full width at half maximum of equivalent mirror displacement; curve (*b*), as recorded much closer to laser threshold, has only a 1.6 μm full width at half maximum. The shift in displacement between curves (*a*) and (*b*) is probably due to some slow cavity length drift [e.g., a temperature drift of (0.02 °C)/(30 min) would be sufficient]. In this experiment, the gain was not proportional to the electron current, mainly because of the anomalous bunch lengthening and energy spreading at high current; these effects make the gain versus ring current reach a maximum and then decrease. One consequence of this is that the ratio of gain to cavity losses always remained just above 1 during laser operation. Wider detuning curves are expected for higher gain/loss ratios.

Figure 2 presents the horizontal and vertical transverse profiles of the laser output. They are in a very good agreement with the expected cavity TEM_{00} profile. The slight discrepancies might arise from some residual instability of the laser too close to threshold or nonuniform mirror reflectivity.

Figure 3 shows the laser time structure in a 200-ms total time scale. Quasirandom peaks appear in curve (*a*). Curve (*b*) is obtained by increasing the detector sensitivity and shows some substructure in the peaks. Although not seen in Fig. 3, each subpeak is also usually more or less modulated at 13 kHz, very close to the theoretical rf synchrotron frequency, and also shows a typical rise time around 200 μs corresponding to a gain minus cavity losses of 2×10^{-4}/pass. It should be noted that this time structure highly de-

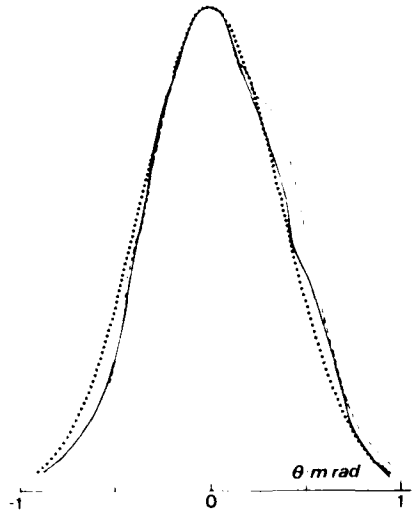

FIG. 2. Experimental laser horizontal (solid curve), vertical (dashed curve) transverse profiles, and the calculated (dotted curve) cavity TEM_{00} profile.

pends on how far the laser is from threshold. Quasiperiodic peaks have sometimes been seen near a 40-Hz frequency. And the laser variation also reproduces the pulsed 27.2-MHz structure of the electron beam.

Figure 4 presents two spectra: (a) is recorded without amplification (optical cavity completely detuned) and (b) is recorded at laser operation (cavity tuned). For case (b), the laser oscillates at three wavelengths, with the strongly dominant one being at $\lambda = 6476$ Å; each wavelength is located at a maximum of the gain versus wavelength curve.[5] Smaller gain/loss ratios would restrict the number of laser wavelengths to two or one. Typical laser lines are Gaussian if averaged over a long time scale of $\gtrsim 1$ sec, with 2 to 4 Å full width at half maximum. Figure 4 also shows an enlargement of the main laser-line spectrum recorded by using a one-dimensional charge-coupled-device (CCD) detector instead of the usual monochromator exit slit. The aperture time is 3 ms. Each narrow square peak in this curve is recorded on only one CCD element and corresponds to a 0.3 A spectral width which is of the same order as the monochromator resolution. We conclude that there is a residual inhomogeneous contribution to the laser linewidth probably connected with the long-time-scale laser-pulse structure (see Fig. 4). The central wavelength of any line is always equal to the wavelength of maximum emission of spontaneous emission with the cavity completely detuned (no amplification) plus 0.15

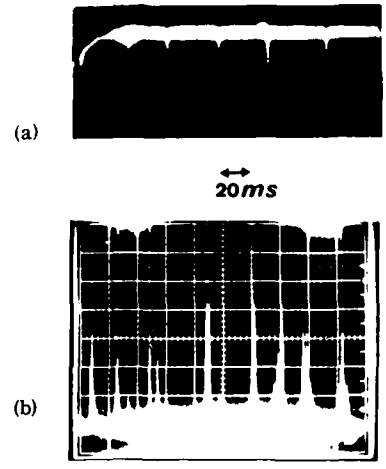

FIG. 3. Laser time structure over a 200-ms interval. Curve *b* is recorded in the same condition as *a*, but with a higher detector sensitivity.

of the wavelength interfringe distance (see Fig. 4) instead of 0.25 as predicted from Madey's theorem.[6] This discrepancy is probably due to the transverse multimode content of the spontaneous emission stored in the cavity; laser operation is only achieved on the TEM_{00} mode. Laser tunability was obtained between 640 and 655 nm by changing the magnetic gap [equivalent to a change of K in Eq. (1)]. The range of tunability is in fact limited for the moment by the mirror reflectivity.

A typical 75-μW average output power has been recorded at 50-mA current of 166-MeV electrons. This corresponds to a typical 60-mW output peak

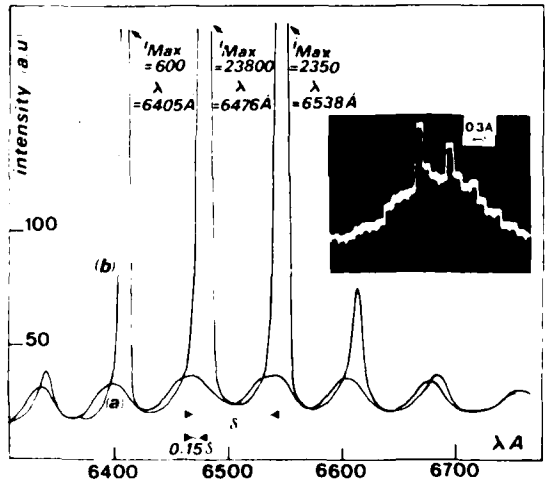

FIG. 4. Spectra of the cavity output radiation under two conditions: curve *a*, cavity detuned (no amplification) and curve *b*, cavity tuned (laser on).

power over the 1-ns electron bunch length (including effects of both the long- and short-time-scale pulse structure of the laser), and a 2-kW intracavity peak power. 75 μW give a 2.4×10^{-5} efficiency with respect to the 3.1 W of total synchrotron radiation power generated in the whole storage ring at this energy and current. This efficiency is about 0.4 the Renieri typical efficiency[7]

$$\eta=(\sigma_E/E)\eta_{\mathrm{mir}},$$

where

$$\eta_{\mathrm{mir}}=\frac{\text{mirror transmission}}{\text{round trip cavity losses}}$$

and $\sigma_E/E=1.2\times10^{-3}$ is the RMS relative energy spread. In this experiment $\eta_{\mathrm{mir}}=0.043$. This low mirror efficiency is mainly due to the high absorption in the mirror dielectric compared to its transmission. The rather low Renieri average output power is therefore the result of high sensitivity of the OK to energy spread, poor mirror efficiency, and weak total synchrotron radiation power at 166 MeV (power is proportional to the fourth power of the electron energy). The laser output power always decreases with the electron beam current and, except in regions too close to threshold, is usually proportional to the current as predicted by the same model. However, important discrepancies appear in the structure for long time scales (see Fig. 3) which is predicted to be constant. Moreover, bunch shortening instead of bunch lengthening has been seen at laser turnon; such an effect has already been seen at much lower current by simulating the FEL with an argon laser.[8]

In summary, this work demonstrates for the first time the feasibility of the storage-ring free-electron laser. Future experiments will continue to analyze the saturation mechanism, and the long- and short-time-scale structure. Higher gain/loss ratios are expected from the use of better mirrors, a second rf cavity, and smaller beam transverse dimensions obtained by using positrons instead of electrons.

This work was supported by the Direction des Recherches Etudes et Techniques under Contract No. 81/131 and by the U. S. Air Force Office of Scientific Research under Contract No. F 49620-80-C-0068.

The authors are greatly indebted to Yves Farge who initiated this research and to the technical support staff of the Laboratoire pour l'Utilisation du Rayonnement Electromagnétique for their invaluable help. Also, they thank the storage-ring staff of the Laboratoire de l'Accelerateur Lineaire, Orsay, for many fruitful discussions and the "Service Aimant" of the Laboratoire de l'Accelerateur Lineaire, Orsay, for experimental assistance.

---

[a]Permanent address: Ecole Supérieure de Physique et Chimie, 10 rue Vauquelin, F-75231 Paris Cedex 05, France.

[b]Permanent address: Département de Physico-Chimie, Service de Photophysique, Centre d'Etudes Nucléaires de Saclay, F-91191 Gif-sur-Yvette, France.

[c]Permanent address: Laboratoire de Photophysique Moléculaire, Bâtiment 213, Université de Paris-Sud, F-91405 Orsay, France.

[d]Permanent address: Deacon Research, 754 Duncardine Way, Sunnyvale, Cal. 94087.

[1]D. A. G. Deacon, L. R. Elias, J. M. J. Madey, G. J. Ramian, H. A. Schwettman, and T. I. Smith, Phys. Rev. Lett. 38, 892 (1977).

[2]J. M. Ortega, C. Bazin, D. A. G. Deacon, C. Depautex, and P. Elleaume, Nucl. Instrum. Methods 206, 281 (1983).

[3]M. Billardon, D. A. G. Deacon, P. Elleaume, J. M. Ortega, K. E. Robinson, C. Bazin, M. Bergher, J. M. J. Madey, Y. Petroff, and M. Velghe, J. Phys. (Paris), Colloq. 44, C1-29 (1983).

[4]N. A. Vinokurov and A. N. Skrinsky, Institute of Nuclear Physics, Novosibirsk, Report No. INP 77-59, 1977 (unpublished); see also N. A. Vinokurov, in *Proceedings of the Tenth International Conference on High Energy Charged Particle Accelerators, Serpukhov, 1977* (Institute Siziki Zysokikh Energie, Serpukhov, U.S.S.R., 1977), Vol. 2, p. 454.

[5]P. Elleaume, J. Phys. (Paris), Colloq. 44, C1-333 (1983). See also P. Elleaume, *Physics of Quantum Electronics* (Addison-Wesley, Reading, Mass., 1982), Vol. 8, Chap. 5, p. 119.

[6]J. M. J. Madey, Nuovo Cimento B50, 64 (1979).

[7]A. Renieri, Nuovo Cimento B53, 160 (1979); G. Dattoli and A. Renieri, Nuovo Cimento B59, 1 (1980).

[8]K. E. Robinson, D. A. G. Deacon, M. F. Velghe, and J. M. J. Madey, IEEE J. Quantum Electron. 19, 365 (1983).

OCTOBER (MARCH) 1984 To be published in: IEEE J. Quant. Elect.

MEASUREMENT OF STIMULATED TRANSVERSE MODE MIXING IN A FREE ELECTRON LASER

D.A.G.DEACON[1], P.ELLEAUME[2], M.XIE[3], C.BAZIN, M.BERGHER, M.BILLARDON[4], B.GIRARD, J.M.J.MADEY[3], J.M.ORTEGA[4], Y.PETROFF, K.E.ROBINSON[3], M.VELGHE[5]

LURE, Batiment 209C, Universite de Paris-Sud, 91405 Orsay, FRANCE

1) Deacon Research, 754 Duncardine Way, Sunnyvale, CA 94087

2) Departement de Physico-Chimie, Service de Photophysique, CEN Saclay, 91191 Gif-sur-Yvette, FRANCE

3) High Energy Physics Lab, Stanford University, Stanford, CA 94305

4) Ecole superieure de Physique et Chimie, 10 rue Vauquelin, 75231 Paris Cedex, FRANCE

5) Laboratoire de Photophysique Moleculaire, Batiment 213, Universite de Paris-Sud, 91405 Orsay, FRANCE

ABSTRACT

We report the first measurement of the off-diagonal terms in the transverse gain matrix in a free electron laser. We show that the higher order transverse modes stimulated in the FEL interaction diminish in amplitude as the electron beam size is increased, that the far field and the near field effects of the excited modes are not equivalent, and that in this low divergence case, the mode mixing is insensitive to the resonance parameter. Remarkably close agreement is demonstrated with the theory [1]. The effects of a multiple mode input beam are also observed, and the theoretical expression is derived.

I. INTRODUCTION

Beginning in 1980 a series of amplifier measurements have been performed of the stimulated emission of the Orsay storage ring free electron laser. These measurements were part of the successful effort to achieve oscillation using the ACO storage ring system [2,3]. The original gain experiments [4,5] on the superconducting undulator, and a later series of measurements [6,7] on the permanent magnet undulator NOEL and its optical klystron configuration demonstrated that the amplitude and the spectrum of the gain could be correctly calculated by the classical independent particle theory [8]. These experiments were sensitive to the total energy emitted by the stimulated emission process, and did not provide any information on the spatial structure of the amplification process. In this paper we report on an extension of these measurements which probes the three dimensional nature of the interaction.

By means of an adjustable aperture placed in the amplified beam, we have been able to measure the excitation of higher order

transverse modes induced by the nonuniform transverse profile of the electron beam. This information is mapped into the spatial distribution of the electric field at the analyzing aperture. The ratio of the transmitted stimulated power to the transmitted power of the external laser is measured as a function of the aperture diameter. The functional dependence of the ratio on the aperture diameter is a diagnostic on the transverse mode mixing which has occurred during the amplification process.

If the spatial distribution of the stimulated radiation is identical to that of the incident laser, their diffraction characteristics are identical, and the ratio of the powers transmitted through the aperture will be independent of its diameter. A dependence will be seen only if the stimulated radiation contains a different combination of transverse modes than the incident radiation. The aperture dependence of this ratio is therefore a good diagnostic of mode mixing in the amplifier.

In a free electron laser, the input laser mode is perfectly replicated only under the conditions that the electron beam is uniform across the optical mode, the electric field strength remains below the saturated level, and the divergence of the laser is negligible in the interaction region. If the electron beam

dimensions are comparable to those of the optical mode, if saturation occurs, or if the divergence is significant, higher order modes will be excited. In most configurations of practical interest, one or more of the latter conditions will hold.

The mode content of the optical field propagating through the FEL can be conveniently thought of as a vector whose elements are the amplitudes and phases of the modes. As the beam propagates through free space, the phases evolve in a fashion characteristic of each mode, but the amplitudes remain constant (in the absence of losses). The amplifier contributes an additional vector of complex field amplitudes which describes the stimulated radiation, and which is in general not parallel to the input vector [1]. The field vector at the output of the FEL amplifier is the sum of the input vector propagated to the output and the stimulated emission vector. The magnitude squared of the resultant will be larger than that of the input by a factor which is the net amplification, and it will be rotated in the multi-dimensional mode space. If the gain is large and mode mixing occurs, the output field vector will be strongly rotated. Under these circumstances, the laser can be expected to run multi-mode, or even to couple the modes so strongly that the modal decomposition becomes useless as in the guided wave case. A self-consistent calculation of the high gain field distribution must be performed to identify the steady state field vector and the gain it experiences. In a low gain

oscillator, however, the same level of mode mixing will produce no effects because the rotation of the field vector by the gain is negligible.

The gain of the Orsay FEL is very low, on the order of 10^{-3} [4-7]. Even though the conditions for mode mixing are present (the dimensions of laser and electron beam are comparable), the rotation of the field vector is minuscule. As could be expected under these conditions, the oscillator produced a nearly pure TEMoo Gaussian mode [3]. (Even the Stanford oscillator which has a gain of about 10% [9] produces a Gaussian mode [10]). The newer FEL systems now under construction at Stanford, Orsay, and elsewhere are projected to have gain on the order of unity. The mixing phenomena of the transverse modes will play an important role in the operation of these new devices. Our measurement technique permits us to obtain some information on the three dimensional amplification problem even in a devicewith such a low gain that no effects can be observed in the modes of the oscillator.

Two series of experiments have been performed, both with the undulator NOEL modified into the optical klystron configuration [7]. The first series of experiments (which we will identify as series I) served to identify the phenomenon, and stimulated our theoretical effort [1] on the problem. A second series (series II) was planned in order to extend the comparison between theory and experiment by changing the placement of the analyzing aperture. We report here on the results of these two experiments.

In section II we review the theoretical results and extend them to the case of multimude input. We describe the experimental technique in section III, and discuss the results and their implications in sections IV and V.

II. MODE MIXING THEORY APPLIED TO THE GAIN-VS-APERTURE EXPERIMENT

Elleaume and Deacon [1] have identified the equations of motion for the excitation of the higher order transverse modes in an undulator and solved them in the low field case. Their principal low field results are that the complex mode amplitudes c_m evolve according to

$$c_m^{out} = \left(\underline{I} + \underline{G}\right)_{mn} c_n^{in} \tag{1}$$

The linear relationship between input and output mode amplitudes holds even in the high gain region [1], although the transformation becomes difficult to calculate. In what follows, we restrict our examples to the small gain limit. In this limit, for low divergence, and for small beam slippage parameter (as in the Orsay experiment), the elements of the gain matrix $\underline{G}$ are

$$g_{mn} = \int \frac{dx\,dy}{\pi w_0^2}\, r(x,y)\, E_m(x,y)\, E_n(x,y)\, e^{-i\Psi_m(x,y)}\, e^{-i\Psi_n(x,y)}$$

$$\cdot \left\{ \frac{1-\cos\nu - \frac{\nu}{2}\sin\nu}{\nu^3} + i\,\frac{-\frac{\nu}{2} - \frac{\nu}{2}\cos\nu + \sin\nu}{\nu^3} \right\} \tag{2}$$

We note that this result does not include the effects of the divergence of the optical modes or the electron beam, a valid approximation in the case of the Orsay experiment, where the Rayleigh length is 1.7 times the length of the optical klystron, and the beta functions are 1.5 to 3 times longer.

In the large divergence case, the time integrals in equation (30) of reference [1] depend on both the mode numbers and the transverse position. The spectral term between the curly brackets of (2) which is generated by this time integral is therefore intimately tied to the transverse integral and cannot be factored out of the gain matrix. Under these conditions, the mode mixing phenomena may have a strong dependence on the resonance parameter. A full treatment of the problem including divergence would probably involve a numerical solution.

We can apply the low divergence results to the case of the optical klystron (or the tapered wiggler) since there is no essential change in the physics which goes into the derivation of (2). Within the same approximations, the only change is in the longitudinal dimension. The time integrals which lead to (2) become more complex so that the spectral term changes its form. Since this term factors out in the low divergence case, for a

fixed frequency experiment such as our amplifier work, the spectral term is optimized once and remains constant during the experiments. As long as the longitudinal dynamics are separable mathematically, the mode mixing phenomena will depend only on the beam dimensions, the resonator configuration, and the gain.

Let us apply equations (1) and (2), following [1], to the case in which the incident beam contains an arbitrary number of modes. The input field is

$$E^I = c_j E_j e^{i\Psi_j} \tag{3}$$

where we use the summation convention: repeated indices are summed. The functions $E_j(x,y)$, and $\Psi_j(x,y)$ are defined in [1] as the normalized amplitude and the phase of the mode. The output field is, from (1),

$$E^o = E^I + E_j e^{i\Psi_j} g_{jk} c_k \tag{4}$$

The gain measured in this experiment, which is the ratio of the stimulated power to the incident power transmitted through the aperture, is, for small gain systems,

$$G = \frac{\int_A dS \left(|E^o|^2 - |E^I|^2 \right)}{\int_A dS \, |E^I|^2} \tag{5}$$

where the integral is over the surface of the aperture opening. For simplicity of notation, we define a normalized mode integral

$$t_{mn} \equiv \frac{\int_A dS \; E_m E_n e^{-i(\psi_m - \psi_n)}}{\int_A dS \; E_o^2} \tag{6}$$

which defines the elements of a Hermitian matrix $\underline{T}$. Since the integral is over the surface out to the aperture, it is clear that these quantities depend on the diameter. Due to the different mode structures, each t_{mn} has its own aperture dependence, and its own unique phase. Substituting into (5), the gain becomes

$$G = \frac{t_{ki} g_{ij} c_j c_k^* + t_{ik} g_{ij}^* c_k c_j^* + t_{ki} g_{ij} g_{ke}^* c_j c_e^*}{t_{ki} c_i c_k^*} \tag{7}$$

This relation can be expressed more compactly in matrix notation. Adopting C as the vector of complex mode amplitudes, we find the result

$$G = \frac{2\,\mathrm{Re}\left\{ \langle C | \left(\underline{I} + \tfrac{1}{2}\underline{G}\right)^{H} \underline{T}\,\underline{G}\, | C \rangle \right\}}{\langle C | \underline{T} | C \rangle} \qquad (8)$$

where the superscript H means Hermitian conjugate. Physically speaking, this result is not hard to understand. The numerator is the stimulated power term. Each input mode c_j produces a set of stimulated modes via the gain matrix g_{ij} : the vector of stimulated modes is $\underline{G}|C\rangle$. Each stimulated mode "beats" with another mode c_k when it passes through the aperture; this other mode is either an incident mode $\langle C|\underline{I}^{H}$ or an amplified mode $\langle C|\underline{G}^{H}$. Each combination of modes produces a nonzero contribution to the transmitted power when the aperture diameter is finite. This contribution is proportional to a particular mode integral, whose amplitude is given by $\underline{T}_{kj}$. The measured gain is the ratio of the stimulated power to the incident power, and the denominator takes care of the effects of the iris on the incident beam.

To make the situation more clear, let us look at the explicit sums in the case of two input modes, "o" and "p". We assume that the input beam is predominantly "o", and linearize in c_p. Equation (8) reduces to

$$G = 2\,Re\left\{ g_{oo} + \sum_{m=1}^{\infty} t_{om} g_{mo} + t_{op}\left(g_{pp} - g_{oo}\right)\frac{c_p}{c_o} + \sum_{m=1}^{\infty} t_{pm} g_{mo}\,\frac{c_p^*}{c_o^*} + \sum_{\substack{m=o \\ m\neq p}}^{\infty} t_{om} g_{mp}\,\frac{c_p}{c_o} \right\} \tag{9}$$

where we have rationalized the denominator, and collected the off-diagonal terms in the sums.

We note here that for single mode input ($c_p = 0$), this result reduces to that of equation (48) in [1]. The additional terms are the various beating terms of the stimulated emission with the input modes, integrated across the iris. The last term, for example, is the product of the mth stimulated mode (produced via g_{mp} from the pth input mode) and the 0th input mode, integrated across the analyzing aperture, and normalized to the input intensity. It is the last three sums which are apparently responsible for the difference between the experimental points in figures 7 and 8 and the single input mode theory of [1].

If the electron beam is very large compared to the laser beam, the off-diagonal terms (2) of $\underline{G}$ go to zero by the orthogonality of the modes. The diagonal terms all have the same magnitude due to the mode normalization. Equation (9) reduces, under these circumstances, to

$$G = 2\ \mathrm{Re}\{g_{nn}\} \qquad \text{(large electron beam)} \qquad (10)$$

which means that the gain for a combination of two modes is the same as that of one of them alone. If we redefine the sum of two modes as our new starting mode, it is clear that an arbitrary third mode amplitude can be added without changing the result. It follows by induction that for an arbitrary combination of modes, the direction of the mode vector is not changed by the FEL amplification process for a large beam.

A measurement of the gain under these circumstances will show no variation as a function of the transverse position in the beam (as shown, (10) is independent of iris diameter). Any variation of the gain in the transverse plane is proof of mode mixing. Although the data of figures 7 and 8 were taken with an unknown multiple mode input, the deviation from unity of the results are a clear indication of the presence of mode mixing. The finite beam size allows off-diagonal terms in (2), and thereby produces the mode mixing observed in this experiment.

III. EXPERIMENTAL METHOD

The apparatus we used was essentially identical to that reported in the original gain measurements [4-7]. Those unfamiliar with the details of the setup should refer to the schematic diagram in [4] along with the associated description of the experiment and the calibration proceedure. A chopped external argon laser is focussed coaxially onto the electron beam in the optical klystron where it is amplified by the FEL interaction. The output beam is passed through an adjustible aperture, filtered in a monochromator, and detected in a resonant detector. The amplified power is extracted in a double demodulation scheme: a 13 Mhz lock-in detects the sum of the spontaneous and the stimulated power, and a subsequent lock-in operating at the frequency of the chopper extracts a signal proportional to the stimulated power at the detector. The FEL gain is given by the ratio of the stimulated power to the incident laser power.

In this experiment, the gain is measured as a function of the opening of an iris aligned on the amplified laser. Both the stimulated power and the incident laser power are measured for several apertures; their ratio is the "gain" as a function of the

iris diameter. If both beams were pure TEMoo modes, the gain measured this way would be independent of the iris. If, on the other hand, the stimulated radiation is a combination of modes, the measured ratio will show some variation as the aperture is varied, since closing the aperture breaks the orthogonality of the modes. A measurement of the gain as a function of the iris is therefore a source of information on the mode content of the stimulated radiation. As explained below, we have measured the mode amplitudes stimulated from a single mode input beam, which provides direct information on the cross terms in the transverse gain matrix.

In setting up for the experiment, the undulator gap is scanned to set a maximum of the optical klystron gain spectrum [7] at the laser wavelength. Alignment of the incident laser on the electron beam is performed by optimizing the amplitude of the stimulated power when adjusting the angle and position of the electron beam. A half-wave plate in the laser input beam is also adjusted to ensure that the polarization of the input mode is parallel to that of the undulator emission.

One analyzing aperture was set up as close as possible to the interaction region: just outside the exit window at a distance of

288 cm from the center of the optical klystron. This unit was a set of fixed apertures of diameters .5, 1.0, 1.5, 2.0, and 2.5 mm, mounted on a rotating exchanger block. The selected aperture could be rotated into position and aligned precisely in the plane transverse to the laser. Before each measurement, the new aperture was aligned by recentering the diffracted beam downstream of the aperture onto the original axis. A second aperture was placed far from the interaction region at a distance of 14.7 m. Since the laser beam was larger here, a minimum aperture of 2 mm was sufficient, and an adjustible iris was used, eliminating the need for realignment on each change in diameter. The powers of the transmitted laser and of the stimulated emission were measured in separate channels and recorded for about 100 seconds. The laser was then blocked in order to permit a measurement of the noise background; the aperture diameter was readjusted; the aperture was realigned (if necessary); and the two power measurements were repeated. The curves of figures 4-8 were taken by this method.

In order to verify that no detection artifacts were masquerading as real effects, we verified first the linearity of the vacuum photodiode detector, and then the position sensitivity of its high and low frequency response. By inserting a series of broadband filters up to a neutral density of .8, we simulated the

reduction in power produced by closing the aperture diameter without changing the ratio of laser to stimulated power. The measured ratio remained within a fraction of one standard deviation from unity. The detector was also moved from side to side with a focussed input to check that spatial variations in its sensitivity were not responsible for the signal. The same negative result was obtained: the detection system is linear and sensitive only to the power transmitted through the analyzing iris.

Since our goal is to measure the dependence of the stimulated power on the aperture, it is important to be sure that no portion of the laser output mode is scraped off at any point in the optical transport system. (In confirmation of this fact, we note that the aperture dependance of the gain disappeared when the monochromator slits were closed down, thereby scraping off a portion of the focal area). During set-up, the laser mode was centered on the transport mirrors, and the monochromator slits were opened to ensure that when the analyzing operture was open, all of the stimulated power entered the detector. When the analyzing aperture was placed in its farthest position from the undulator, no problem was observed in power transport. When the aperture was placed in its near position to the undulator, and set at its minimum opening, the growth of the output beam due to

diffraction did result in perhaps a 5% power loss on one of the beam transport mirrors.

The interpretation of the results demands an accurate knowledge of the electron and optical beam sizes. In an attempt to simplify the comparison with theory, considerable effort was expended to make the external Argon laser run in a single transverse mode. For series I, this effort was successful. For the later series, the aged laser plasma tube performed less well, and even with an iris internal to the Argon laser oscillator closed and optimized, the beam showed significant higher order mode power.

The laser beam sizes were repeatedly measured before and during series II. The input laser mode was measured with a Reticon diode array with a 25 micron diode separation. The beam shape and the full width at half maximum was recorded at five positions about the focus, both in the vertical and the horizontal dimensions. These measurements were fit to a Gaussian TEMoo mode to extract the beam waist and focal position information. The fits, shown in figure 1, show moderate agreement with the data, but cannot be used reliably to estimate the higher mode intensities. The astigmatism of the Argon laser's asymmetric cavity

is apparent; as expected, the vertical focus is tighter than the horizontal, and occurs slightly before it. Figure 2 shows the transverse profile of the intensity at the center of the undulator (nearly Gaussian), and 4.3 m before the focus, where the higher mode power becomes apparent.

For the data analysis, we also require a knowledge of the size of the laser beam at the aperture. This information is obtained from the dependence of the total detected laser power on the diameter. If the diameter is known and the aperture is well aligned, the laser beam size can be calculated from the reduction of the transmitted laser power, under the assumption of a Gaussian beam.

The electron beam size is less well known. It is measured as shown in figure 3. The synchrotron radiation emitted from the beam in the dipole magnet 158 cm in front of the center of the optical klystron is imaged onto the Reticon. The vertical and the horizontal beam shapes are typically observed to be Gaussian, with a width which varies according to the current in the ring. These dimensions also change with the tunes of the ring, so separate electron beam measurements are required on each injection during the experiment. No diagnostics are available on the beam size in

the center of the optical klystron. This is an unfortunate limitation since the beta functions of ACO have not been measured with the sextupoles in operation. In the absence of the trajectory errors induced by the sextupoles, the theoretical model of the ACO optics predicts that the beam sizes change by less than 25% and 6%, respectively in the horizontal and the vertical planes, when moving from the electron beam measurement point to the center of the OK. These numbers can be taken as an estimate of the systematic error in the electron beam size determination.

For the second series of experiments the extraction mirror had been removed for the repair of an intracavity iris in the same assembly. We were therefore obliged to run with the probe laser beam exiting the vacuum system through the rear oscillator mirror. This mirror was tilted slightly so that the reflected beam could be intercepted on a beam stopper. The transmission of this mirror, a high reflector at 6328 A, is about 80% at the Argon 5145 A wavelength. It acts as a defocussing lens with a focal length of about -5.2 m. These experiments also had to be performed at low energy (166 MeV) in order to avoid damaging [9] the oscillator mirrors with the UV generated in the optical klystron. All measurements were done with the 5145 A laser line; in Series I, Nd = 80, K = 1.89, and Wo = 670 microns; in Series II, Nd = 70, K = .9, and Wo = 610 microns.

IV. RESULTS OF THE EXPERIMENTS

One data scan taken in series I is compared with theory in figure 4. This scan was taken under optimum conditions with well characterized electron and optical beam sizes. Here, the input laser beam is a pure TEMoo mode, and the amplified beam propagates freely for 14.3 m before being analyzed with the iris. The error bars can be estimated from the accuracy with which the two consecutive scans overlap. The solid curve is the theoretical calculation [1] based on the measured distances and beam sizes; no fitting has been done. The agreement is excellent.

This experiment is the first to demonstrate the existence of the off-diagonal terms in the gain matrix (transverse mode mixing), and the agreement between theory and experiment in figure 4 establishes the validity of our theoretical understanding of mode mixing in FELs in the weak field limit. In the calculation of the theoretical curve, the amplitudes of the first few terms in the matrix are found to be $|g_{10}/g_{00}| = .46$, and $|g_{20}/g_{00}| = .17$; the higher terms are less than 10%. This means that the amplitudes added to the two higher order modes are .46 and .17 of the amplitude added to the lowest order mode, respectively.

(The power added to the higher order modes is very low in this experiment, 10^{-9} and 10^{-10} of the laser power vs. $4X10^{-4}$ for the lowest mode, because the gain is low and no higher order mode power is present in the input beam.) It is clear that significant mode mixing is ocurring with an electron beam to laser beam size ratio of $\eta = 2\bar{\sigma}/Wo = 0.96$. If a laser of moderately high gain is operated with such a beam ratio, the oscillator mode will differ significantly from a Gaussian.

The data of Figures 5 and 6 were taken during the initial investigations of the effect. For these curves, the laser beam dimensions are not as well characterized as for Figure 4, so theoretical curves are not available for comparison. However, this data illustrate certain qualitative features of the mode mixing effect such as the effect of changing the electron beam size and the resonance parameter.

Figure 5 show the results of two series I measurements taken as the stored current decayed by a factor of 1.9; the resonance parameter was changed only a small amount ($\delta\nu$=.1) between the two scans. Significant differences are apparent between these curves. This data demonstrates the effect of a reduction of the electron beam size.

In ACO the transverse dimensions are strongly dependent on the current stored in the ring because of the multiple Touschek effect and ion trapping. Between these two scans, the electron beam dimensions have fallen from approximately σ = 620 microns at 79 ma of average beam current to σ = 480 microns at 42 ma, which makes the beam ratios η=1.9 and 1.4, respectively. The direct effect of the current on the size of the gain is removed by the normalization, leaving only the effect of the beam size. The curve taken with the smallest electron beam shows the largest gain depression at small aperture. This confirms the theoretical expectation that smaller electron beam sizes result in more excitation of the higher order transverse modes. All off-diagonal terms in the gain matrix tend towards zero as the electron beam becomes large -- see equation (2). The shape of each curve depends on the detailed structure of the mode integrals (6) and their relative amplitudes. The shape changes as the beam size drops and modes of progressively higher order are excited. This effect is also visible in figure 8.

Figure 6 shows a later set of data taken after the lifetime of the stored beam had stabilized to a larger value. These three sets of points were taken consecutively at approximately the same electron beam size (σ= 420, 380, and 350 microns), but widely

varying resonance parameters (ν= 3.6, 3.0 ,and -3.0), which correspond to the fourth-from-the-center gain and absorption peaks on either side of the optical klystron spectrum. No systematic deviation appears between these curves, and we conclude that the transverse mode coupling is independent of the resonance parameter, as predicted by the low divergence theory. It is apparent from (2) that in the low divergence limit, the spectral term has separated out as an independent factor. This implies that both the relative amplitudes and phases of the gain matrix and therefore the shape of the gain-vs.-iris curve are independant of the resonance parameter.

This result is supported by a second type of measurement. For a given aperture diameter, a scan was taken vs. the resonance parameter. The peak positions were identified, and a new scan was taken for another diameter. No spectral shifts or changes in the shape of the spectrum were observed over a range of iris openings between full open and .9 on the horizontal scale of the figures.

The data of series II were taken with the primary goal of verifying the dependence on the distance of the aperture from the interaction region. The evidence of multiple mode input discussed above implies that the full equation (8) must be used to

calculate the aperture dependence of the gain. Unlike the case of figure 4 where an ab initio calculation is possible, here several fitting parameters would be needed since the C vector of the mode amplitudes and phases is unknown. Since these quantities cannot be obtained from the measurements of figures 1 and 2, and since we judge the results of a multi-parameter fit to be useless, no theoretical values are calculated for the Series II measurements. The experimental results alone are sufficient for the identification of a very important phenomenon which can occur in free electron lasers: active guiding.

Figure 7 shows a composite of three successive measurement scans taken in the near field at a distance from the center of the optical klystron of 2.88 m, only 13 cm from the output mirror. The large fluctuations in the amplitude are caused by the need to realign the aperture each time a new opening is selected. A large increase in the gain is observed at small aperture openings. A set of data was also taken in the far field at a distance of 14.3 m, and is presented in figure 8. The error bars for this set are comparable to those of the other 14.3 m data of figures 4-6.

The data of figure 8 were taken under the same conditions as those of figure 7. There is a large and significant difference between the data sets taken at the different distances. In the near field, we observe that the amplitude of the stimulated radiation is concentrated at the center of the amplified laser

mode. The on axis gain is enhanced by almost 50%. In the far field on the other hand, the higher order modes diverge and shift phase with respect to one another so that the enhancement disappears. A change in the distance at which the aperture is placed shifts the phases of the $\underline{T}$ matrix elements of equation (6), and therefore changes the shape of the gain-vs.-iris curve. For single mode input, the stimulated amplitude is actually reduced on axis in the far field as we have seen in figure 4.

The significance of these observations lie mainly in the implications they have for the high gain mode of operation. If the amplification is large, the propagation of the growing wave becomes dominated by the near field diffractive behavior of the stimulated radiation. We infer from the results of figure 7 that the mode which propagates in a high gain system will be more strongly concentrated about the electron beam than the freely diffracting unamplified input wave. If the gain per Rayleigh range is large, this phenomenon can lead to guided propagation in which the shape of the growing mode is unchanged throughout the interaction region. This phenomenon, in which the effects of diffraction are compensated by strong axial amplification [11], is called "gain focussing".

Although the imaginary part of the gain matrix (2) cannot be seen in a low gain experiment, in a high gain system it can shift the phase of the propagating wave significantly. As Tang and Sprangle [12] have observed, the optical phase is

retarded by the interaction on the positive gain side of the resonance curve. This implies that the stimulated wave, which we have observed to be localized to the axis of the system, tends to distort the phase fronts of the input wave in such a way as to produce a real focussing of the optical mode. Both the real and the imaginary parts of the gain conspire to actively guide the mode in the high gain case as is discussed in a recent theoretical paper by Scharlemann et al. [13].

The results of figure 4 demonstrate that our present understanding of the three dimensional effects of amplification is numerically correct. The results of figure 7 show that the gain is enhanced on axis in the near field. Taken together, these two results lend strong experimental support to the theoretical prediction of active guiding in FEL systems.

V. CONCLUSION

This experiment is the first capable of resolving an excitation of the higher order transverse modes in a free electron laser, and has established the existence of off-diagonal terms in the transverse gain matrix. The technique we have developed is a useful diagnostic of the transverse mode mixing effect which is invisible in today's FEL oscillators due to the low gain, but which will play a dominant role in the operation of the high gain devices now being constructed or planned.

High gain free electron lasers will show strong effects of mode mixing in any system in which the electron and laser beam sizes are comparable. We have demonstrated that mode mixing effects are typically large in free electron lasers but that they have been masked in the existing devices by the low value of the gain. The results of this experiment indicate that the basic theory is valid, and that it is complete in the linear regime. As discussed in the [illegible] section, these results lend strong experimental support to the theoretical prediction of active guiding in high gain free electron laser systems.

Acknowledgements: This research was supported in part by the Advanced Research Projects Agency of the Department of Defense, and the Air Force Office of Scientific Research under contracts F49620-83-C-0149 and F49620-83-K-0030, by the Direction des Recherches, Etudes et Techniques contract 81/131.

REFERENCES

1) P. Elleaume, D. A. G. Deacon, "Transverse Mode Dynamics in a Free Electron Laser", Appl. Phys. B33, 9-16 (1984).

2) M. Billardon, P. Elleaume, J. M. Ortega, C. Bazin, M. Bergher, M. Velghe, Y. Petroff, D. A. G. Deacon, K. E. Robinson, J. M. J. Madey, "First Operation of a Storage Ring Free Electron Laser", Phys. Rev. Lett. 51, 1652-1655 (1983).

3) P. Elleaume, J. M. Ortega, M. Billardon, C. Bazin, M. Bergher, M. Velghe, Y. Petroff, D. A. G. Deacon, K. E. Robinson, J. M. J. Madey, "Results of the Free Electron Laser Oscillation Experiments on the ACO Storage Ring", Journ. de Phys. 45, 989-996 (1984).

4) D. A. G. Deacon, J. M. J. Madey, K. E. Robinson, C. Bazin, M. Billardon, P. Elleaume, Y. Farge, J. M. Ortega, Y. Petroff, M. F. Velghe, "Gain Measurement on the ACO Storage Ring Laser", IEEE Trans. Nucl. Sci. NS-28, 3142-3144 (1981).

5) D. A. G. Deacon, K. E. Robinson, J. M. J. Madey, C. Bazin, M. Billardon, P. Elleaume, Y. Farge, J. M. Ortega, Y. Petroff, M. F. Velghe, "Gain Measurements vs. Theory for the ACO Storage Ring Laser", Opt. Commun. 40, 373-378 (1982)

6) J. M. Ortega, C. Bazin, D. A. G. Deacon, "Optimization of a Permanent Magnet Undulator for Free Electron Laser Studies on the ACO Storage Ring", J. Appl. Phys. 54, 4776-4783 (1983).

7) D. A. G. Deacon, M. Billardon, P. Elleaume, J. M. Ortega, K. E. Robinson, C. Bazin, M. Bergher, M. Velghe, J. M. J. Madey, Y. Petroff, "Optical Klystron Experiments for the ACO Storage Ring Free Electron Laser", Appl. Phys. B34, 207-219 (1984).

8) W. B. Colson, "One Body Analysis of Free Electron Lasers", in Physics of Quantum Electronics, 5, 157-196 (1978), eds. S. F. Jacobs, M. Sargent III, M. O. Scully, (Addison-Wesley, Reading, Mass.)

9) S. Benson, D. A. G. Deacon, J. N. Eckstein, J. M. J. Madey, K. Robinson, T. I. Smith, R. Taber, "Review of Recent Experimental Results From the Stanford 3 micron Free Electron Laser", Journ. de Phys. C1, 353-362 (1983), eds. D. A. G. Deacon, M. Billardon, (Editions de Physique, Les Ulis, France).

10) G. R. Neil, J. A. Edighoffer, "Measurements of Optical Beam Quality in an FEL", SPIE 453, 114-117 (1984), eds. C. A. Brau, S. F. Jacobs, M. A. Scully, (SPIE Bellingham, Washington).

11) H. Kogelnik, Appl. Opt. 4, 1562 (1965), and B. N. Perry, P. Rabinowitz, and M. Newstein, "Wave Propagation in media with focused gain", Phys. Rev. A27, 1989-2002 (1983).

12) C. M. Tang, P. Sprangle, "The Three Dimensional Non-Linear Theory of the FEL Amplifier", in Physics of Quantum Electronics 9, S. F. Jacobs, G. T. Moore, H. S. Pilloff, M. Sargent III, M. O. Scully, R. Spitzer (eds), 627-650 (1982).

13) E. T. Scharlemann, A. M. Sessler, J. S. Wurtele, "Optical Guiding in a Free Electron Laser", (unpublished) UCRL-91476 Preprint, Technical Information Department, Lawrence Livermore National Laboratory, Livermore, CA 94550.

FIGURE CAPTIONS

Figure 1

The laser beam was measured with a Reticon diode array to determine its mode characteristics. The beam parameter W(z) measured in Series II is plotted and compared to a TEMoo Gaussian fit. The beam is well focussed into the klystron, whose position is indicated at the center of the horizontal axis.

Figure 2

Photographs of the transverse laser profiles during series II, taken by the Reticon at two longitudinal positions: at the center of the optical klystron, and 4.3 m in front of it. In the center of the laser interaction region, the laser profiles can be fit well with a Gaussian shape. However, far from the focus, the profiles acquire a significant non-Gaussian pedestal which is apparent in the photo on the left (the discontinuity in the vertical profile is an artifact caused by a bad diode). This data

shows the laser beam in its most Gaussian configuration for the Series II measurements. Much cleaner Gaussian behavior was obtained in Series I.

Figure 3

The electron beam measurement scheme. Synchrotron light emitted in the bending magnet before the klystron is imaged onto the Reticon.

Figure 4

Measured ratio of stimulated power to incident laser power transmitted through an analyzing aperture as a function of its diameter. The diameter of the aperture is normalized to the laser beam wai parameter at the measurement point, and the gain ratio is normalized to unity at large aperture opening. The points were measured on two successive scans; the error bars can be estimated by the deviation of the points from each other. The solid curve is the theoretical [1] result, using the measured beam parameters: Wo = 670 microns for the laser, and σ = 320 microns for the electron beam. The iris was placed in the far field at 14.3 m from the optical klystron, where the optical wave had grown to w_o = 3.2 mm.

Figure 5

The gain is measured as a function of the iris diameter as in figure 4, but now for two different electron beam sizes. The triangles, taken for the small electron beam size, show the largest deviation from unity, and therefore the largest excitation of the higher order modes. As explained in the text, smaller electron beam sizes result in larger values for the off-diagonal terms in the transverse gain matrix. The shift in the resonance parameter between the two curves is inconsequential, as shown in figure 6.

Figure 6

The gain is measured as a function of the iris diameter for three different values of the resonance parameter which correspond to gain and absorption peaks displaced by four optical klystron fringes (more than half of the gain curve) from the center. The data all fall along the same curve within the error bars, and we conclude that the mode mixing effect does not depend on detuning in this low divergence experiment. The changes in the beam size are small (and unavoidable due to the current decay in ACO during these measurements).

Figure 7

In the second series of experiments, the gain is measured as a function of aperture for a position as close to the output of the

optical klystron as possible. The error bars are large here because of the constant realignment of the aperture position. The beam sizes are $\sigma_H = 450\,\mu$ and $\sigma_V = 310\,\mu$ for the triangles, and $\sigma_H = 340\,\mu$ and $\sigma_V = 290\,\mu$ for the remaining points. The input laser is operating multimode (see figure 2).

Figure 8

Two scans of the gain vs. diameter taken in the far field of the interaction region under the same conditions as those of figure 7. The deviation of these results from those of figure 7 is due to the difference between the near-field and the far-field phases of the higher order excited modes. As was seen in figure 5, the scan with the smaller electron beam $\sigma_H = 360\,\mu$ and $\sigma_V = 330\,\mu$ (the solid points) shows a larger deviation from unity than that with the larger beam $\sigma_H = 450\,\mu$ and $\sigma_V = 420\,\mu$ (the open squares).

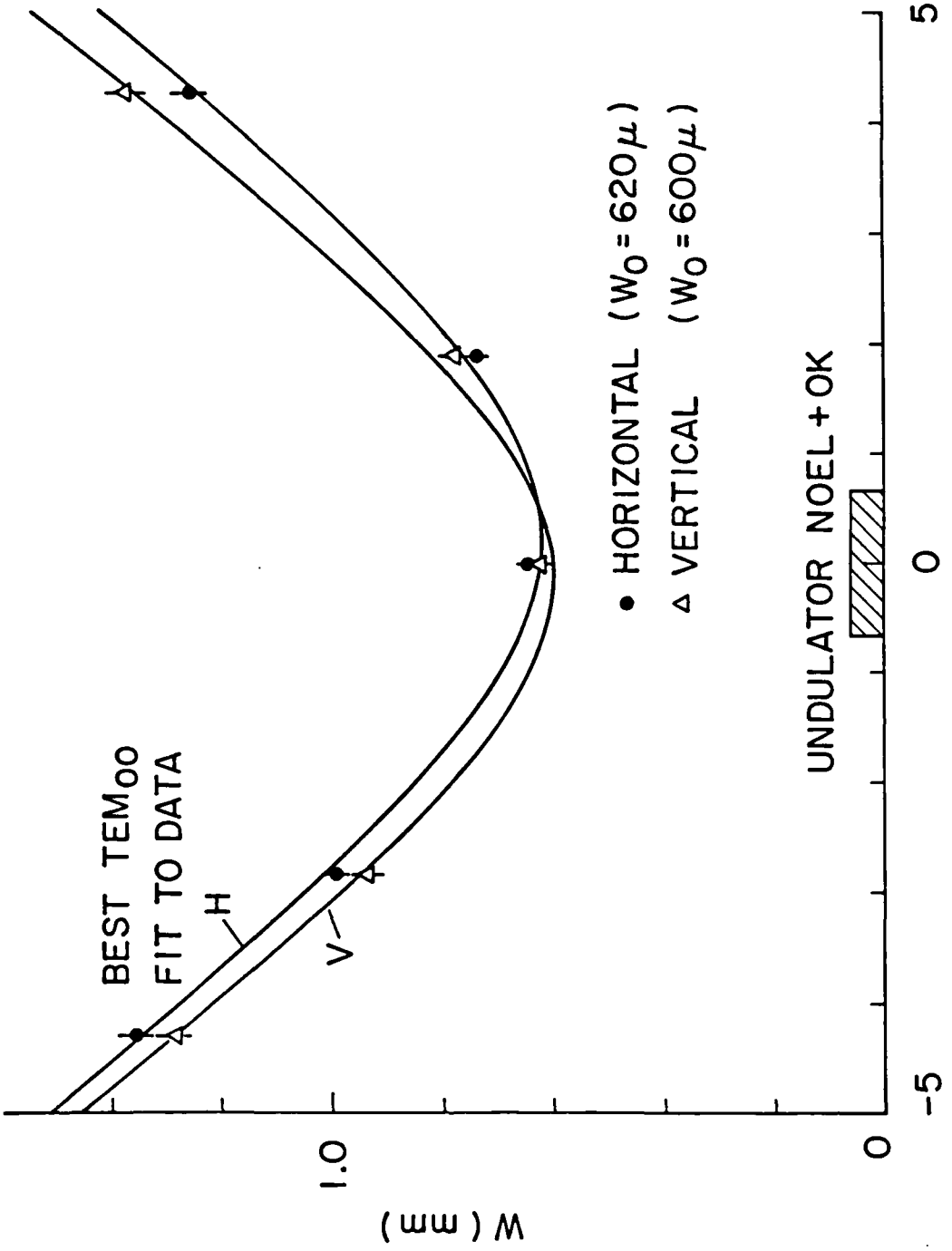
BEST TEM00
FIT TO DATA
H
V
• HORIZONTAL (W0 = 620μ)
Δ VERTICAL (W0 = 600μ)
UNDULATOR NOEL + OK
W (mm)
1.0
0
-5
0
5
z (m)

FIGURE 1

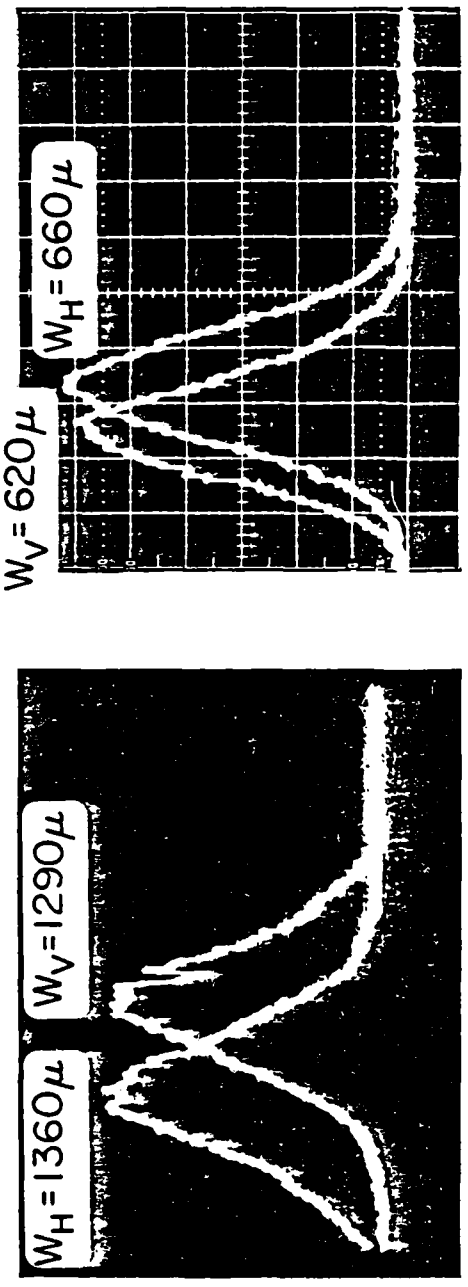

FIGURE 2

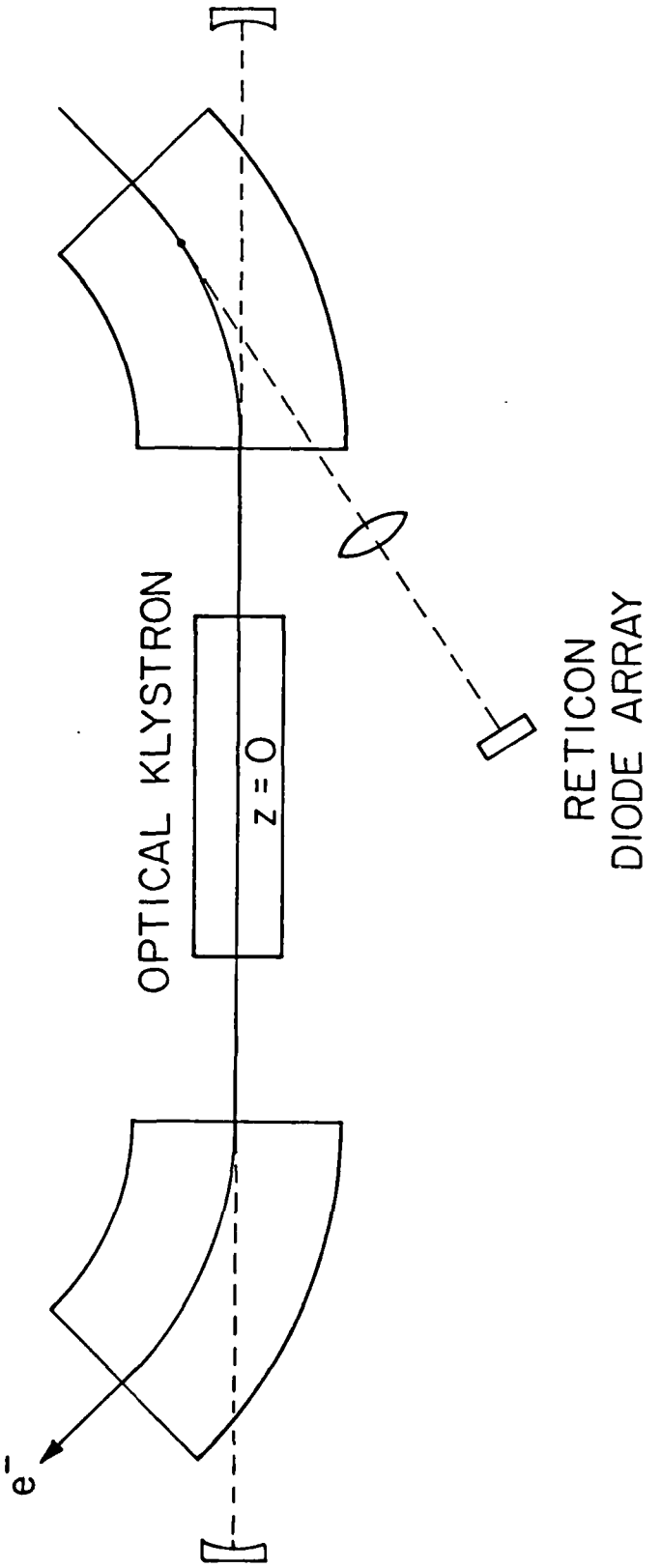

FIGURE 3

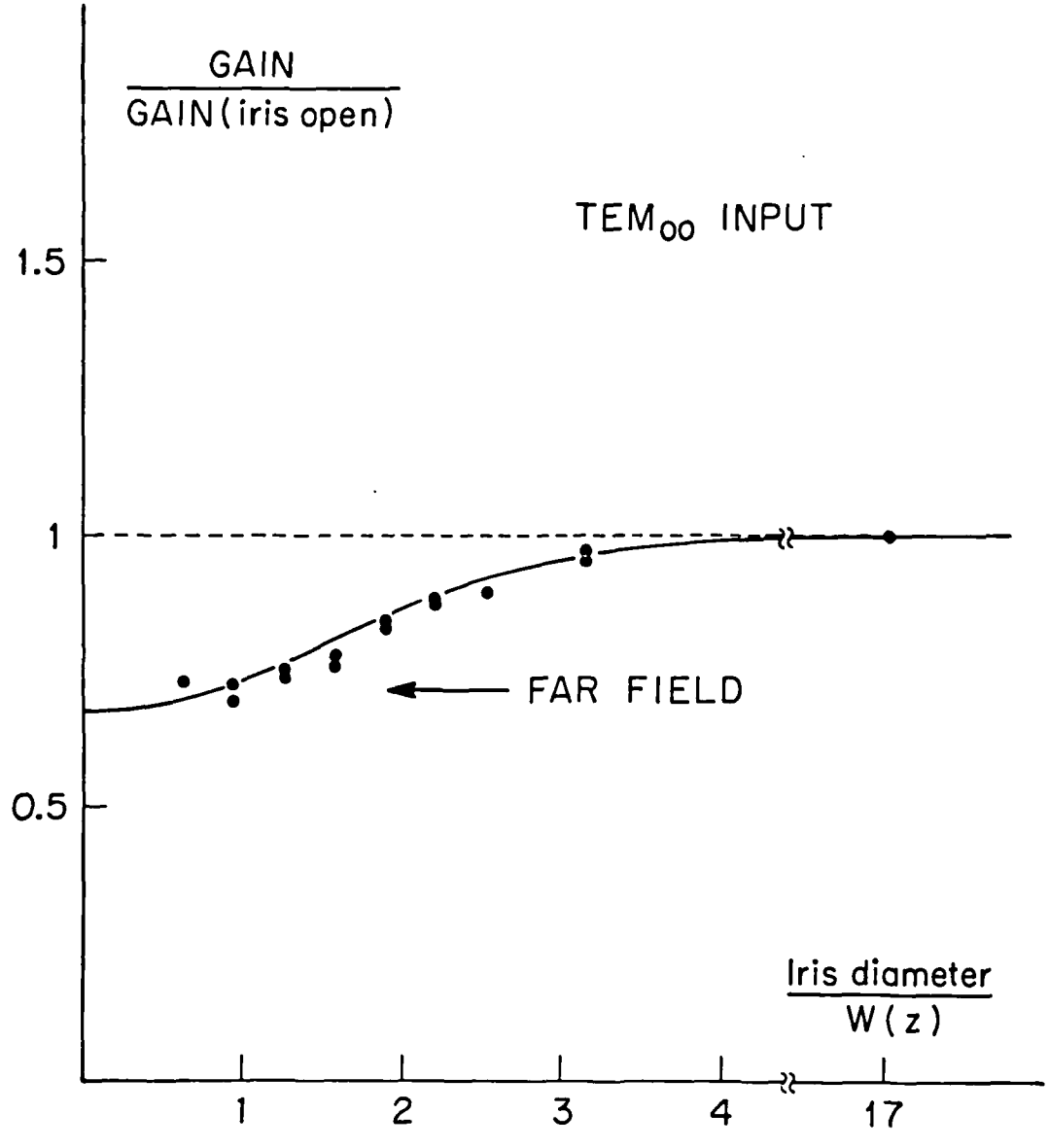
GAIN
GAIN(iris open)
TEM00 INPUT
1.5
1
0.5
FAR FIELD
Iris diameter
W(z)
1
2
3
4
17

FIGURE 4

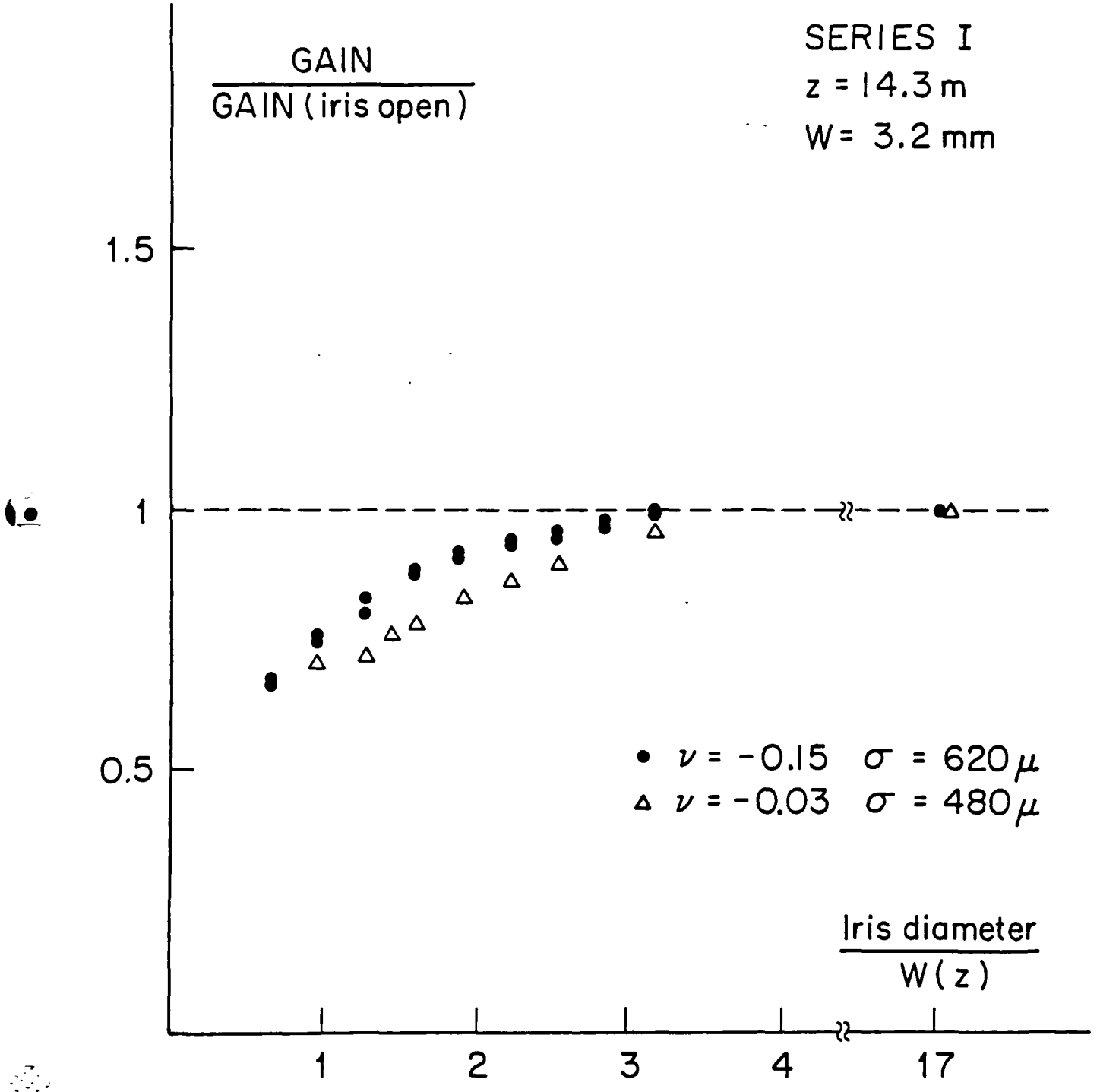
GAIN
GAIN (iris open)
SERIES I
z = 14.3 m
W = 3.2 mm
1.5
1
0.5
• ν = -0.15 σ = 620 μ
△ ν = -0.03 σ = 480 μ
Iris diameter
W(z)
1
2
3
4
17

FIGURE 5

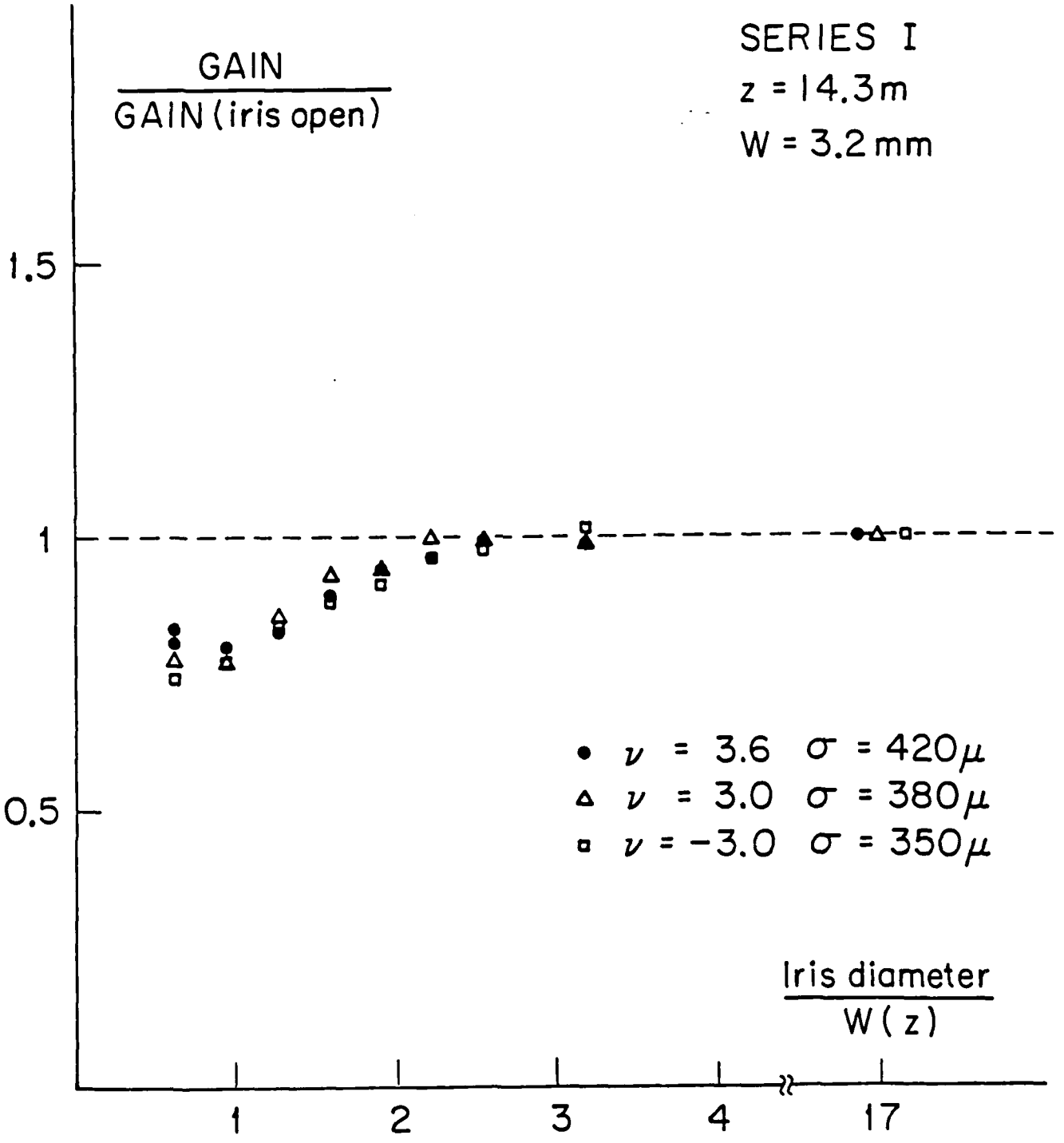
GAIN
GAIN (iris open)
SERIES I
z = 14.3m
W = 3.2 mm
1.5
1
0.5
• ν = 3.6 σ = 420μ
△ ν = 3.0 σ = 380μ
▫ ν = −3.0 σ = 350μ
Iris diameter
W(z)
1
2
3
4
17

FIGURE 6

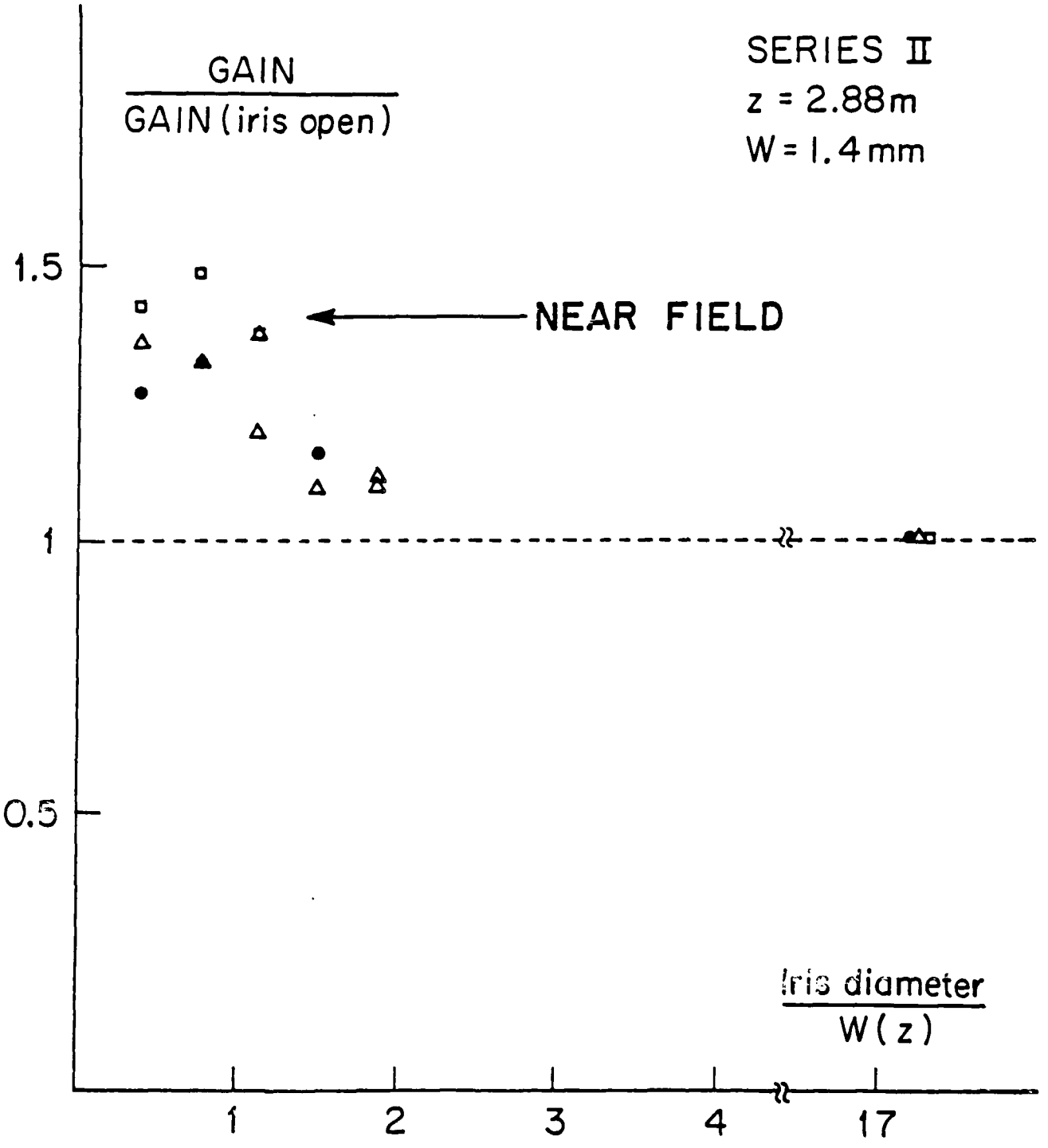
GAIN
GAIN (iris open)
SERIES II
z = 2.88m
W = 1.4mm
1.5
NEAR FIELD
1
0.5
Iris diameter
W(z)
1
2
3
4
17

FIGURE 7

5044-3
(REV A)

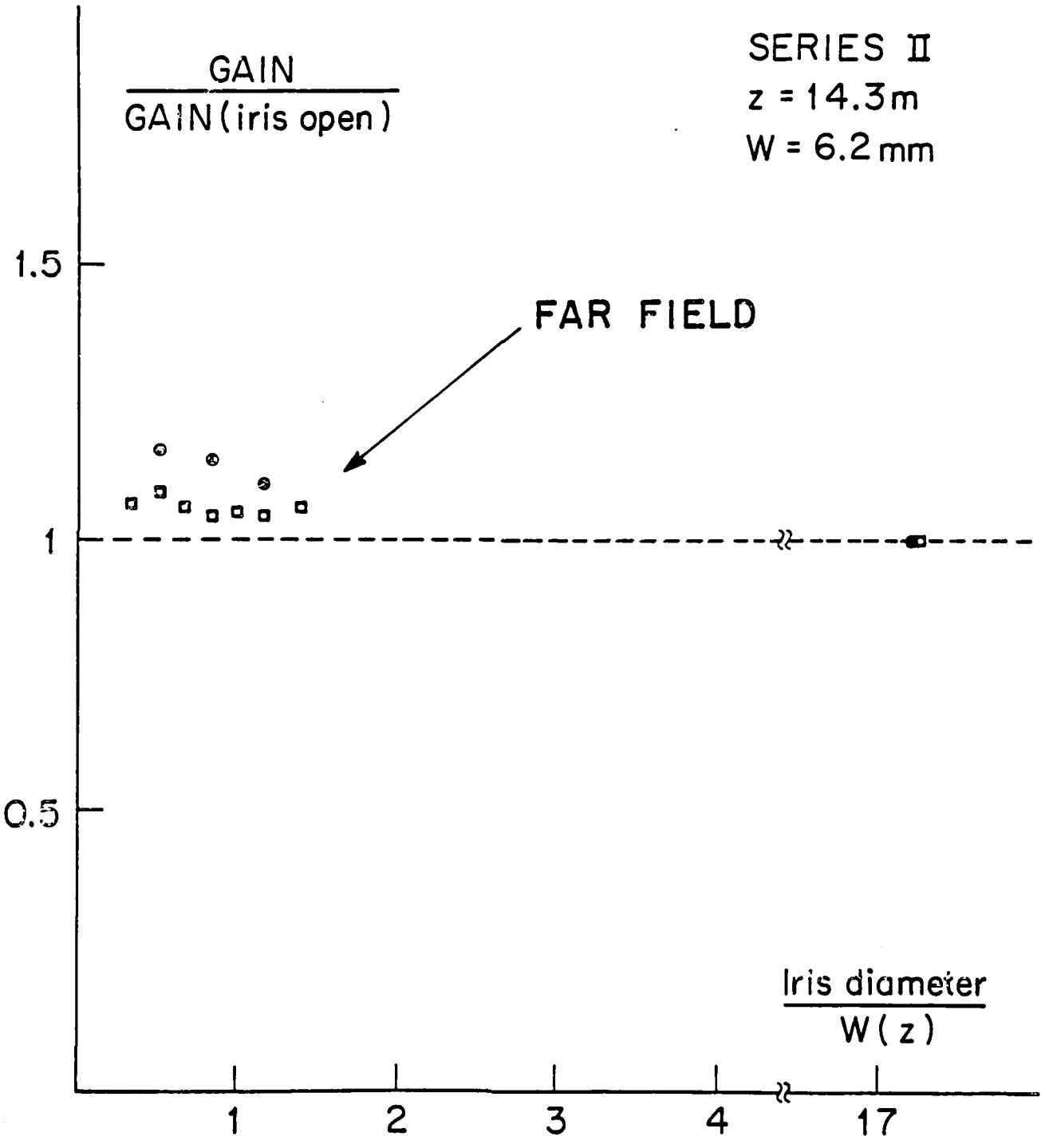

FIGURE 8

Classification
Physics Abstracts
42.55T — 42.60B — 29.20D

Results of the free electron laser oscillation experiments on the ACO storage ring

P. Elleaume ([a]), J. M. Ortéga ([b]), M. Billardon ([b]), C. Bazin, M. Bergher, M. Velghe ([c]), Y. Petroff

Laboratoire pour l'Utilisation du Rayonnement Electromagnétique,
L.P. CNRS 008, Bâtiment 209-C, Université de Paris-Sud, 91405 Orsay, France

D. A. G. Deacon ([d]), K. E. Robinson and J. M. J. Madey

High Energy Physics Laboratory, Stanford University, Stanford, CA 94305, U.S.A.

(*Reçu le 28 décembre 1983, accepté le 9 février 1984*)

Résumé. — On a fait fonctionner un laser à électrons libres sur anneau de stockage à 6 500 Å de longueur d'onde. L'effet laser a été obtenu avec des électrons de 166 MeV circulant dans l'anneau de stockage ACO. La lumière émise par les électrons lorsqu'ils passent à travers un klystron optique (une version modifiée de l'onduleur) est stockée dans une cavité optique à faibles pertes. On analyse tout d'abord les phénomènes sous le seuil. La seconde partie décrit les caractéristiques spectrales et macrotemporelles du laser. On montre que la puissance moyenne est en accord avec la limite imposée par le chauffage du paquet d'électrons (limite de Renieri). Finalement une augmentation d'un facteur 100 de la puissance crête, a été obtenue en asservissant le laser à un générateur extérieur de signaux basse fréquence.

Abstract. — A storage ring free-electron laser oscillator has been operated above threshold at a visible wavelength $\lambda \simeq 6\,500$ Å. This laser was obtained with electrons of 166 MeV circulating in the storage ring ACO. The light emitted by the electrons passing through an optical klystron (a modified version of an undulator) is stored in a high-Q optical cavity. First some below laser threshold phenomena are reported. Then the spectral and macrotemporal structure of the laser are described. The average power is shown to be consistent with the limit imposed by the heating of the electron beam (Renieri's limit). Finally a factor of 100 enhancement in the peak power, over the Renieri's limit, has been obtained by driving the laser with an external low frequency generator.

In recent years, much attention has been given to radiation emitted by relativistic electrons. This is principally synchrotron radiation in a dipole field [1], in an undulator [1] or from a free electron laser. The free electron laser (F.E.L.) is a very promising source of coherent radiation in the spectral range from the far I.R. to the V.U.V.; the earliest proposals for such a device were made by Ginzburg [2] and Motz [3].

There are basically two classes of F.E.L. One type operates in the « collective » regime where the electronic density and Coulomb interaction are very strong, the electron energy is rather low (a few MeV) and the radiation is emitted in the far I.R. [4]. The order class operates in the low density or « Compton » regime, where Coulomb interactions are negligible, the energy is high (10-10^3 MeV) and the emission comes at short wavelengths (I.R., Visible, U.V.). Our experiment belongs to the second category. This type of F.E.L. has been studied by Madey [5] and his group at Stanford where the first laser action was achieved in 1977 in I.R. [5]. Since that time many theoretical and experimental studies have been done on this subject [6].

Most F.E.L. experiments involve either linear accelerators and microtrons [7] or electron storage rings [8]. One expects the storage ring D.E.L. to reach much shorter wavelengths, particularly in the U.V.

([a]) Département de Physico-Chimie, Service de Photophysique, CEN Saclay, 91191 Gif-sur-Yvette, France.

([b]) Ecole Supérieure de Physique et Chimie, 10, rue Vauquelin, 75231 Paris Cedex 05, France.

([c]) Laboratoire de Photophysique Moléculaire, Bât. 213, Université de Paris-Sud, 91405 Orsay, France.

([d]) Deacon Research, 754 Duncardine Way, Sunnyvale, CA 94087, U.S.A.

and V.U.V. spectral range. Our experiment is the first example of an F.E.L. working on a storage ring. We have recently reported the first operation of the laser [9]. In this paper we described in more detail the operation of the F.E.L., its behaviour as a driven pulsed laser and the interpretation of its macro-temporal structure. We have used the Orsay storage ring ACO, an « old » machine, first operated in 1965. Its characteristics for this experiment are given in table I.

Table I.

ACO characteristics in the F.E.L. experiment

Energy	160-166 MeV
Circumference	22 m
Bunch to bunch distance	11 m
Electron beam current for oscillation	16 to 100 mA
R.M.S. bunch length σ_l	0.5 to 1 ns
R.M.S. bunch transverse dimensions σ_x, σ_y	0.3 to 0.5 mm
R.M.S. angular spread σ'_x, σ'_y	0.1 to 0.2 mrad
R.M.S. relative energy spread	0.9 to 1.3 × 10^{-3}
Electron beam life time	60 to 90 min
R.F. frequency	27.2361 MHz

The core of an F.E.L. is an undulator (periodic transverse magnetic field) on passage through which high energy electrons radiate a series of harmonics of a fundamental line of wavelength, λ, given by :

$$\lambda = \frac{\lambda_0}{2\gamma^2}\left[1 + \frac{K^2}{2} + \gamma^2\theta^2\right] \qquad (1)$$

where γ is the electron energy normalized to their energy at rest, λ_0 the undulator period and θ the angle of observation with respect to the electron trajectory axis. K is the deflection parameter of the undulator given by :

$$K = \frac{eB_0\lambda_0}{2\pi m_0 c} = 93.4\, B_0\, \lambda_0 \text{ in S.I. units} \qquad (2)$$

where B_0 is the peak undulator magnetic field, e and m_0 the electron charge and mass. The characteristics of our undulator/optical klystron are listed in table II.

A light beam of convenient wavelength in coïncidence with an electron beam is amplified when passing through an undulator. The magnitude of the optical gain was first calculated by Madey [5]. We have measured the gain of the Orsay undulator made with 17 periods of 7.8 cm [10] placed on the ACO storage ring working at 240 MeV. The stimulating light was an argon laser at 5 145 Å. The measured gain value was near 2 × 10^{-4} [11]. This gain is too small to achieve laser oscillation; therefore, we have transformed our undulator into an optical klystron [12] (O.K.). This is done by replacing the 3 central

Table II.

Optical klystron characteristics	
Overall length	1.3 m
Type	SmCo5 permanent magnets
Undulators	
Number of periods	2 × 7
Period	78 mm
Transverse pole width	100 mm
Minimum magnetic gap	33 mm
Maximum field	0.31 T
K	0 to 2.3
K in the F.E.L. experiments	1.1 to 1.2
Dispersive section	
Length	240 mm
Maximum field	0.58 T
N_d (see text)	70 to 100
N_d in the F.E.L. experiments	95

periods of the undulator by a longer period, analogous to a 3-pole wiggler, called the dispersive section. The rôle of this section is to « bunch » the electronic density faster than a regular undulator [12]. Therefore, the optical klystron gain, $G_{o.k.}$ is larger than the gain $G_{und.}$ of the undulator of same length by a maximum factor of :

$$\frac{G_{o.k.}}{G_{und.}} \simeq \frac{3.6 \times 10^{-3}}{\sigma_E/E} \qquad (3)$$

where σ_E/E is the R.M.S. relative energy spread of the electrons circulating in the ring.

The synchrotron light emitted by the O.K. exhibits a characteristic modulation [13] which is shown on figure 1a. The optical gain (Fig. 1b) which by virtue of the Madey's theorem [14] is the derivative of the spontaneous emission with respect to energy, also appears modulated. For a given fundamental wavelength $G_{o.k.}/G_{und.}$ depends on the magnetic gap and on the energy spread. The measured value confirms a predicted factor of 4 gain enhancement at 240 MeV and 1 × 10^{-3} energy spread.

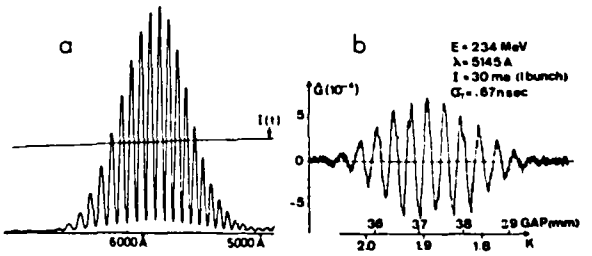

Fig. 1. — (a) On axis spectral distribution of the optical klystron spontaneous emission measured using 240 MeV electrons and a magnetic gap of 34.4 mm. (b) The corresponding gain curve *versus* magnetic gap measured with an external laser.

In this paper we present results obtained with our optical klystron working at a low electron energy (166 MeV). This energy range was chosen in order to minimize the cavity mirror degradation due to V.U.V. emissions [11] from the undulator and dispersive section.

The light emitted by the O.K. was stored in the highest-Q optical cavity that we could obtain (Table III). The measured average round trip losses

Table III.

Optical cavity characteristics

Length	5.5 m
Mirror radius of curvature	3 m
Rayleigh range	1 m
Wavelength of maximum Q	620 to 680 nm
Average mirror reflectivity at 6 328 Å	99.965 %
Round trip cavity losses at 6 328 Å	7×10^{-4}
Mirror transmission	3×10^{-5}

for the mirrors that we used were near 2×10^{-4} at 6 328 Å when the mirrors were in the air. However when placed in the ultra-vacuum of the cavity and irradiated with the light produced by the undulator or optical klystron the losses grow rapidly [11]. At 240 MeV the degradation drives the losses almost instantaneously above 1 or 2×10^{-3}. However it is possible to operate the O.K. at lower electron energy by increasing the magnet gap (thereby decreasing K) in order to keep the emitted wavelength near 6 500 Å, wavelength of maximum reflectivity for the mirrors used in these experiments. A lower K decreases the harmonics content of the undulator emission and therefore the U.V. flux received by the mirrors. The O.K. was finally operated at $K = 1.1$ to 1.2 with a dispersive section characterized by [13] $N_d \simeq 95$ where N_d is the number of laser optical wavelengths passing over an electron in the dispersive section.

At a low energy of 150 MeV, after an initial degradation the losses were stabilized near $(7 \pm 1).10^{-4}$. At this energy the optical gain is only slightly smaller than the losses and very interesting « below threshold » phenomena may be observed (§ 1). At higher energy (160-166 MeV) an intense amplification of the stored emission is observed (laser effect). The various characteristics of the laser are detailed in § 2 and discussed in § 3.

1. Below threshold phenomena (150 MeV).

When the optical cavity mirrors are set parallel to each other, the spontaneous emission of the O.K. is stored in the cavity. The resulting optical spectrum (Fig. 2, lower curve) is the spontaneous emission spectrum modified by the phase shifts of the various cavity transverse modes in which it is stored [15] and by the output mirror transmission. When the cavity length is exactly matched with the electron round-trip time

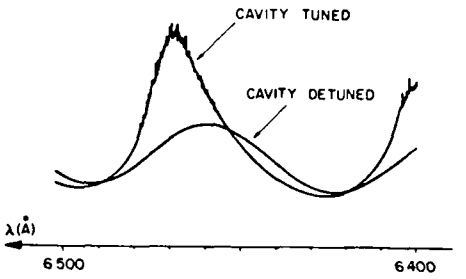

Fig. 2. — Fine structure spectrum of the stored spontaneous emission from the optical klystron. The « cavity tuned » curve is obtained for a perfect time synchronism between light and electron pulses in the cavity. The « cavity detuned » curve is obtained for complete desynchronism. Gain and absorption appear on the higher and lower wavelength side of the maximum.

in the ring the cavity is considered to be « tuned ». Then amplification of the stored spontaneous emission occurs through the gain mechanism mentioned above. One clearly sees in figure 2 an amplification at $\lambda \simeq 6\,470$ Å by a factor close to 2 and an absorption at $\lambda \simeq 6\,440$ Å by a factor 0.8. This amplification occurs at several wavelengths along the spontaneous emission curve with a maximum depending mostly on the mirrors reflectivity curve. The spectral distribution of the amplified beam is no longer proportional to the derivative of the stored spontaneous emission because of the non-linearity of the multipass amplification when the gain value is close to the cavity losses. Also the noise that can be seen at the top of the amplified curve is clearly related to the fact that we are very near the laser threshold. A small gain variation produces a large amplification variation. By aligning the optical cavity axis and the electron beam trajectory within 0.1 mm, a maximum amplification ratio of 3 has been observed for a 50 mA ring current. Figure 3 shows horizontal and vertical transverse profiles of the stored spontaneous emission recorded at $\lambda \simeq 6\,470$ Å, corresponding to the most amplified wavelength. The net amplification (obtained by subtracting the cavity detuned curve from the cavity tuned one) has a profile very close to the fundamental cavity TEM_{00} profile.

The amplification is a sharp function of the adjustment of the cavity length. The dependence of its value *versus* the detuning of this length is shown on figure 4. The amplification as a function of the mirror displacement from the tuned position, δ, can be computed by summing the contributions over the electron positions (characterized by δ_0) inside the electron bunch and over a quasi-infinite number of pass, n, in the optical cavity. Let $F(\delta)$ be that sum, then :

$$F(\delta) = (1 - \overline{R}^2) \int \sum_{n=0}^{n} \overline{R}^{2n} \times \times \prod_{p=0}^{n} [1 + g_p f(\delta_0 + 2p\delta)] f(\delta_0)\, d\delta_0 \quad (4)$$

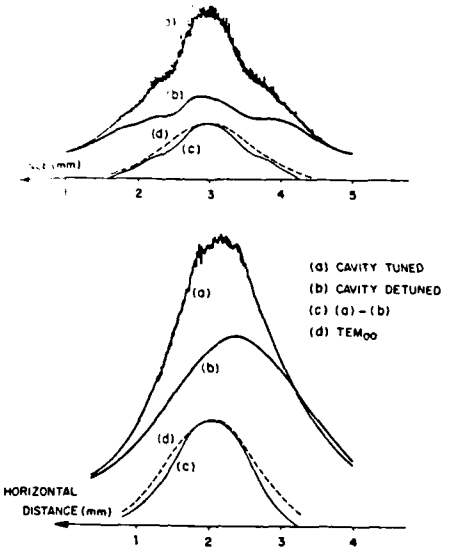

Fig. 3. — Horizontal and vertical profiles of the stored spontaneous emission at the wavelength of maximum gain. The difference between the « cavity tuned » and « cavity detuned » curves show a good agreement with the cavity TEM_{00} profile.

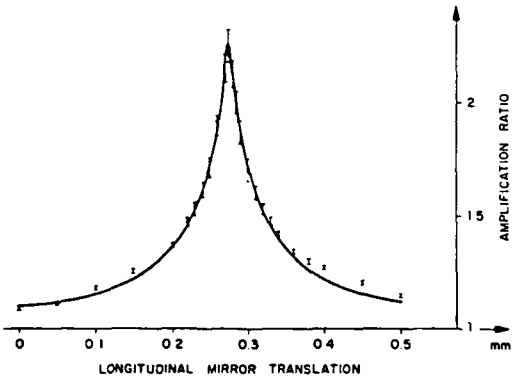

Fig. 4. — Maximum on axis amplification ratio *versus* cavity length. The dark curve shows the theoretical prediction for 0.23 m R.M.S. bunch length, 3.6×10^{-4} average loss per mirror and 5.1×10^{-4} peak gain per pass.

where $\bar{R}$ is the average reflectivity per mirror, $f(\delta_0)$ is the normalized shape function of the electron bunch and g_p the peak gain at the wavelength considered. From (4) one deduces :

$$F(\delta = \infty) = 1 \quad \text{and} \quad F(\delta = 0) = \int \frac{f(\delta_0)\, d\delta_0}{1 - \dfrac{g_p f(\delta_0)}{1 - \bar{R}^2}} \tag{5}$$

valid for $g_p < 1 - \bar{R}^2 = P$.

For a uniform distribution of the electrons inside the bunch (5) reduces to :

$$F(\delta = 0) = [1 - g_p/P]^{-1}.$$

This would yield $g_p/P = 0.60$ in the case of figure 4 (amplification by 2.5). In our case (Gaussian electronic distribution) the integral has been computed numerically using the measured R.M.S. bunch length of 0.23 m. The best fit to the experimental results shown in figure 4 was obtained for $P = 7.2 \times 10^{-4}$ (close to the measured value of 7.0×10^{-4}) and $g_p/P = 0.71$.

Very good agreement has also been found in the tail of this detuning curve showing a significant amplification of 1.02 for a detuning as high as 0.8 mm.

2. Above threshold phenomena.

At 166 MeV laser oscillation is obtained by a careful alignment of the electron beam on the cavity axis (within 0.1 mm and 0.1 mrad) and maximization of emission as a function of the storage ring R.F. cavity voltage and the optical cavity length. Laser operation requires very precise synchronism between the light pulse round trip frequency and the bunch revolution frequency. To avoid backlash and mirror misalignment, fine tuning was performed by slightly changing the R.F. frequency instead of translating the mirrors. Laser oscillation lasted typically 1 h after each electron injection.

Due to the weak gain/loss ratio the cavity length (or R.F. frequency) is a very crucial parameter. Figure 5 shows two « detuning curves » of laser power (normalized to the maximum) *versus* R.F. frequency variation and equivalent mirror displacement. Curve (a) has a 3.4 μm F.W.H.M. of equivalent mirror displacement; curve (b), recorded much closer to laser threshold, has only a 1.6 μm F.W.H.M. The shift in displacement between curves (a) and (b) is probably

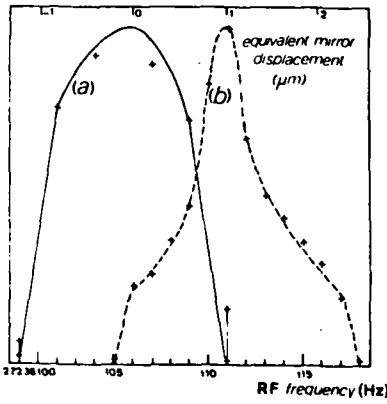

Fig. 5. — Normalized laser power as a function of R.F. frequency and equivalent mirror displacement. Curve (a) is recorded close to the maximum gain/loss ratio and curve (b) close to the laser threshold. The shift between the two curves is probably due to some slight cavity length drift. The upper scale has to be multiplied by a factor 2.

due to a slow cavity length drift (a temperature drift of 0.02 °C in 30 min would be sufficient). However the length of the cavity was stable enough to allow laser operation without adjustments during typically more than half an hour.

The horizontal and vertical transverse profiles of the laser mode are very close to the cavity TEM_{00} mode (Fig. 6) as expected from the below threshold measurement. The small observed discrepancies may arise from some residual instability of the laser too close to threshold or from non uniform mirror reflectivity.

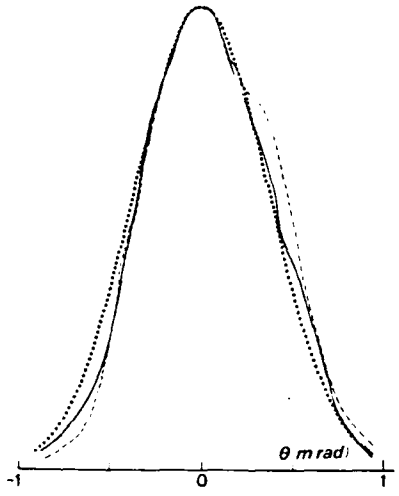

Fig. 6. — Experimental laser horizontal (——) and vertical (- - -) transverse profiles and the calculated (...) cavity TEM_{00} profile

The laser exhibits a particular time structure : (i) it is pulsed at the ACO storage ring frequency (27.2 MHz with two bunches in the ring), (ii) its structure on a long time scale (of the order of 1 s) is quite irregular as shown by the photograph in figure 7a, (iii) the laser may be triggered by an external low-frequency generator (Fig. 7b). This will be discussed in section 3.

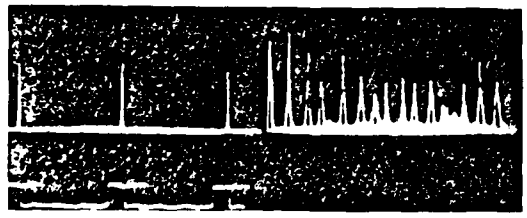

(b) (a)

Fig. 7. — Laser time structure over a 200 ms total interval, (a) « natural » time structure; (b) time structure when the electron beam transverse position is modulated (upper trace). The vertical scale is 1/4 the scale on (a) (see text).

Figure 8 presents two spectra : (a) is recorded without amplification (optical cavity completely detuned), (b) is recorded at laser operation (cavity tuned).

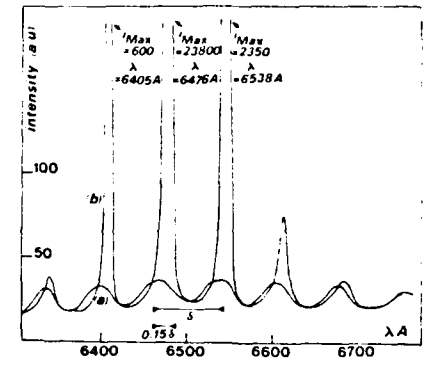

Fig. 8. — Spectra of the cavity output radiation under two conditions : (a) cavity detuned (no amplification), (b) cavity tuned (laser on).

For case (b), the laser oscillates at three wavelengths, with a strongly dominant one at $\lambda = 6\,476$ Å ; each wavelength is located at a maximum of the gain *versus* wavelength curve [5]. Typical laser lines are Gaussian if averaged over a long time scale of $\geqslant 1$ s with 2 to 4 Å F.W.H.M.

The central wavelength of any line is always equal to the wavelength of maximum emission of spontaneous emission with the cavity completely detuned (no amplification) plus 0.15 of the wavelength interfringe distance (see Fig. 8) instead of 0.25 as predicted from Madey's theorem [14]. This discrepancy is probably due to the transverse multimode content of the spontaneous emission stored in the cavity ; laser operation is only achieved on the TEM_{00} mode. Laser tunability was obtained between 640 nm to 655 nm by changing the magnetic gap (equivalent to a change of K in Eq. (1)). The range of tunability is limited for the moment by the mirror reflectivity bandwidth.

The laser spectrum has also been recorded on a Reticon diode array. The laser was driven by the Reticon « start » signal in order to synchronize the laser pulses with the Reticon read out. For a driving frequency of $\sim$ 800 Hz, as discussed in section 3, the laser pulse intensities were unstable and it was observed that the higher the pulse the narrower its spectral line. For the higher pulses the observed spectral width is less than 1 Å (Fig. 9) well below the above mentioned spectral width.

In the experiments the gain is not directly proportional to the electron current, mainly due to the anomalous bunch lengthening and energy spreading at high current. These effects make that the gain *versus* ring current reaches a broad maximum near 50 mA and then decreases. However despite this effect and despite the irregular pulsed time structure described above the laser average power is very stable and depends almost linearly on the ring current as shown by the recording of figure 10. This fact shows clearly that the free electron laser has saturated and reached its equilibrium average power.

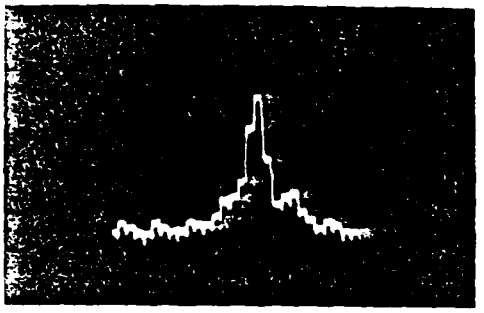

Fig. 9. — Recording of the spectral distribution of a laser pulse on a reticon diode array. The laser was driven at a frequency of 8.8 kHz (see text). Each diode corresponds to 0.3 Å in wavelength which is also the spectral resolution of the monochromator used.

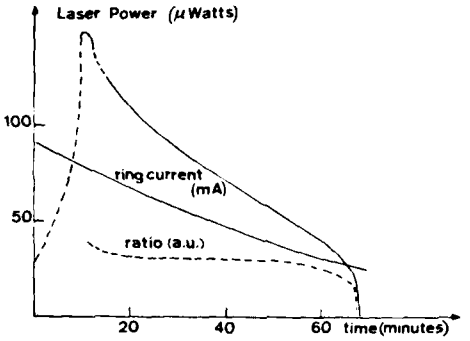

Fig. 10. — Recording of the laser average output power together with the ring current. The ratio of the two quantities is a constant on most of the laser operation range.

3. Laser saturation and peak power enhancement

It has been shown that storage ring F.E.L. would saturate by laser induced electron energy spread which would decrease the gain by inhomogeneous broadening [16]. The energy spreading is also expected to lengthen the electron bunch and decrease the peak density and therefore the peak gain [17]. Renieri [16] has shown that the average power (P_a) is a fraction η of the total synchrotron radiation (P_s) emitted by a single bunch in the whole storage ring. η represents the laser efficiency since it is the ratio between the laser power and the Radio Frequency (R.F.) power given by the R.F. cavity to the electron beam to compensate for the power lost by electrons by synchrotron radiation emission. η has been calculated for a weakly saturated optical klystron to be (18) :

$$\eta = \eta_c \frac{f}{2\pi(N + N_d)} \operatorname{Ln}(g_0/P)$$

where

$$\eta_c = \frac{\text{output mirror transmission}}{\text{round trip cavity losses}} \qquad (7)$$

η_c is the cavity efficiency, f is the optical klystron modulation rate [13]. N is the number of periods of one of the two identical undulators constituting the optical klystron. g_0/P is the ratio between the start-up peak-gain and the round trip cavity losses.

The laser output power always decreases with the electron beam current and, except in regions too close to threshold, is usually proportional to the current (see Fig. 10). Such a result is in good agreement with the theory since P_s is proportional to the current but η is only weakly current dependent. A typical 75 μW average output power has been recorded at 50 mA current of 166 MeV electrons; this corresponds to an efficiency $\eta = 4.8 \times 10^{-5}$ with respect to the 1.55 W of single bunch total synchrotron radiation. Taking the following measured quantities, $\eta_c = 0.047$ (due to the high absorption losses in the dielectric layers of the mirrors compared to the transmission), $f = 0.7$, $N + N_d \simeq 100$ and assuming $g_0/P = 3$, one calculates $\eta = 5.7 \times 10^{-5}$.

Considering the errors in the calibration of ring current and power meter and the uncertainty in the determination of g_0/P, one concludes in the good agreement of the measured average power with the one predicted by theory [18]. This theory does not consider the anomalous bunch lengthening and energy spreading as observed on ACO and on almost every storage ring. The most striking example of this anomalous behaviour was the observed bunch shortening and electron energy spread reduction at the initial laser start-up. Although, as we shall see later, the bunch lengthens when the laser saturates as predicted by the theory.

The rather low average output power is therefore the result of the weak total synchrotron radiation power at 166 MeV, the low cavity efficiency and the high sensitivity of the optical klystron to the energy spread.

Figure 7a shows the observed F.E.L. time structure over a 200 ms time interval. The irregular time structure of the laser is the result of the large difference in magnitude between the fast laser rise time, τ_m, of the order of 50 to 100 μs, and the slow response time τ_s of the electron beam, which is 200 ms at 166 MeV. It has long been anticipated that at the instant of laser turn-on in a storage ring laser, the power would dramatically overshoot the equilibrium value and perharps oscillate until the electron beam had a chance to stabilize at a level which saturates the gain. Our results show that such an equilibrium may be very difficult to obtain due to fluctuations in the gain. Elleaume [19] has recently studied the stability of the laser, and found that although the equilibrium situation is stable, it is only weakly damped. The laser operation is resonant at a period T_r of the order of $2\pi\sqrt{\tau_s \tau_m/2}$ (15-25 ms for these experiments as shown in Fig. 7a), and even a very small fluctuation of the electron energy spread, the bunch length, or the electron beam position with this period will cause the laser to pulse on and off.

In more than 15 successive experimental runs, involving ring currents ranging from 80 to 15 mA, continuous operation has never been observed. The laser always pulses in an irregular, pseudo-periodic fashion with a period of 10 to 25 ms. Sometimes, the peaks are more or less modulated at the ring synchrotron frequency (~ 13 kHz).

As a consequence of this high sensitivity to gain fluctuations, the laser may be triggered by an external low-frequency signal. Stable pulsed operation has now been achieved by modulating either the transverse beam position or the R.F. frequency. Figure 7b shows a single trace of the laser output when the transverse position of the electron beam is periodically displaced. The peak power has been increased by a factor of 4 over that of figure 7a; the horizontal time scale is the same. This result was obtained by turning on the gain long enough for the pulse to develop, heat the beam, and decay, and turning it off again for a long time to allow the beam to cool down. A vertical displacement of 160 μm is enough to turn off the laser. The beam motion is adiabatic with respect to the betatron motion in the ring, so the transverse dimensions are not affected by the periodic orbit distortion. Stable driven pulses have also been obtained by modulating the R.F. frequency back and forth from the synchronism condition, but this procedure presents the disadvantage of inducing synchrotron oscillation of the electron bunch.

When driven by beam displacement as shown in figure 7b, pulse widths less than 1 ms are obtained with periods from 1 to 60 ms. No change in the average power is observed over this range, although the peak power can be adjusted by more than a factor of ten. A peak power 100 times larger than the average power has been obtained so far.

This pulsed operation of the laser allows another test of the saturation theory. Figure 11 presents the laser pulse structure together with a signal proportionnal to the bunch length. The bunch length measurement technics is described in [17]. A negative variation corresponds to a bunch lengthening. One clearly sees a fast bunch lengthening induced by the laser pulse followed by a slow relaxation time. The bunch length curve appears to be the integral of the laser pulse shape. These results were precisely predicted to occur with energy spread [18] and therefore

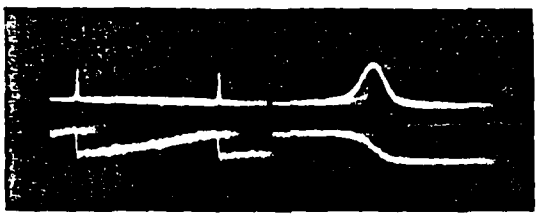

Fig. 11. — Time recording of the laser intensity (upper trace) together with the bunch length evolution (lower trace). A negative signal corresponds to a lengthening of the bunch. The total time interval is 100 ms for the left picture and 5 ms for the right one.

bunch length since energy spreading automatically induces a bunch lengthening in a time of the order of the synchrotron period (0.08 ms) which is much shorter than the pulse duration.

Therefore the laser time structure can be understood by a simple model [19] where the fast increase in energy spreading is responsible of the off-equilibrium behaviour of the system. The energy spread evolution has been verified experimentally through the time-resolved recording of the electron bunch length. Moreover we have shown that this off-equilibrium laser behaviour offers an opportunity to drive the laser intensity by an external trigger and to obtain a pulsed laser without any lost of average power.

The experiments will continue in the future to analyse the short time structure of the laser with a streak camera. Also higher gain/loss ratios are expected to be obtainable at higher energy and from the use of better mirrors, a second R.F. cavity and positrons instead of electrons. This should extend the range of tunability of the laser towards the U.V. region.

This work was supported by DRET contract no. 81/131 and AFOSR contract no. F 49620-80-C-0068.

Acknowledgments.

The authors are greatly indebted to Yves Farge who initiated this research, to the technical support staff of the L.U.R.E. laboratory for their invaluable help. Also, they thank the storage ring staff of the LAL for many fruitful discussions.

References

[1] For the calculation of the synchrotron radiation see : JACKSON, J. D., *Classical electrodynamics* 2nd Ed. Section 14.5 (Wiley and Sons NY) 1975.
For the undulator radiation see for example : HOFMAN, A., *Nucl. Instrum. Meth.* **152** (1978) 17 and COISSON, R., *Phys. Rev. A* **20** (1979) 524.
For a review of the practical possibilities on a storage ring see : THOMPSON, D. J. and POOLE, M. W., European Synchrotron Radiation Facility, Supp. II, the Machine (E.S.F., Strasbourg, France) 1979 p. 52.

[2] GINZBURG, V. L., *Bull. Acad. Sc. U.S.S.R., Sov. Phys.* **11** (1947) 165.

[3] MOTZ, H., *J. Appl. Phys.* **22** (1951) 527.
MOTZ, H., THON, W., WHITEHURST, R. N., *J. Appl. Phys.* **24** (1953) 826.

[4] MACDERMOTT, D. B., MARSHALL, T. C., SCHLESINGER, S. P., PARKER, R. K., GRANASTEIN, V. L., *Phys. Rev. Lett.* **41** (1978) 1368.

[5] MADEY, J. M. J., *J. Appl. Phys.* **42** (1971) 1906.
DEACON, D. A. G., ELIAS, L. R., MADEY, J. M. J., RAMINA, G. L., SCHWETTMAN, H. A. and SMITH, T. I., *Phys. Rev. Lett.* **38** (1977) 892.

[6] Free Electron Generators of Coherent Radiation, Physics of Quantum Electronics, vols. 8 and 9 (Addison-Wesley, New York) 1982 ; many chapters are devoted to existing or future FEL projects.

[7] See ref. [6] chapters 2-3-17 and :
COOPER, R. K., MORTON, P. L., WILSON, P. B., KEEFE, D., FALTENS, A., *J. Physique Colloq.* **44** (1983) C1-185.

[8] See ref. [6], chapters 4-6-7-8 and :
WIEDEMAN, H., *J. Physique Colloq.* **44** (1983) C1-201.
LE DUFF, J., *J. Physique Colloq.* **44** (1983) C1-217.

[9] BILLARDON, M., ELLEAUME, P., ORTEGA, J. H., BAZIN, C., BERGHER, M., VELGHE, M., PETROFF, Y. and DEACON, D. A. G., ROBINSON, K. E. and MADEY, J. M. J., *Phys. Rev. Lett.* **51** (1983) 1652.

[10] ORTEGA, J. M., BAZIN, C., DEACON, D. A. G., DEPEAUTEX, C., ELLEAUME, P., *Nucl. Instrum. Meth.* **206** (1983) 281.
ORTEGA, J. M., BAZIN, C., DEACON, D. A. G., *J. Appl. Phys.* **54** (1983) 4776.

[11] BILLARDON, M., DEACON, D. A. G., ELLEAUME, P., ORTEGA, J. M., ROBINSON, K. E., BAZIN, C., BERGHER, M., MADEY, J. M. J., PETROFF, Y., VELGHE, M., *J. Physique Colloq.* **44** (1983) C1-73.

[12] VINOKUROV, N. A. and SKRINSKII, A. N., Preprint INP 77.59 (Novosibirsk, 1977).
VINOKUROV, N. A., Proc. 10th Int. Conf. on high energy charged particle accelerators, Serpukhov, **2** (1977) 454.

[13] ELLEAUME, P., *J. Physique Colloq.* **44** (1983) C1-333 and *Physics of Quantum Electronics*, vol. 8, ch. 5 (Addison-Wesley, New York) 1982.

[14] MADEY, J. M. J., *Il Nuevo Cimento* **B 50** (1979) 64.
KROLL, N. M. and ROSENBLUTH, M. N., *J. Physique Colloq.* **44** (1983) C1-85.
DEACON, D., ROBINSON, M., MADEY, J., BAZIN, C., BILLARDON, M., ELLEAUME, P., FARGE, Y., ORTEGA, J. M., PETROFF, Y., VELGHE, M., *Optics Commun.* **40** (1982) 373.

[15] ELLEAUME, P., DEACON, D. A. G., to be published in *Appl. Phys. B* (1983).

[16] RENIERI, A., *Il Nuovo Cimento* **B 53** (1979) 160.
DATTOLI, G. and RENIERI, A., *Il Nuovo Cimento*, **59B** (1980) 1.

[17] ROBINSON, K. E., DEACON, D. A. G., VELGHE, M. F., MADEY, J. M. J., *IEEE J. Quantum Electron.* **QE-19** (1983) 365.

[18] ELLEAUME, P., to be published in *Appl. Phys. B* and thèse de doctorat (unpublished).

[19] ELLEAUME, P., Submitted to *J. Physique*.

Reprinted from SPIE Vol. 453—Free-Electron Generators of Coherent Radiation

First operation of a Storage Ring Free-Electron Laser

M.Billardon[a], P.Elleaume[b], J.M. Ortega[a], C.Bazin, M.Bergher, Y.Petroff, M.Velghe[c], D.A.G. Deacon[d], J.M.J.Madey[e]

L.U.R.E. - Bâtiment 209-C
Université de Paris-Sud, 91405 ORSAY (France)

(a) Ecole Supérieure de Physique et Chimie, 10 rue Vauquelin, 75231 Paris Cedex 05 (France)
(b) Département de Physico-Chimie, Service de Photophysique, CEN Saclay, 91191 Gif-sur-Yvette (France)
(c) Laboratoire de Photophysique Moléculaire, Bâtiment 213, Université de Paris-Sud, 91405 Orsay (France)
(d) Deacon Research, 3790 El Camino Real, n° 162, Palo Alto, CA 94306 (U.S.A.)
(e) High Energy Physics Lab., Stanford University, Stanford, CA 94305 (U.S.A.)

Abstract

A storage ring free-electron laser oscillator has been operated at a visible wavelength $\lambda \simeq 6500$ Å .

Introduction

The purpose of the Orsay experiment is to test the feasability of a visible Storage Ring Free-Electron Laser (F.E.L.). The realization of the permanent magnet undulator NOEL was achieved in January 1982 [1]. Detailed results concerning the spontaneous emission, the gain measured using an external laser, the laser induced bunch lengthening have been reported at the 1982 Bendor meeting [2]. Improvement of the original low gain (a few parts in 10^{-4} per pass) was achieved in July 1982 by modifying the undulator into an optical klystron [3,4] (O.K.). The O.K. optimization and early results on the spontaneous emission have also been reported at the Bendor meeting[2]. The gain has been measured using an external argon laser [5] and laser induced bunch lengthening has been reported [6]. All the measurements turned out to be in a very good agreement with the classical theory[4]. The maximum gain (at the best electron beam current and energy) is now about 10^{-3} per pass. Therefore, operation of the F.E.L. above threshold requires very high reflectivity mirrors having losses less than $5\ 10^{-4}$ (or reflectivity > 99.95 %). Mirrors having losses less than 10^{-4} have been tested, unfortunately they have shown reflectivity degradation mainly due to the U.V. part of the undulator or optical klystron synchrotron radiation [2,7]. To minimize this degradation, experiments were carried out at 150, 160 and 166 MeV electron energy (as opposed to the original 240 MeV optimization energy for the undulator) in Spring 1983. Despite an initial quick degradation from 10^{-4} up to $3.5\ 10^{-4}$ average losses per mirror, stability of the cavity Q was observed at this last value. The gain at 150 MeV turned out to be less than $6\ 10^{-4}$ preventing from crossing the oscillation threshold. However, operation of the storage ring at 160 MeV and then at 166 MeV brought an improvement of the electron beam quality (mainly bunch length and energy spread) and allowed the oscillator to cross threshold.

Description of the experiment

We have used the Orsay storage ring ACO, an older machine first operated in 1965. Its characteristics for this experiment are given in the following table.

Energy	160-166 MeV
Circumference	22 m
Bunch to bunch distance	11 m
Electron beam current for oscillation	16 to 100 mA
RMS bunch length σ_l	0.5 to 1 ns
RMS bunch transverse dimensions σ_x, σ_y	0.3 to 0.5 mm
RMS angular spread σ'_x, σ'_y	0.1 to 0.2 mrad
RMS relative energy spread	0.9 to 1.3 10^{-3}
Electron beam life time	60 to 90 minutes

The optical klystron main characteristics are :

Full length	1.33 m

Undulators

Number of periods	2 x 7
Period	78 mm
Transverse pole width	100 mm
Minimum magnetic gap	33 mm
Maximum field	0.31 T
K	0 to 2.3
K in the F.E.L. oscillator experiment	1.1 to 1.2

Dispersive section

Length	234 mm
Maximum field	0.58 T
N_d (4)	70 to 100
N_d in the F.E.L. oscillator experiment	95

The characteristics of the optical cavity used in this experiment are the following :

Length	5.5 m
Mirror radius of curvature	3 m
Rayleigh range	1 m
Wavelength of maximum Q	620 to 680 nm
Average mirror reflectivity at 6328 Å	99.965 %
Round trip cavity losses at 6328 Å	$7\ 10^{-4}$
Mirror transmission	$3\ 10^{-5}$

Optical measurements were made using the experimental set-up shown in figure 1.

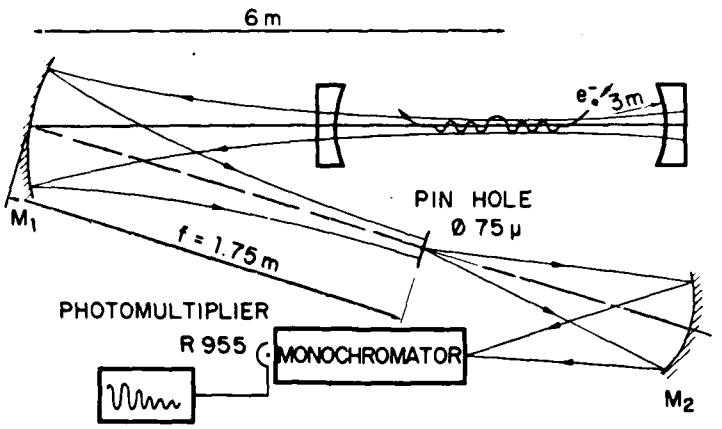

Figure 1. Experimental set-up

This set-up was originally used to investigate the spontaneous emission[8]. The transmitted part of the synchrotron radiation stored in the cavity is refocused by an aluminium mirror M_1 of 1.75 m focal distance. A pinhole of 75 μ diameter pinhole is placed at the mirror focal distance. The light passing through the pinhole is sent to a monochromator by an aluminium mirror M_2. Typical monochromator bandwith was 0.3 Å. The light coming out from the monochromator is detected in a photomultiplier, the signal being sent to a strip-chart recorder. The pinhole is mounted on a horizontal and vertical translation plate for transverse profiles records.

Results

Laser oscillation was obtained after a careful alignment of the electron beam on the cavity axis (within 0.1 mm all along the 1.3 m O.K. length) and maximization of emission as a function of the storage ring radio frequency cavity voltage and the optical cavity length. Laser operation requires very precise synchronism between light pulse reflections and electron-bunch revolution frequency. To avoid backlash and mirror misalignment, fine tuning of the cavity length was performed by slightly changing the R.F. frequency instead of translating the mirrors.

Fig. 2 shows two "detuning curves" of laser power (normalized to the maximum) versus R.F. frequency variation and equivalent mirror displacement.

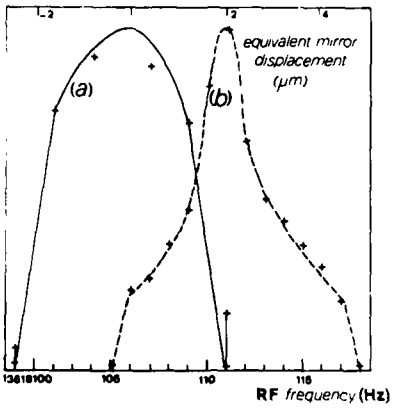

Figure 2. Normalized laser power as a function of RF frequency and equivalent mirror displacement. Curve (a) is recorded close to the maximum gain/loss ratio and curve (b) close to the laser threshold. The shift between the two curves is probably due to some slight cavity length drift.

Curve (a) has a 3.7 μm F.W.H.M. of equivalent mirror displacement ; curve (b) as recorded much closer to laser threshold, has only a 1.6 μm F.W.H.M. The shift in displacement between curves (a) and (b) is probably due to some slow cavity length drift (e.g. a temperature drift of 0.02 °C/30 minutes would be sufficient). In this experiment, the gain was not proportional to the electron current, mainly due to the anomalous bunch lengthening and energy spreading at high current ; these effects make the gain versus ring current reach a maximum and then decrease. One consequence of this is that the ratio of gain to cavity losses always remained just above 1 for laser operation. Wider detuning curves are expected for higher gain/losses ratios.

Fig. 3 presents the horizontal and vertical transverse profiles of the laser output. They are in a very good agreement with the expected cavities TEM_{oo} profile. The slight discrepancies might arise from some residual instability of the laser too close to threshold or non uniform mirror reflectivity.

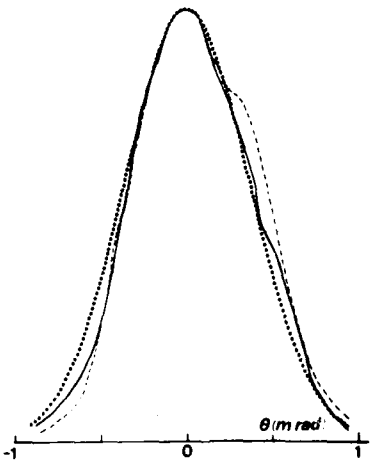

Figure 3. Experimental laser horizontal and vertical transverse profiles and the calculated cavity TEM_{oo} profile.

Fig. 4 shows the laser time structure in a 200 ms total time scale. Although not seen in fig. 4, the laser reproduces the pulsed 27 MHz structure of the electron laser. As it can be seen on fig. 4, the laser adopts a quasirandom pulsed structure over a long time scale with a typical rise time around 200 μs (corresponding to a gain minus losses of $2.\ 10^{-4}$ per pass) and a quasirandom period of about 20 to 40 ms.

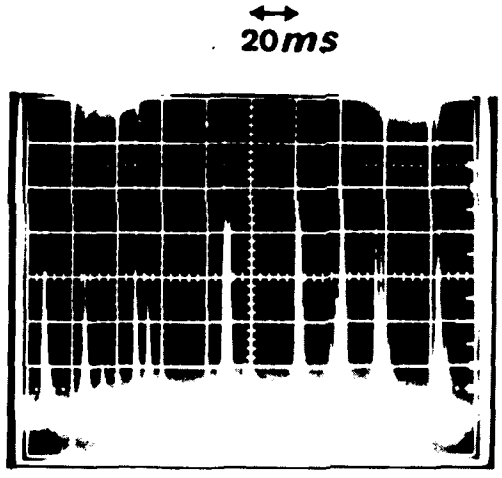

Figure 4. Laser time structure over a 200 ms interval.

Each subpeak is also usually more or less modulated at 13 KHz very close to the theoretical R.F. synchrotron frequency. It should be noted that this time structrure depends on the electron energy and also how far the laser is from threshold.

Fig. 5 presents two spectra : a) is recorded without amplification (optical cavity detuned), b) is recorded at laser operation (cavity tuned). Usually, the laser oscillates simultaneously at three wavelength with a wrontly dominant central line. Each wavelength is located at a maximum of the gain versus wavelength curve[4]. Laser tunability was obtained from 640 nm to 655 nm by changing the magnetic gap. In fact, the range of tunability is limited for the moment by the mirror reflectivity.

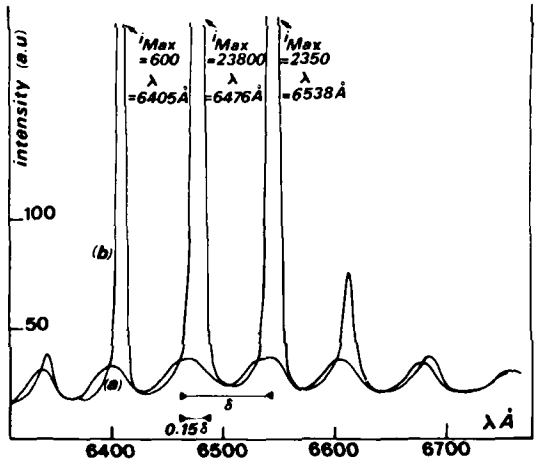

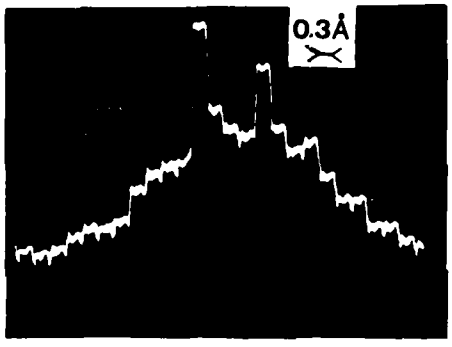

Figure 5. Spectra ot the cavity output radiation under two conditions ; (a) cavity detuned (no amplification), (b) cavity tuned (laser on).

Fig. 5 shows an enlargement of the main laser line spectrum recorded by using a one dimensional C.C.D. detector instead of the usual monochromator exit slit. The aperture time is 3ms. Each narrow square peak in this curve is recorded on only one C.C.D. element and corresponds to a 0.3 Å spectral width of the same order as monochromator resolution. We conclude that there is a residual inhomogeneous contribution to the laser line--width probably connected with the long time scale laser pulsed structure (see fig. 4), so that typical laser lines are gaussian with about 3 Å F.W.H.M. if averaged over a time scale of ≈ 1 sec.

The central wavelength of any line is always equal to the wavelength of maximum emission of spontaneous emission with the cavity completely detuned (no amplification) plus 0.15 of the wavelength interfringe distance (see fig. 5) instead of 0.25 as predicted from Madey's theorem[9]. This discrepancy is probably due

to the transverse multimode content of the spontaneous emission stored in the cavity, whereas the measured transverse profiles of the laser output show that laser operation is only achieved on the TEM_{oo} mode.

A typical 75 μW average output power has been recorded at 50 mA current of 166 MeV electrons. This corresponds to a typical 60 mW output peak power over the 1 ns electron bunch length (including effects of both long and short time scale pulsed structure of the laser), and a 2 kW intracavity peak power. This gives a 2.4×10^{-5} efficiency with respect to the 3.1 watt ot total synchrotron radiation power generated in the whole storage ring at this energy and current. This efficiency is about 0.4 the Renieri typical efficiency (10) :

$$\eta = \frac{\sigma_E}{E} \times \eta_{mir} \quad \text{where } \eta_{mir} = \frac{\text{mirror transmission}}{\text{round trip cavity losses}}$$

and $\frac{\sigma_E}{E} = 1.2 \times 10^{-3}$ is the R.M.S. relative energy spread. In this experiment $\eta_{mir} = 0.043$.

This low mirror efficiency is mainly due to the high absorption in the mirror dielectric layers compared to its transmission. The rather low Renieri average output power is therefore the result of high sensitivity of the O.K. to energy spread, poor mirror efficiency, and weak total synchrotron radiation power at 166 MeV (power is proportional to the fourth power of the electron energy). As shown in Fig. 6, the laser output power decreases with the electron beam current and, except in regions too close to threshold is usually proportional to the current as predicted by the same model.

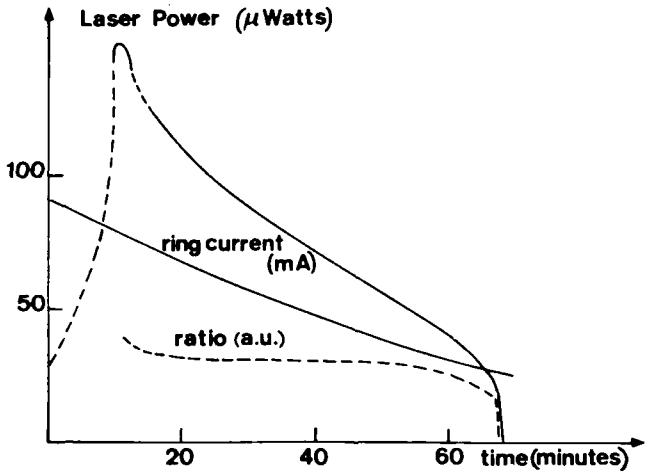

Figure 6. Laser power together with electron beam current versus time.

However, important discrepancies appear in the structure for long time scales (see Fig. 3) which is predicted to be constant. Moreover, bunch shortening instead of bunch lengthening has been seen at laser turn on ; such an effect has already been seen at much lower current by stimulating the F.E.L. with an argon laser (11).

Conclusions

In summary, this work demonstrates for the first time the feasability of the storage ring Free-Electron Laser. Future experiments will continue to analyze the saturation mechanism and the long and short time scale structure. Higher gain/losses ratios are expected from the use of better mirrors, a second RF cavity, and positrons instead of electrons.

Acknowledgements

The authors are greatly indebted to Yves Farge who initiated this research, to the technical support staff of the L.U.R.E. laboratory for there invaluable help. Also, they

AD-A164 192 STORAGE RING TECHNOLOGY FOR FREE ELECTRON LASERS(U) 3/3
STANFORD UNIV CA J M MADEY ET AL. APR 84
AFOSR-TR-85-1223 F49620-83-K-0030

UNCLASSIFIED F/G 20/5 NL

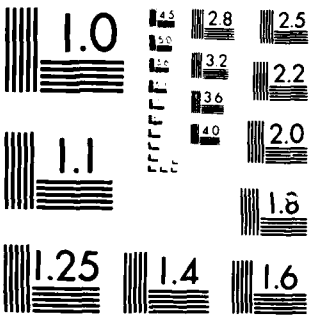

thank the storage ring staff of the LAL for many fruitful discussions and the "Service Aimant" of the LAL for experimental assistance. This work was supported by DRET contract No. 81/131 and AFOSR contract No. F 49620-80-C-0068.

References

1. J.M. Ortéga, C. Bazin, D.A.G. Deacon, C. Depeautex and P. Elleaume, Nucl. Inst. and Methods, 206, 281 (1983)
2. M. Billardon, D.A.G. Deacon, P. Elleaume, J.M. Ortéga, K.E. Robinson, C. Bazin, M. Bergher, J.M.J. Madey, Y. Petroff and M. Velghe, Journal de Physique, Colloque C1, 44, 29 (1983)
3. N.A. Vinokurov and A.N. Skrinsky, Preprint INP 77-59, Novosibirsk (1977) ; see also N.A. Vinokurov, Proc. 10th Int. Conf. on high energy charged particle accelerators, Serpukhov, vol. 2, 454 (1977)
4. P. Elleaume, Journal de Physique, Colloque C1, 44, 333 (1983). See also P. Elleaume Physics of Quantum Electronics, Addison-Wesley, 8, chapter 5, 119 (1982)
5. M. Velghe, M. Bergher, C. Bazin, M. Billardon, D.A.G. Deacon, P. Elleaume, J.M.J. Madey, J.M. Ortéga, Y. Petroff and K.E. Robinson, to be published in the Proceedings of the International Conference on Lasers' 82
6. K.E. Robinson, D.A.G. Deacon, M.F. Velghe, J.M.J. Madey, Journal de Physique, Colloque C1, 44, 379 (1983).
7. P. Elleaume, D.A.G. Deacon, M. Billardon, J.M. Ortéga, to be published in the proceedings of CLEO' 83.
8. C. Bazin, M. Billardon, D.A.G. Deacon, P. Elleaume, Y. Farge, J.M.J. Madey, J.M. Ortéga, Y. Petroff, K.E. Robinson and M. Velghe, Physics of Quantum Electronics, 8, 89 (Addison-Wesley 1982)
9. J.M.J. Madey, Il Nuovo Cimento, 50 B, 64 (1979)
10. A. Renieri, Nuov. Cim., 53B, 160 (1979), G. Dattoli and A. Renieri, Nuov. Cim., 59B, 1 (1980)
11. K.E. Robinson, D.A.G. Deacon, M.F. Velghe, J.M.J. Madey, IEEE J. Quant. Electron., QE-19, 365 (1983).

END

FILMED

4-86

DTIC